

AD-A040 707

GENERAL DYNAMICS/FORT WORTH TEX FORT WORTH DIV
ASD ADVANCED PROGRAM RESEARCH INLET DATA ANALYSIS REPORT FOR 1/--ETC(U)
JAN 77 C C MANN, J.E GARNER

F/G 21/5

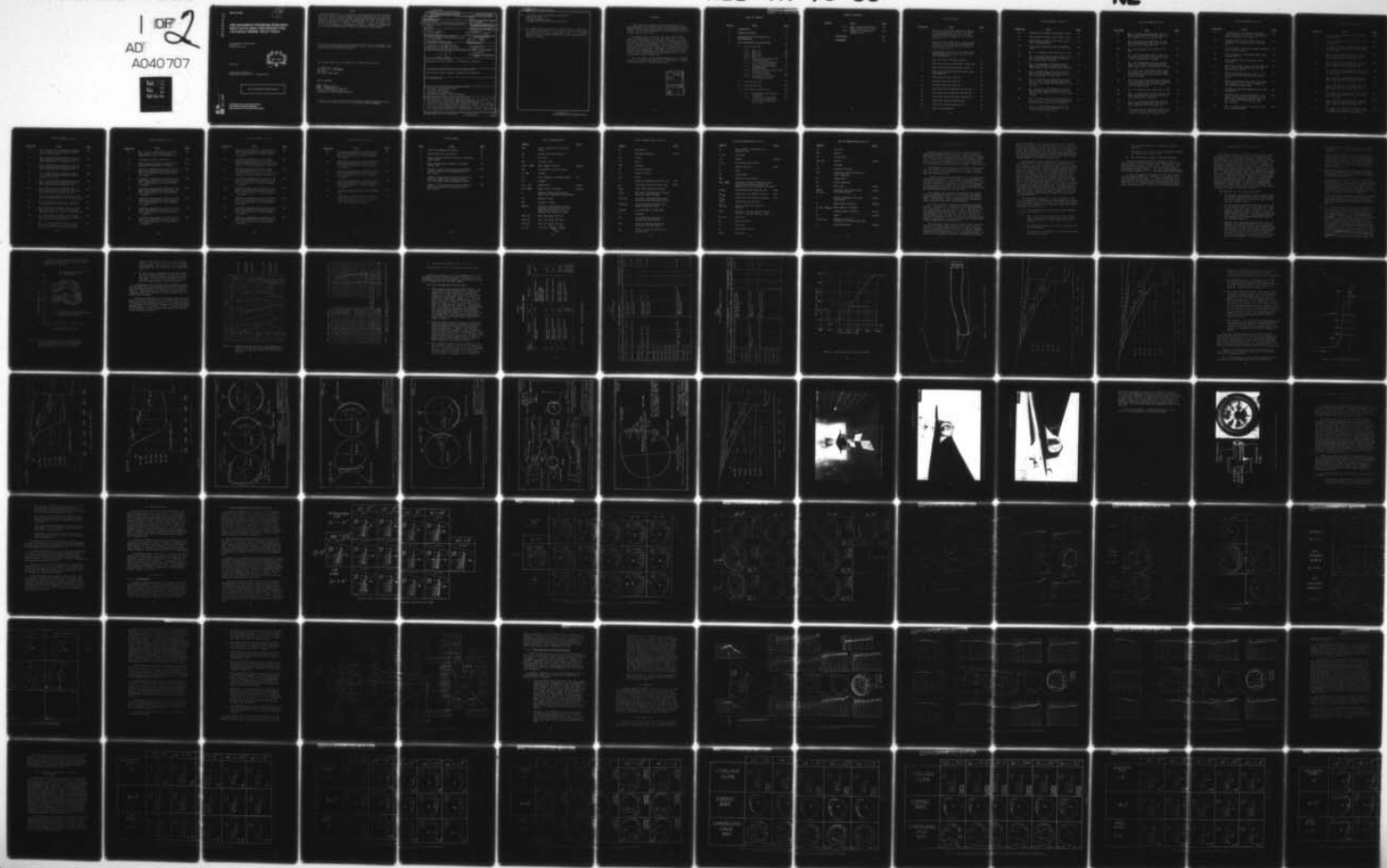
F33615-75-C-5289

UNCLASSIFIED

ASD-TR-76-35

NL

1 OF 2
AD
A040 707



AD A 040707

ASD-TR-76-35

12
NW

ASD ADVANCED PROGRAM RESEARCH INLET DATA ANALYSIS REPORT FOR 1/5.2 SCALE MODEL INLET TESTS

*General Dynamics Fort Worth Division
P.O. Box 748
Fort Worth, Texas 76101*

January 1977

DDC
RECEIVED
JUN 20 1977
B

Technical Report ASD-TR-76-35
Final Report for Period 14 July 1975 - 1 September 1976

Approved for Public Release: Distribution Unlimited

AD No. _____
DDC FILE COPY

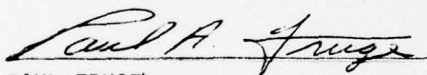
AERONAUTICAL SYSTEMS DIVISION
AIR FORCE SYSTEMS COMMAND
Wright-Patterson Air Force Base, Ohio 45433

NOTICE

When Government drawings, specifications, or other data are used for any purpose other than in connection with a definitely related Government procurement operation, the United States Government thereby incurs no responsibility nor any obligation whatsoever; and the fact that the government may have formulated, furnished, or in any way supplied the said drawings, specifications, or other data, is not to be regarded by implication or otherwise as in any manner licensing the holder or any other person or corporation, or conveying any rights or permission to manufacture, use, or sell any patented invention that may in any way be related thereto.

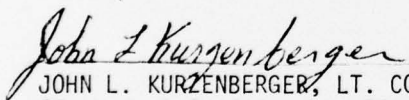
This report has been reviewed by the Information Office (IO) and is releasable to the National Technical Information Service (NTIS). At NTIS, it will be available to the general public, including foreign nations.

This technical report has been reviewed and is approved for publication.



PAUL FRUGE
Air Force Program Manager

FOR THE COMMANDER



JOHN L. KURZENBERGER, LT. COL, USAF
(Technical Assistant to Director)
Directorate of Flight Systems Engineering

Copies of this report should not be returned unless return is required by security considerations, contractual obligations, or notice on a specific document.

Unclassified

SECURITY CLASSIFICATION OF THIS PAGE (When Data Entered)

19 REPORT DOCUMENTATION PAGE		READ INSTRUCTIONS BEFORE COMPLETING FORM	
1. REPORT NUMBER ASD-TR-76-35	2. GOVT ACCESSION NO.	3. RECIPIENT'S CATALOG NUMBER	
4. TITLE (and Subtitle) ASD Advanced Program Research Inlet Data Analysis Report for 1/5.2-Scale Inlet Tests.		5. TYPE OF REPORT & PERIOD COVERED Final Report, for Period 7/14/75-9/1/76	
7. AUTHOR(s) Charles C. Mann Jack E. Garner		6. PERFORMING ORG. REPORT NUMBER 14 Jul 75 - 1 Sep 76	
9. PERFORMING ORGANIZATION NAME AND ADDRESS General Dynamics' Fort Worth Division P. O. Box 748 Fort Worth, Texas 76101		8. CONTRACT OR GRANT NUMBER(s) Contract F33615-75-C-5289/new	
11. CONTROLLING OFFICE NAME AND ADDRESS Aeronautical Systems Division Wright-Patterson AFB, Ohio 45433		10. PROGRAM ELEMENT, PROJECT, TASK AREA & WORK UNIT NUMBERS 11 Jan 77	
14. MONITORING AGENCY NAME & ADDRESS (if different from Controlling Office) 12-185p.		12. REPORT DATE	
		13. NUMBER OF PAGES 184	
		15. SECURITY CLASS. (of this report) Unclassified	
		15a. DECLASSIFICATION/DOWNGRADING SCHEDULE	
16. DISTRIBUTION STATEMENT (of this Report) Approved for public release: Distribution unlimited.			
17. DISTRIBUTION STATEMENT (of the abstract entered in Block 20, if different from Report) Approved for public release: Distribution unlimited.			
18. SUPPLEMENTARY NOTES			
19. KEY WORDS (Continue on reverse side if necessary and identify by block number) Open-nose, normal-shock inlet wing-body flow field engine/inlet compatibility subsonic/supersonic inlet performance			
20. ABSTRACT (Continue on reverse side if necessary and identify by block number) The analysis of wind-tunnel data from tests of a 1/5.2-scale inlet research model covered was conducted in PWT 16S and 16T. The tests were conducted by GD under contract from ASD. Inlet design and engine/inlet compatibility criteria are based on the F101-GE-100 engine characteristics and requirements. Detailed inlet flow-field analyses are discussed. Inlet pressure recovery, distortion,			

Unclassified

SECURITY CLASSIFICATION OF THIS PAGE(When Data Entered)

19. hi-response data acquisition and analysis
duct-blowing/VGs
fuselage boundary layer
boundary layer diverters/splitter plates
20. → and compatibility parameters are presented for a basic configuration from Mach 0.55 to Mach 2.0. Data for an alternate configuration are presented for Mach 0.55 to 1.5. A limited amount of data are also presented for other configurations that were tested.

Unclassified

SECURITY CLASSIFICATION OF THIS PAGE(When Data Entered)

FOREWORD

This report was prepared by General Dynamics' Fort Worth Division for the Aeronautical Systems Division, ASD, Wright-Patterson AFB, Dayton, Ohio, under Contract F33615-75-C-5289. It covers an analysis of the test data from an advanced research inlet test.

In this program, a simple, open-nose, normal-shock inlet was designed and tested in the influence of a wing-body flow field, which at supersonic speeds has its associated shocks and precompression effects. To evaluate the inlets performance and operation, the General Electric F101-GE-100 engine-airflow and compatibility characteristics were selected as the criteria. The report documents inlet performance and compatibility from Mach 0.55 to Mach 2.0 for a primary inlet configuration and from Mach 0.55 to 1.5 for an alternate inlet configuration.

Mr. Paul Fruge' was the ASD Program Monitor. Preparation of this report was made by C. C. Mann and J. E. Garner of General Dynamics' Fort Worth Division.

ACCESSION for	
RTIS	White Section <input checked="" type="checkbox"/>
BDC	Buff Section <input type="checkbox"/>
UNANNOUNCED	<input type="checkbox"/>
JUSTIFICATION	
BY	
DISTRIBUTION/AVAILABILITY CODES	
Dist. AVAIL. and/or SPECIAL	
A	

TABLE OF CONTENTS

<u>Section</u>	<u>Title</u>	<u>Page</u>
1.	INTRODUCTION	1
2.	SUMMARY OF RESULTS	4
3.	DESCRIPTION OF TEST PROGRAM AND CONFIGURATIONS	10
4.	DATA PRESENTATION AND DISCUSSION	33
4.1	Inlet Flow Field	35
4.1.1	Mach 1.6	35
4.1.2	Mach 0.5	54
4.1.3	Mach 0.85	54
4.1.4	Mach 1.2	62
4.1.5	Research Model Flow Field Versus Mach Number	62
4.1.6	F-111 and Research-Model Flow Field Comparisons	81
4.1.7	Alternate Splitter-Plate Configurations	87
4.1.8	Effect of Splitter-Plate Size/ Standoff-Distance	91
4.1.9	Flow Field Summary	91
4.1.10	Fuselage Boundary-Layer System Modifications	92
4.2	Internal Duct Flow	99
4.3	Inlet Performance	102
4.4	Engine/Inlet Compatibility	128
4.4.1	Hi-Response Data Analysis Techniques	128
4.4.2	Compatibility Assessment of the Basic Long-Plow/ Splitter-Plate Inlet at B.L. 45.64	132

TABLE OF CONTENTS

<u>Section</u>	<u>Title</u>	<u>Page</u>
4.4.3	Basic Long-Plow/Splitter- Plate Inlet at B.L. 43.82	145
4.4.4	Summary of Engine/Inlet Compatibility	160
5.	CONCLUSIONS	163
	REFERENCES	165

LIST OF FIGURES

<u>Figure No.</u>	<u>Title</u>	<u>Page</u>
1	Effect of steady-state-distortion pattern on dynamic-distortion level of the Basic Long-Plow/Splitter-Plate Inlet at B.L. 43.82 at design airflows for $\alpha = 5^\circ$ and $\beta = 0^\circ$	6
2	Predicted versus model test inlet pressure recovery of the Basic Long-Plow/Splitter-Plate Inlet @ B.L. 43.82, $A_i = 1214 \text{ in.}^2$, $\alpha = 5^\circ$, and $\beta = 0^\circ$	8
3	Compatibility envelopes of the Basic Long-Plow/Splitter-Plate Inlet at B.L. 45.64 with VG Pattern 3	9
4	Duct area curve (0.8 Mach throat)	14
5	Plan view of the research model inlet duct	15
6	Basic Long-Plow/Splitter-Plate Inlet	16
7	Basic Long and Short Splitter-Plate Inlet configurations	17
8	Inlet buttock line locations	19
9	Alternate Splitter Plate No. 1	20
10	Alternate Splitter Plate No. 2	21
11	Inlet-duct Vortex Generator Pattern No. 1	22
12	Inlet-duct Vortex Generator Pattern No. 2	23
13	Inlet-duct Vortex Generator Pattern No. 3	24
14	Inlet-duct outboard blowing jets	25
15	Inlet-duct inboard blowing jets	26
16	Inlet instrumentation	27

LIST OF FIGURES (Cont'd)

<u>Figure No.</u>	<u>Title</u>	<u>Page</u>
17	ASD advanced research inlet model in 16T	28
18	ASD advanced research inlet model in 16S	29
19	ASD advanced research inlet model flow-field instrumentation	30
20	Inlet-model-compressor-face instrumentation	32
21	$M_0 = 1.6$ fuselage flow field at F.S. 390	37
22	$M_0 = 1.6$ throat-rake contour maps for the Basic Long-Plow/Splitter-Plate Inlet at B.L. 45.64 at $W_c = 310$ pps	39
23	$M_0 = 1.6$ compressor-face-rake contour maps for the Basic Long-Plow/Splitter-Plate Inlet at B.L. 43.82 at $W_c = 310$ pps	41
24	$M_0 = 1.6$ inlet-flow-field data for the Basic Long-Plow/Splitter-Plate Inlet at B.L. 43.82 at $\alpha = 2^\circ$ and $\beta = 0^\circ$	43
25a	$M_0 = 1.6$ throat and compressor-face maps for the Basic Long-Plow/Splitter-Plate Inlet at $\alpha = 2^\circ$ and $\beta = 0^\circ$ for $W_c = 365$ - 310 pps	45
25b	$M_0 = 1.6$ throat and compressor-face maps for the Basic Long-Plow/Splitter-Plate Inlet at $\alpha = 2^\circ$ and $\beta = 0^\circ$ for $W_c = 280$ - 195 pps	47
26	$M_0 = 1.6$ inlet flow field versus angle of attack ($\beta = 0^\circ$) for the Basic Long-Plow/Splitter-Plate Inlet at $W_c = 310$ pps	51
27	$M_0 = 1.6$ inlet-flow-field data for the Short-Plow/Splitter-Plate Inlet at B.L. 43.82 at $\alpha = 2^\circ$ and $\beta = 0^\circ$	55

LIST OF FIGURES (Cont'd)

<u>Figure No.</u>	<u>Title</u>	<u>Page</u>
28	$M_0 = 0.5$ inlet-flow-field data for the Basic Long-Plow/Splitter-Plate Inlet at B.L. 43.82 at $\alpha = 2^\circ$ and $\beta = 0^\circ$	57
29	$M_0 = 0.5$ inlet-flow-field data for the Short-Plow/Splitter-Plate Inlet at B.L. 45.64 at $\alpha = 2^\circ$ and $\beta = 0^\circ$	59
30	$M_0 = 0.85$ fuselage flow field at F.S. 390	63
31	$M_0 = 0.85$ throat-rake contour maps for the Basic Long-Plow/Splitter-Plate Inlet at B.L. 43.82 at $W_c = 310$ pps	65
32	$M_0 = 0.85$ compressor-face-rake contour maps for the Basic Long-Plow/Splitter-Plate Inlet at B.L. 43.82 at $W_c = 310$ pps	67
33	$M_0 = 0.85$ inlet flow field versus angle of attack ($\beta = 0^\circ$) for the Basic Long-Plow/Splitter-Plate Inlet at B.L. 43.82 at $W_c = 357$ pps	69
34	$M_0 = 0.85$ inlet-flow-field data during an airflow excursion for the Basic Long-Plow/Splitter-Plate Inlet at B.L. 43.82 at $\alpha = 5^\circ$ and $\beta = 0^\circ$	71
35	$M_0 = 1.2$ fuselage flow field at F.S. 390	73
36	$M_0 = 1.2$ throat-rake contour maps for the Basic Long-Plow/Splitter-Plate Inlet at B.L. 43.82 at $W_c = 354$ pps	75
37	$M_0 = 1.2$ inlet-flow-field data for the Basic Long-Plow/Splitter-Plate Inlet at B.L. 43.82 at $\alpha = 5^\circ$ and $\beta = 0^\circ$	77
38	Inlet flow field versus Mach number for the Basic Long-Plow/Splitter-Plate Inlet at B.L. 43.82 at $\alpha = 5^\circ$ and $\beta = 0^\circ$	79

LIST OF FIGURES (Cont'd)

<u>Figure No.</u>	<u>Title</u>	<u>Page</u>
39	A comparison of the fuselage boundary layers measured on the F-111 and research models for Mach 0.75 to Mach 1.6	83
40	Theoretical flat-plate versus measured boundary-layer heights at $M_0 = 0.85$ and $M_0 = 1.2$	86
41	F-111 airplane and model-fuselage-boundary-layer pressure survey	88
42	F-111 flight-test fuselage-boundary-layer pressure survey	89
43	F-111 Triple Plow II inlet-model face-rake data	90
44	Effect of splitter-plate size and shape at $M_0 = 0.85$ on inlet-throat flow for the inlet at B.L. 43.82	93
45	Effect of splitter-plates at $M_0 = 1.5$ on inlet-throat flow for the inlet at B.L. 43.82	95
46	Effect of splitter-plate shape and stand-off distance at $M_0 = 0.85$ on compressor-face-pressure contour maps	97
47	A potential fuselage-boundary-layer system modification	100
48	Effectiveness of duct-blowing/VGs in reducing compressor-face distortion of the Basic Long-Plow/Splitter-Plate Inlet at $M_0 = 0.85$, $\alpha = 5^\circ$ and $\beta = 0^\circ$, and $W_c = 354$ pps	101
49	$M_0 = 1.6$ inlet pressure recovery of four inlet configurations	103

LIST OF FIGURES (Cont'd)

<u>Figure No.</u>	<u>Title</u>	<u>Page</u>
50	$M_0 = 1.6$ inlet distortion of four inlet configurations	104
51	$M_0 = 1.6$ inlet performance of four inlet configurations	105
52	$M_0 = 0.55-1.2$ inlet pressure recovery for the Basic Long-Plow/Splitter-Plate Inlet at B.L. 43.82	107
53	$M_0 = 0.55-1.2$ inlet distortion of the Basic Long-Plow/Splitter-Plate Inlet at B.L. 43.82 for $\alpha = 5^\circ$ and $\beta = 0^\circ$	108
54	$M_0 = 0.55-1.2$ inlet turbulence of the Basic Long-Plow/Splitter-Plate Inlet at B.L. 43.82 for $\alpha = 5^\circ$ and $\beta = 0^\circ$	109
55	$M_0 = 1.20-1.70$ inlet pressure recovery for the Basic Long-Plow/Splitter-Plate Inlet at B.L. 43.82	110
56	$M_0 = 1.20-1.70$ inlet distortion for the Basic Long-Plow/Splitter-Plate Inlet at B.L. 43.82 for $\alpha = 5^\circ$ and $\beta = 0^\circ$	111
57	$M_0 = 1.20-1.70$ inlet turbulence for the Basic Long-Plow/Splitter-Plate Inlet at B.L. 43.82 for $\alpha = 5^\circ$ and $\beta = 0^\circ$	112
58	$M_0 = 1.62-2.00$ inlet pressure recovery for the Basic Long-Plow/Splitter-Plate Inlet at B.L. 43.82	113
59	$M_0 = 1.62-2.00$ inlet distortion for the Basic Long-Plow/Splitter-Plate Inlet at B.L. 43.82 for $\alpha = 5^\circ$ and $\beta = 0^\circ$	114
60	$M_0 = \text{Mach } 1.62-2.00$ inlet turbulence for the Basic Long-Plow/Splitter-Plate Inlet at B.L. 43.82 for $\alpha = 5^\circ$ and $\beta = 0^\circ$	115

LIST OF FIGURES (Cont'd)

<u>Figure No.</u>	<u>Title</u>	<u>Page</u>
61	$M_0 = 0.55-0.85$ inlet pressure recovery for the Basic Long-Plow/Splitter-Plate Inlet at B.L. 45.64	116
62	$M_0 = 0.55-0.85$ inlet distortion for the Basic Long-Plow/Splitter-Plate Inlet at B.L. 45.64 for $\alpha = 5^\circ$ and $\beta = 0^\circ$	117
63	$M_0 = 0.55-0.85$ inlet turbulence for the Basic Long-Plow/Splitter-Plate Inlet at B.L. 45.64 for $\alpha = 5^\circ$ and $\beta = 0^\circ$	118
64	$M_0 = 1.20-1.50$ inlet pressure recovery of the Basic Long-Plow/Splitter-Plate Inlet at B.L. 45.64	119
65	$M_0 = 1.20-1.50$ inlet distortion for the Basic Long-Plow/Splitter-Plate Inlet at B.L. 45.64 for $\alpha = 5^\circ$ and $\beta = 0^\circ$	120
66	$M_0 = 1.20-1.50$ inlet turbulence for the Basic Long-Plow/Splitter-Plate Inlet at B.L. 45.64 for $\alpha = 5^\circ$ and $\beta = 0^\circ$	121
67	$M_0 = 0.85$ inlet pressure recovery of four inlet configurations at $\alpha = 5^\circ$ and $\beta = 0^\circ$	122
68	$M_0 = 0.85$ inlet distortion of four inlet configurations at $\alpha = 5^\circ$ and $\beta = 0^\circ$	123
69	$M_0 = 0.85$ inlet pressure recovery of the Basic Long Splitter Plate and Alternate Splitter Plate No. 2 at $\alpha = 5^\circ$ and $\beta = 0^\circ$	124
70	$M_0 = 0.85$ inlet distortion of the Basic Long Splitter Plate and Alternate Splitter No. 2 at $\alpha = 5^\circ$ and $\beta = 0^\circ$	125
71	$M_0 = 1.5$ inlet pressure recovery of the Basic Long Splitter Plate and Alternate Splitter No. 2 at $\alpha = 5^\circ$ and $\beta = 0^\circ$	126

LIST OF FIGURES (Cont'd)

<u>Figure No.</u>	<u>Title</u>	<u>Page</u>
72	$M_0 = 1.5$ inlet distortion of the Basic Long Splitter Plate and Alternate Splitter No. 2 at $\alpha = 5^\circ$ and $\beta = 0^\circ$	127
73	Hi-response analysis procedure	129
74	Mach-altitude envelope selected for engine/inlet compatibility analysis	131
75	Estimated compatibility envelope of the Basic Long-Plow/Splitter-Plate Inlet at B.L. 45.64 with $M_0 = 0.85$ and altitude = 35,500 ft	135
76	Estimated compatibility envelope of the Basic Long-Plow/Splitter-Plate Inlet at B.L. 45.64 with $M_0 = 1.2$ and altitude = 45,000 ft	136
77	Estimated compatibility envelope of the Basic Long-Plow/Splitter-Plate Inlet at B.L. 45.64 with $M_0 = 1.4$ and altitude = 48,000 ft	137
78	Estimated compatibility envelope of the Basic Long-Plow/Splitter-Plate Inlet at B.L. 45.64 with $M_0 = 1.5$ and altitude = 49,500 ft	138
79	Estimated compatibility envelope of the Basic Long-Plow/Splitter-Plate Inlet at B.L. 45.64 with $M_0 = 1.2$ and altitude = 36,000 ft	139
80	Estimated compatibility envelope of the Basic Long-Plow/Splitter-Plate Inlet at B.L. 45.64 with $M_0 = 1.4$ and altitude = 40,000 ft	140

LIST OF FIGURES (Cont'd)

<u>Figure No.</u>	<u>Title</u>	<u>Page</u>
81	Estimated compatibility envelope of the Basic Long-Plow/Splitter-Plate Inlet at B.L. 45.64 with $M_0 = 1.5$ and altitude = 44,000 ft	141
82	Estimated compatibility of the Basic Long-Plow/Splitter-Plate Inlet, with Vortex Generator Pattern 3, at B.L. 45.64 with $M_0 = 0.85$ and altitude = 35,500 ft	143
83	Estimated compatibility of the Basic Long-Plow/Splitter-Plate Inlet, with Vortex Generator Pattern 3, at B.L. 45.64 with $M_0 = 1.4$ and altitude = 48,000 ft	144
84	Estimated compatibility envelope of the Basic Long-Plow/Splitter-Plate Inlet at B.L. 43.82 with $M = 0.85$ and altitude = 35,500 ft	149
85	Estimated compatibility envelope of the Basic Long-Plow/Splitter-Plate Inlet at B.L. 43.82 with $M_0 = 1.2$ and altitude = 45,000 ft	150
86	Estimated compatibility envelope of the Basic Long-Plow/Splitter-Plate Inlet at B.L. 43.82 with $M_0 = 1.4$ and altitude = 48,000 ft	151
87	Estimated compatibility envelope of the Basic Long-Plow/Splitter-Plate Inlet at B.L. 43.82 with $M_0 = 1.5$ and altitude = 49,500 ft	152
88	Estimated compatibility envelope of the Basic Long-Plow/Splitter-Plate Inlet at B.L. 43.82 with $M = 1.6$ and altitude = 50,000 ft	153

LIST OF FIGURES (Cont'd)

<u>Figure No.</u>	<u>Title</u>	<u>Page</u>
89	Estimated compatibility envelope of the Basic Long-Plow/Splitter-Plate Inlet at B.L. 43.82 with $M_0 = 1.7$ and altitude = 50,500 ft	154
90	Estimated compatibility envelope of the Basic Long-Plow/Splitter-Plate Inlet at B.L. 43.82 with $M_0 = 1.2$ and altitude = 36,000 ft	155
91	Estimated compatibility envelope of the Basic Long-Plow/Splitter-Plate Inlet at B.L. 43.82 with $M_0 = 1.4$ and altitude = 40,000 ft	156
92	Estimated compatibility envelope of the Basic Long-Plow/Splitter-Plate Inlet at B.L. 43.82 with $M_0 = 1.5$ and altitude = 44,000 ft	157
93	Left-Hand Compressor-Face Probe Designation	159
94	Compatibility prediction of the Basic Long-Plow/Splitter-Plate Inlet with the low-energy defect corrected: $\alpha = 5^\circ$, $\beta = 0^\circ$, and design airflows	161

LIST OF TABLES

<u>Table</u>	<u>Title</u>	<u>Page</u>
1	16S Test Configuration Summary	11
2	Summary PWT 16T Test Program	12
3	Research Model Predicted Flat-Plate Boundary-Layer Height	82
4	Model Boundary Layer Height at Fuselage Station 390	85
5	Summary of Points Selected for Hi-Response Analysis, Basic Inlet Configuration at B.L. 45.64	133
6	Summary of Points Selected for Hi-Response Analysis, Basic Inlet Configuration at B.L. 45.64 With Vortex Generator Pattern 3	142
7	Summary of Points Selected for Hi-Response Analysis, Basic Inlet Configuration at B.L. 43.82	146

LIST OF ABBREVIATIONS

<u>Symbols</u>		<u>Units</u>
AEDC	Arnold Engineering Development Center	
ADA	Analog Distortion Analyzer	
AF	Air Force	
AFB	Air Force Base	
Alpha, ALPHA	Model Angle of Attack	degrees
ASD	Aeronautical Systems Division	
AV, AVG	Average	
A_i	Inlet Capture or Reference Area	in ²
A/P	Airplane	
B.L., B/L	Buttock Line	inches
Beta, BETA	Model Angle of Sideslip	degrees
b	Emprical Superposition Factor Used in the Distortion Calculations	
C.F.	Compressor Face	
DIV	Diverter or Flow	
DUCT 45	L/H Inlet, Duct Static Pressure Recovery Data Measured Down the Inlet Duct Along the 45° Line Looking Into Inlet from Front	
DUCT 135	Same, But Along 135° Line	
DUCT 225	Same, But Along 225° Line	
DUCT 315	Same, But Along 315° Line	
D ₂ , D ₂ L	L/H Inlet, $\frac{P_{T2MAX} - P_{T2MIN}}{P_{T2av}}$	


LIST OF ABBREVIATIONS (Cont'd.)

<u>Symbols</u>		<u>Units</u>
FF	Flow Field	
FS	Fuselage Station, X	inches
Flt	Flight	
Ft	Feet	
FUS	Fuselage	
GD	General Dynamics	
GE	General Electric	
GLV	Glove	
H	Total or Stagnation Pressure, P_T	psia
H_0	Free-Stream Total Pressure, P_{T0}	psia
H/H_0	Pitot Total Pressure Recovery	
H_2/H_0	L/H Inlet, Average Total Pressure Recovery, RECL, P_{T2}/P_{T0}	
IDCL MAX	L/H Inlet, Maximum Steady-State Circumferential Distortion Index	
IDRL MAX	L/H Inlet, Maximum Steady-State Radial Distortion Index	
IDL MAX	$b K_C \text{ IDCL MAX} + K_R \text{ IDRL MAX}$	
K	Thousand	
K_C	Circumferential Distortion Sensitivity Coefficient	
KD2	Pratt and Whitney Distortion Parameter for TF30 Engines	
K_R	Radial Distortion Sensitivity Coefficient	

LIST OF ABBREVIATIONS (Cont'd.)

<u>Symbols</u>		<u>Units</u>
L/D	Duct Length to Compressor Face Diameter Ratio	
L, L/H	Left Hand	
l, ℓ	Length	inches
M, M_0	Free-Stream Mach number	
P	Static Pressure	psia
PL	Plate	
PN	Point Number	
PWT	Propulsion Wind Tunnel	
PRMS, $\overline{P_{RMS}}$	L/H Inlet, Average Turbulence Index, TI2 Root-Mean-Square Average of Compressor Face, Hi-Response Pressures	
P_T, P_{T0}	Free-Stream Total Pressure, H_0	psia
P_{T2MAX}	Compressor Face Maximum Pressure	psia
P_{T2MIN}	Compressor Face Minimum Pressure	psia
P/P_T	Static Pressure Recovery	
$\overline{P_{T2}}/P_{T0}$	Inlet Average Total Pressure Recovery	
RECL	L/H Inlet, Average <u>Total</u> Pressure Recovery, P_{T2}/P_{T0} , $\overline{P_{T2}}/P_{T0}$, H_2/H_0	
RH, R/H	Right Hand	
R_N	Reynolds Number	
S	Supersonic	
SF	Supersonic Facility	
SIDE	Sideplate	

LIST OF ABBREVIATIONS (Cont'd.)

<u>Symbols</u>		<u>Units</u>
SL	Sea Level	
SPL	Splitter	
SS	Steady State	
STA, Sta	Station	inches
T	Transonic	
TF	Transonic Facility	
TI2	L/H Inlet, Average Turbulence Index, P_{RMS}/P_{t2}	
TP	Triple Flow	
VG	Vortex Generator	
WL	Water Line	inches
WPLFS W_C, W_{C2}	L/H Inlet, Full-Scale Total Corrected Airflow	lb/sec
X	Distance Measured from Inlet Lip Station	inches
α	Model Angle of Attack	degrees
$\beta, \beta_M, \beta_{Model}$	Model Angle of Sideslip	
δ	Boundary Layer Thickness	inches
θ	Angle	degrees
$\beta_{Flow\ R/H}$	Opposite Sign of β , Pertains to R/H Flow Field Data	
	Wing-Sweep Angle	degrees

1. INTRODUCTION

Advanced research inlet tests were conducted in the Arnold Engineering Development Center (AEDC) Propulsion Wind Tunnel (PWT) 16-foot supersonic (16S) tunnel in November 1975 and in the 16-foot transonic (16T) tunnel in March 1976. These tests, designated as SF-178 and TF-399, were conducted by the Fort Worth Division of General Dynamics for the Aeronautical Systems Division (ASD) of the Air Force.

The purpose of the tests was to evaluate inlet performance and engine/inlet compatibility of a simple, normal-shock inlet in a wing-body flow field to extend the data base for designing inlets.

In the Tailor-Mate program (Reference 1), blended wing-body configurations were investigated but a non-blended wing-body configuration, such as that employed on the F-111, was not investigated. Therefore, to extend the data base on inlet design, a research inlet program to investigate the integration of a simple, normal-shock inlet with a pure wing-body was contracted by the Air Force.

The research inlet program incorporated the General Electric F101-GE-100 engine for inlet sizing and engine/inlet compatibility. Thus, a new generation engine and a simple, normal-shock inlet configuration were integrated with a wing-body flow field for evaluation.

The design and test program was an advance research program. Consequently, a minimum of inlet configurations were investigated, and no concerted effort was made to correct flow-field or boundary-layer problems that became recognizable during the program. However, methods to correct boundary-layer spillage into the inlet and ways to minimize flow separation off of a duct bend have been identified to improve the overall performance and compatibility of the configurations investigated.

The full-scale length of the forebody on the research model was 73 inches longer (ahead of the inlet) than it was on F-111 models previously tested by General Dynamics. A long forebody, such as this, was in keeping with similar configurations investigated in the Tailor-Mate program. A check of the theoretical flat-plate boundary-layer height

showed the boundary layer would be thicker on this model. However, placement of the upper inboard corner of the inlet at the same location, Buttock Line (B.L.) 43, as that of the Triple Plow II (TP II) F-111 inlet, would put the inlet on the boundary-layer outer edge with high inlet performance expected. By keeping the same relative inlet-fuselage spacing, a baseline for comparing the inlet flow fields of the research model to the F-111 could be made.

Two questions that were addressed during the inlet design were what the maximum expected Mach number could be for a simple, open-nose, normal-shock-type inlet in a wing-body flow field and whether splitter plates would be necessary. A review of F-111 flight test data revealed that the local Mach number at the inlet's terminal (normal) shock reached a maximum of 1.6 (for free-stream Mach of 2.4-2.5) and that the terminal shock was impinging on the Triple Plow II fuselage boundary layer without a splitter plate. Thus, it was expected that the research model normal-shock inlet could operate satisfactorily up to Mach 1.7 or 1.8. But, it was felt that some splitter plate would be necessary to prevent the fuselage boundary layer from spilling into the inlet as it was being plowed off. A splitter plate of this type is not necessary on the Triple Plow II inlet because TP II has a double-cone-spike pressure field to control the boundary layer behind the spike and not allow it to enter the inlet.

The Tailor-Mate (Reference 1) model flow-plug, beam, and compressor-face hi-response instrumentation was selected for the research-model inlet tests. The ratio of the model compressor-face diameter to the diameter of the F101 engine compressor face was 1/5.2.

The inlet-configuration variables that were evaluated during the tests were:

1. The length of the fuselage ahead of the inlet.
(The research-model fuselage extended 73 inches further ahead of the inlet than it does on the F-111.)
2. The standoff distance of the inlet from the side of the fuselage.
3. The length and steepness of the fuselage and glove boundary-layer plows.

4. The length and shape of the fuselage splitter plates.
5. The size of the throat (throat design Mach number) and capture area of the inlet.
6. The duct vortex generators and duct blowing.

Flow field and configuration evaluations had to be done at Mach 1.6 in 16S because a scheduling priority moved the 16T tests to follow the 16S tests. Consequently, the 16S tests were conducted first even though this was not the desired testing sequence. The basic configuration was then tested at Mach 1.6 to 2.0 for performance documentation.

In 16T, the primary evaluations and flow-field assessment was done at Mach 0.85. Additional evaluations were made from Mach 1.2 to Mach 1.5. Full documentation of the basic and an alternate inlet configuration was made from Mach 0.55 to 1.5. Representative combinations of angles of attack and sideslip were tested over the full Mach range.

2. SUMMARY OF RESULTS

The overall results of the research-model inlet tests determined that a normal-shock inlet can operate while in the influence of a wing-body flow field. The Basic Long-Plow and Splitter-Plate Inlet, located at either B.L. 43.82 or B.L. 45.64, has acceptable inlet pressure recovery. Engine/inlet compatibility also was found to be acceptable throughout most of the Mach-altitude envelope where it was analyzed, the exception being at Mach 1.2 at the top of the Mach-altitude envelope selected for the compatibility analysis. In those speed regimes where compatibility is marginal, it was the result of fuselage boundary-layer spillage into the inlet or the result of flow separation off the outboard bend on the outboard duct wall. However, the analysis of the test results shows that correction of the duct-bend problem will greatly improve engine/inlet compatibility throughout the Mach range. As tested, the outboard inlet location has a larger compatibility envelope (at the top of the flight envelope) for all Mach numbers.

Specifically, the test results show that:

1. The fuselage boundary-layer of the research model at Fuselage Station 390 is similar to but thicker than the boundary layer measured on the F-111 at the same fuselage station.
2. The measured boundary-layer thickness at F.S. 390 on the research model is thicker than that calculated by flat-plate theory below Mach 1.6. (The greatest difference occurs at Mach 1.2 where the model boundary layer was 0.42 inches thicker (full scale) than theoretical. Corresponding theoretical flat-plate and measured thicknesses for the F-111 agreed closely.)
3. Spillage of the fuselage boundary-layer over the fuselage side splitter-plate into the inlet degraded inlet pressure recovery and increased inlet distortion at all Mach conditions. This phenomena was initially analyzed as a shock/boundary-layer interaction problem from the 16S test results. But since the subsonic tests showed similar inlet throat-flow patterns, it is now concluded that

spillage preceded and contributed to any shock/boundary-layer interaction that occurred supersonically.

4. Increasing the standoff distance by moving the inlet outboard to B.L. 45.64 made some improvement in inlet pressure recovery and engine/inlet compatibility. Increasing the standoff distance further resulted in a loss in inlet pressure recovery at Mach 1.6. The most outboard position was not tested in 16T.
5. Revising the splitter-plate shape and size improved flow conditions at the throat, but these improvements were not realized in the compressor-face distortion patterns.
6. An outboard bend in the inlet duct caused some duct separation. This resulted in a loss in pressure recovery and an increase in distortion in the outboard portion of the compressor face. But it was demonstrated during the tests that this flow defect can be corrected with a minimum duct vortex generator pattern or with duct blowing.
7. Inlet performance (pressure recovery) is acceptable at all Mach numbers for the Basic Long-Flow/Splitter-Plate Inlet even though it was slightly below the predicted levels below Mach 1.5 and at Mach 2.0.
8. The flow separation off the back of the bend in the inlet duct creates a low-energy region of air on the outboard side of the compressor face. This caused a high level of steady-state distortion which completely biased the compatibility assessment. The low-energy region can be minimized by correcting the duct separation as stated in Item 6. This correction would reduce the steady-state distortion without a significant increase in turbulence. The predicted improvement in compatibility is shown in Figure 1 at $\alpha = 5^\circ$, $\beta = 0^\circ$ for design airflows across the Mach range. Notice that the dynamic distortion level for an "improved" duct configuration is less than the steady-state distortion level for the duct tested. Also, from Mach 0.85 to 1.6 the predicted dynamic distortion

For altitudes along upper boundary of Mach-altitude envelope selected for engine/inlet compatibility analysis.

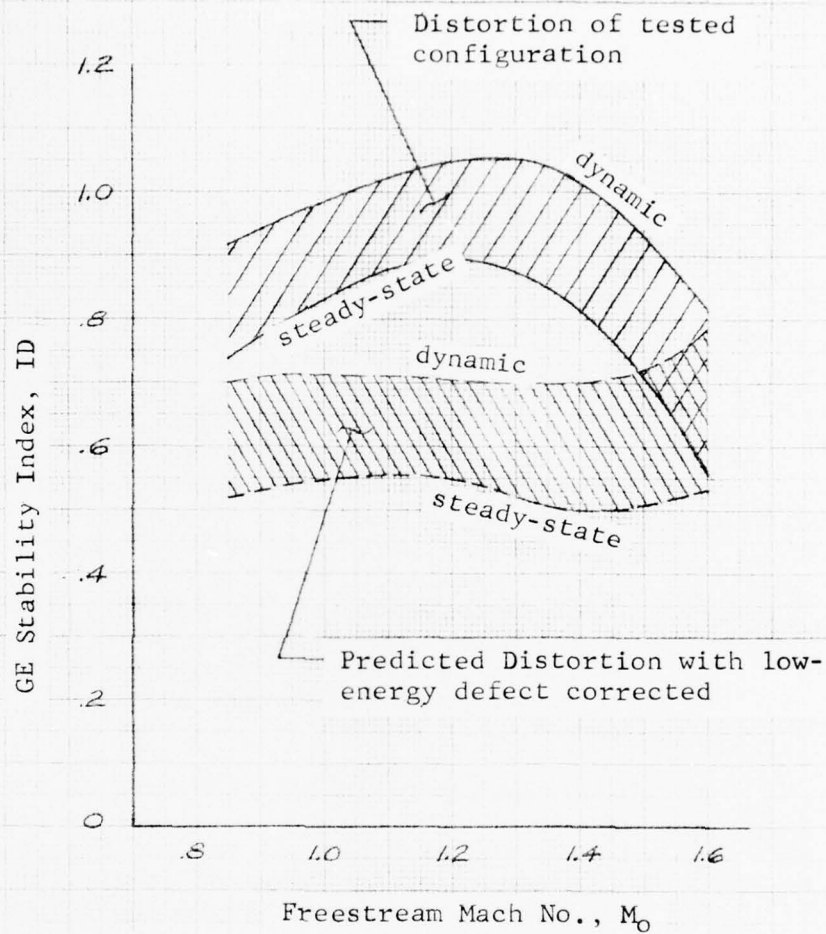


Figure 1. Effect of steady-state-distortion pattern on dynamic-distortion level of the Basic Long-Plow/Splitter Plate Inlet at B.L. 43.82 at design airflow for $\alpha = 5^\circ$ and $\beta = 0^\circ$

level is less than an ID of 0.8, which is well within the acceptable limit (< 1.0) for surge-free operation. The details of this prediction with supporting data are discussed in Subsection 4.4.3.

9. The duct noise or turbulence is low up to Mach 1.6 and increases rapidly to a high level above Mach 1.8. The low overall turbulence level is attributed to the long duct length ($L/D = 5.6$) and the fixed-geometry, normal-shock inlet.

A comparison of the predicted inlet pressure recovery with the model-test inlet-pressure recovery for the Basic Long-Plow/Splitter-Plate Inlet at B.L. 43.82 is shown in Figure 2. These data are for 5° angle of attack and 0° sideslip. Noted for reference on the curves are the acceleration path airflows.

Engine/inlet compatibility envelopes at Mach 0.85 and Mach 1.4 are given in Figure 3 for the Basic Inlet at B.L. 45.64 with Vortex Generator Pattern No. 3. These envelopes are indicative of those to be expected after the duct-bend problem (Item 6) is corrected. Also, at 5° angle of attack and 0° sideslip, these envelopes substantiate the predictions contained in Figure 1.

Sym	Part	M_o	Sym	Part	M_o
○	20	1.6	▽	363	.65
□	155	1.7	▷	276	.85
△	123	1.8	△	337	1.2
◇	144	1.9	◻	320	1.4
◻	141	2.0	◇	305	1.5

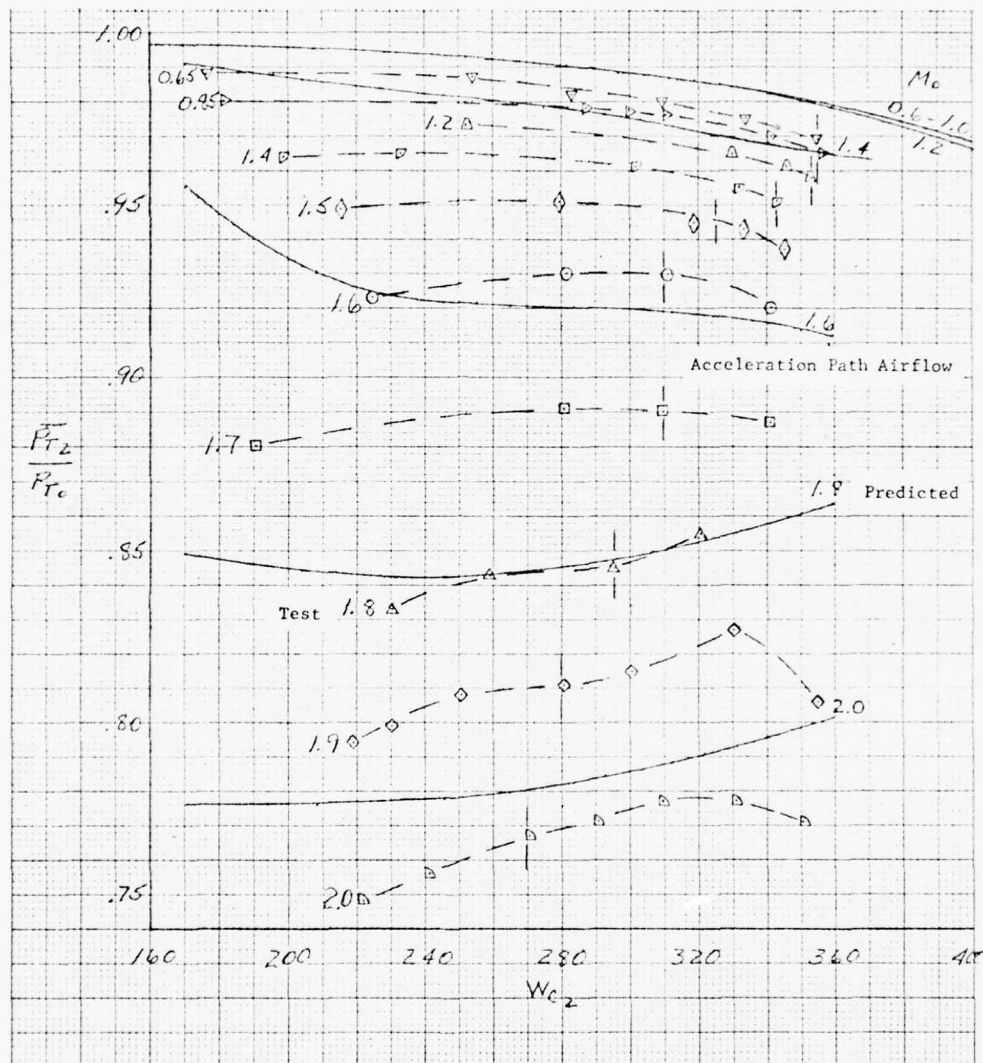
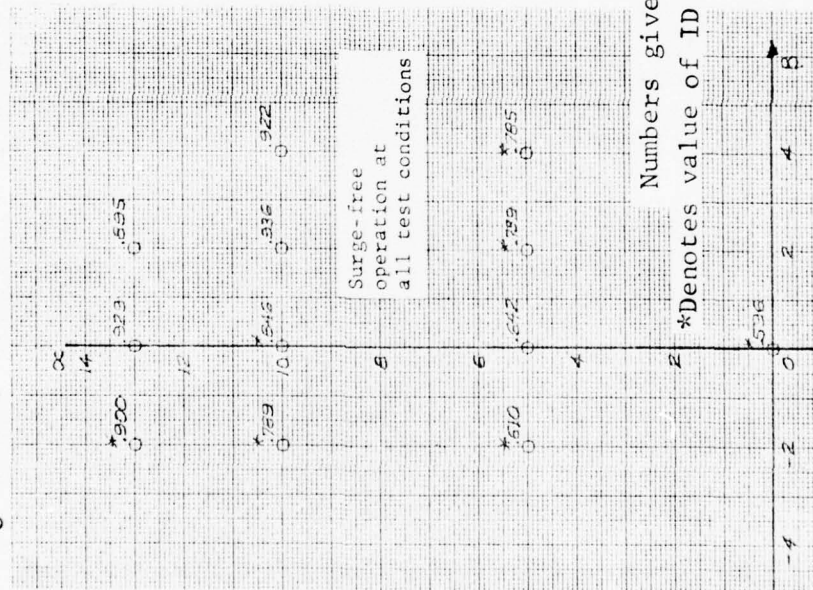


Figure 2. Predicted versus model test inlet pressure recovery of the Basic Long-Plow/Splitter-Plate Inlet @ B.L. 43.82, $A_i = 1214 \text{ in.}^2$, $\alpha = 5^\circ$, and $\beta = 0^\circ$.

$M_0 = 0.85$, altitude = 35,500 ft



$M_0 = 1.4$, altitude = 48,000 ft

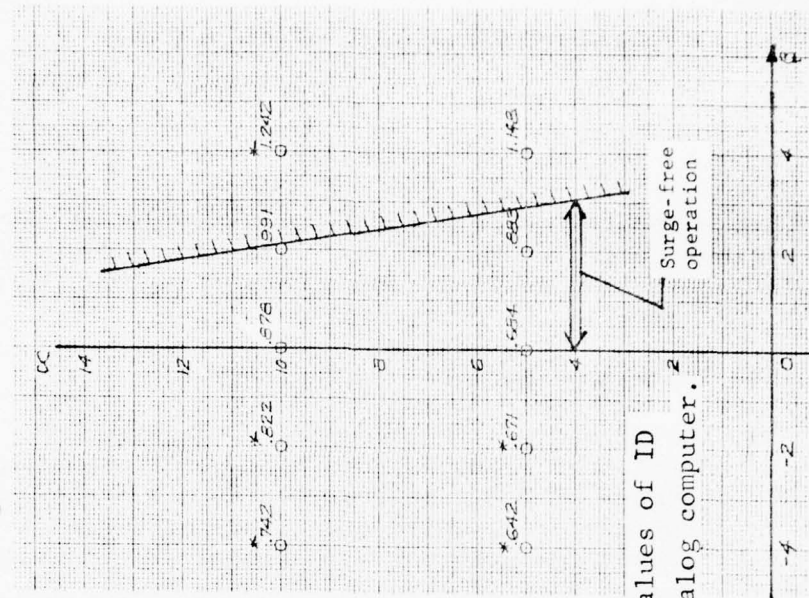


Figure 3. Compatibility envelopes of the Basic Long-Plow/Splitter-Plate Inlet at B.L. 45.64 with VG Pattern 3.

3. DESCRIPTION OF TEST PROGRAM AND CONFIGURATIONS

Presented in Tables 1 and 2 are summaries of the configurations tested in PWT 16S and 16T, respectively. In the tables are the test part numbers that pertain to a specific configuration and test Mach number.

The inlet-configuration variables were:

1. Inlet capture area and throat Mach number. The left-hand inlet was designed for a throat Mach number of 0.8 that resulted in a 1214-sq-in. capture area, while the right-hand inlet was designed for a throat-Mach number of 0.7 that resulted in a 1281-sq-in. capture area. The duct area curve for the Mach 0.8 throat design is shown in Figure 4. The duct area curve for the Mach 0.7 throat design is similar. Both had an $L/D = 5.6$, based on the throat to compressor-face duct length and the compressor-face diameter. The area distribution per unit length of both ducts was made the same as it is on the YF-16 inlet because that inlet duct has low turbulence. A plan view of the research-model inlet duct is shown in Figure 5.
2. Length of splitter plate and plow. A Basic Long Plow and Splitter Plate was designed and tested with both inlets (L/H and R/H) as the primary inlet configuration. A Basic Short Plow and Splitter Plate was designed for the 0.8 Mach L/H inlet as an alternate inlet configuration. It was tested at Mach 1.6 and 0.5 in 16S. The Basic Long Splitter-Plate Inlet configuration is shown in Figure 6 and the Short Splitter-Plate Inlet is shown relative to the long in Figure 7.
3. Inlet standoff distance from the fuselage. The upper inboard corner of the inlet was located at B.L. 43. To compensate for growth in the fuselage boundary layer on the model at the model test Reynolds number, the inlets were moved outboard to B.L. 43.82. In addition to B.L. 43.82, the

Table 1

16S

TEST CONFIGURATION SUMMARY

Test Shift	L/H Inlet	M _O	R/H Inlet	Part Nos.
1a.	· Long Plows/Splitters @ B/L 43.82	1.6	· Long Plows/Splitters @ B/L 45.64 · Fuselage Rakes · Splitter Rakes · Throat Rakes	12-30
1b.	· Long Plows/Splitters @ B/L 47.45	1.6	· Fuselage Rakes Removed	32-48
2a.	· Short Plows/Splitters @ B/L 43.82	1.6	· Splitter Rakes Removed	54-78
2b.	· Short Plows/Splitters @ B/L 45.64	1.6 0.5	· Throat Rakes Removed - Clean inlet @ 45.64	81-102 103-105
3.	· Long Plows/Splitters @ B/L 43.82	1.8 2.0* 1.9* 1.7 0.5	· Long Plows/Splitters @ B/L 43.82	114-136 138-141 142-145 146-165 167-172

*Just a few points. Inlets had high noise.

Table 2

SUMMARY
PWT 16T TEST PROGRAM

PN	M _O	INLET CONFIGURATION		AEDC CONFIG CODE		DATE
		L/H	R/H	L/H	R/H	
207-226	0.85	Basic at 43.82, VG Pat #1	Alt Sp1 #1 at B/L 43.82, Throat Rakes	3	3	3-19-76
240-256	0.85	Alt Sp1 #2 at B/L 43.82	Alt Sp1 #2 at B/L 43.82, Throat Rakes	2	2	3-22-76
262-271	1.5	"	"	2	2	3-22-76
276-284	0.85	Basic at B/L 43.82	Basic at B/L 43.82, Throat Rakes	1	1	3-22-76
291-297	0.85	Basic at B/L 43.82	Basic at B/L 43.82, Throat Rakes	1	1	3-23-76
300-315	1.5	"	"	"	"	"
317-330	1.4	"	"	"	"	"
333-347	1.2	"	"	"	"	"
349-359	0.75	"	"	"	"	"
362-366	0.65	"	"	"	"	"
367-371	0.55	"	"	"	"	"
380-397	0.85	Basic at B/L 45.64 with VG Pat. No. 2	Basic at B/L 43.82 Fuse. FF Rakes at Station 390, Throat Rakes	4	4	3-24-76
400-414	1.2	"	"	"	"	"
415-430	1.4	"	"	"	"	"

Table 2
SUMMARY
PWT 16T TEST PROGRAM (continued)

PN	M ₀	INLET CONFIGURATION		AEDC CONFIG CODE		DATE
		L/H	R/H	L/H	R/H	
435-450	0.85	Basic at B/L 45.64, No VG's	Alt Spl #1 at B/L 43.82 Fuse FF Rakes at Station 390, Throat Rakes	5	5	3-24-76
451-464	1.2	"	"	"	"	"
465-481	1.4	"	"	"	"	"
487-512	0.85	Basic at B/L 45.64, VG Pat. No. 3	Basic at B/L 43.82 + Duct Blowing Jets	6	6	3-25-76
513-523	1.4	"	"	"	"	"
527-528	0.55	Basic at B/L 45.64, No VG's	Basic at B/L 43.82, Spl. Pl. Tip Removed, Duct Jets	5	7	3-25-76
529-530	0.65	"	"	"	"	"
531-532	0.75	"	"	"	"	"
533-540	0.85	"	"	"	"	"
541-557	1.5	"	"	"	"	"

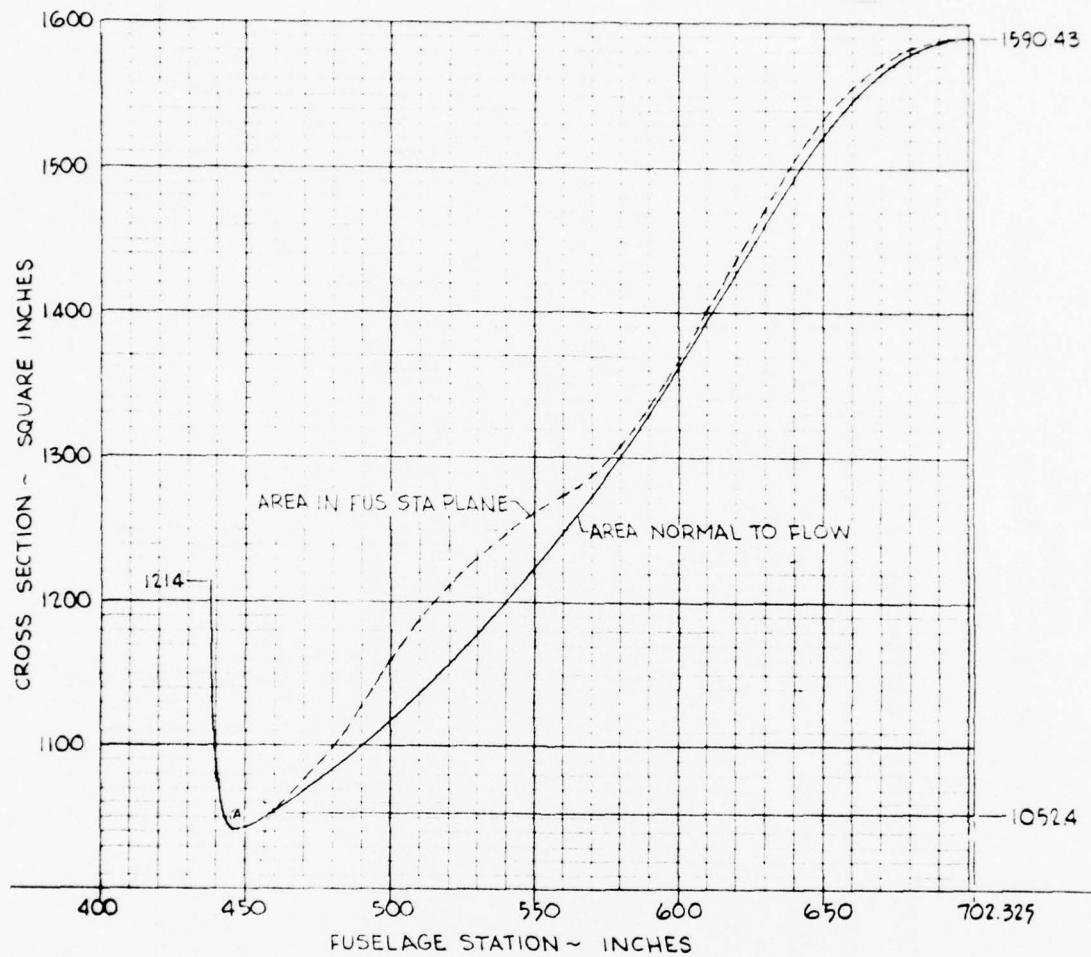


Figure 4. Duct area curve (0.8 Mach throat).

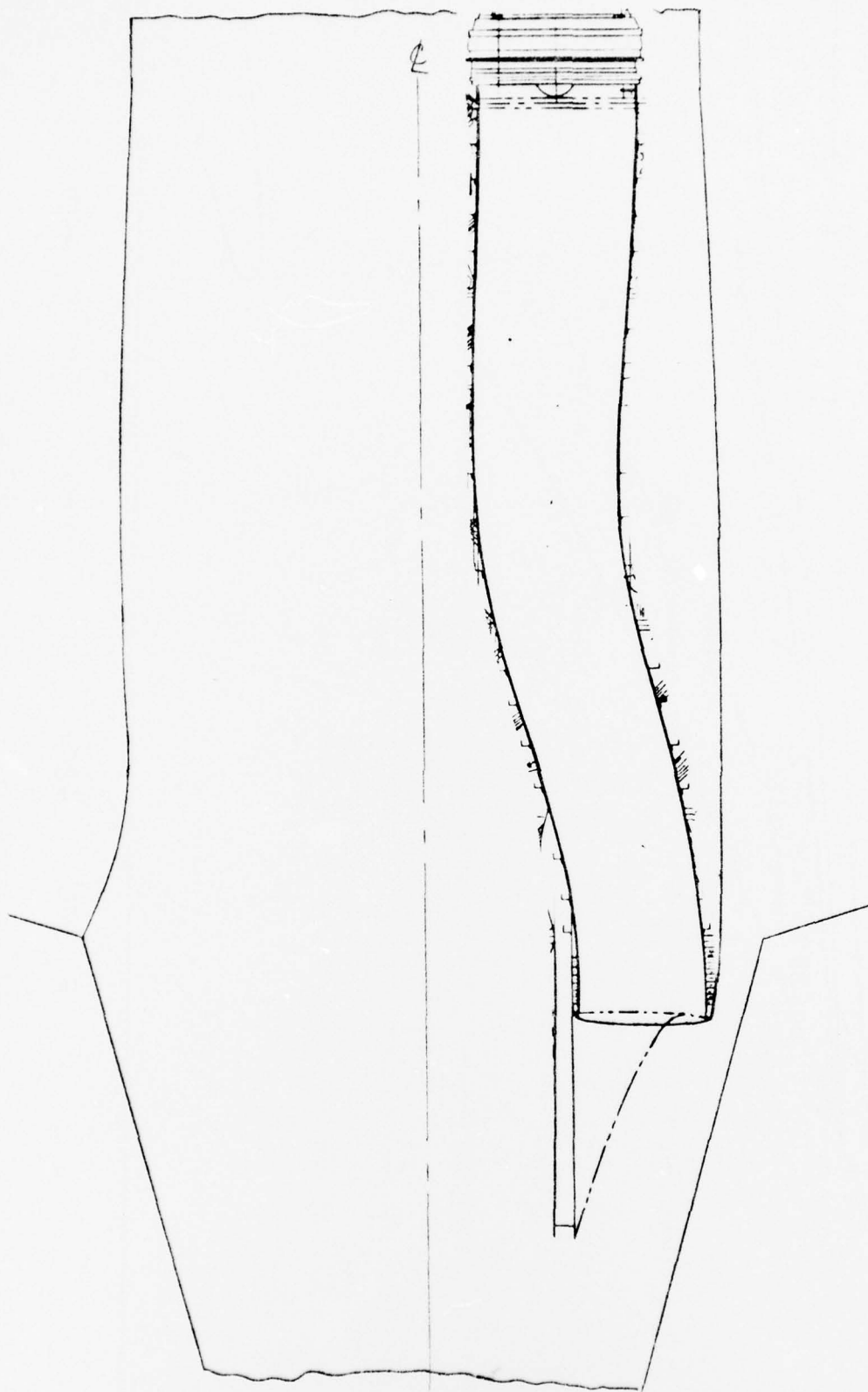


Figure 5. Plan view of the research model inlet duct.

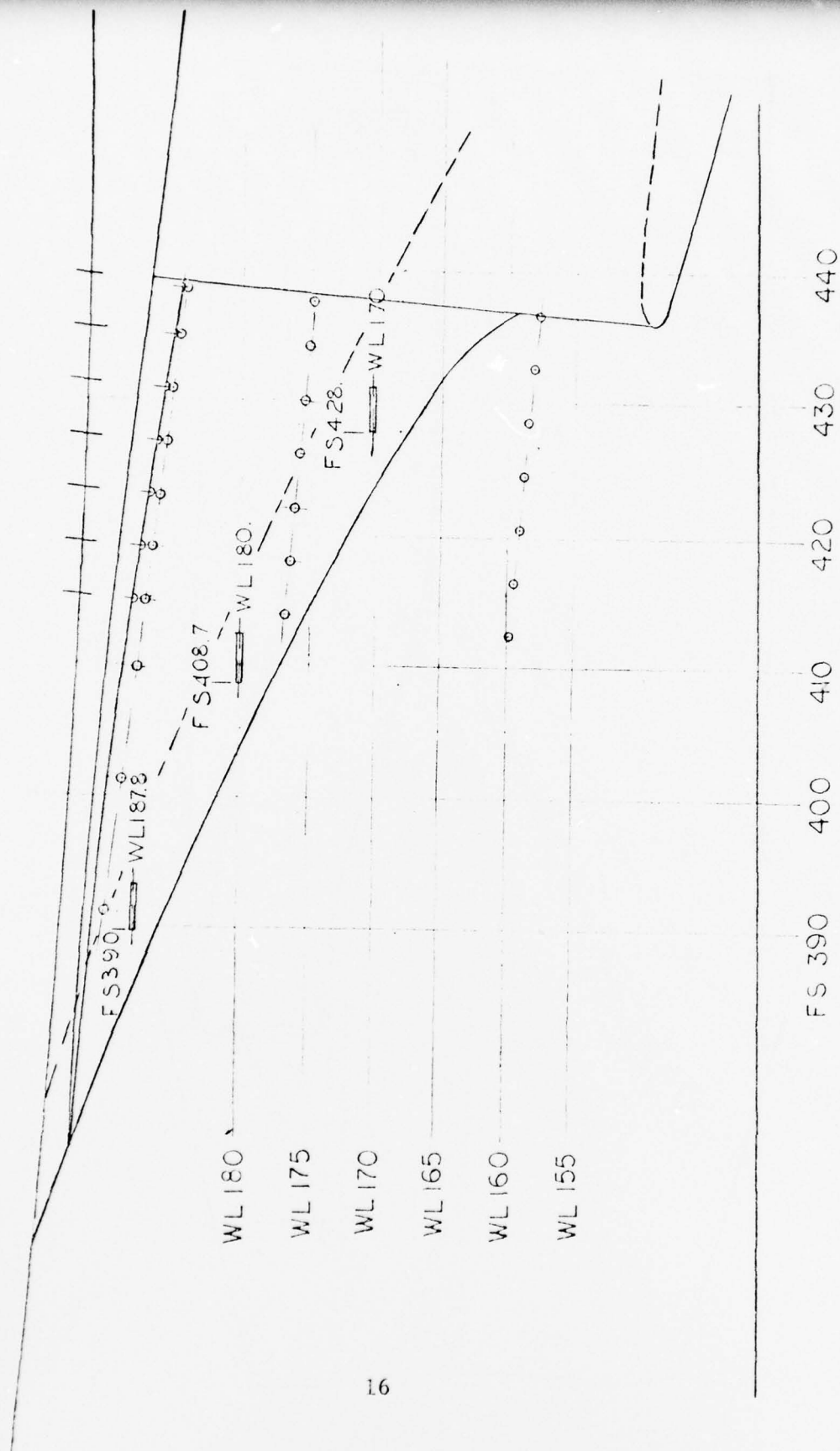


Figure 6. Basic Long-flow/Splitter-Plate Inlet.

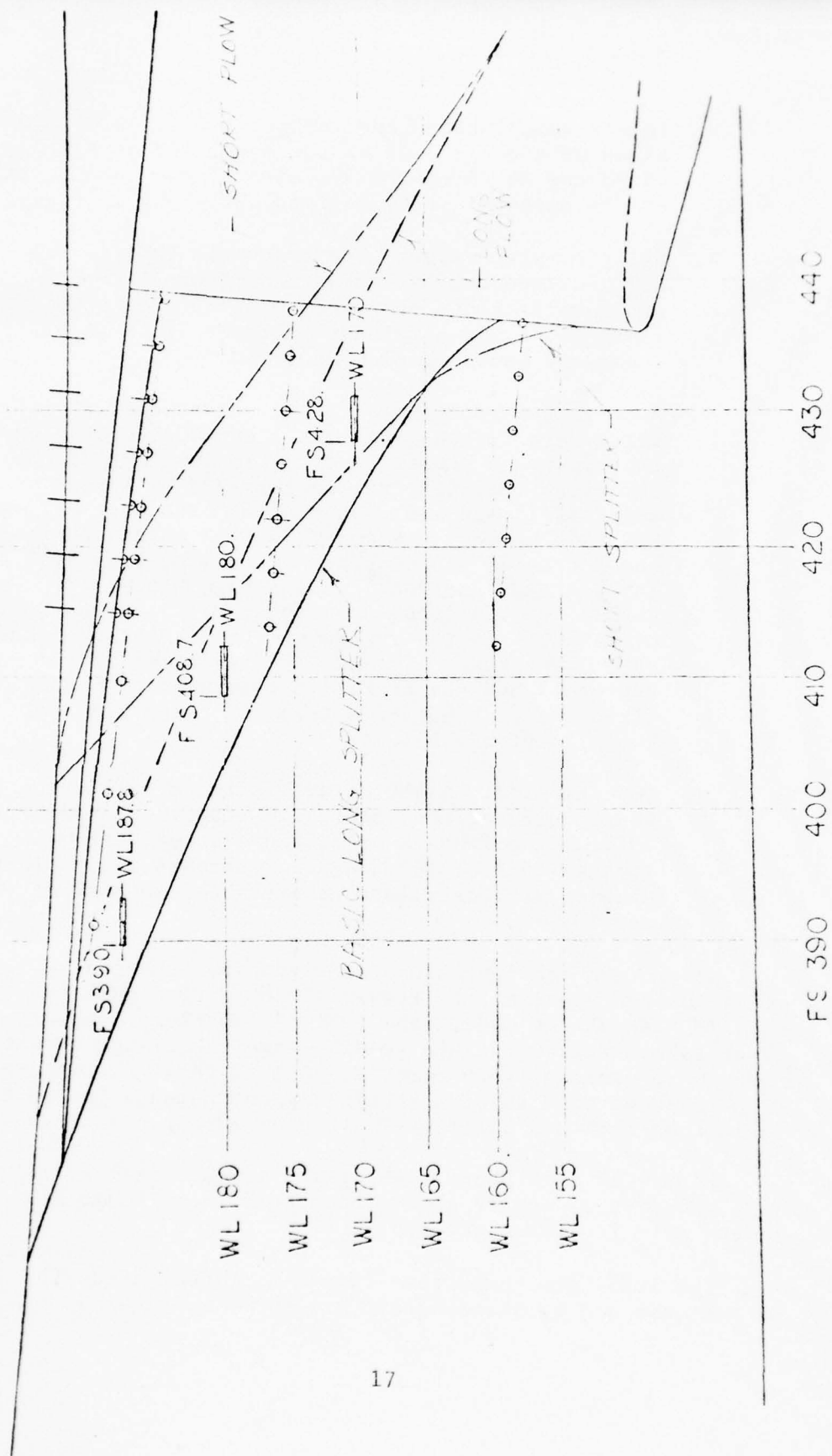


Figure 7. Basic Long and Short Splitter-Plate Inlet configurations.

inlets were located and tested at B.L. 45.64 and 47.45 on the L/H side of the model and at B.L. 43.82 and 45.64 on the R/H side of the model. Each of the buttock line locations are shown in Figure 8.

4. Splitter-plate size. The transonic test in PWT 16T included the Basic Long Splitter Plate and two modifications referred to as Alternate Splitter Plate No. 1 and Alternate Splitter Plate No. 2. These are shown in Figures 9 and 10.
5. Duct vortex generators (VGs). Three duct VG patterns were tested. Pattern 1 had VGs located on the upper and inboard duct walls just aft of the throat at F.S. 455 (region surveyed by Throat Rakes 12-13 and 1-6), on the outboard duct wall at F.S. 540 between 45° and 135° , and across the top and bottom of the duct at F.S. 560 between 315° and 45° and 135° and 225° , as shown in Figure 11. Pattern 2 had VGs located on the throat inboard wall at F.S. 455 in the region of Throat Rakes 2-5 and at F.S. 540 between 45° and 135° , as shown in Figure 12. Pattern 3 had VGs at F.S. 540 between $67\frac{1}{2}^{\circ}$ and $112\frac{1}{2}^{\circ}$ and at F.S. 560 between 135° and 225° , as shown in Figure 13.
6. Duct blowing. A set of aft-facing duct-blowing jets was located at Cowl Station 52 (approximately F.S. 492) on the inboard wall, and a second set was located at F.S. 592.8 on the outboard wall. These blowing jet installations are shown in Figures 14 and 15.

Other test configurations resulted from changes in model instrumentation. As flow-field data were gathered on the R/H side of the model, the F.S. 390 fuselage boundary-layer rakes, splitter-plate leading-edge rakes, and throat rakes were progressively removed. All of this instrumentation is shown with the L/H static-tap instrumentation on the Basic Long-Flow and Splitter-Plate configuration in Figure 16.

Figure 17 is a photograph of the model installed in 16T. Figures 18 and 19 show closeups of the L/H and R/H inlets with instrumentation.

The left-hand compressor face was instrumented with 40 hi-response and 40 steady-state pressure transducers,

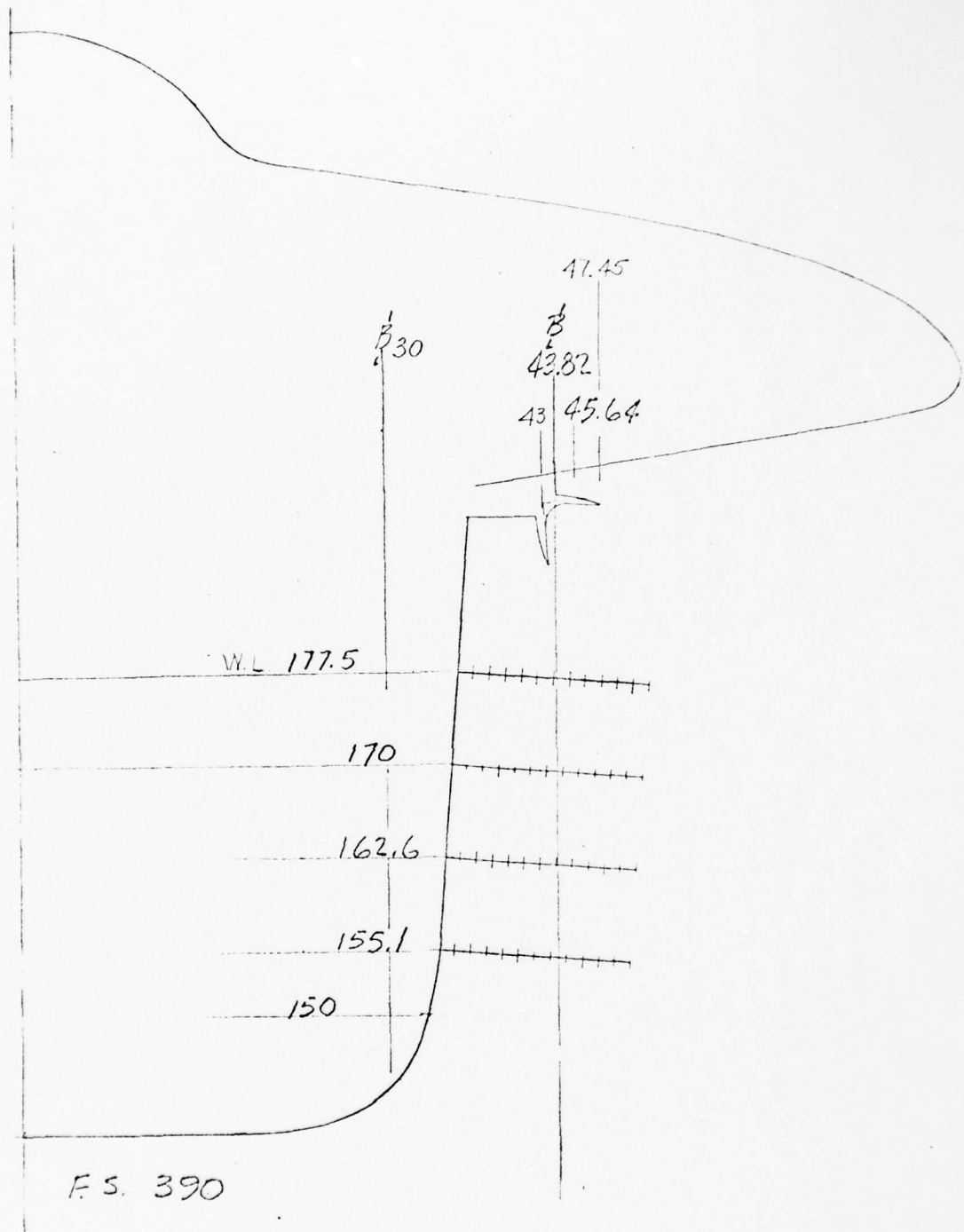


Figure 8. Inlet buttock line locations.

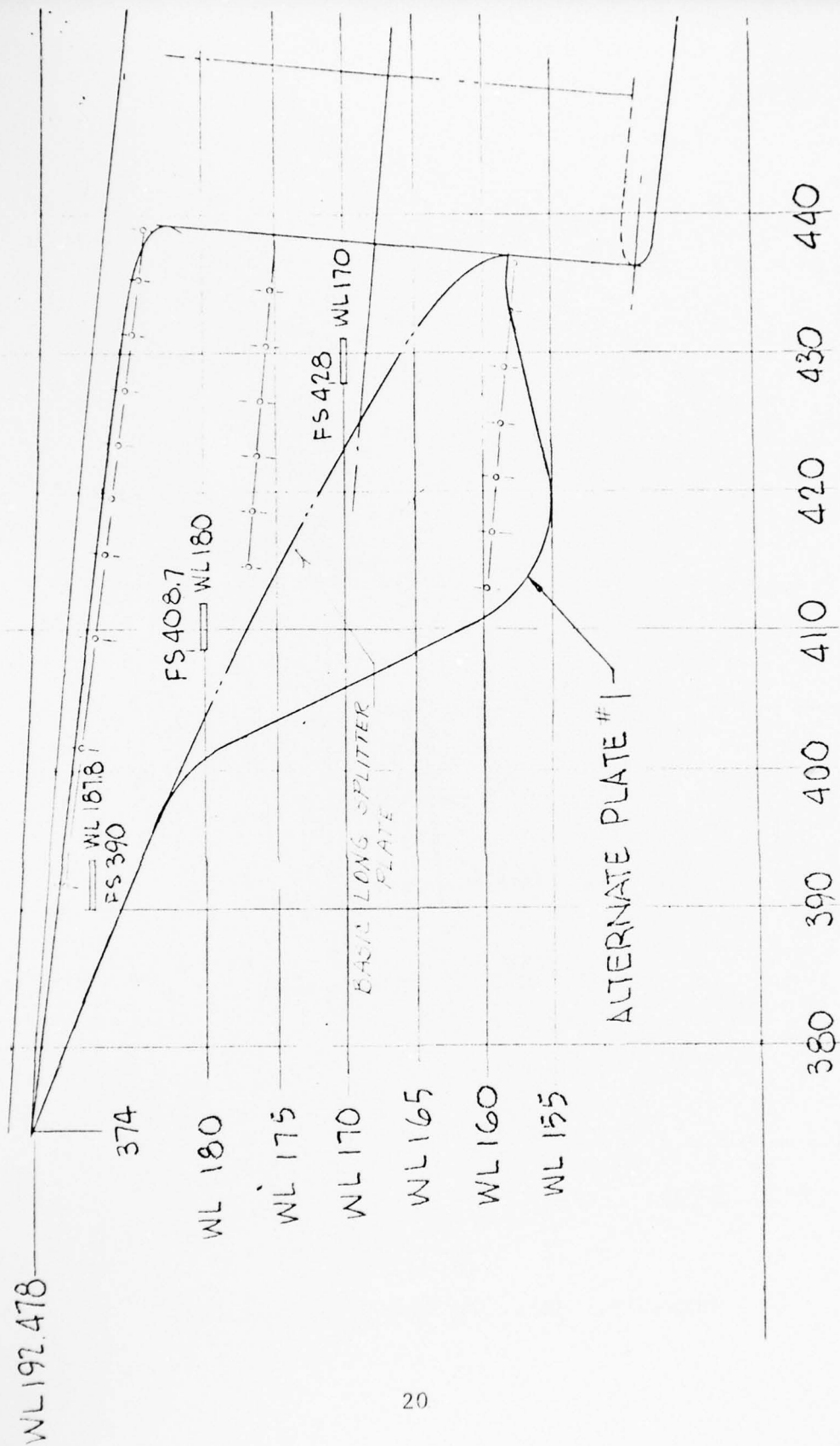


Figure 9. Alternate Splitter Plate No. 1.

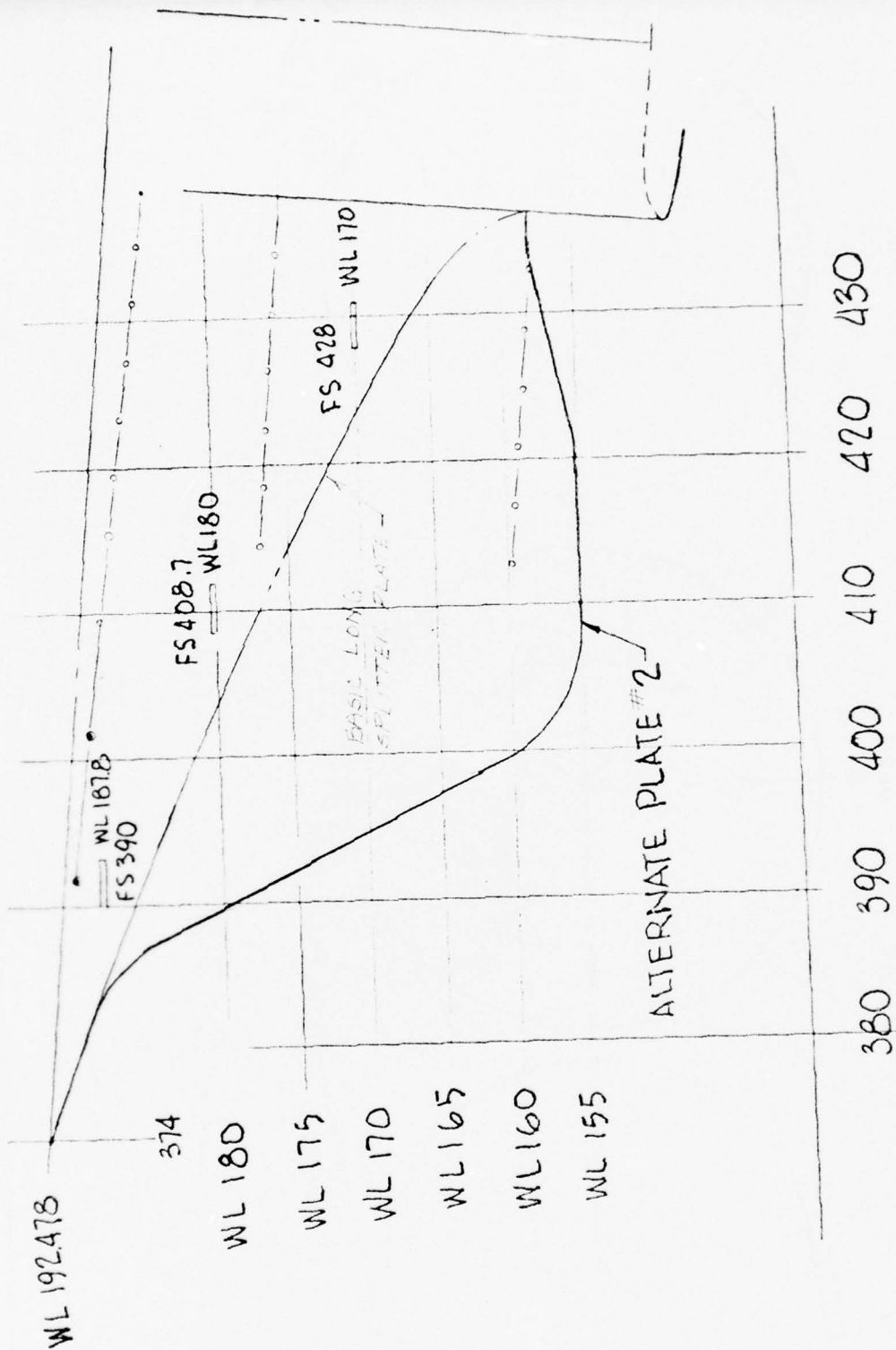


Figure 10. Alternate Splitter Plate No. 2.

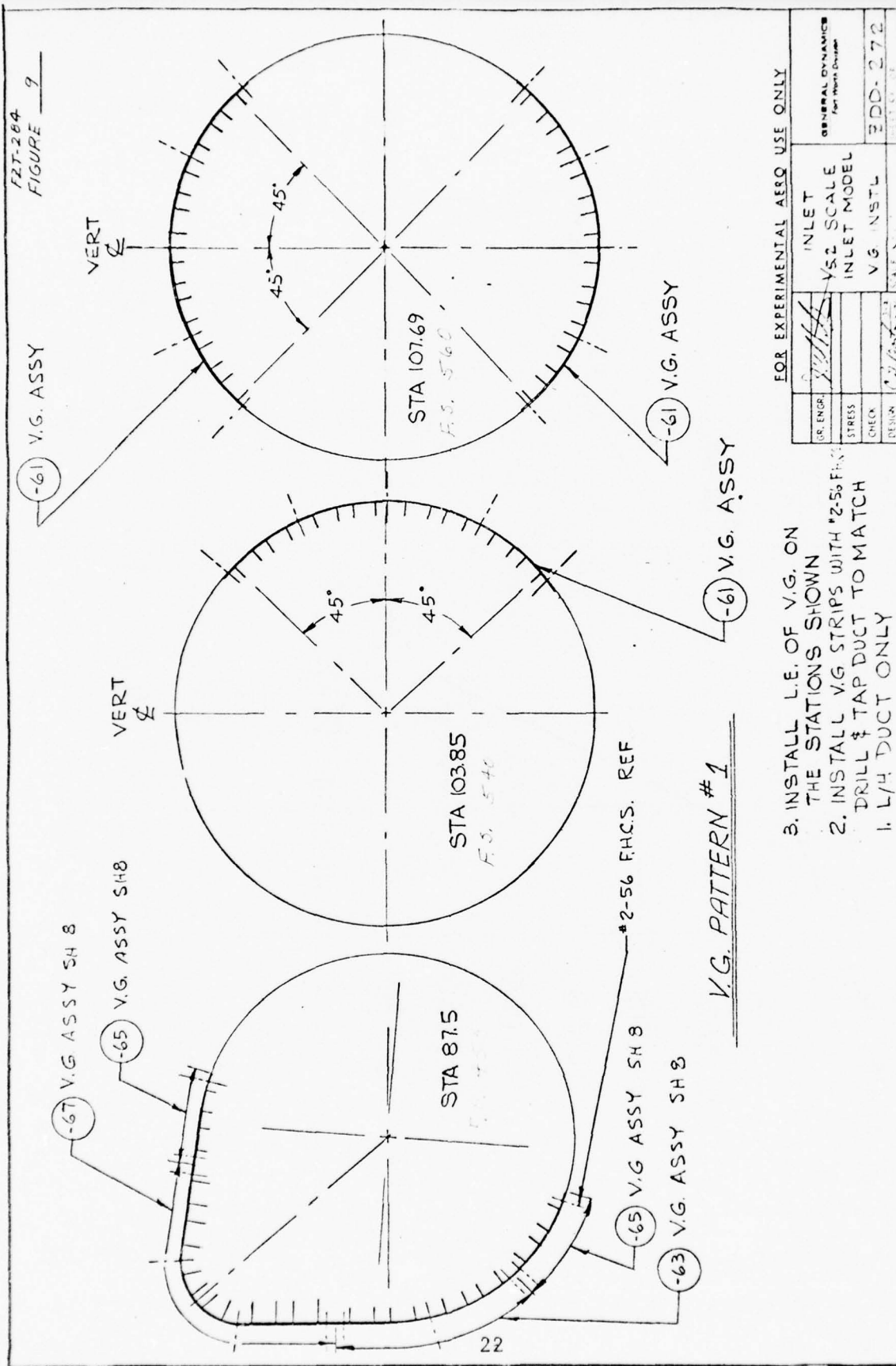
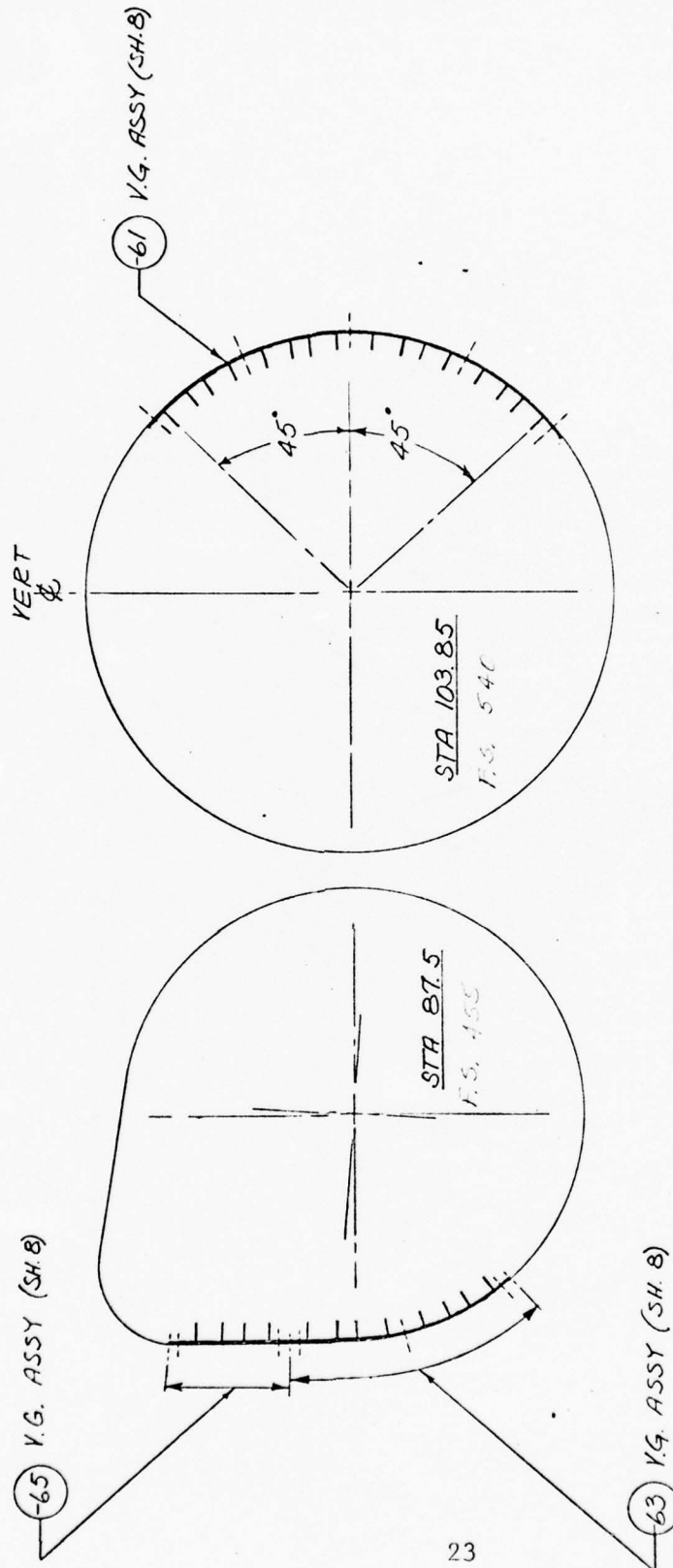


Figure 11. Inlet-duct Vortex Generator Pattern No. 1.

F27-284

FIGURE 10

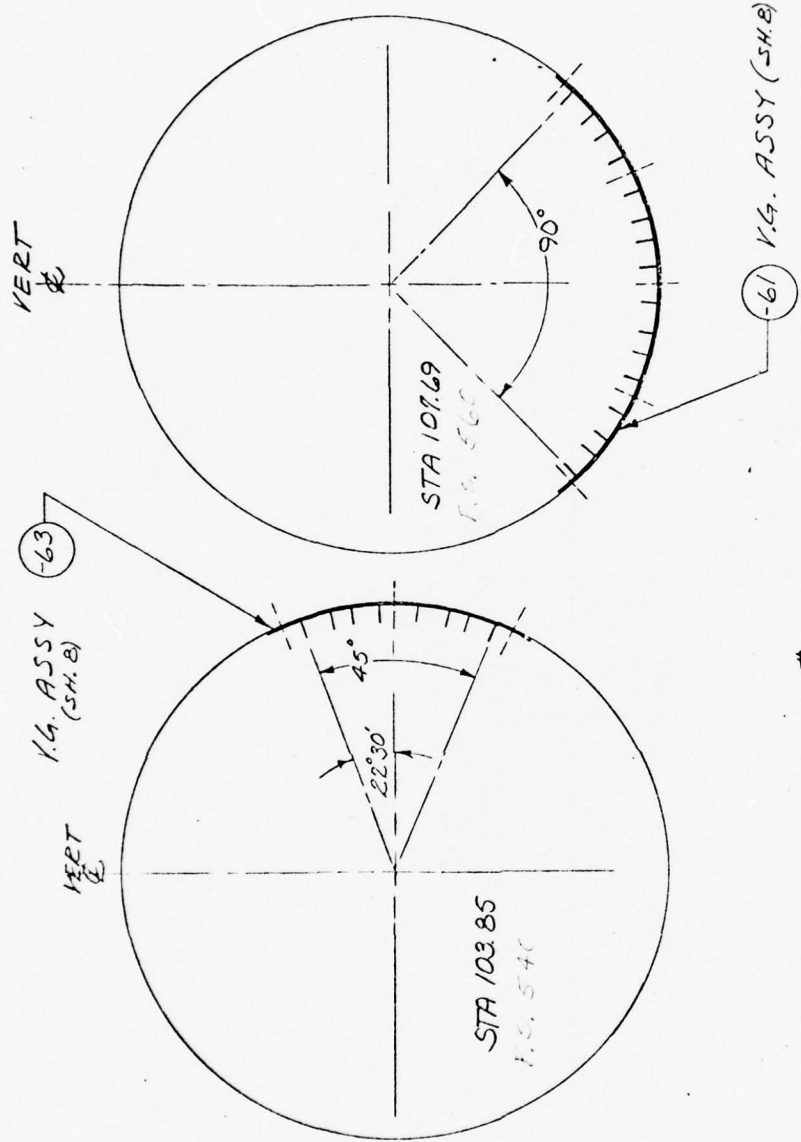


V.G. PATTERN # 2

FOR EXPERIMENTAL AERO USE ONLY

DR. ENGR.	INLET	GENERAL DYNAMICS
STRESS	1/52 SCALE	Port Mach Division
CHECK	INLET MODEL	
DESIGN	V.G. PAT # 2	FDD-272
	SCALE 20:1	REVISED

Figure 12. Inlet-duct Vortex Generator Pattern No. 2.



V.G. PATTERN # 3

FOR EXPERIMENTAL AERO USE ONLY

GR. ENGR.	INLET	GENERAL DYNAMICS Part No. 10-1000
STRESS	1/2 SCALE	
CHECKED BY	INLET MODEL	
DESIGN	V.G. PATT # 3	FDD-272

Figure 13. Inlet-duct Vortex Generator Pattern No. 3.

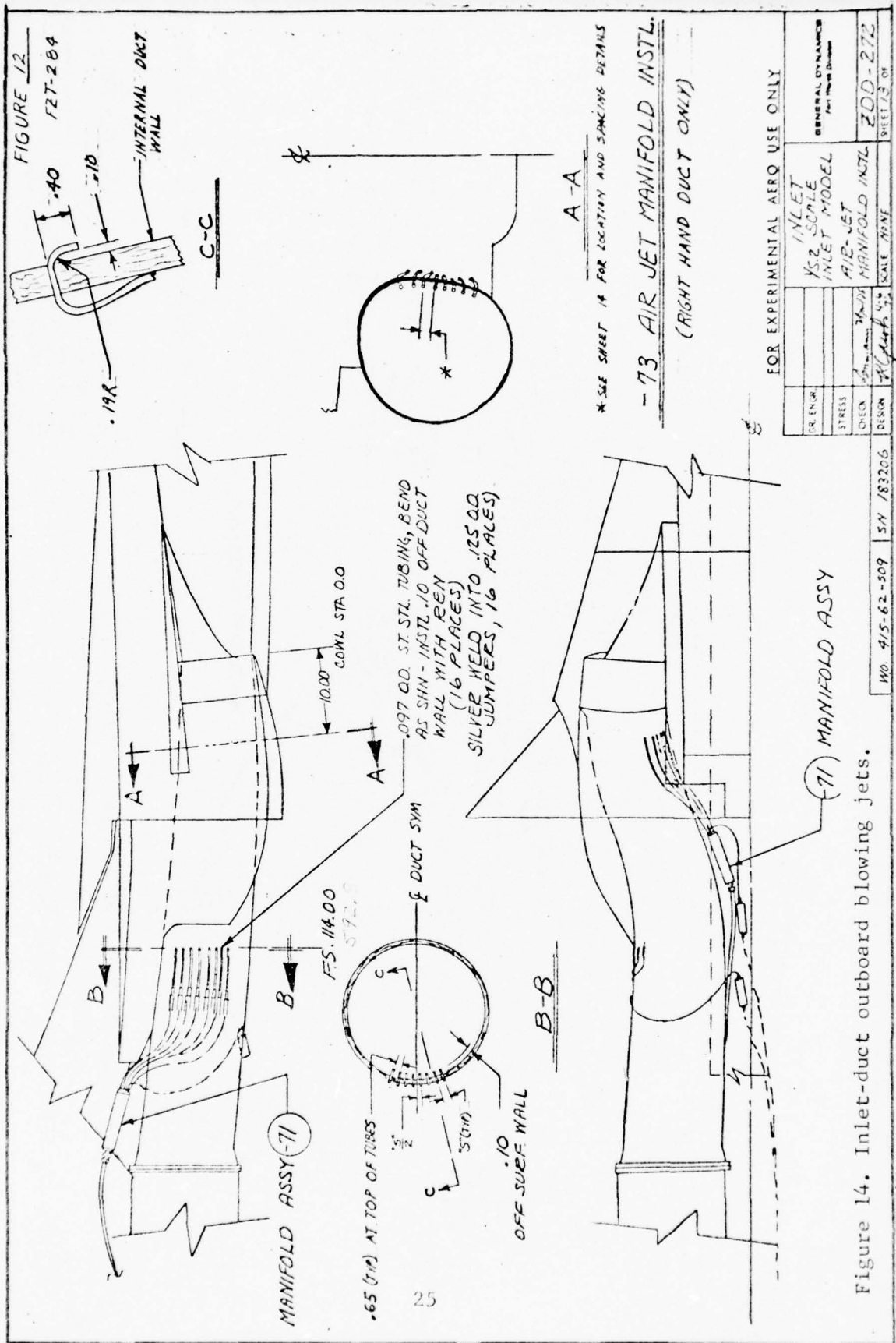
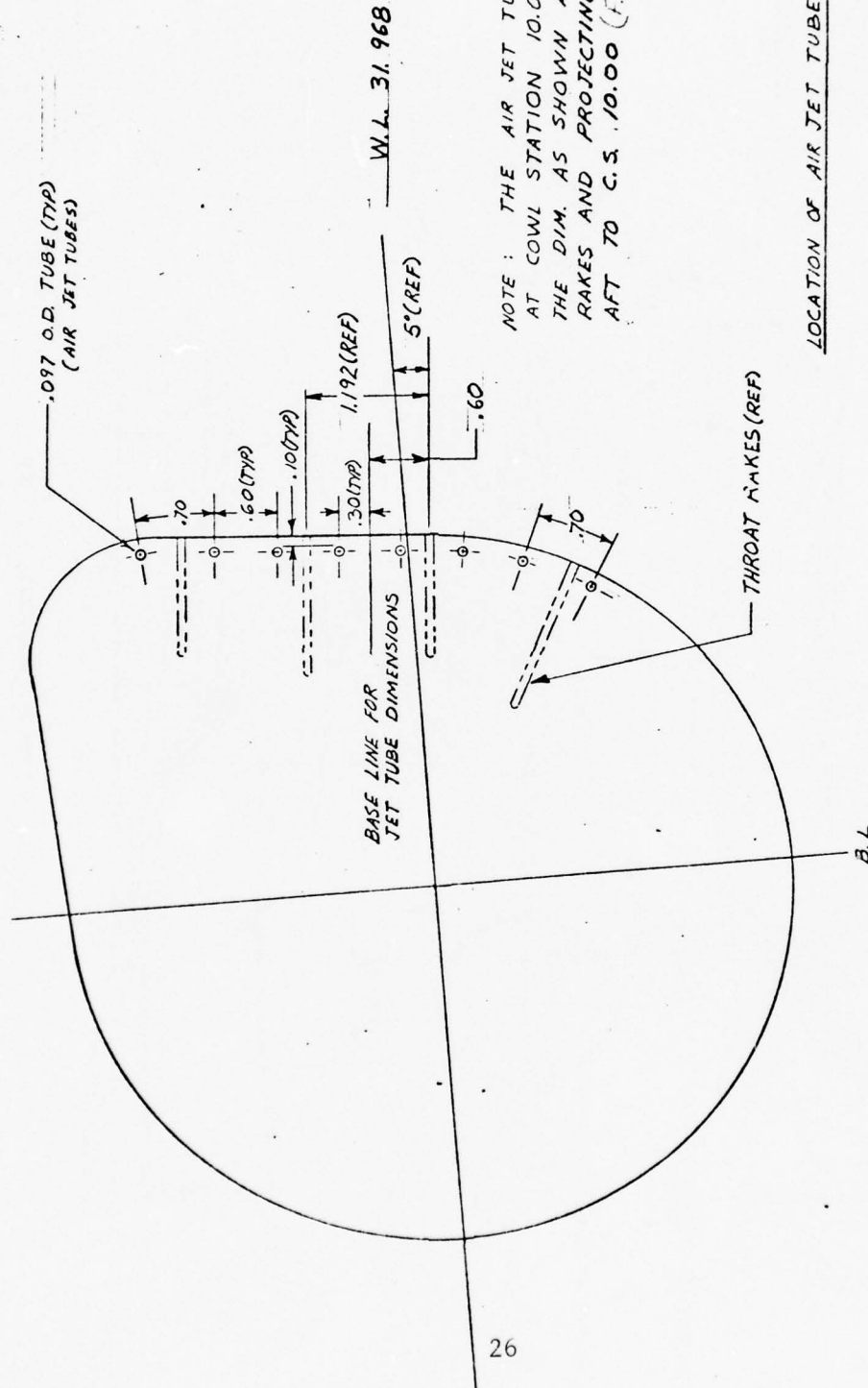


Figure 14. Inlet-duct outboard blowing jets.

FIGURE 13
F2T-284



NOTE: THE AIR JET TUBES ARE LOCATED AT COWL STATION 10.00 BY LOCATING THE DIM. AS SHOWN AT THE THROAT RAKES AND PROJECTING THESE DIM. AFT TO C.S. 10.00 (F.S. 52.0)

LOCATION OF AIR JET TUBES AT C.S. 10.00

RIGHT HAND COWL THROAT SECTION
(TRUE VIEW LOOKING AFT)

Figure 15. Inlet-duct inbound blowing jets.

FOR EXPERIMENTAL AERO USE ONLY

DESIGN	1/4" MANV 741	SCALE	1/4" MANV 741
CHECK			
STRESS			
DR. ENGR.			
INLET 1/2" SCALE INLET MODEL AIR JET TUBES AT C.S. 10.00			
GENERAL DYNAMICS			
Part Name Division			
ZDD-272			SHEET 14 OF

W.O. 415-62-509 S.N. 183206

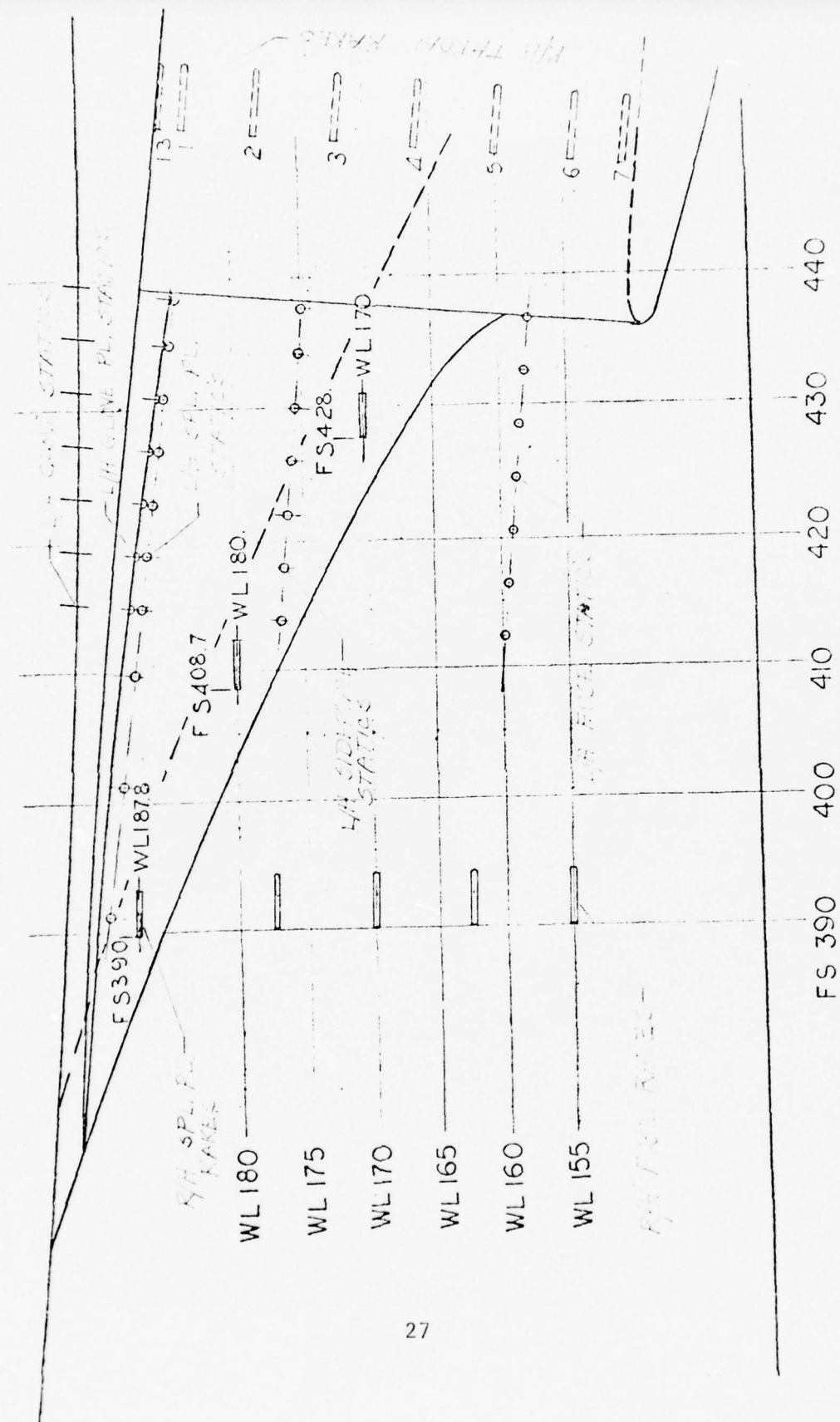


Figure 16. Inlet instrumentation.

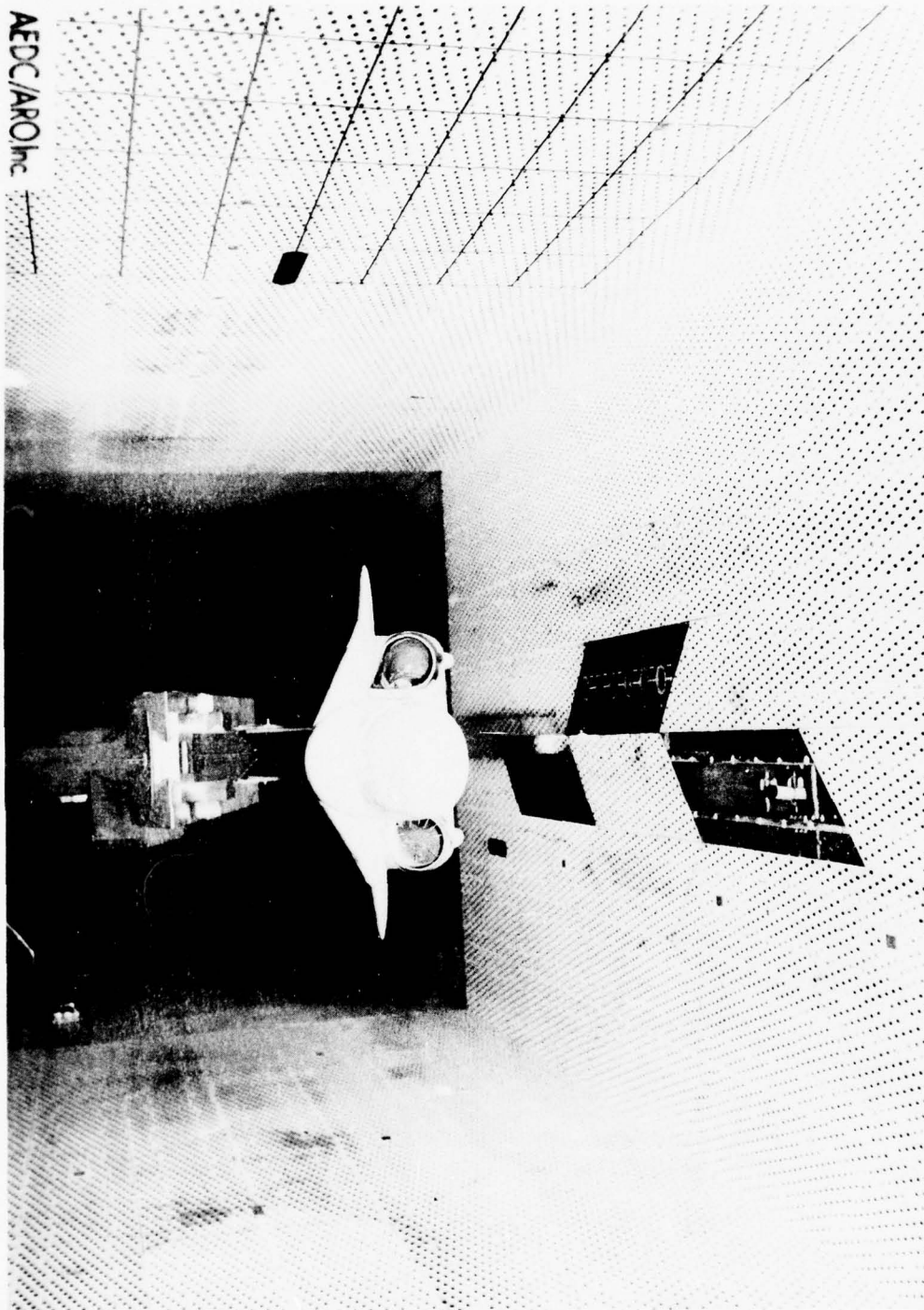


Figure 17. ASD advanced research inlet model in 16T.

AEDC/ARO, Inc.

10338 (11-24-75) PAT-A/A ASD RESEARCH INLET MODEL
IN THE PROPUSSION WIND TUNNEL (165)

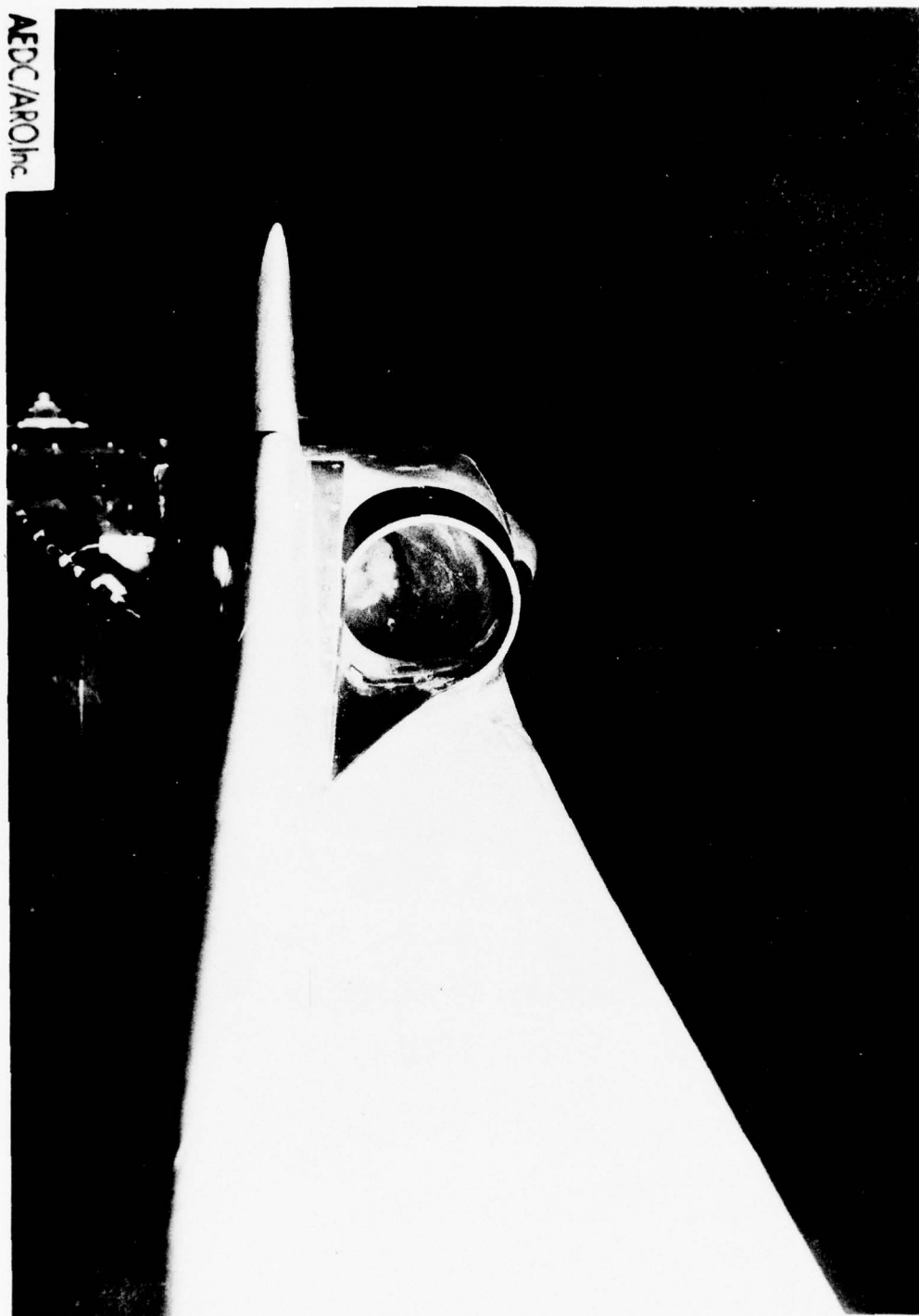


Figure 18. ASD advanced research inlet model in I6S.

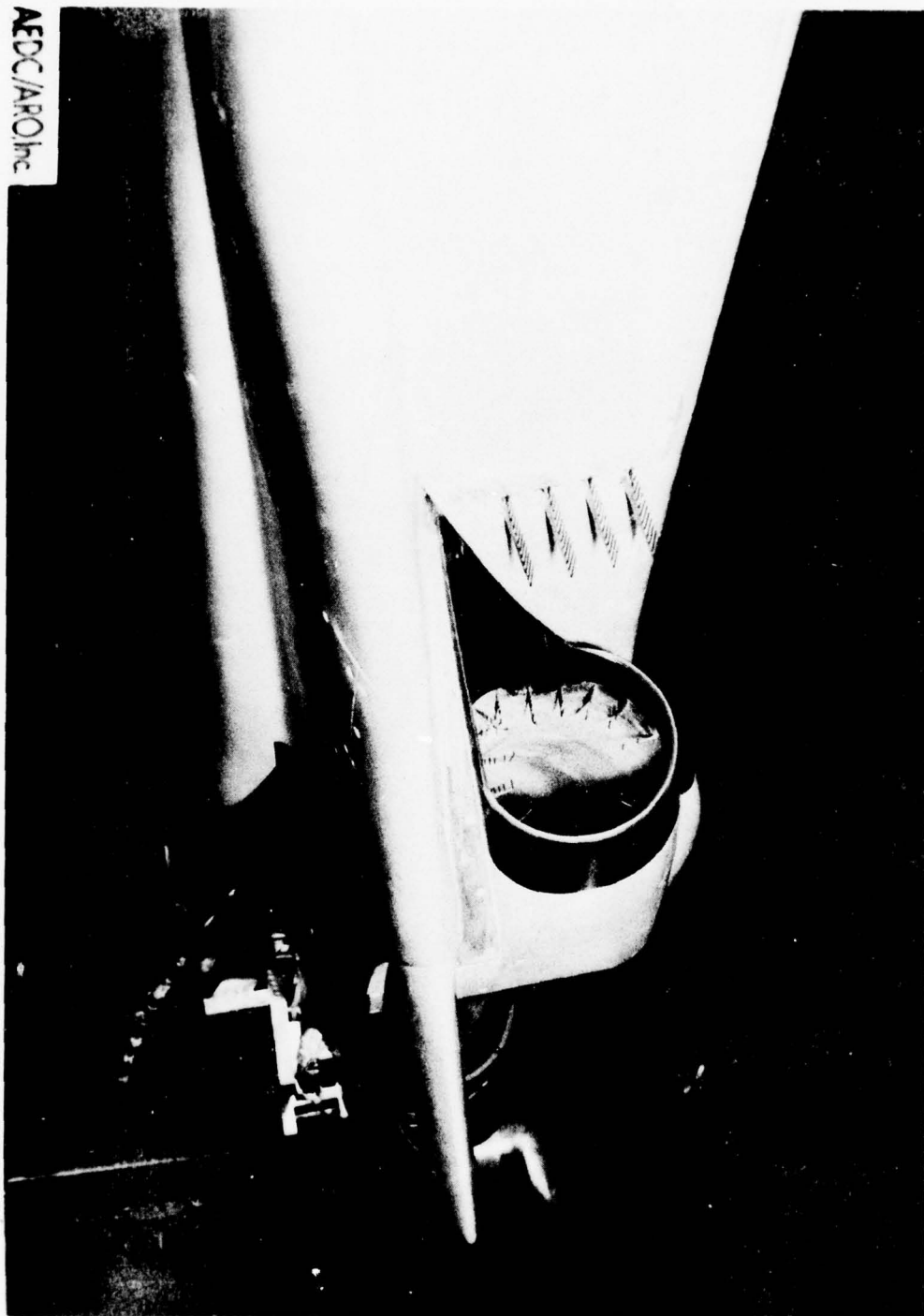


Figure 19. ASD advanced research inlet model flow-field instrumentation.

located on centroids of equal area as shown in Figure 20. The right-hand compressor-face instrumentation consisted of 40 steady-state pressure transducers also located on centroids of equal area. Four rows of duct-static taps ran from the splitter plates to the compressor face in the L/H duct. In addition, several hi-response static taps were located at the throat, in bend areas, and at the compressor face in the L/H duct.

Reference 2 contains a complete description of the model, test configurations, and instrumentation.

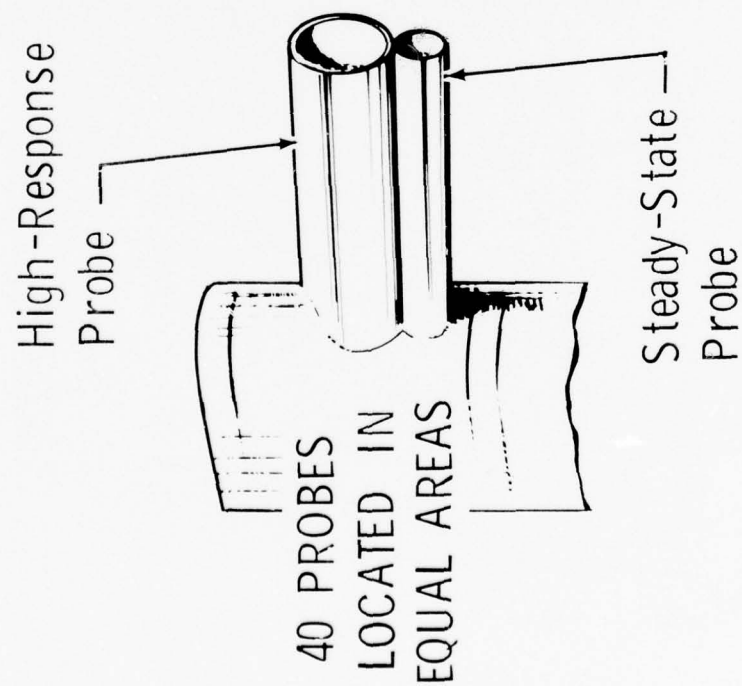
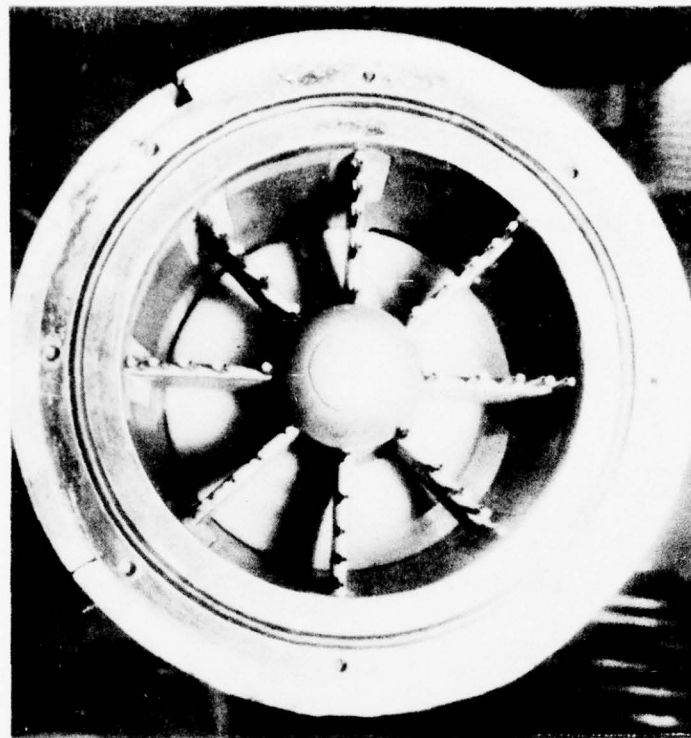


Figure 20. Inlet-model-compressor-face instrumentation.

4. DATA PRESENTATION AND DISCUSSION

The tests were accomplished during three nights of testing in PWT 16S in November 1975 and four nights of testing in PWT 16T in March 1976. A description of the configurations tested, the order in which they were tested, the Mach numbers at which they were tested, and the test facility part numbers were given in Tables 1 and 2.

The basic model consisting of the L/H hi-response compressor-face instrumentation and flow plug, the R/H steady-state compressor-face instrumentation and flow plug, the beam, and the model support and actuation mechanisms was from the Tailor-Mate program and was borrowed from the AF Flight Dynamics Laboratory for these tests. A model scale of 1/5.2 was established from the size of the existing model compressor face compared to the size of the compressor face of the F101-GE-100 engine, the engine selected for this research program. The Tailor-Mate inlet model was selected because of its large size, because it existed and could therefore save some design and fabrication costs, and because the information obtained from the test could supplement the Tailor-Mate inlet-test results. Thus, the test results would extend the data base in evaluating inlet performance and engine/inlet compatibility of a simple, open-nose inlet and the integration of the F101-GE-100 engine placed in a wing-body flow field.

Evaluation of the inlet with a 0.8-Mach number throat with various plow/splitter-plate configurations and standoff distances was done on the left-hand side of the model with both hi-response and steady-state instrumentation. The right-hand side of the model was dedicated primarily to inlet flow-field testing, with steady-state evaluation of the inlet with the larger, 0.7-Mach number throat as a secondary objective.

The recorded data were used primarily to determine the following:

1. The thickness and characteristics of the boundary layer on the fuselage at F.S. 390 ahead of the inlet and at the splitter-plate leading edge.

2. The extent of normal-shock/boundary-layer interaction/separation or fuselage boundary-layer spillage past the splitter plate and the resulting effect on the throat-pressure profiles.
3. The effect of inlet standoff distance and plow/splitter-plate length, size, and shape, and the resulting effect on inlet pressure recovery and distortion.
4. Inlet performance documentation as a function of Mach number, angle of attack, angle of sideslip, and engine corrected airflow.
5. Engine/inlet compatibility angle-of-attack and side-slip envelopes for each Mach for the baseline inlet configuration.

The baseline configuration for which the majority of the data are presented is the Long-Plow/Splitter-Plate Inlet located at B.L. 43.82. The performance for this configuration was documented from Mach 0.55 to 2.0.

It should be noted that all of the throat-pressure profile data and splitter-plate rake data obtained at Mach 1.6 in 16S were taken with the inlet located at B.L. 45.64, while all of the throat-pressure profile data obtained in 16T were taken in the inboard position of 43.82. (No splitter-plate rake data were taken in 16T.)

In addition, it should be noted that no boundary-layer transition strip of any type was applied to the model nose or wing leading-edges for these tests. It may be for this reason that the fuselage boundary layer was thicker than the theoretical flat-plate thickness.

In the subsections that follow, sufficient data will be presented to define the performance of the Basic Long-Plow/Splitter-Plate Inlet at B.L. 43.82 and 45.64. Sufficient data and charts are also provided to present various analyses required to understand the test results. However, no attempt will be made to present all of the data that was recorded during the tests. The complete set of data is presented in Reference 3.

4.1 INLET FLOW FIELD

The flow field of an inlet located alongside a fuselage and under a wing can be very complex. The boundary-layer characteristics of the fuselage are not wholly predictable even though a flat-plate thickness can be calculated. Because the forward fuselage is a lifting body it generates lifting vortices. Such vortices tend to lift off the body surface at relatively sharp corners or where the cross-flow component turning angle is large. Additional complexities can be introduced because of the wing. Its pressure field can feed down along the fuselage surface, forcing separation and then trapping the vortex beneath the wing. Frequently the path of such vortices is outward and downward so that they enter the inlet and affect engine/inlet compatibility.

Conversely, locating an inlet in a precompression flow field under a wing can be very beneficial. It reduces local supersonic Mach numbers resulting in smaller inlet sizes, simplification of the variable geometry required (if the inlet geometry is variable), and reduction of the effective range of angle of attack through which the inlet must operate.

The fuselage boundary layer at F.S. 390, splitter-plate flow, inlet-throat flow, and compressor-face flow will be examined in the following subsections in an effort to understand the research-model inlet flow field. This will be done for selected test conditions. In addition, some comparative configurations will be examined. The analysis will also compare the fuselage boundary layer of the research model with that of the F-111, which had a 73-inch shorter fuselage ahead of its inlet.

4.1.1 Mach 1.6

4.1.1.1 Fuselage Flow

The pitot pressure-recovery contour maps of the fuselage boundary layer at F.S. 390 as a function of angle of attack and sideslip are shown for Mach 1.6 in Figure 21. At angles of attack of 5° or less, only the lee-side sideslip of 4° results in a thickened boundary layer that extends outboard of the splitter-plate leading edge at B.L. 43.82. The boundary layer does thicken as the angle of attack increases, but there is no indication of a body vortex.

4.1.1.2 Basic Long-Flow/Splitter-Plate Inlet Flow

Presented in Figure 22 is a set of right-hand-inlet throat maps associated with the fuselage-flow conditions of Figure 21 for an inlet corrected airflow of 310 lb/sec. From these throat maps, it can be seen that low-energy air is entering on the inboard side of the inlet even though the F.S. 390 flows did not indicate a fuselage boundary-layer problem at many of the conditions. However, it is interesting to notice the improvement in the throat flow as the angle of attack is increased. The region of low-energy air is virtually eliminated at 13° angle of attack. Because of the ingestion of this low-energy air at the lower alphas and higher local Mach conditions, a shock-boundary layer interaction problem was suspected.

The corresponding steady-state compressor-face maps for the 310 lb/sec corrected-airflow conditions are shown in Figure 23. A low-energy region at the three o'clock outboard position can be seen on each of these compressor-face maps. This defect has been analyzed as separation off the backside of the bend on the outboard side of the duct. It is interesting to notice that the low-energy air on the inboard wall at the throat is less evident at the compressor face.

Figure 24 is a composite chart drawing upon all of the available left-hand and right-hand instrumentation to analyze the Mach 1.6 inlet flow for the Basic Long-Flow/Splitter-Plate Inlet configuration at B.L. 43.82. Because only one throat and one compressor-face map could be shown in Figure 24, Figures 25a and 25b are included to supplement Figure 24 for the full airflow sweep. Figures 25a and 25b also have some of the turbulence maps that can be compared with the steady-state compressor-face maps for similarity. The darkened lines on Figure 24 correspond to the data for the throat and compressor-face maps shown.

Starting at the left side of Figure 24, the fuselage boundary-layer plot shows good, clean flow at F.S. 390. Proceeding to the right to the three splitter-plate rakes, it can be seen that the pressure profiles measured at F.S. 390 on Rake 1 were unaffected by changing inlet airflow. Thus the normal shock was always behind Rake 1. The profile also shows good flow conditions. However, Rake 2 shows a high sensitivity to inlet flow with a decrease in the pressure profiles as the inlet was throttled. Rake 3 was measuring low-energy air and was relatively insensitive to inlet flow.

WINDWARD
SIDE

$$\beta = -4^\circ$$

$$\alpha = -2\frac{1}{2}^\circ$$

$$\beta = 0^\circ$$

LEE
SIDE

$$\beta = +4^\circ$$

$$\alpha = 2^\circ$$

$$\alpha = 5^\circ$$

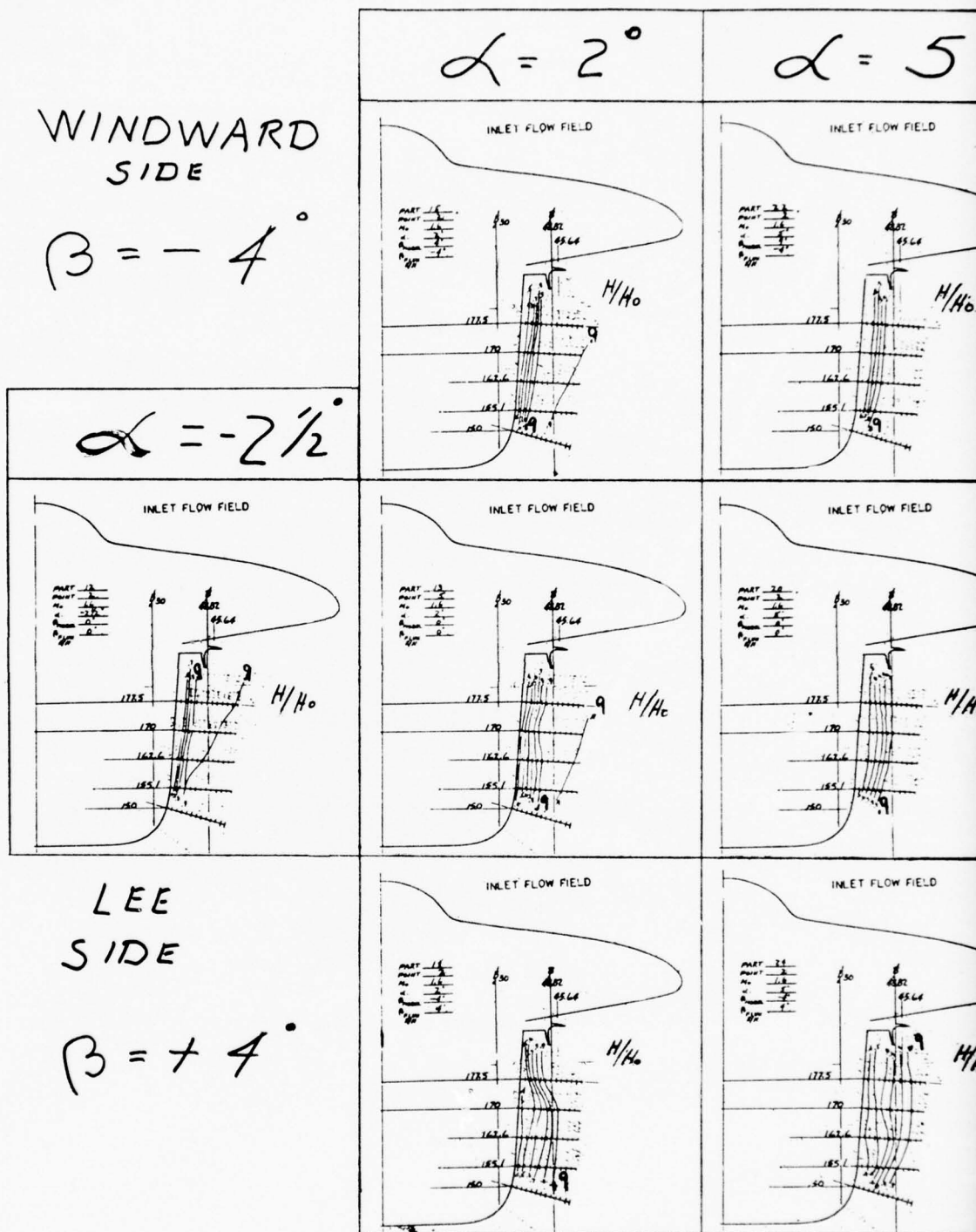


Figure 21. $M_0 = 1.6$ fuselage flow field

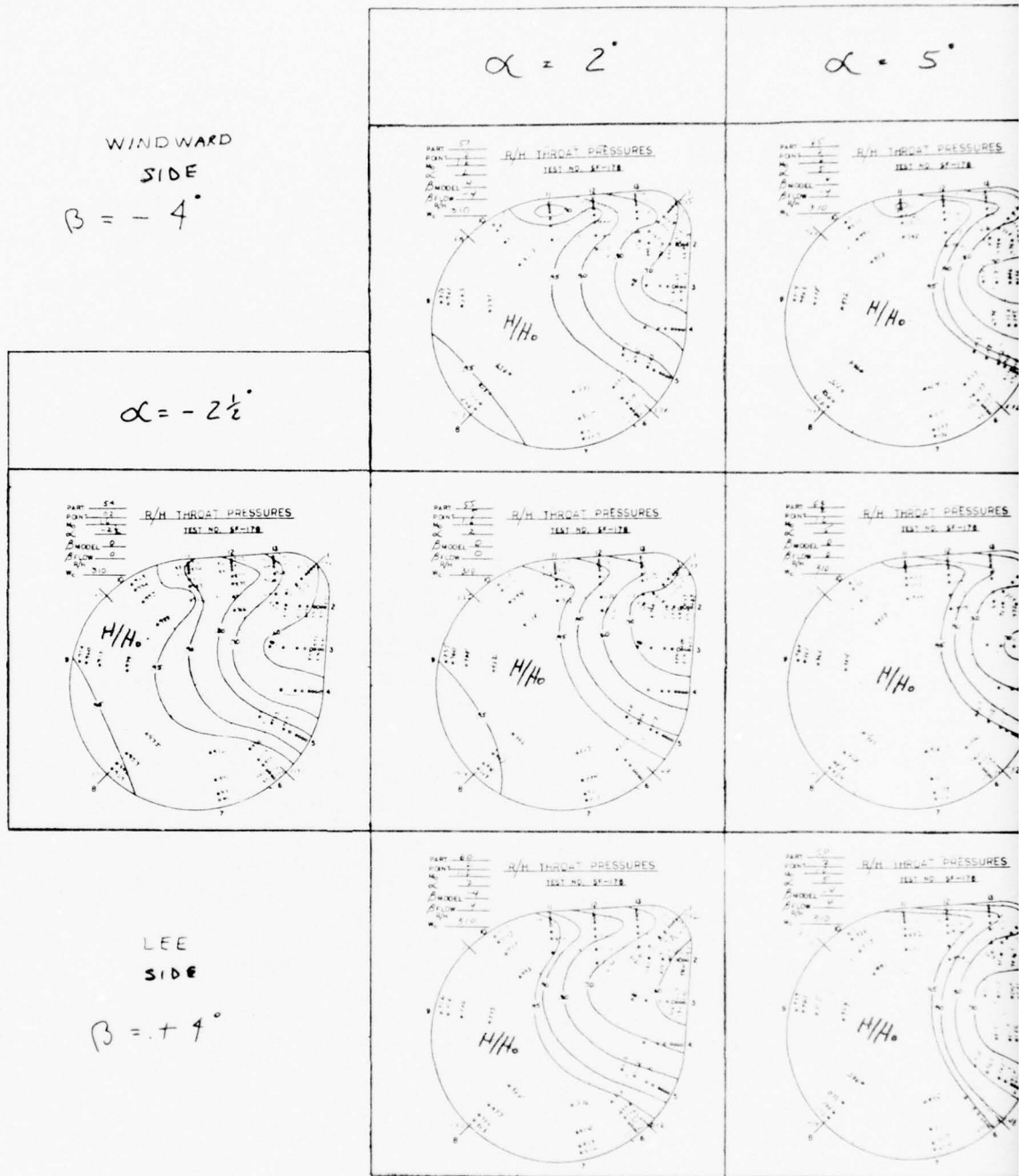
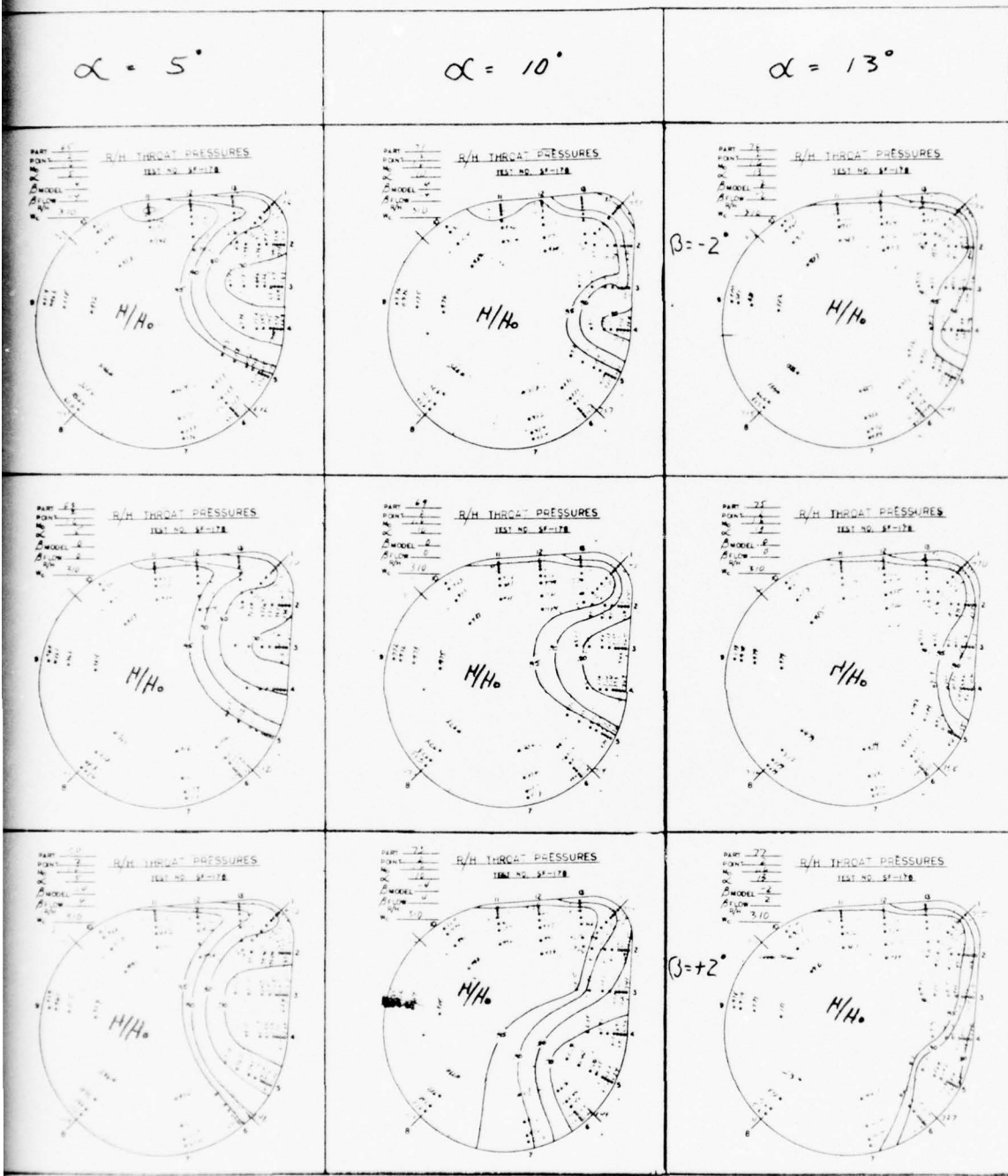


Figure 22. $M_0 = 1.6$ throat-rake contour maps
Inlet at B.L. 45.64 at $W_c = 310$

BEST AVAILABLE COPY



oat-rake contour maps for the Basic Long-Flow/Splitter-Plate
 . 45.64 at $W_c = 310$ pps.

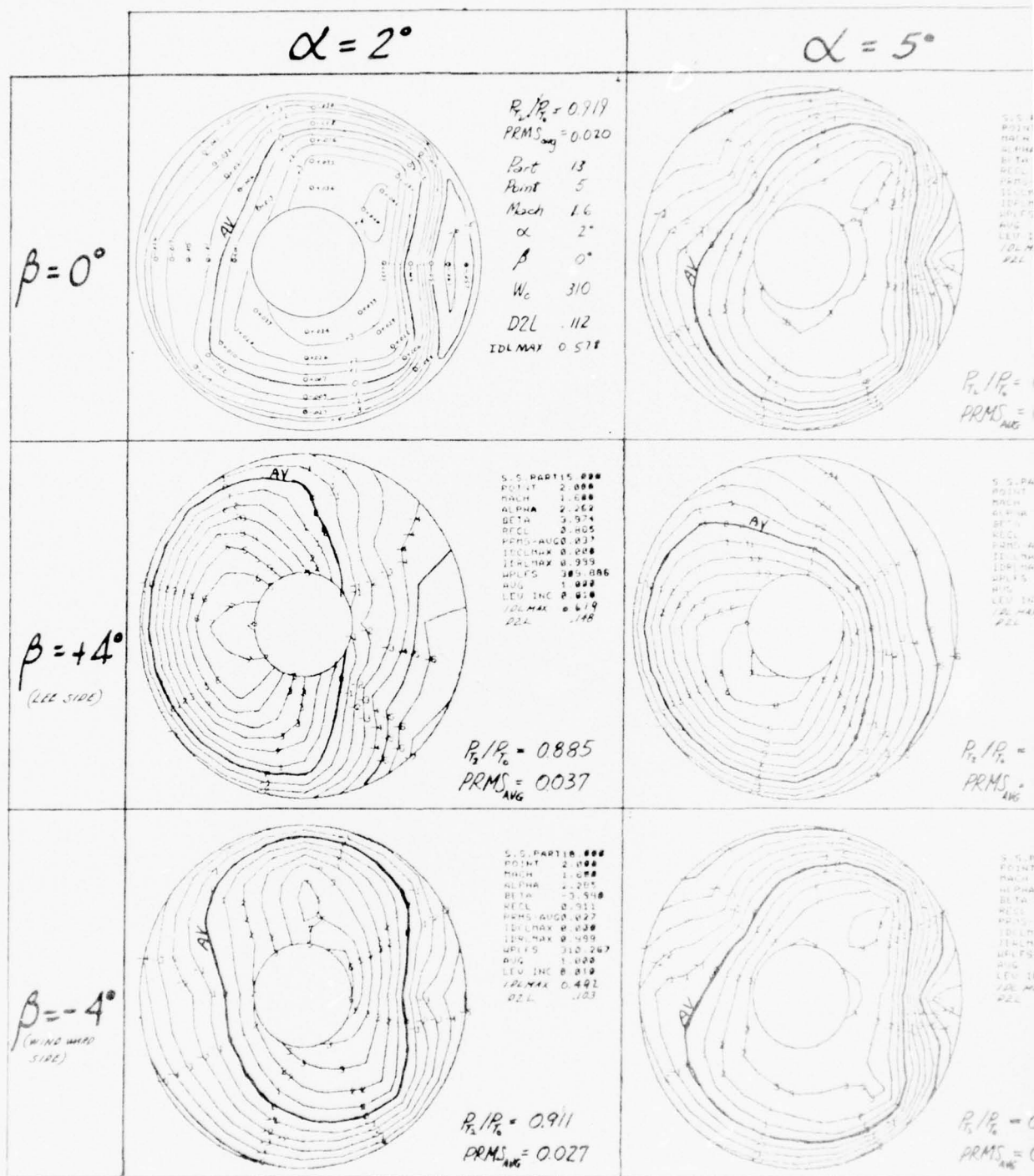
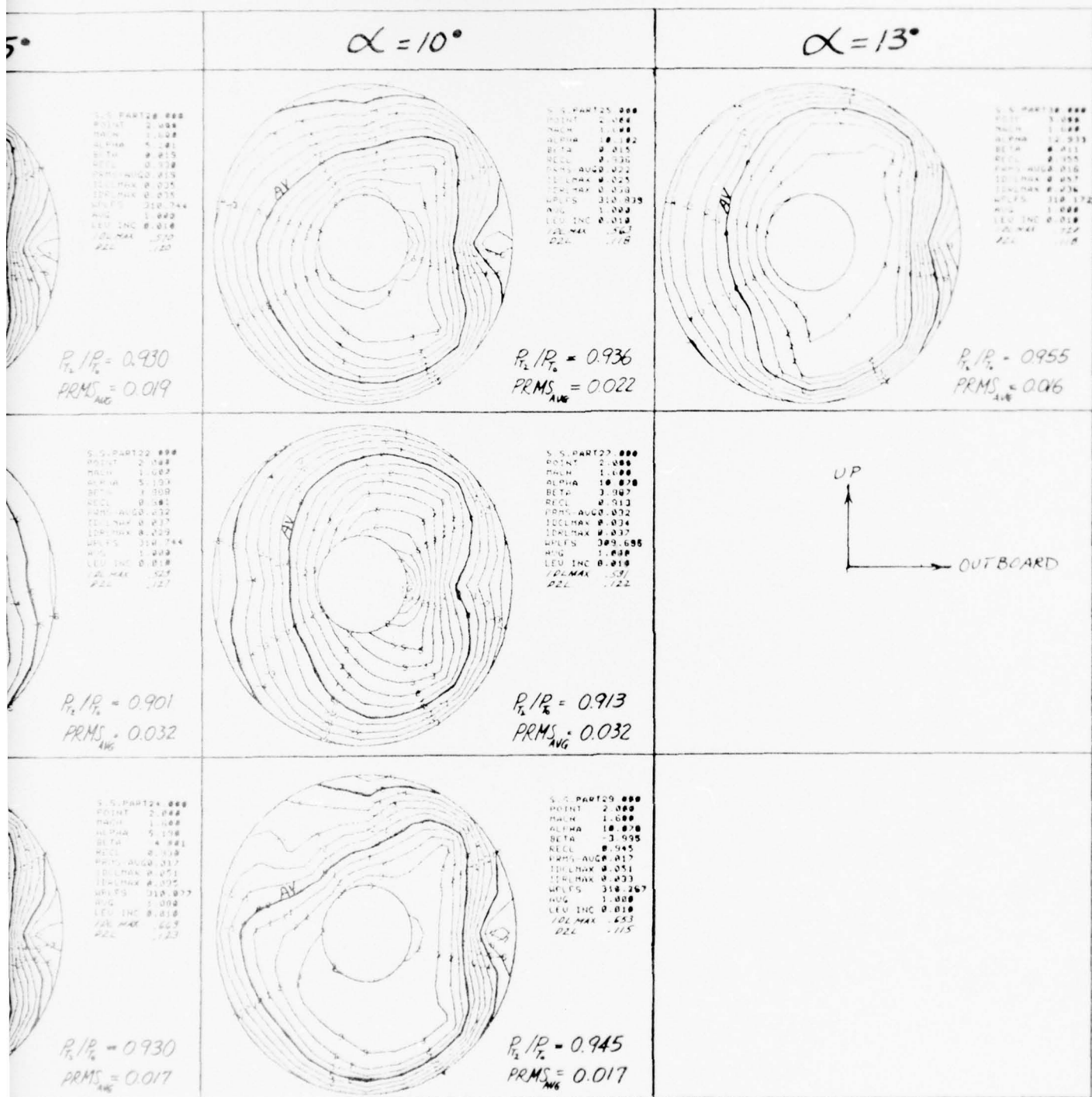


Figure 23. $M_0 = 1.6$ compressor-face-rake c
Splitter-Plate Inlet at B.L. 43

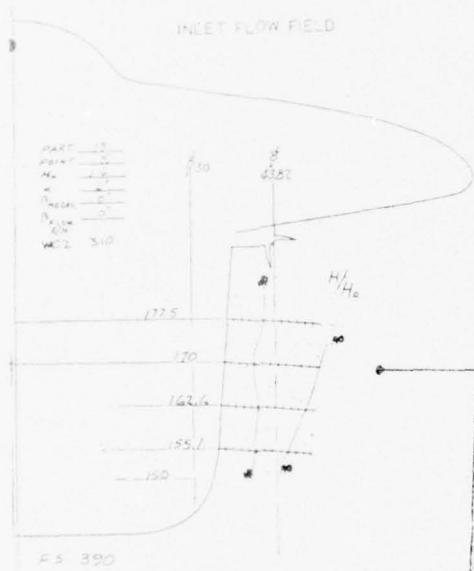
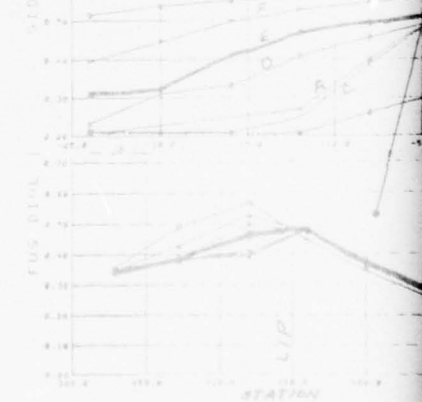
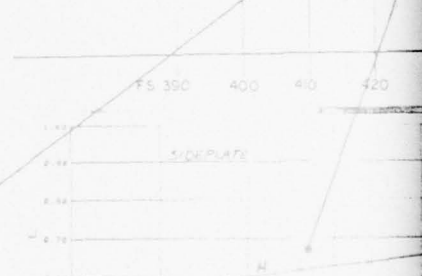
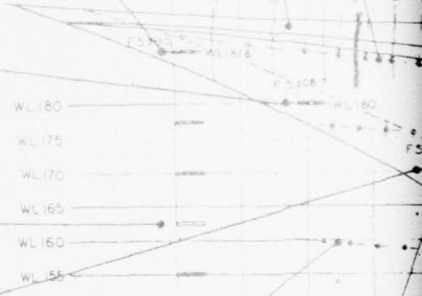
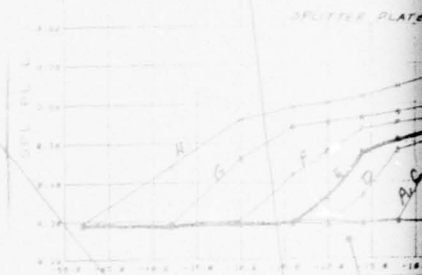
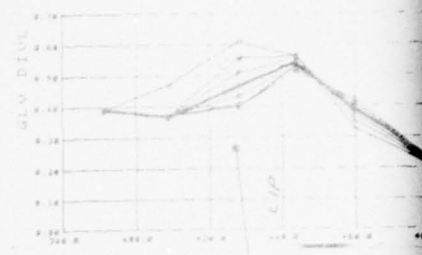
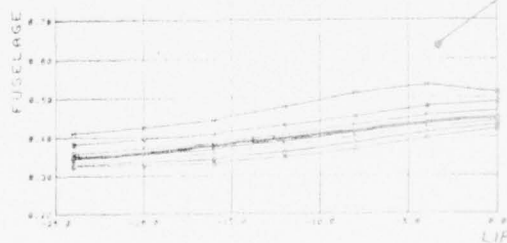
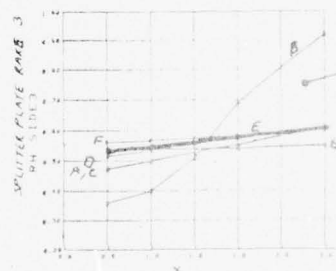
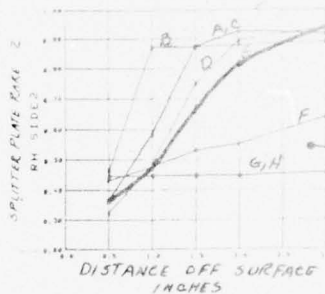
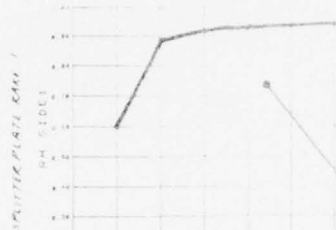


BEST AVAILABLE COPY

face-rake contour maps for the Basic Long-Flow/
at B.L. 43.82 at $W_c = 310$ pps.

PRECEDING PAGE BLANK NOT FILLED

SPL. PL. RAKE DATA
FOR INLET AT B.L. 45.44



SYMBOL	WL - LAMEC
A	340
B	345
C	340
D	323
E	310
F	250
G	250
H	184

BEST AVAILABLE COPY

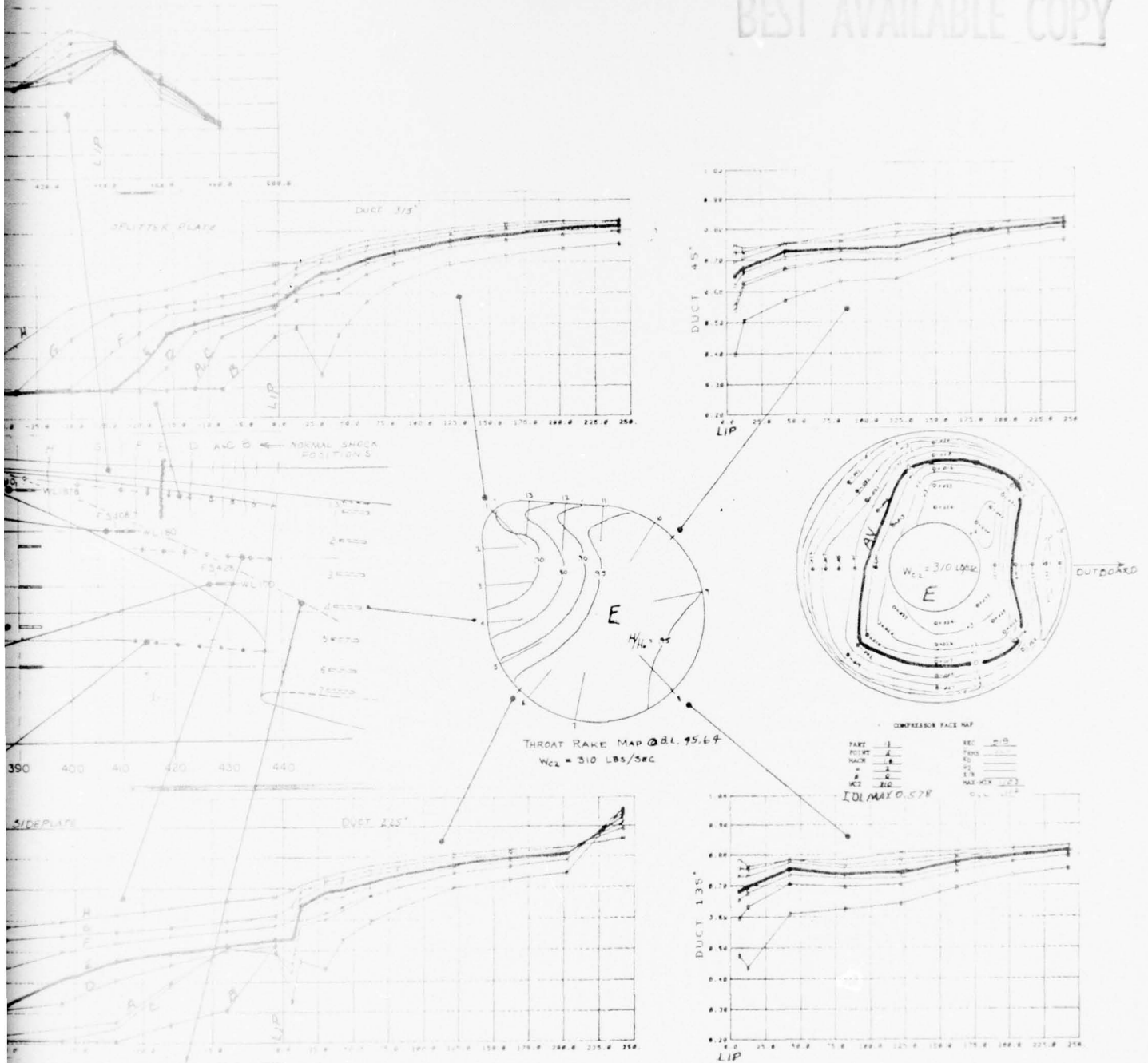
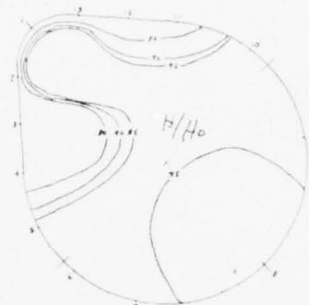


Figure 24. $M_0 = 1.6$ inlet-flow-field data for the Basic Long-Plow/Splitter-Plate Inlet at B.L. 43.82 at $\alpha = 2^\circ$ and $\beta = 0^\circ$.

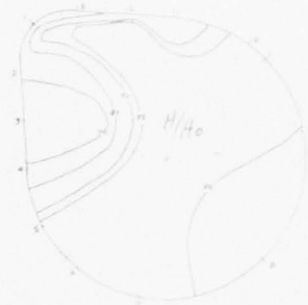
THROAT

@ B.L. 45.64

$W_c = 365$

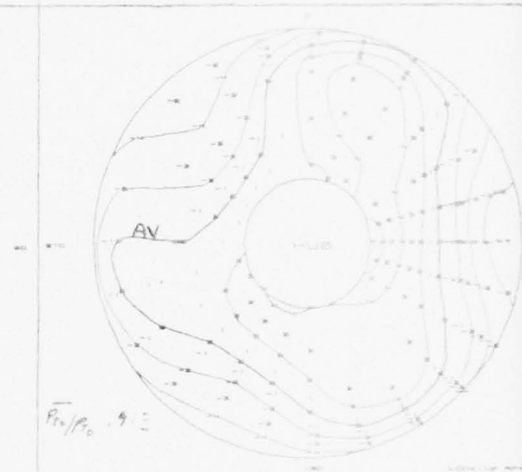
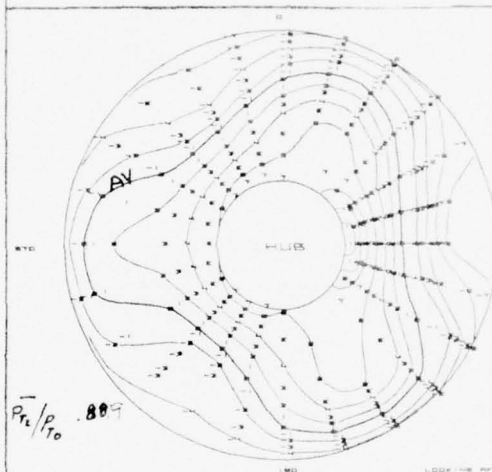


$W_c = 340$



C.F.
STEADY
STATE

@ B.L. 43.82



C.F.
INSTAN-
TANEOUS

@ B.L. 43.82

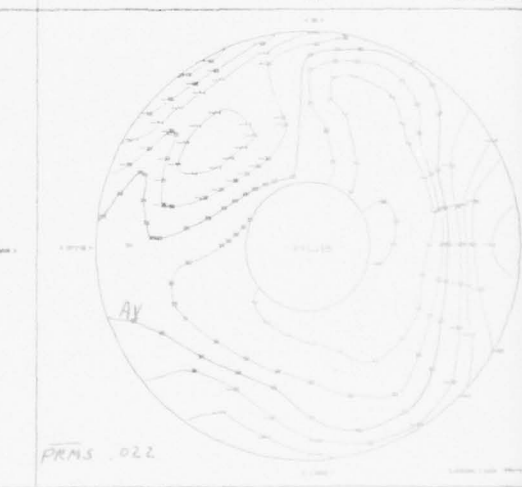
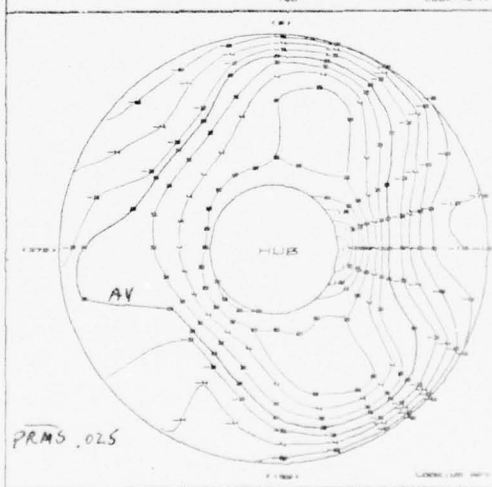
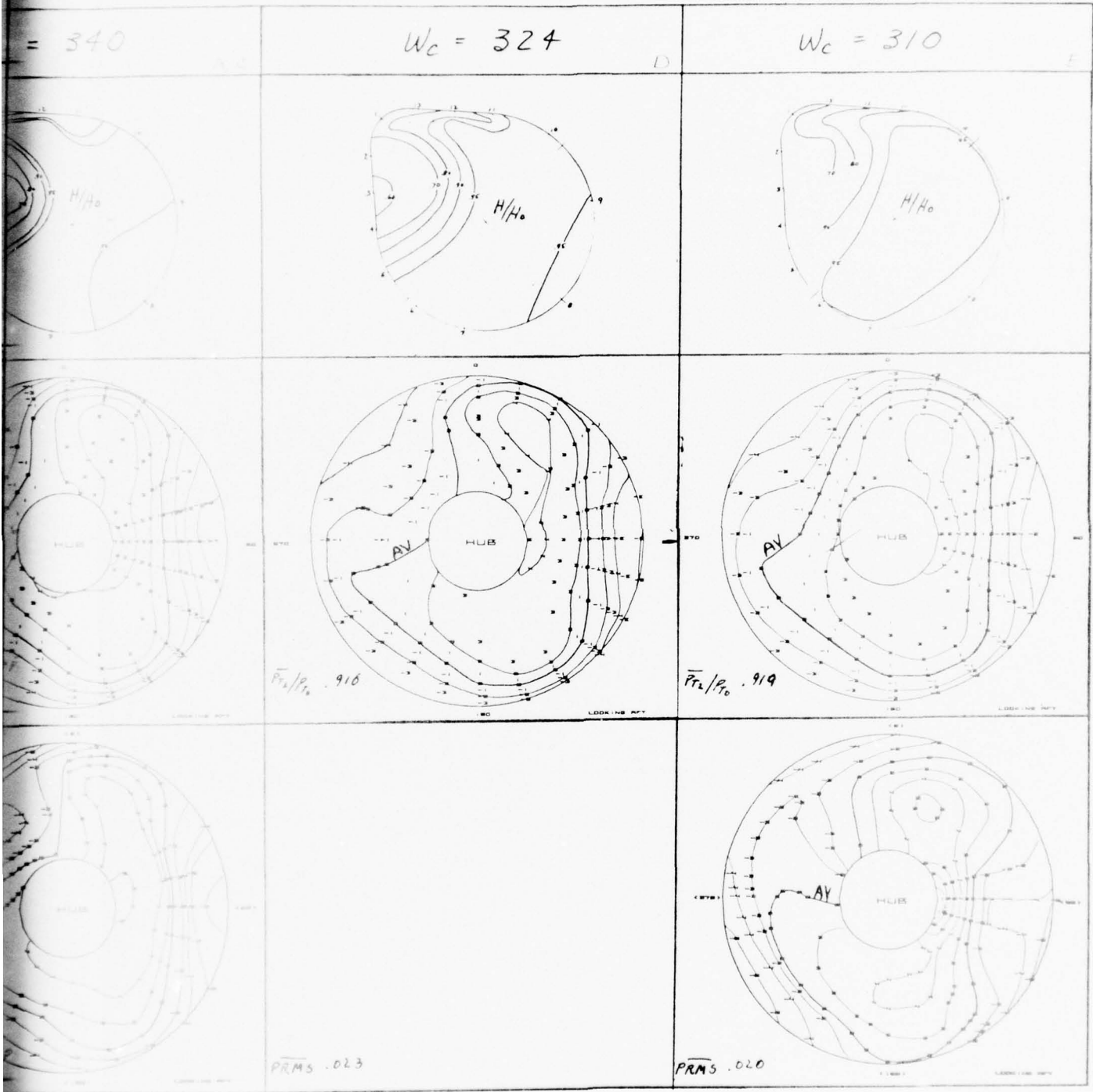


Figure 25a. $M_0 = 1.6$ throat and compressor-face
Splitter-Plate Inlet at $\alpha = 2^\circ$ at

BEST AVAILABLE COPY

2



t and compressor-face maps for the Basic Long-Flow/
Inlet at $\alpha = 2^\circ$ and $\beta = 0^\circ$ for $W_c = 365-310$ pps.

THROAT

@ B.L. 45.64

C.F.
STEADY
STATE

@ B.L. 43.82

C.F.
INSTAN-
TANEOUS

@ B.L. 43.82

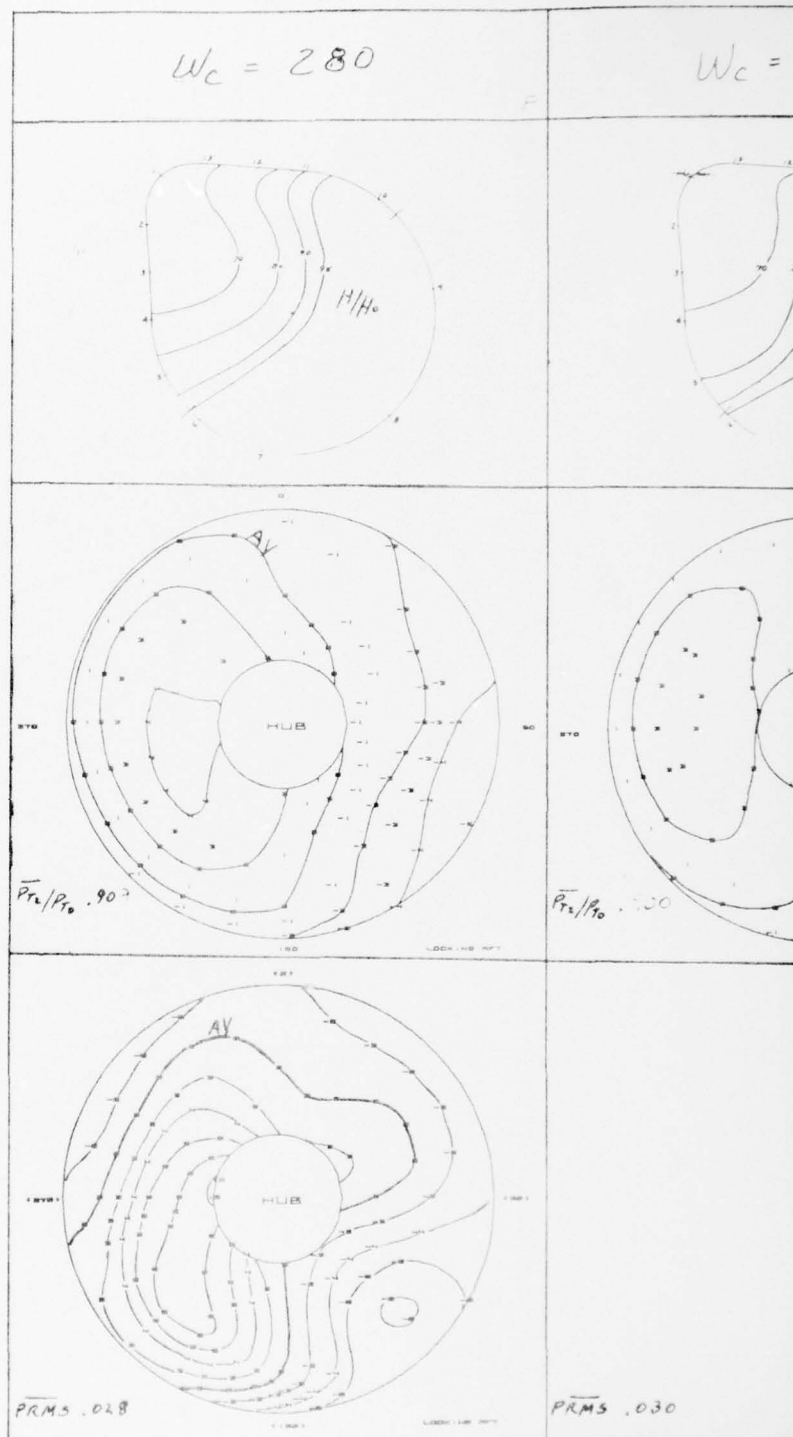
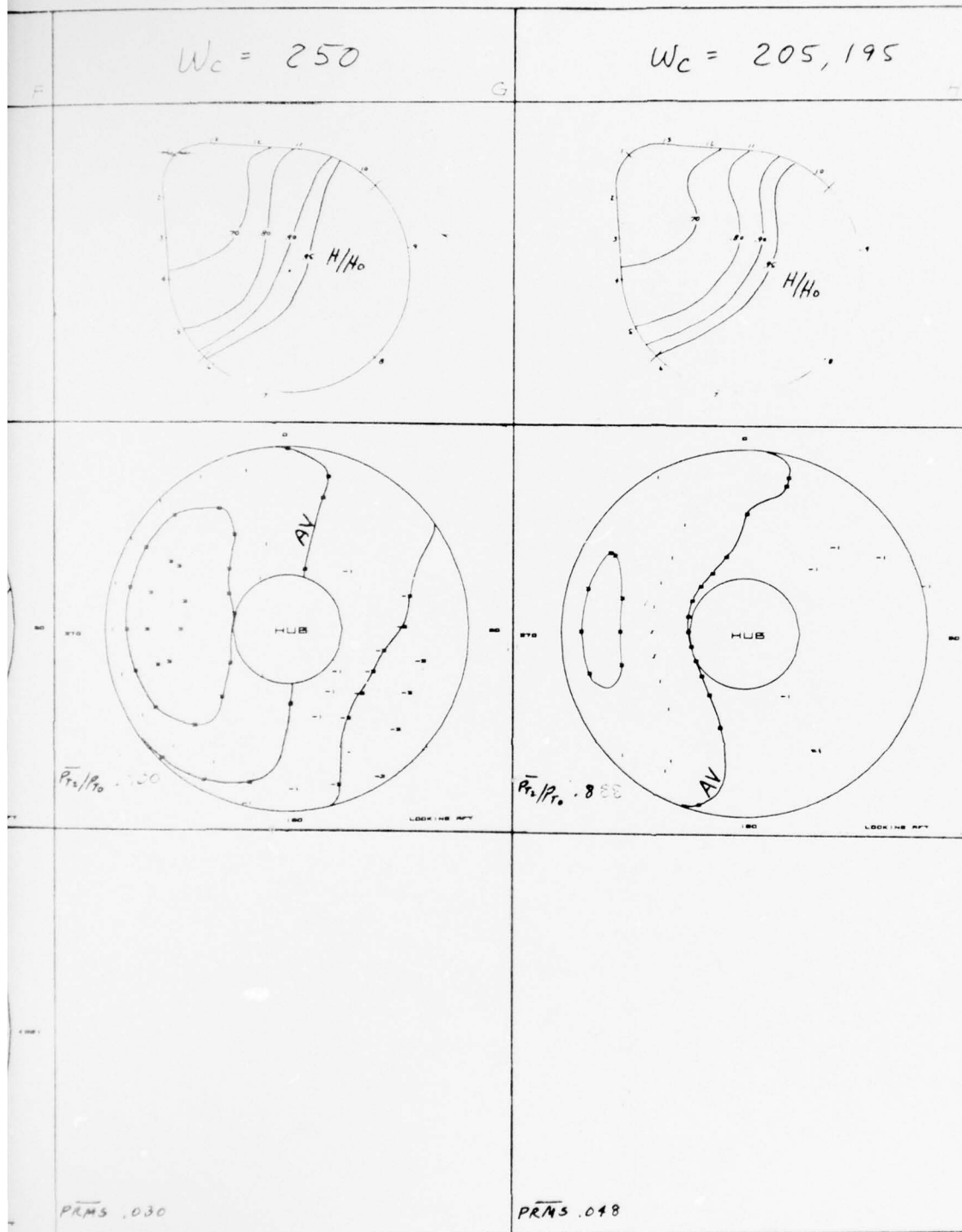


Figure 25b. $M_0 = 1.6$ throat and compressor-face
Splitter-Plate Inlet at $\alpha = 20^\circ$.

2



at and compressor-face maps for the Basic Long-Plow/
e Inlet at $\alpha = 2^\circ$ and $\beta = 0^\circ$ for $W_c = 280-195$ pps.

The corner splitter-plate statics and throat map show good flow in the 315° corner down to a flow of 280 lb/sec (Figure 25). However, the sideplate statics, which form a line midway between Throat Rakes 2 and 3, show a bifurcated (λ) shock system or a separated-flow region at the highest inlet airflow. Re-examining flow-profile B on Splitter-Plate Rake 3, it is difficult to establish whether it is a shock-boundary layer interaction problem or spillage of the fuselage boundary-layer air past the splitter-plate leading edge. However, since Splitter-Plate Rake 2 was sensitive to inlet airflow and thus normal-shock position, it is apparent that the normal-shock-system pressures being imposed on the fuselage boundary layer were affecting the flow at Rake 2. Consequently, it is now concluded that spillage past the splitter-plate leading edge was occurring. (The analysis immediately following the 16S test concluded that it was a classical shock-boundary layer interaction problem that could be fixed with revised splitter plates.)

With further examination of the throat and compressor-face maps, it can be seen that as the inlet airflow is reduced the lower-energy air covers a larger portion of the throat with a reduction in compressor-face distortion. It is significant to notice, from examining all of the throat maps, that there is no evidence of inlet-lip flow problems - no lip separation due to any cause.

Following the transonic tests, additional analysis of the Mach 1.6 flow-field data was made. This was done because it was suspected that the splitter-plate leading-edge spillage was occurring between Water Lines (W.L.) 170 and 180, and the splitter-plate rake data should be examined further. It was decided that these rake data should be examined as a function of angle of attack at a constant inlet airflow to complement the data shown in Figures 22 and 23.

The assembled data plots are shown in Figure 26. As noted, the splitter-plate rake and throat-rake data were recorded on the R/H inlet that was located at B.L. 45.64. All of the inlet static-pressure data are from the L/H inlet that was located at B.L. 43.82.

In analyzing the data of Figure 26, the following observations were made:

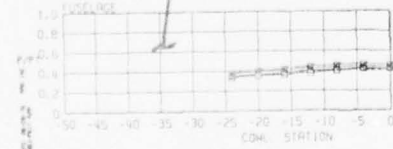
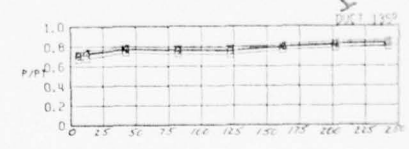
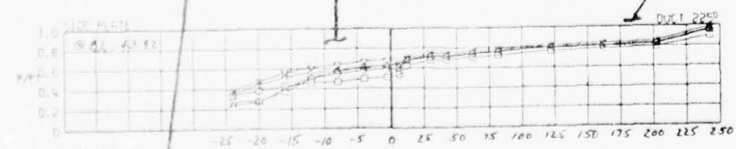
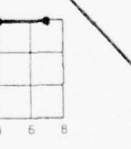
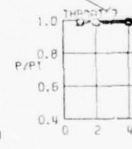
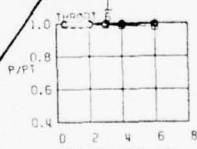
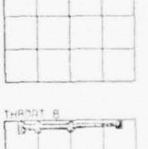
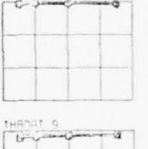
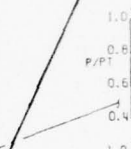
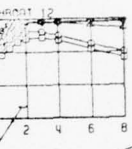
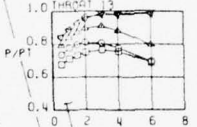
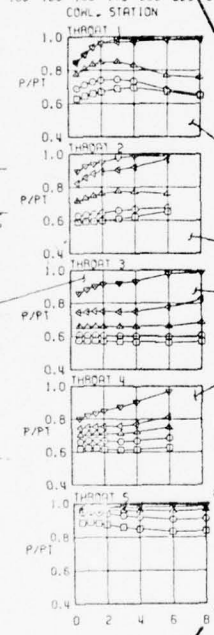
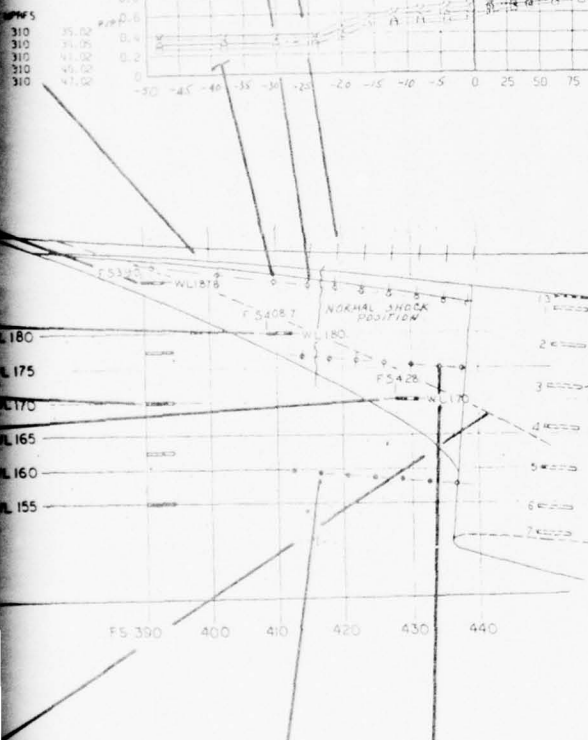
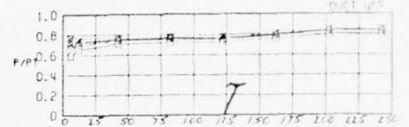
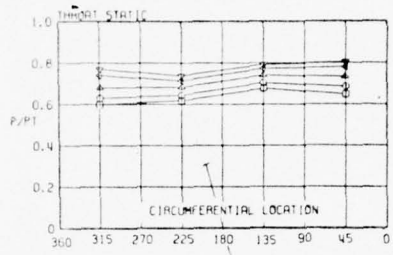
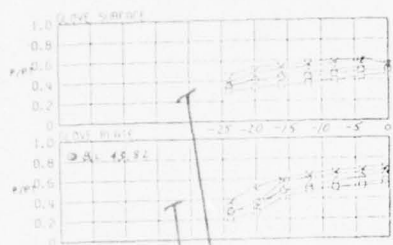
1. The position of the normal shock remained constant for all angles of attack. It did not move forward as local Mach decreased. This can be seen from examining the static-pressure plots from the splitter plate, side plate, and glove plate.
2. The normal shock was the same distance ahead of the inlet lip on the splitter plate, side plate, and glove plate (no skewing due to variations in local Mach) for all angles of attack.
3. The fuselage boundary layer thickened as angle of attack was increased with the lower-energy air progressively extending outboard of the splitter-plate leading edge.
4. In spite of the thickened fuselage boundary layer that occurred with increased angle of attack, the throat-rake profiles show improved pressure levels as angle of attack was increased. This was also evident in Figure 22.
5. Each splitter-plate rake profile improved as angle of attack was increased. The big improvement on Rake 2 occurred at 10° , and the big improvement on Rake 3 occurred at 13° . This indicates that the region of spillage was moving aft, from in front of to behind the normal-shock position, as angle of attack was increased.
6. Referring to the throat-pressure contour maps in Figure 22, it can be seen that the low-pressure defect progressed from Rakes 2 and 3, to Rake 3, to Rakes 3 and 4, to Rake 4 as angle of attack was varied from 2° , to 5° , to 10° , to 13° , respectively. It can also be seen that the value of the low-pressure recovery improved (increased) as angle of attack was increased.
7. The fuselage-diverter (plow) static-pressure levels increased more downstream of the inlet lip than they did forward of the lip as angle of attack was increased.

On the basis of the preceding observations, it is concluded that as the model angle of attack was increased the fuselage boundary layer was compressed enough to enter the

SYMBOL	M	α	θ	CONF	WPPS
□	1.62	-2.1	0.0	2	310
○	1.62	-2.2	0.0	2	310
△	1.62	-5.2	0.0	2	310
◆	1.62	10.1	0.0	2	310
▼	1.62	12.9	0.0	2	310

SYMBOL	M	α	θ	CONF	WPPS
□	1.60	-2.4	0.0	4	310
○	1.60	-2.1	0.0	4	310
△	1.60	5.1	0.0	4	310
◆	1.60	10.0	0.0	4	310
▼	1.60	13.1	0.0	4	310

SYMBOL	M	α	θ	CONF	WPPS
□	1.62	-2.1	0.0	2	310
○	1.62	-2.2	0.0	2	310
△	1.62	-5.2	0.0	2	310
◆	1.62	10.1	0.0	2	310
▼	1.62	12.9	0.0	2	310



t flow field versus angle of attack ($\beta = 0^\circ$) for the Basic
itter-Plate Inlet at $W_c = 310$ pps.

channel between the splitter plate and the fuselage with a minimum of spillage into the inlet. From this analysis and subsequent analyses at other Mach numbers, it appears that the fuselage boundary-layer system can be modified to improve its flow characteristics at all Mach and angle-of-attack conditions. Some possible modifications to accomplish this are discussed in Subsection 4.1.10.

4.1.1.3 Short-Plow/Splitter-Plate Inlet Flow

Inlet flow-analysis data for the Short-Plow/Splitter-Plate Inlet configuration located at B.L. 43.82 are presented in Figure 27. This data can be compared with data for the Long-Plow/Splitter-Plate Inlet of Figure 24. However, a complete comparison cannot be made because splitter-plate rake and throat-map data were not recorded for the short configuration. But it is advantageous to look at their similarities and differences when analyzing the overall inlet-flow conditions.

A summary comparison of the configurations and the recorded pressure data (for the same test conditions) of Figures 24 and 27 follows:

1. Splitter-plate static pressures: The static pressures along the long-splitter plate indicated good, clean flow down to 250 lb/sec, with the normal shock always on the plate. On the short plate, it appears that the normal shock moves off the plate at a higher airflow. Looking at the estimated position of the normal shocks for each inlet, it appears that the normal shock lies approximately 10 inches further ahead of the lip on the short plate. This results in greater diffusion of the flow before entering the inlet and may be part of the reason why the pressure recovery for the short plate was 0.935 versus 0.919 for the long plate for the same inlet corrected airflow of 310 lb/sec.
2. Distance of the fuselage diverter (plow) behind the splitter-plate leading edge: The distance from the splitter-plate leading edge to the plow (edge distance) is greater on the Short Splitter-Plate Inlet than it is on the Long Splitter-Plate Inlet.

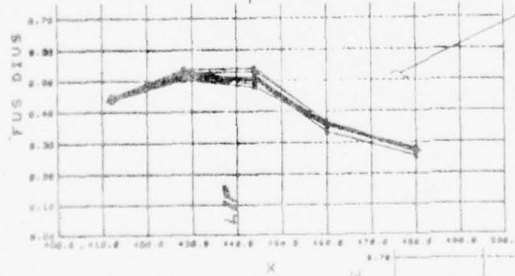
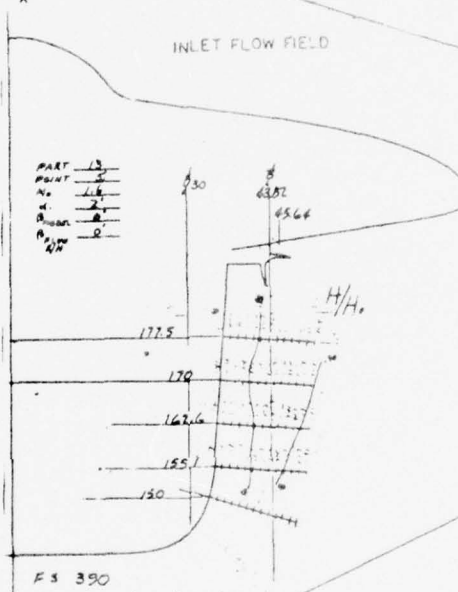
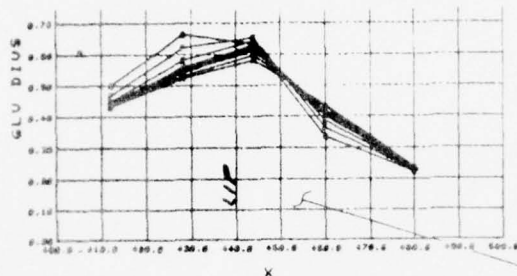
3. Fuselage-diverter and fuselage-surface static pressures: The Short Splitter-Plate configuration with its longer-edge distance was fairly insensitive to inlet-flow variations. The long configuration with a shorter-edge distance showed considerable sensitivity to inlet airflows on those pressure taps that were ahead of the inlet-lip station. Similarly, the fuselage-surface static pressure measurements on the long configuration were more sensitive to the airflow variations. Thus, it is concluded that the higher sensitivity to inlet airflow variations displayed by the Long Splitter-Plate Inlet was due to insufficient fuselage boundary-layer-channel flow area that resulted in spillage into the inlet. However, on the Short Splitter-Plate Inlet, it is speculated that spillage into the inlet was less of a problem. This is based on the compressor-face map in Figure 27 since throat-map data are not available.
4. Duct outboard bend: The defect at the compressor face due to the duct bend discussed earlier is also evident in Figure 27.

4.1.2 Mach 0.5

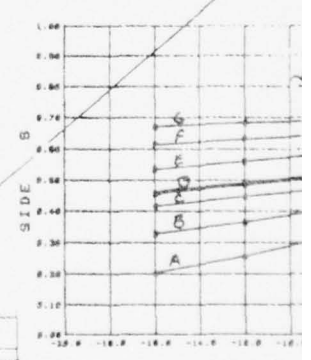
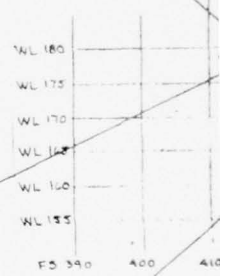
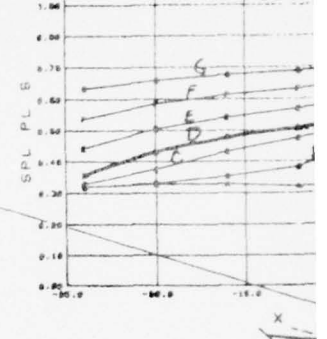
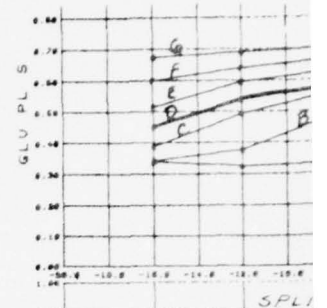
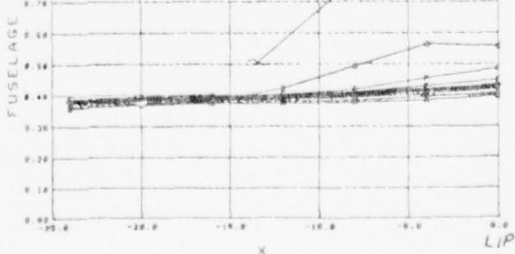
A limited amount of Mach 0.5 data was taken on the Basic Long-Plow/Splitter-Plate Inlet at B.L. 43.82 and on the Short-Plow/Splitter-Plate Inlet at B.L. 45.64 at 0.5 Mach in PWT 16S. These data were obtained with the tunnel in an unstarted flow condition to get some subsonic-performance data for the inlets prior to the 16T tests. From the data presented in Figures 28 and 29, it was concluded that there was essentially no differences in the configurations. This is best seen in the compressor-face contour maps. Both contain the same duct outboard-bend, low-energy defect, and both give some indication of splitter-plate spillage. But since throat-map data was not taken for these configurations at Mach 0.5, no absolute conclusions could be reached.

4.1.3 Mach 0.85

Mach 0.85 was a primary test condition for evaluating the configurations tested in PWT 16T. It also provided an opportunity to obtain data on the inlet flow-field (at a



SYMBOL	$W_{AS} - LB/SEC$
A	365
B	340
C	323
D	310
E	280
F	250
G	205



PART RANGE IS 5502

Figure 27.

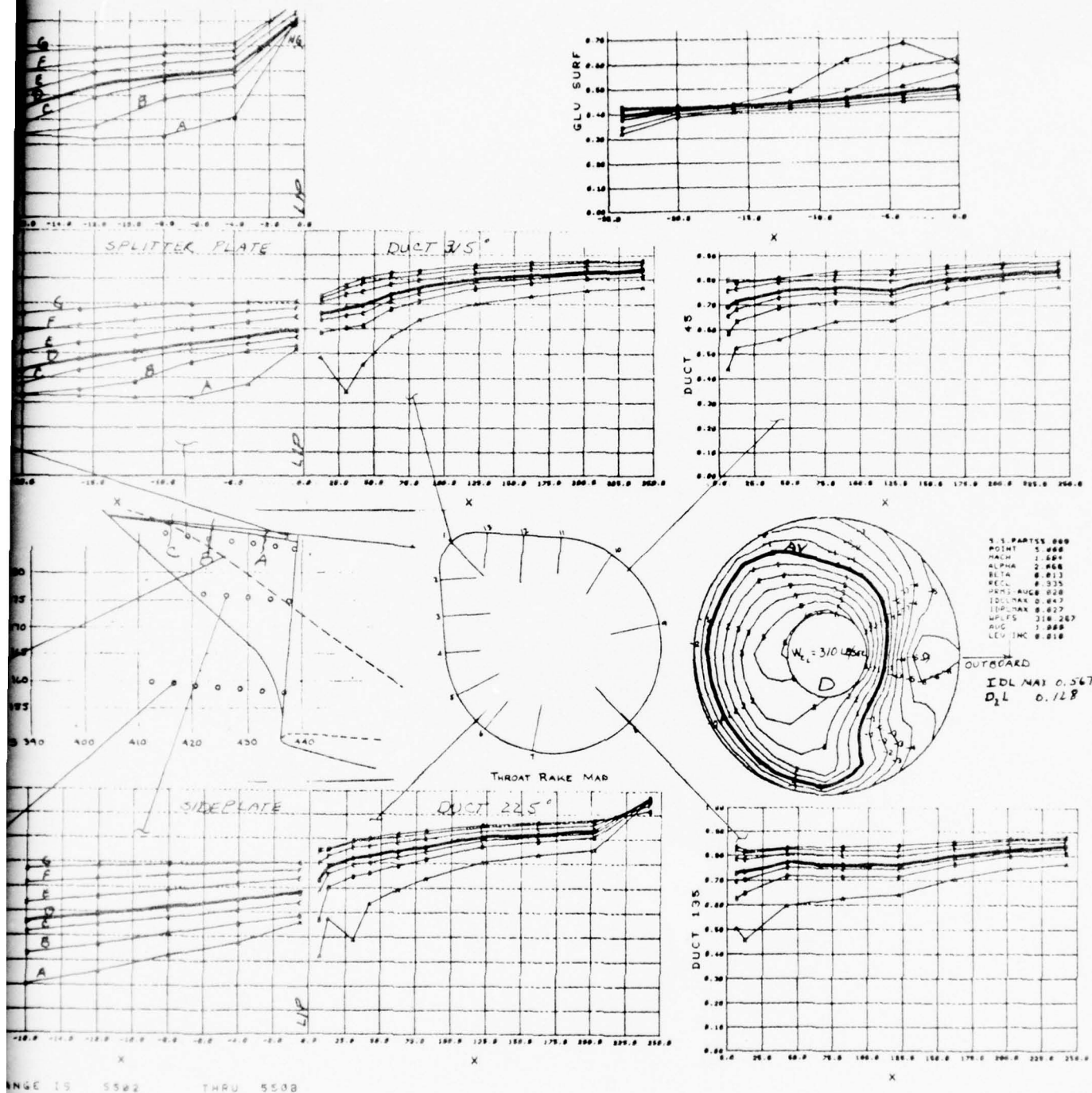
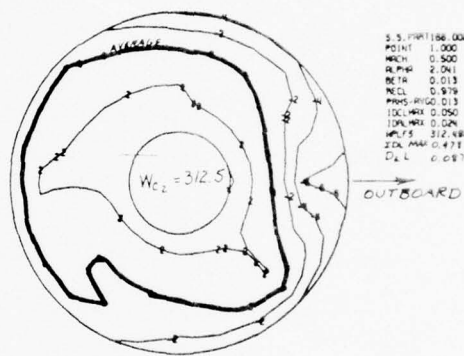
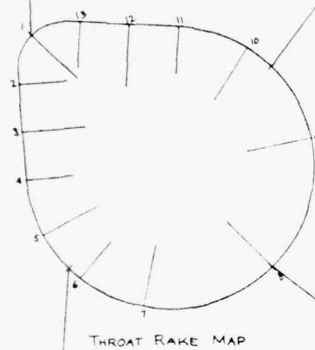
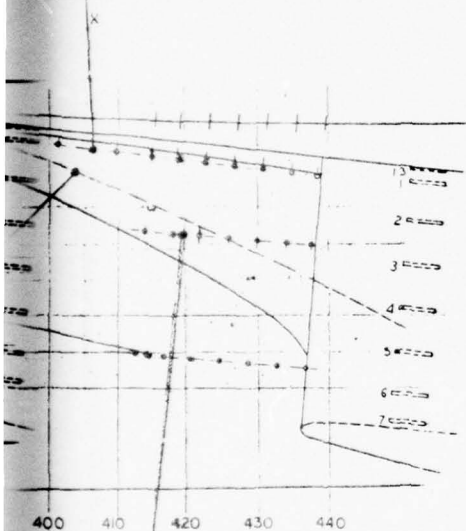
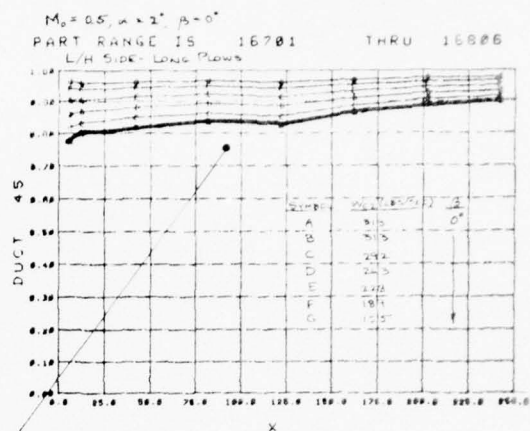
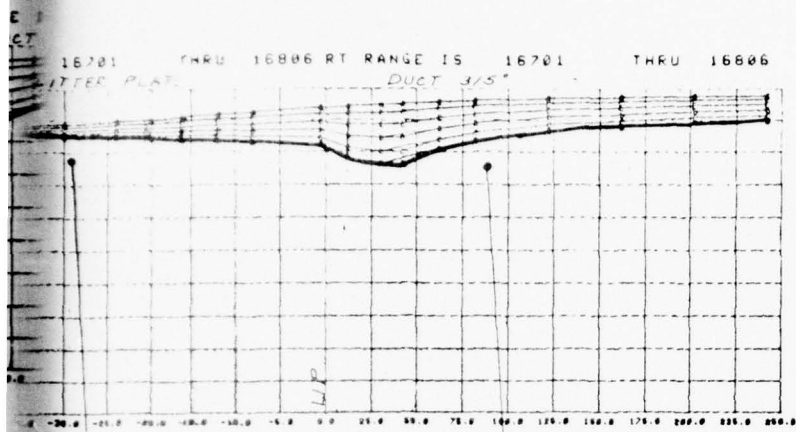
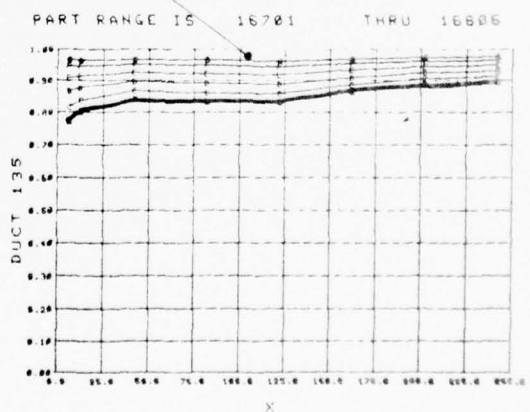
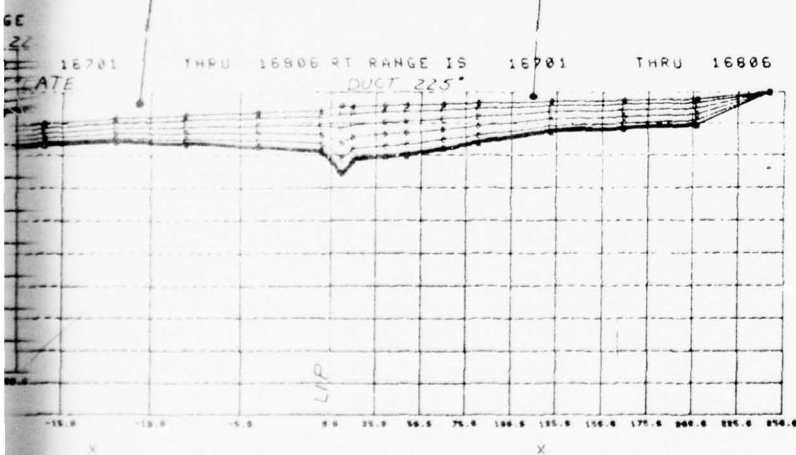


Figure 27. $M_0 = 1.6$ inlet-flow-field data for the Short-Plow/Splitter-Plate Inlet at B.L. 43.82 at $\alpha = 2^\circ$ and $\beta = 0^\circ$.

PRECEDING PAGE BLANK-NOT FILMED



S.S. PART 186.000
 POINT 1.000
 MACH 0.500
 ALPHA 2.001
 BETA 0.013
 RECL 0.979
 PRMS WING 0.113
 DCL WING 0.050
 DCL WING 0.024
 WPLTS 312.480
 ZCL WING 0.471
 DCL 0.687



low-field data for the Basic Long-Plow/Splitter-Plate
 82 at $\alpha = 2^\circ$ and $\beta = 0^\circ$.

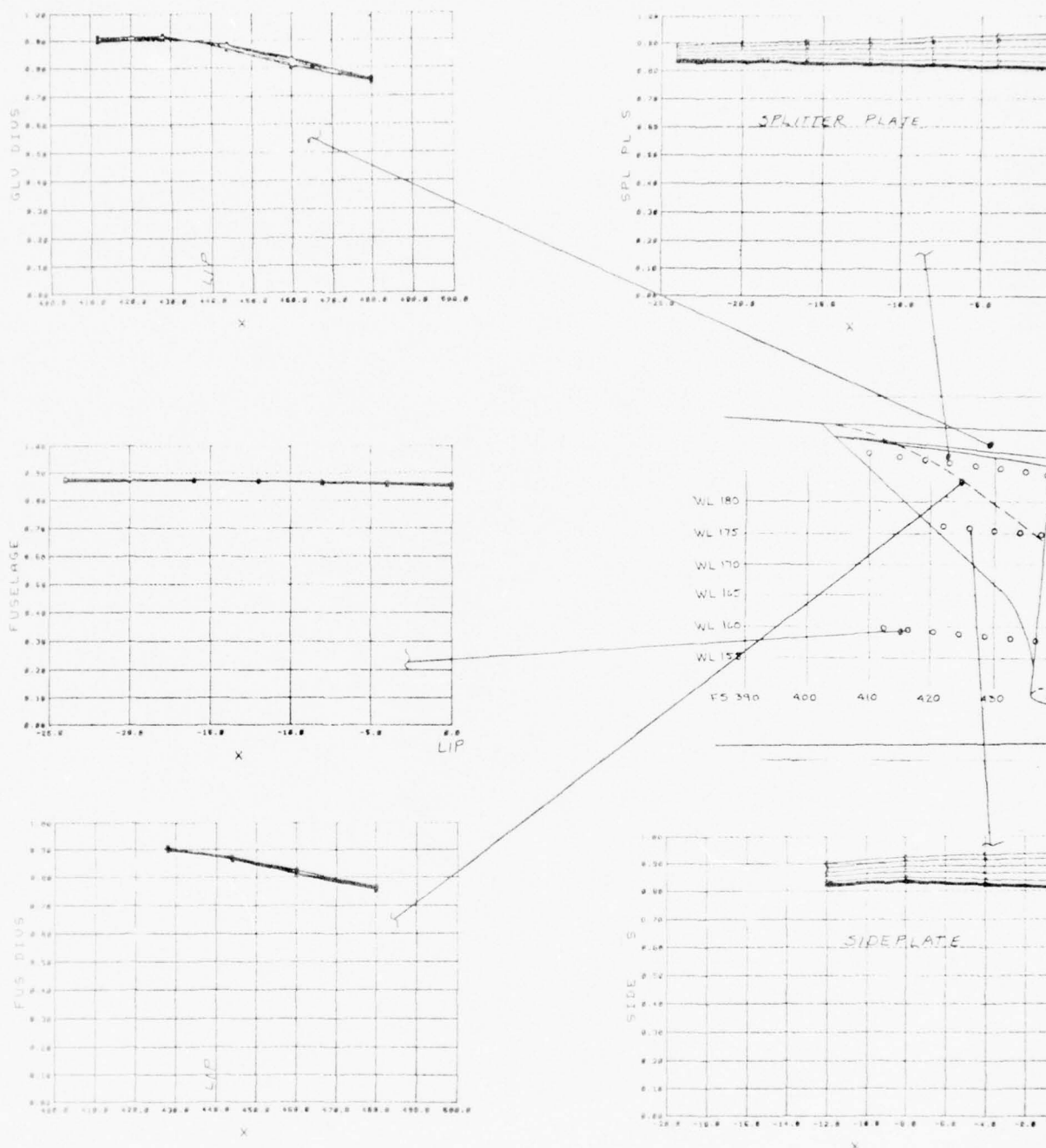
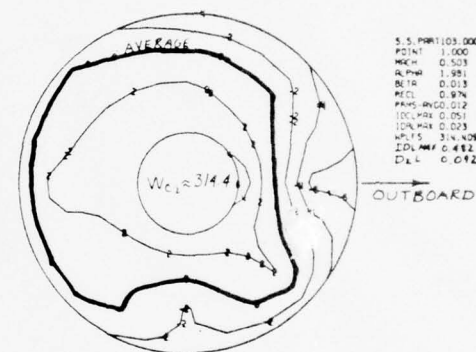
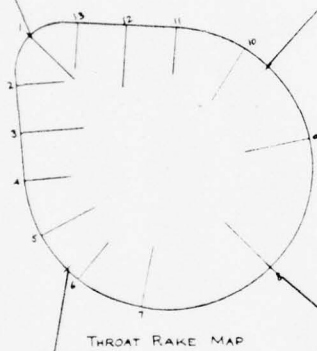
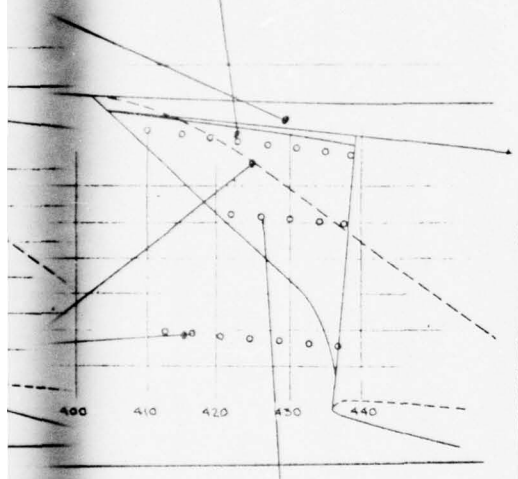
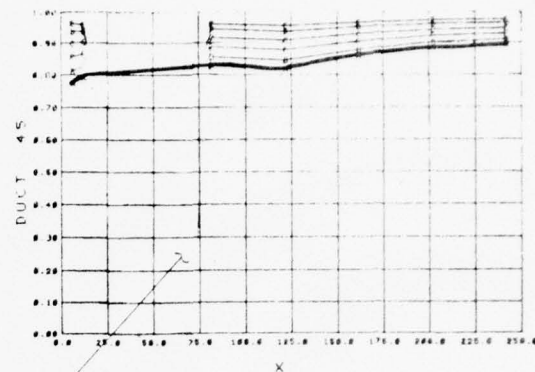
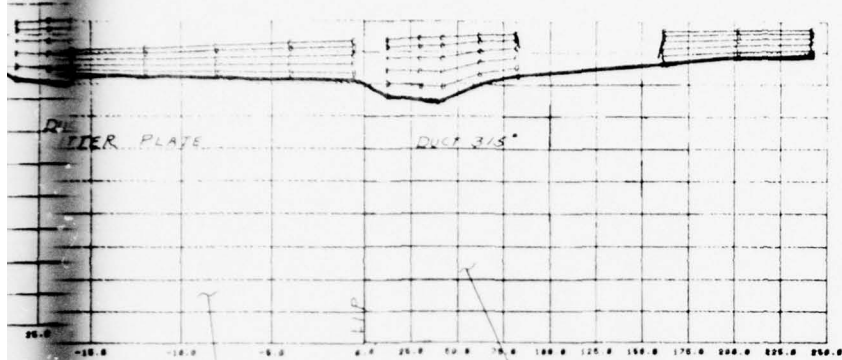
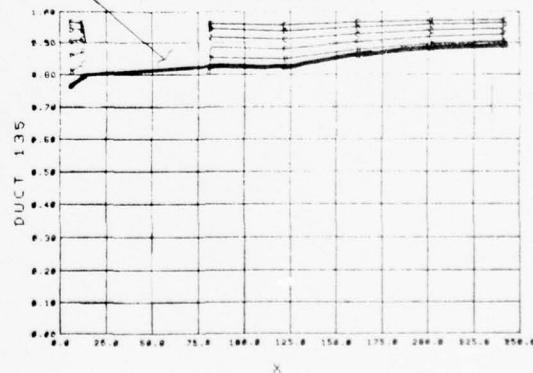
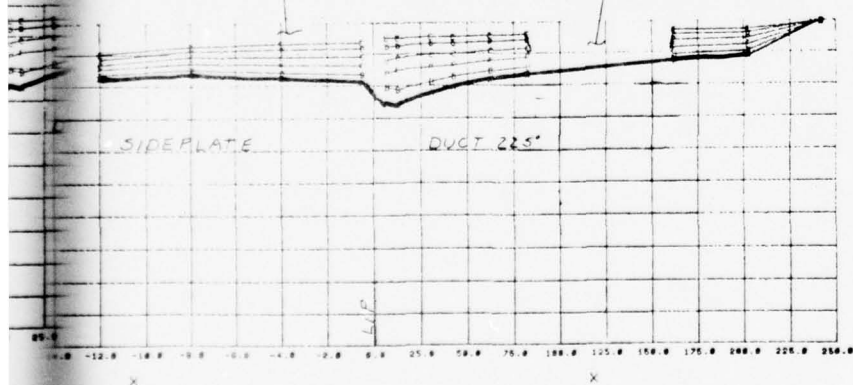


Figure 29. $M_0 = 0.5$ inlet-flow-field data for t at B.L. 45.64 at $\alpha = 2^\circ$ and $\beta = 0^\circ$



S.S. PORT 103.000
 POINT 1.000
 MECH 0.503
 ALPH 1.981
 REFR 0.018
 RECL 0.974
 PANS-MCO 0.012
 LOC-MAX 0.051
 LOC-MIN 0.023
 WETS 3.4408
 EDU-MAX 0.482
 D/L 0.042

OUTBOARD



$\alpha = 2^\circ$ $\beta = 0^\circ$ SHORT-PLow/SPLITTER-PLATE INLET
 PART RANGE IS 10301 THRO 10307

e S₁ low-field data for the Short-Plow/Splitter-Plate Inlet
 $\alpha = 2^\circ$ and $\beta = 0^\circ$

subsonic Mach number) that was not available from the earlier 16S tests at Mach 0.5.

F.S. 390 fuselage boundary-layer data as a function of angle of attack and angle of sideslip are presented in Figure 30. These data are very similar to the data obtained at Mach 1.6 and show that a body vortex is not present. The presented data also shows that locating the inlet at B.L. 43.82 provides adequate standoff distance from the fuselage for the inlet to receive high-energy air.

Right-hand inlet throat-pressure contour maps for the Basic Inlet located at B.L. 43.82 are shown in Figure 31. These data are for an inlet corrected airflow of 310 lb/sec for the angle-of-attack and sideslip angles of Figure 30. It can be seen from these throat maps that an increase in low-energy air on the inboard wall occurs as the angle of attack is increased. The source of the low-energy air could be due to spillage of the fuselage-boundary-layer air into the inlet, due to the lack of compression on the splitter plate because it was parallel to the centerline of the model, or due to a vortex that may be generated along the swept leading edge of the splitter plate because it is at an angle of attack to the approaching flow. To alleviate the source of the low-energy air, some cambering (inboard) of the plate leading edge could possibly help. Additional testing would be necessary to verify that cambering would alleviate this flow condition, but it appears to be a problem that can be readily solved.

The compressor-face maps shown in Figure 32 completes the data for analysis of the 310-lb/sec flow conditions. Evidence of the duct bend and inboard low-energy air is apparent. However, as angle of attack is increased, the high-energy air goes to the lower portion of the duct.

To complete the flow-field analysis at Mach 0.85 for the Basic Long-Flow/Splitter-Plate Inlet at B.L. 43.82, Figures 33 and 34 are presented. The data in Figure 33 show the effect of angle of attack for the high-airflow (357-lb/sec) case, and the data in Figure 34 show similar data for an airflow excursion at 5° angle of attack.

4.1.4 Mach 1.2

A set of fuselage boundary-layer data and a corresponding set of throat-map data are presented for Mach 1.2 in Figures 35 and 36 for the Basic Long-Plow/Splitter-Plate Inlet located at B.L. 43.82. Figure 37 is a composite data plot for the 5° -angle-of-attack and 0° -angle-of-sideslip test condition. The observations and comments made at the other Mach numbers also apply at Mach 1.2.

4.1.5 Research Model Flow Field Versus Mach Number

A survey of the research model inlet flow field from Mach 0.85 to Mach 1.6 is shown in Figure 38. The significant observations are that the throat-pressure defect deepens and encompasses a larger portion of the throat area as the freestream Mach number increases. It also appears that the throat-pressure defect moved up from the Throat Rakes 4-5 position to the Throat Rake 3 position when the inlet was in the more outboard position. Thus, the more outboard position (or increasing the inlet standoff distance) does not alleviate the spillage into the inlet. This tends to fortify the theory that fuselage-boundary-layer air is spilling into the inlet due to insufficient flow divergence and that improving the fuselage boundary-layer system is necessary to improve inlet flow conditions that will result in better engine/inlet compatibility. Improving inlet performance and engine/inlet compatibility by improving the fuselage boundary-layer system appears to be more desirable than moving the inlet outboard because it can be done without increasing an airplane's cross-sectional area.

An examination of the compressor-face maps in Figure 38 reveals that the fundamental pattern is unchanged. The throat-pressure defect simply divides. Some of the lower-energy air moves up to the 315° position while the rest moves to the 225° or 180° position. At a first glance it might be concluded that this is not true at Mach 1.6. However, further examination of Figure 25a reveals that it is also true at the higher airflows.

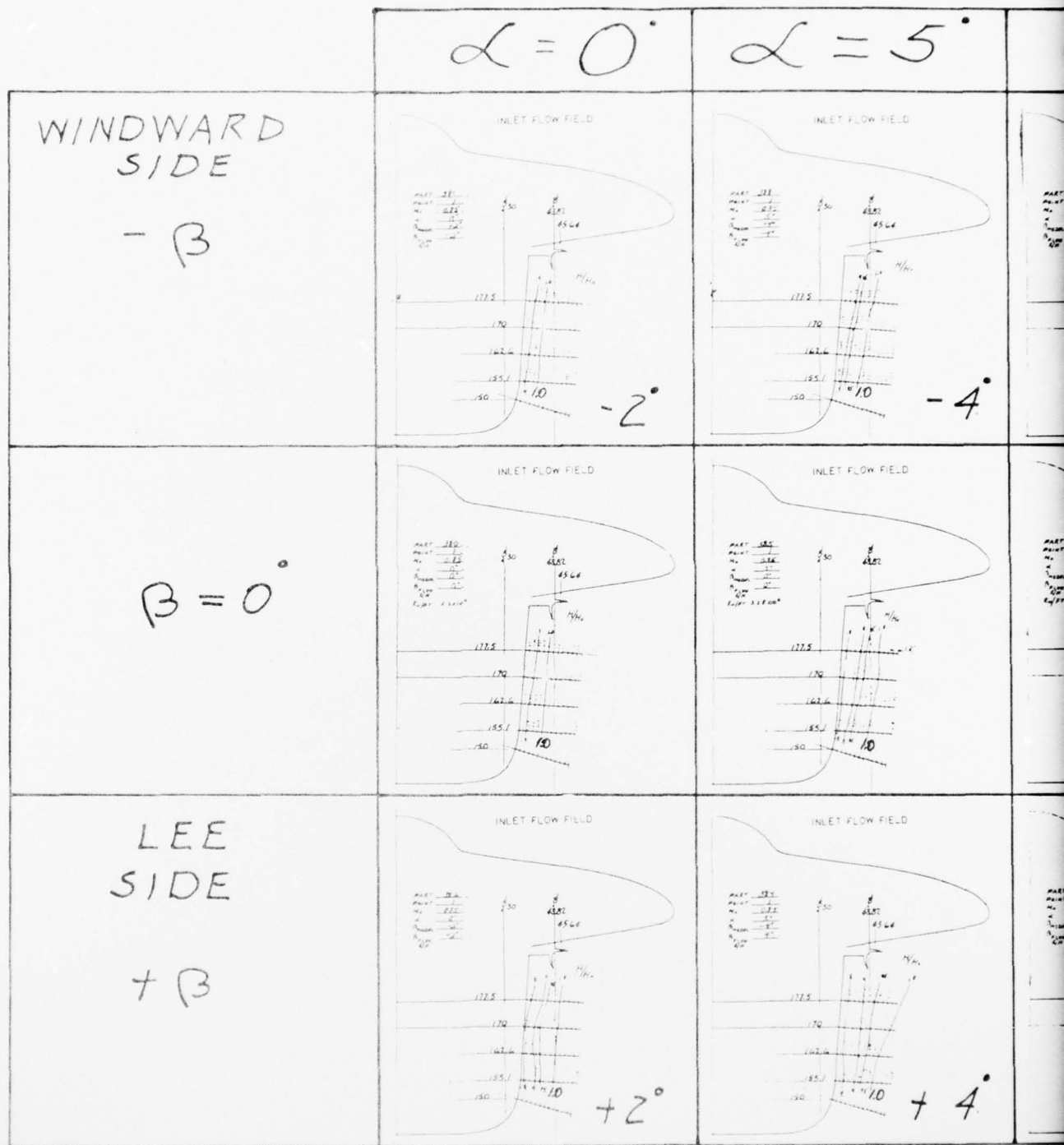
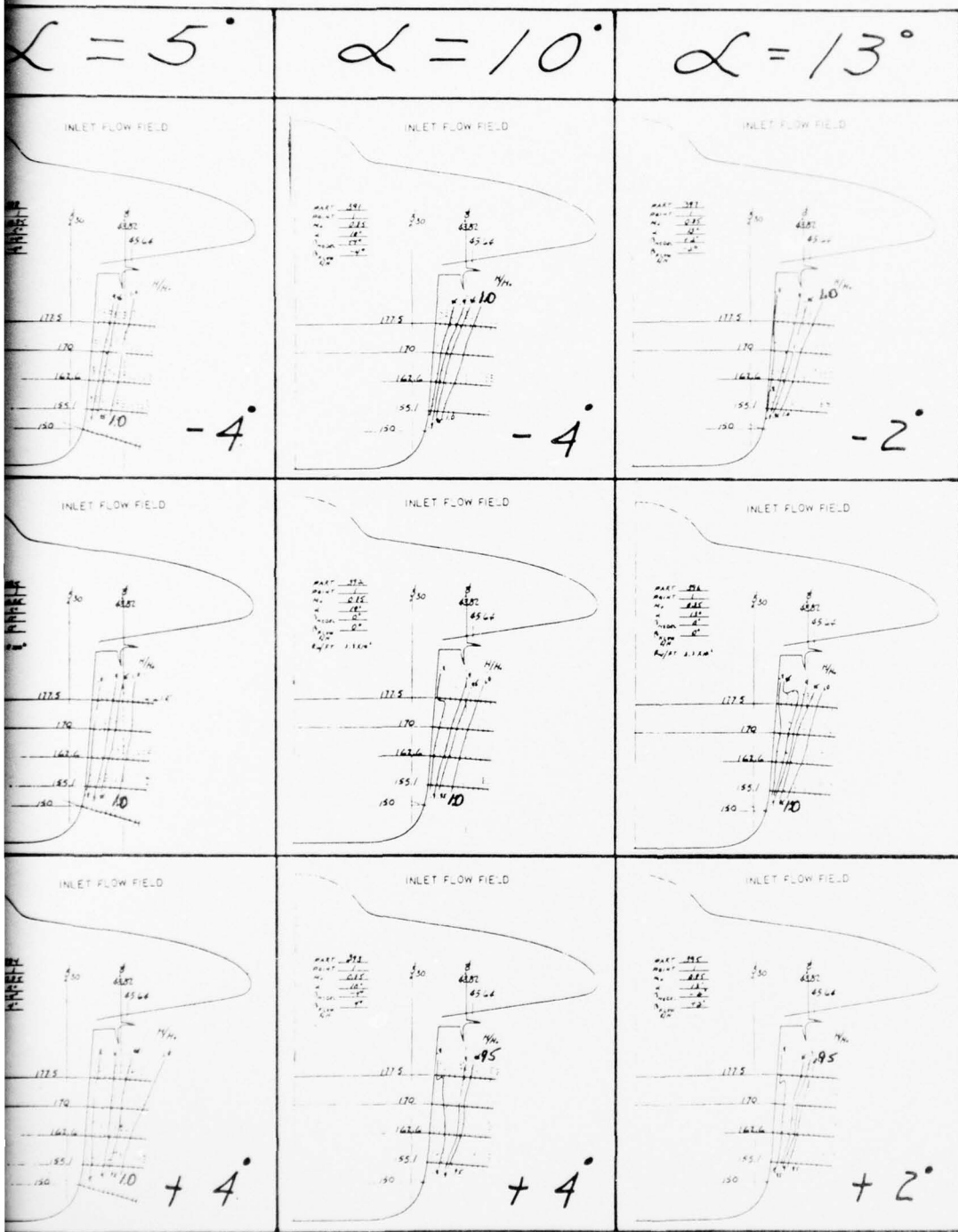


Figure 30. $M_0 = 0.85$ fuselage flow field at F



BEST AVAILABLE COPY

Fuselage flow field at F.S. 390.

PRECEDING PAGE BLANK NOT FILMED

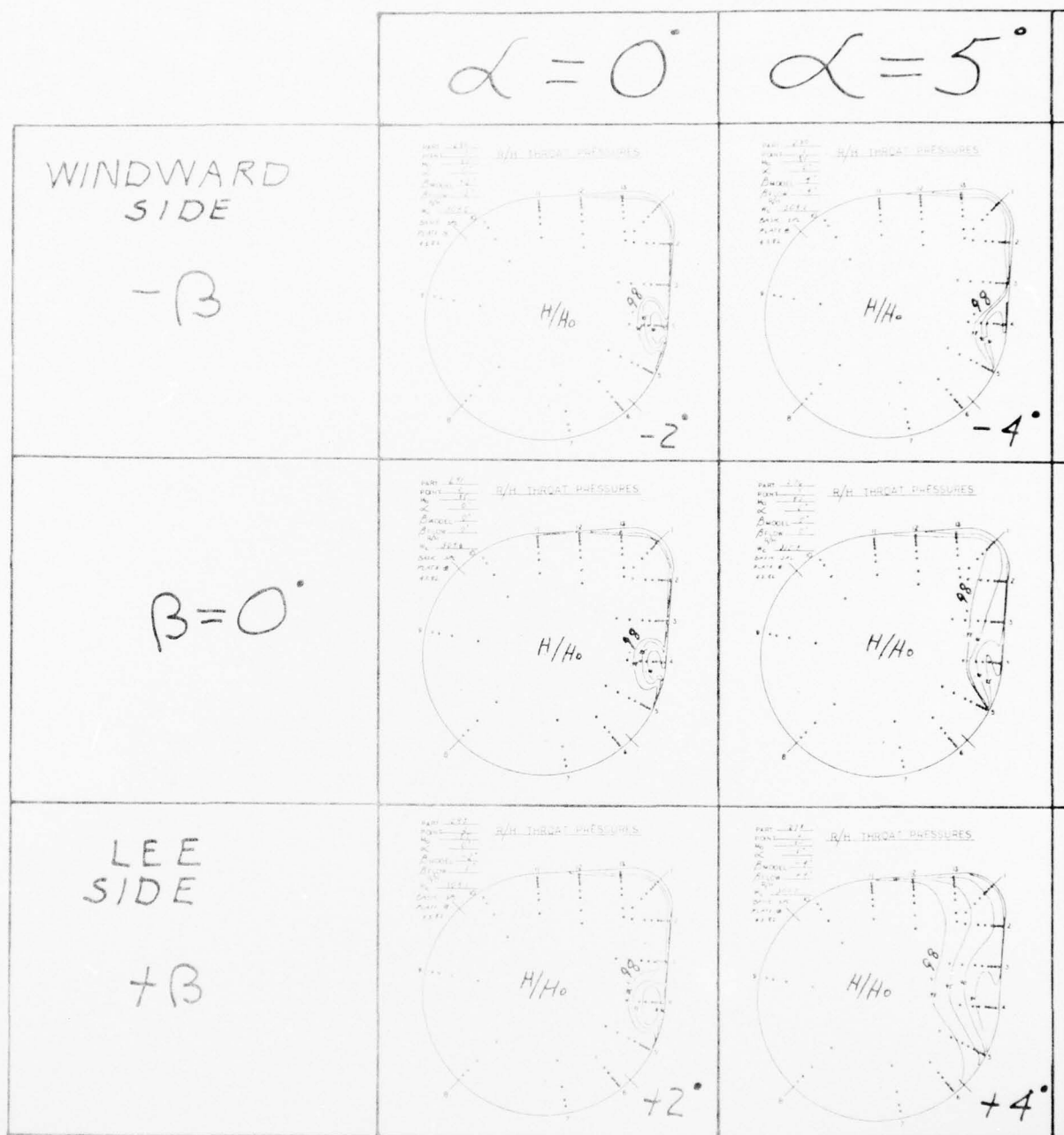
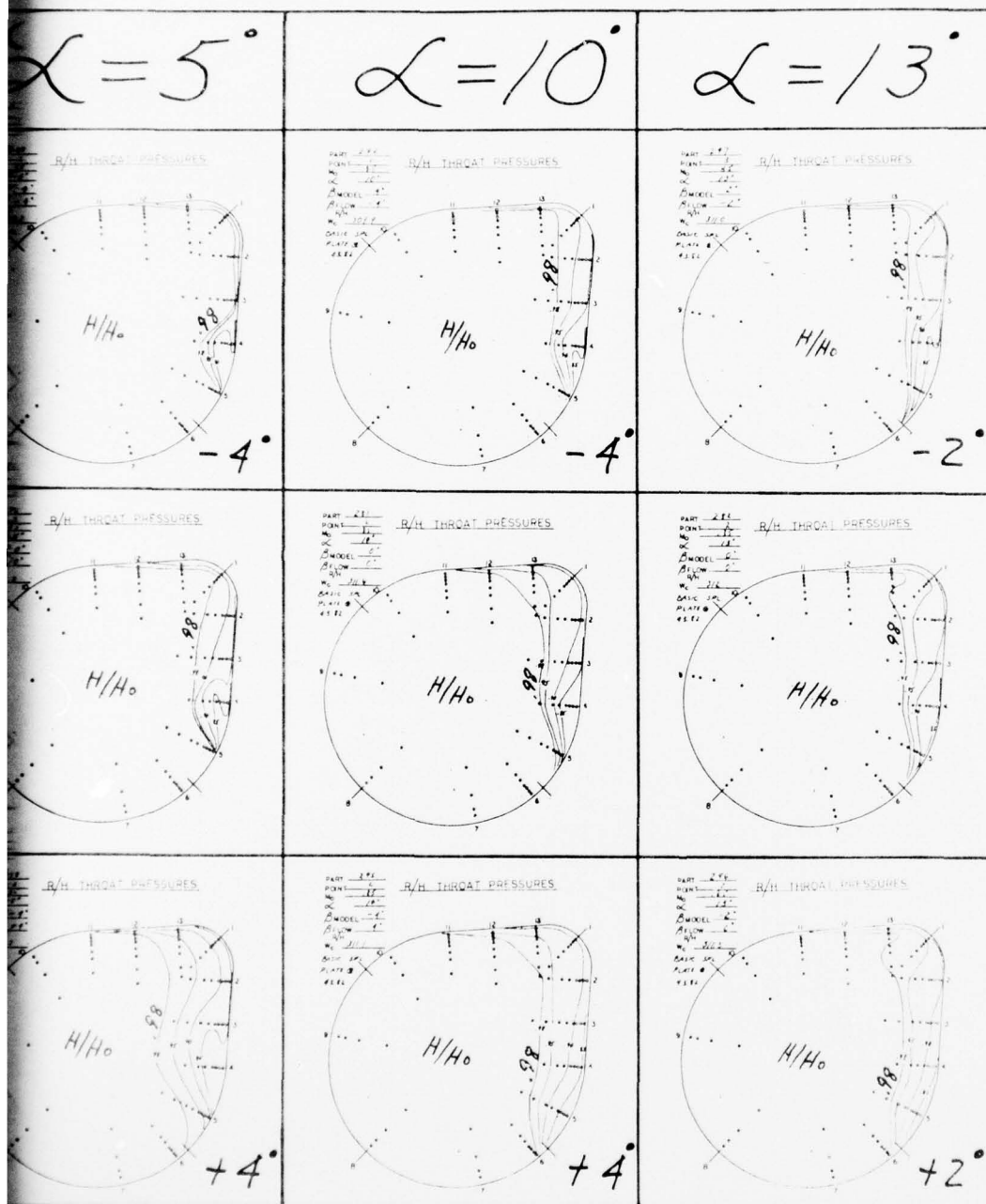


Figure 31. $M_0 = 0.85$ throat-rake contour maps for the F
Plate Inlet at B.L. 43.82 at $W_c = 310$ pps.

2

BEST AVAILABLE COPY



Contour maps for the Basic Long-Flow/Splitter-
 32 at $w_c = 310$ pps.

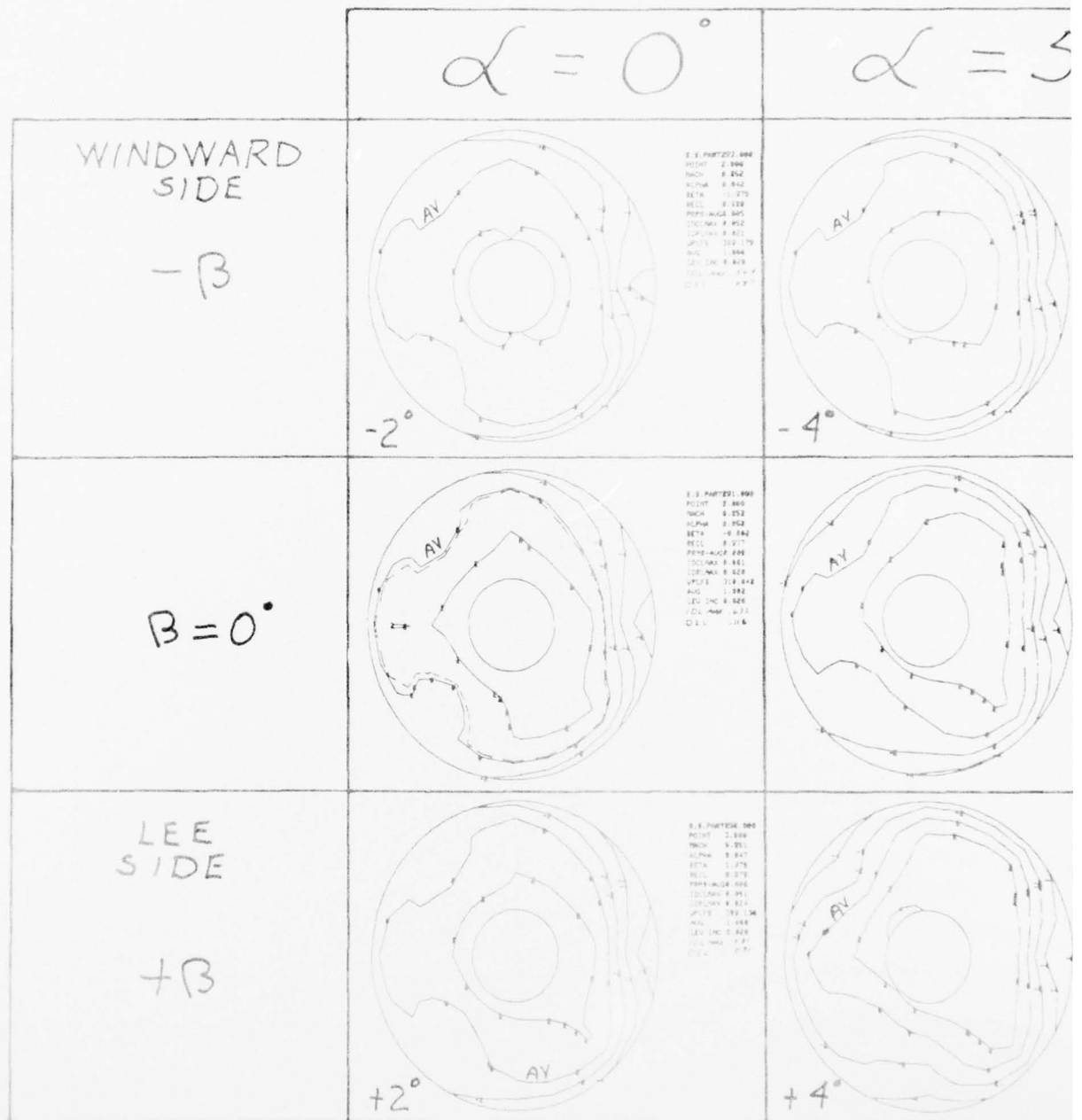
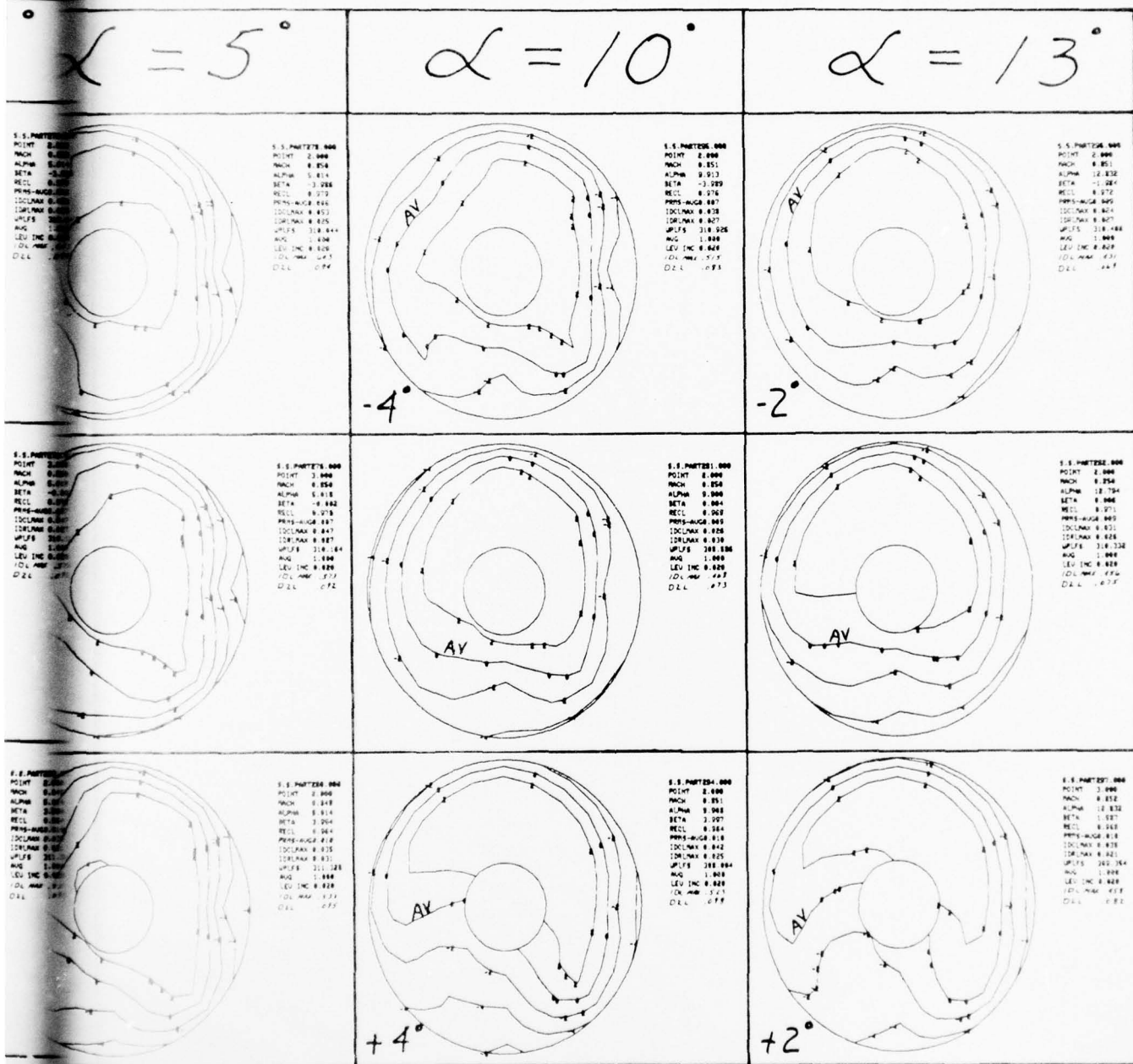


Figure 32. $M_0 = 0.85$ compressor-face-rake contour
Splitter-Plate Inlet at B.L. 43.82 at W

2

BEST AVAILABLE COPY



ps for e-rake contour maps for the Basic Long-Plow/
= 31 B.L. 43.82 at $W_c = 310$ pps.

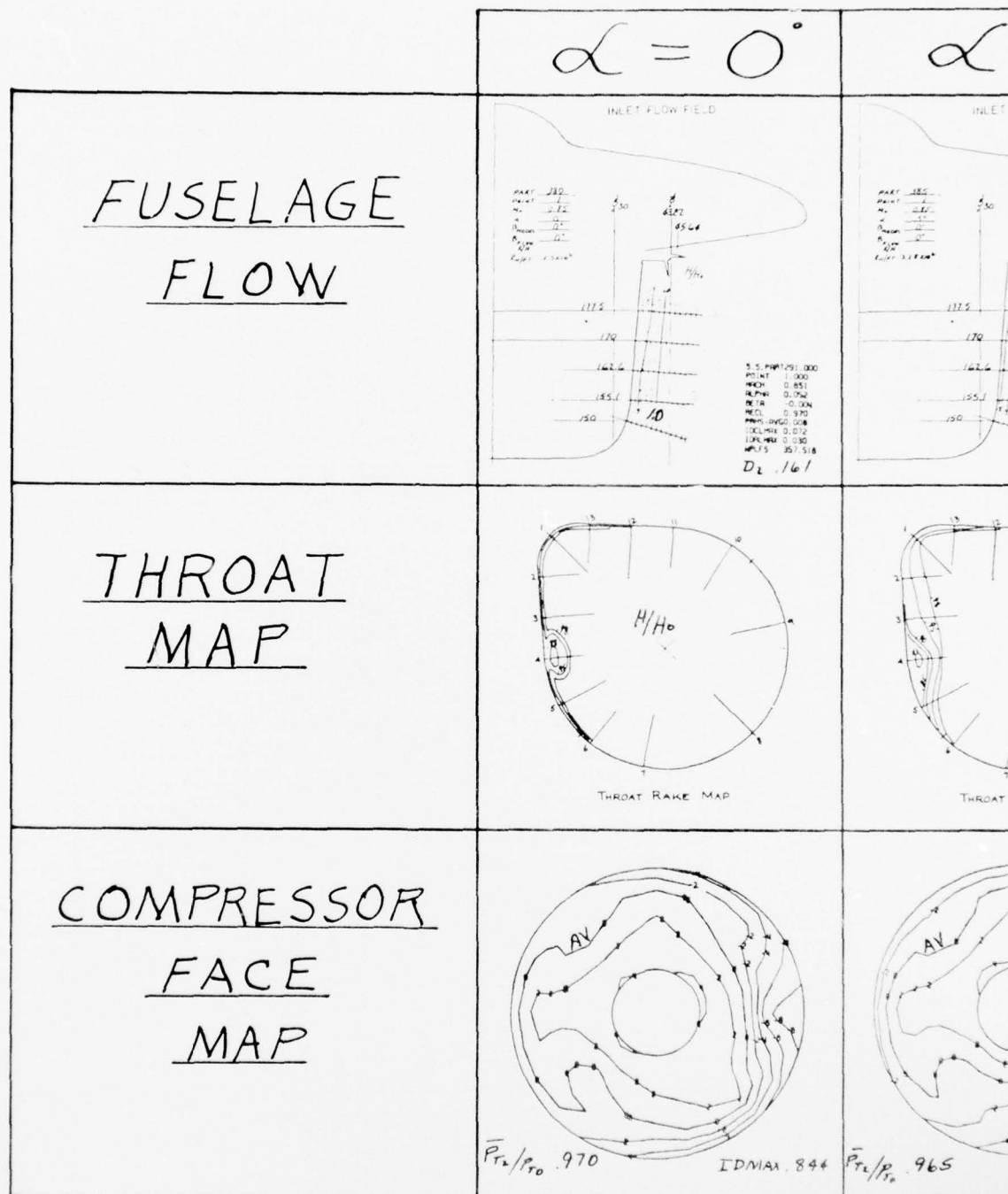
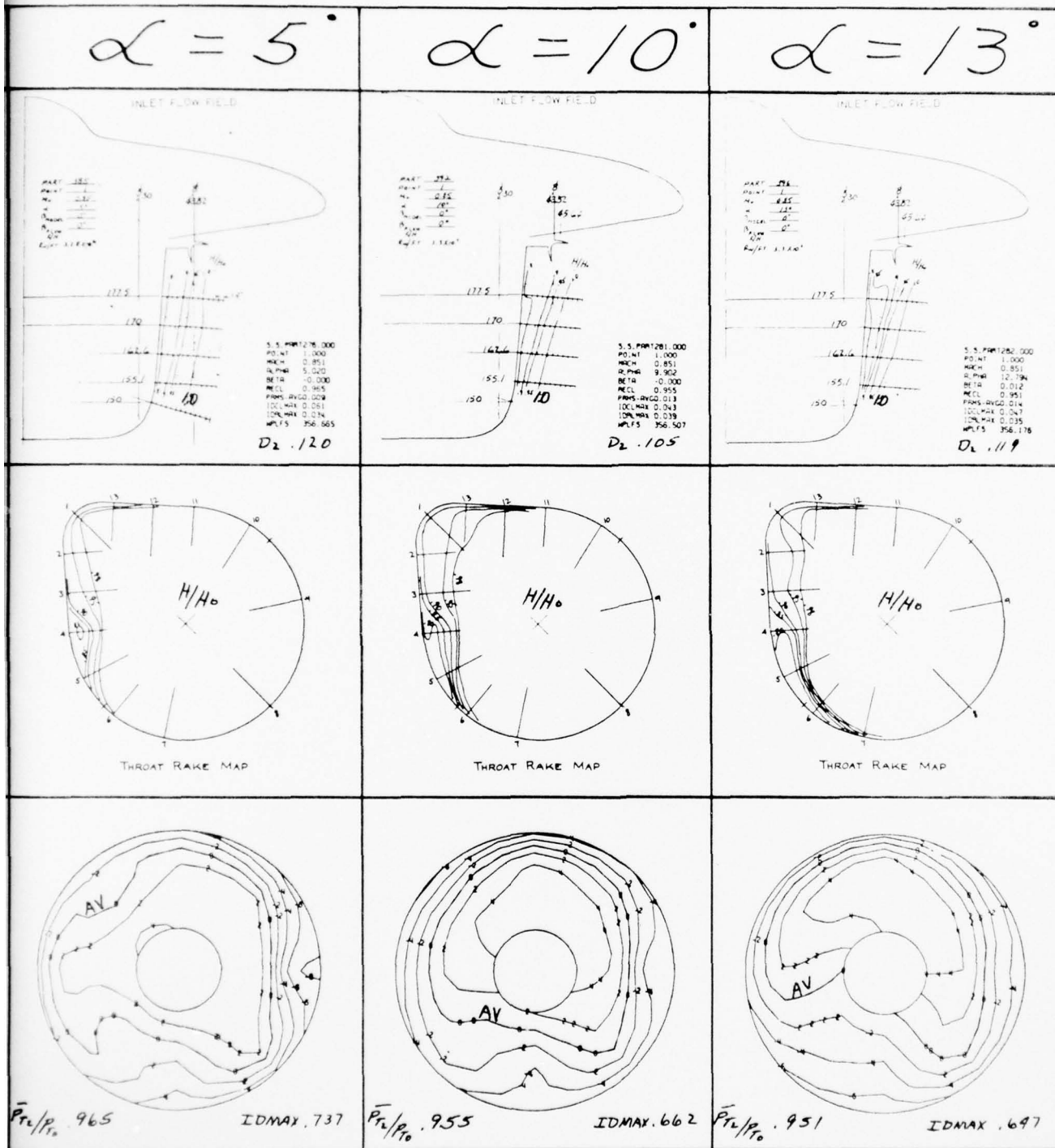


Figure 33. $M_0 = 0.85$ inlet flow field versus Basic Long-Flow/Splitter-Plate



ow field versus angle of attack ($\beta = 0^\circ$) for the litter-Plate Inlet at B.L. 43.82 at $W_c = 357$ pps.

PRECEDING PAGE BLANK-NOT FILMED

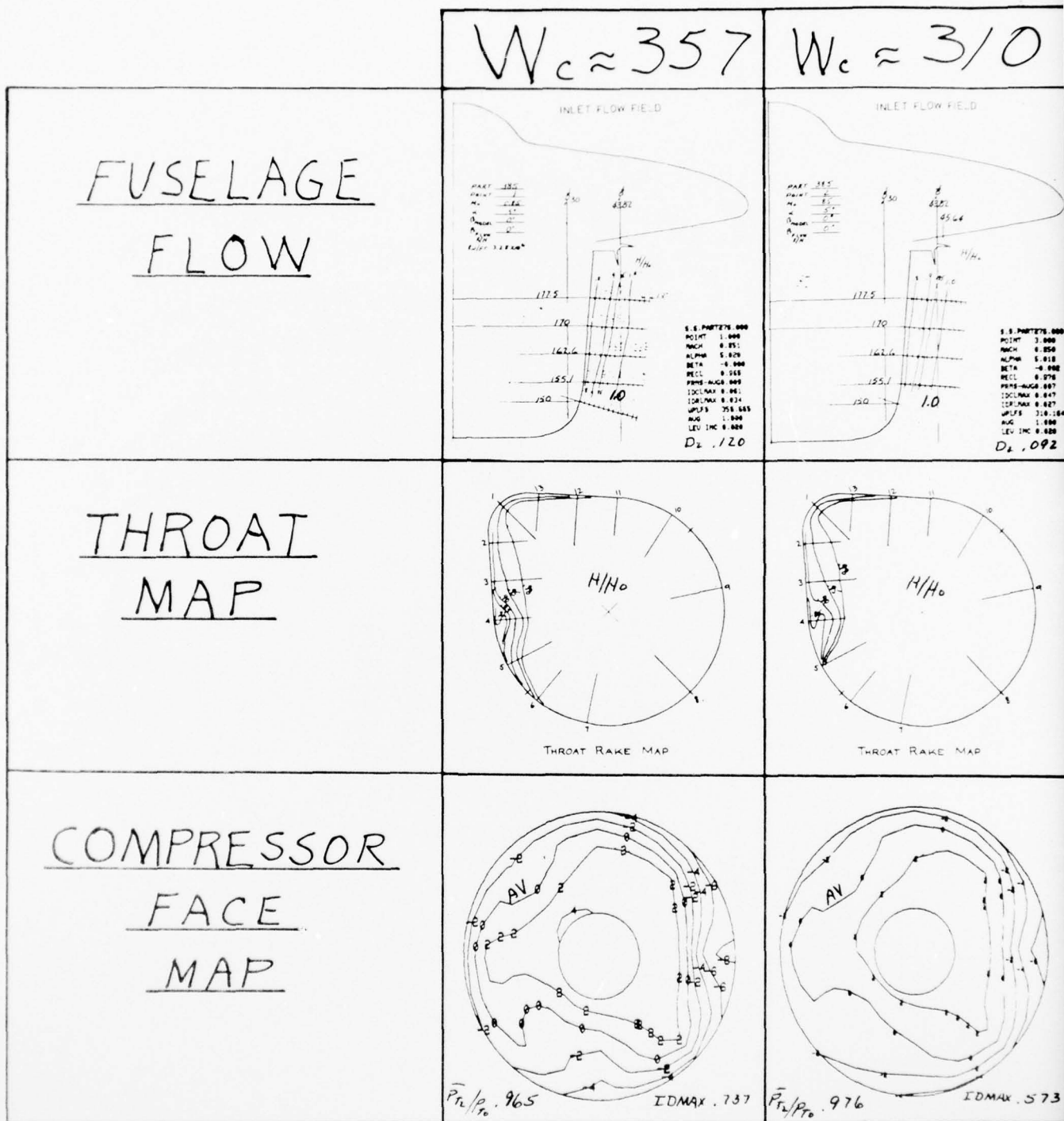
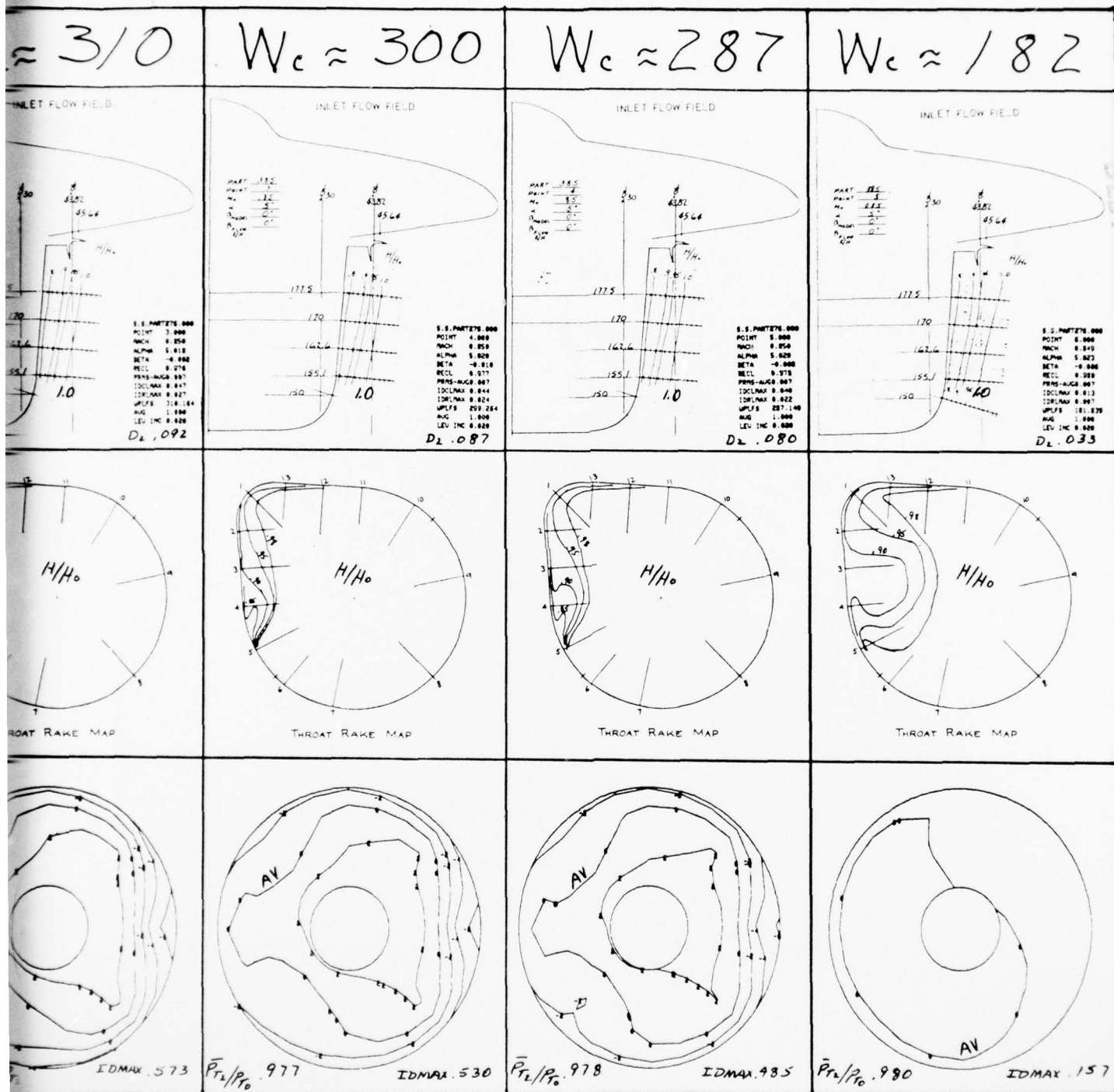


Figure 34. $M_0 = 0.85$ inlet-flow-field data
Basic Long-Flow/Splitter-Plate



flow-field data during an airflow excursion for the Splitter-Plate Inlet at B.L. 43.82 at $\alpha = 5^\circ$ and $\beta = 0^\circ$.

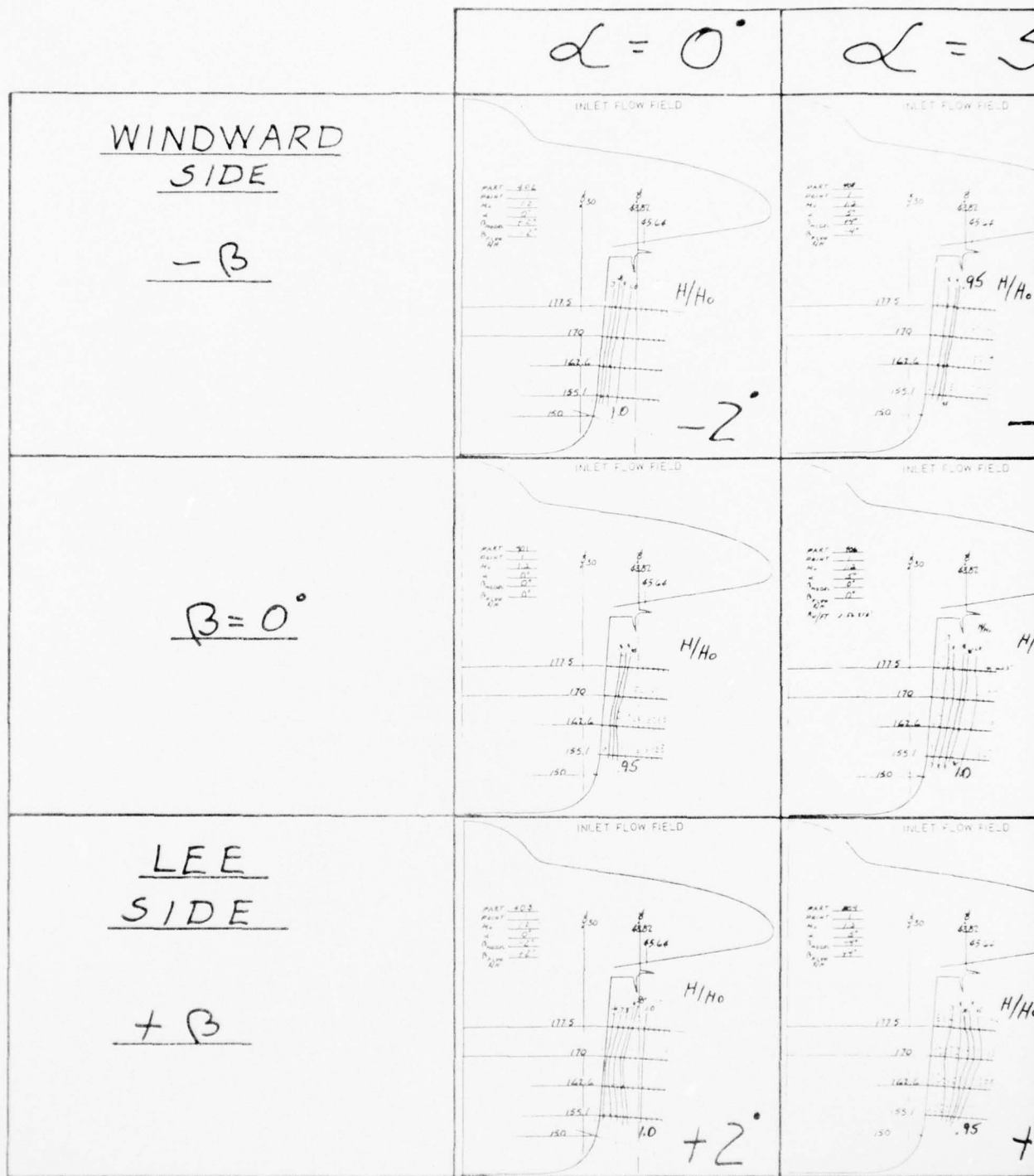
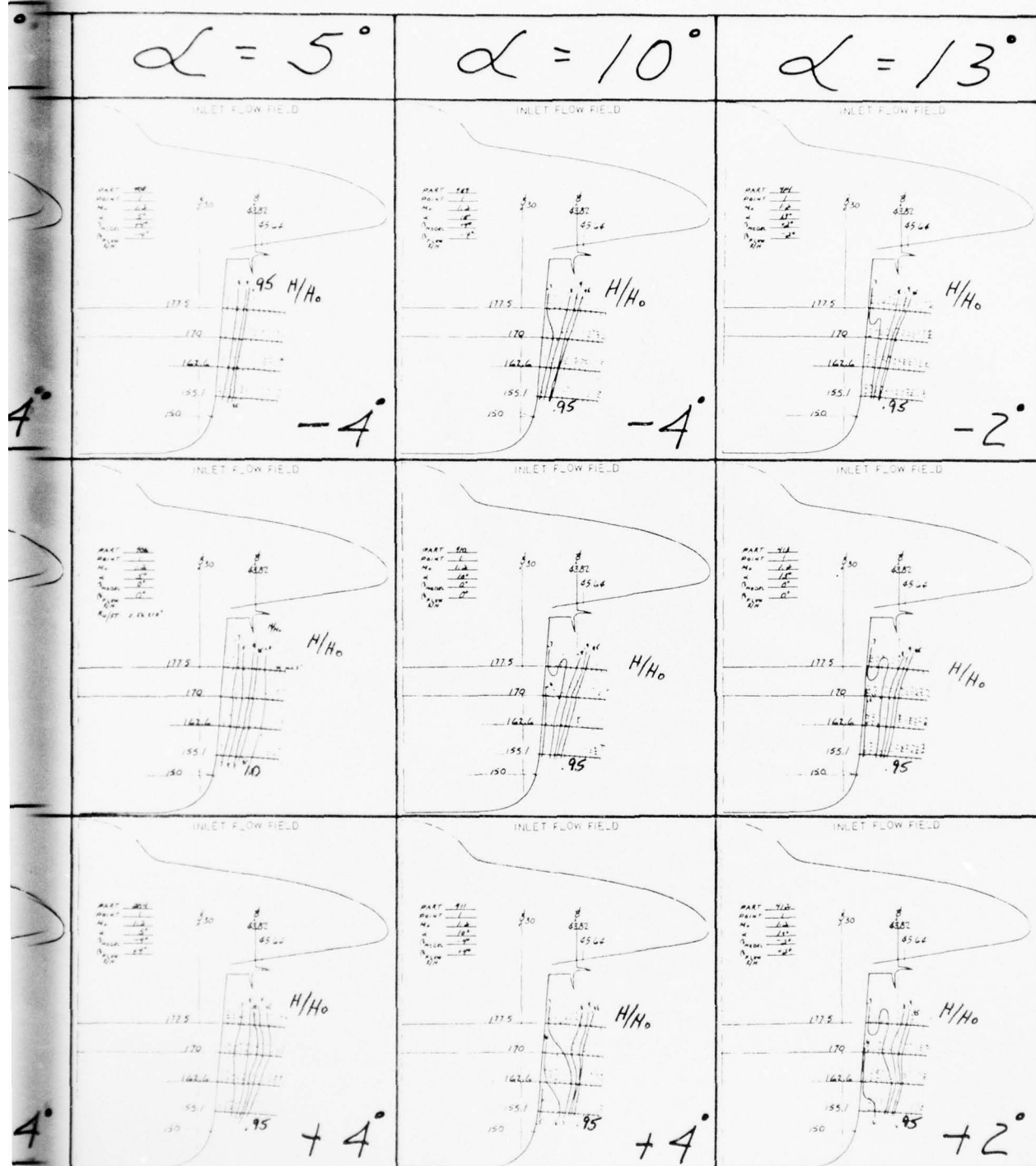


Figure 35. $M_0 = 1.2$ fuselage flow

BEST AVAILABLE COPY



$f_{M_0} = 1.2$ fuselage flow field at F.S. 390.

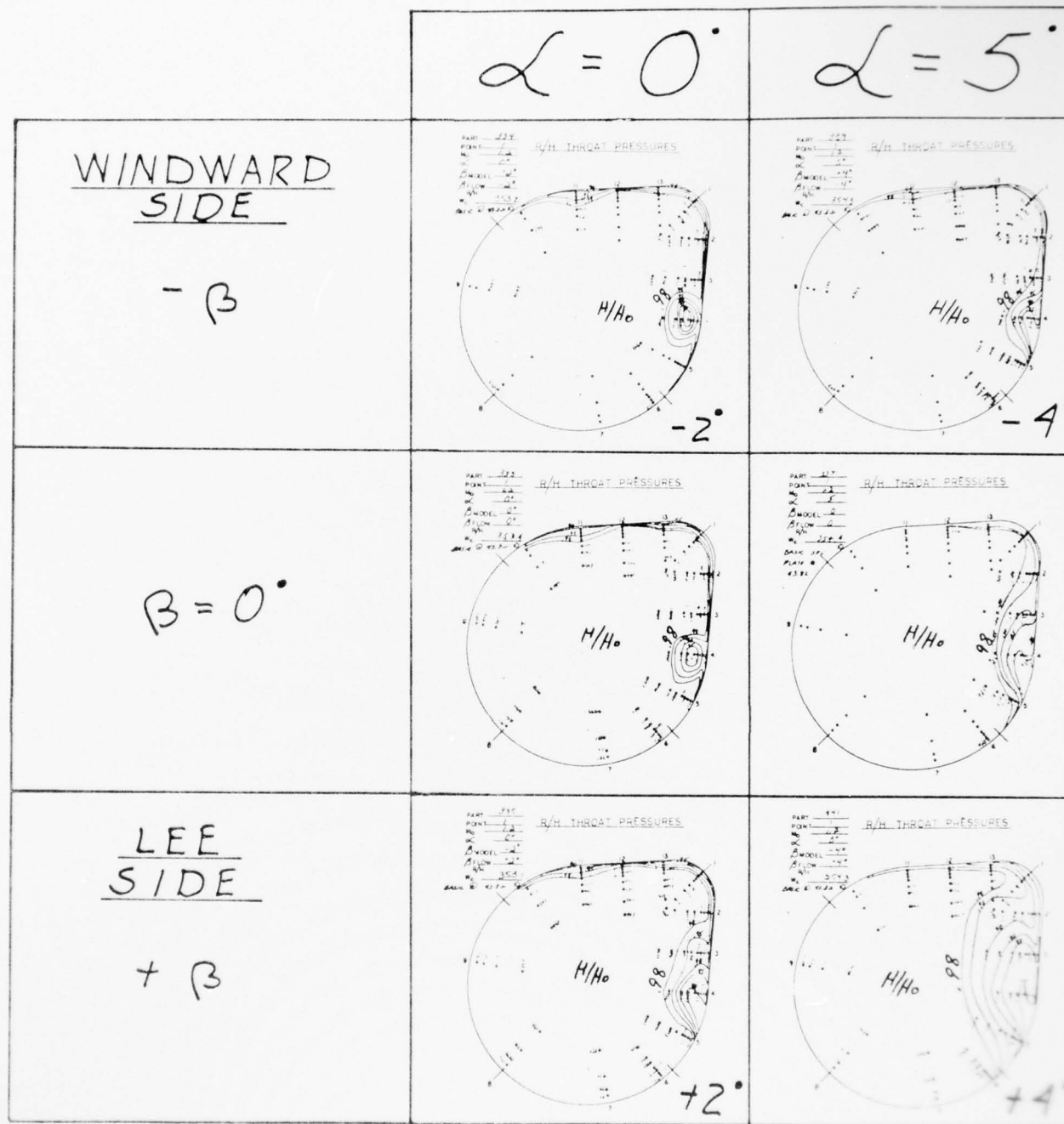


Figure 36. $M_0 = 1.2$ throat-rake contour maps for the
Inlet at B.L. 43.82 at $W_c = 354$ pps.

AD-A040 707

GENERAL DYNAMICS/FORT WORTH TEX FORT WORTH DIV
ASD ADVANCED PROGRAM RESEARCH INLET DATA ANALYSIS REPORT FOR 1/--ETC(U)
JAN 77 C C MANN, J.E GARNER

F/G 21/5

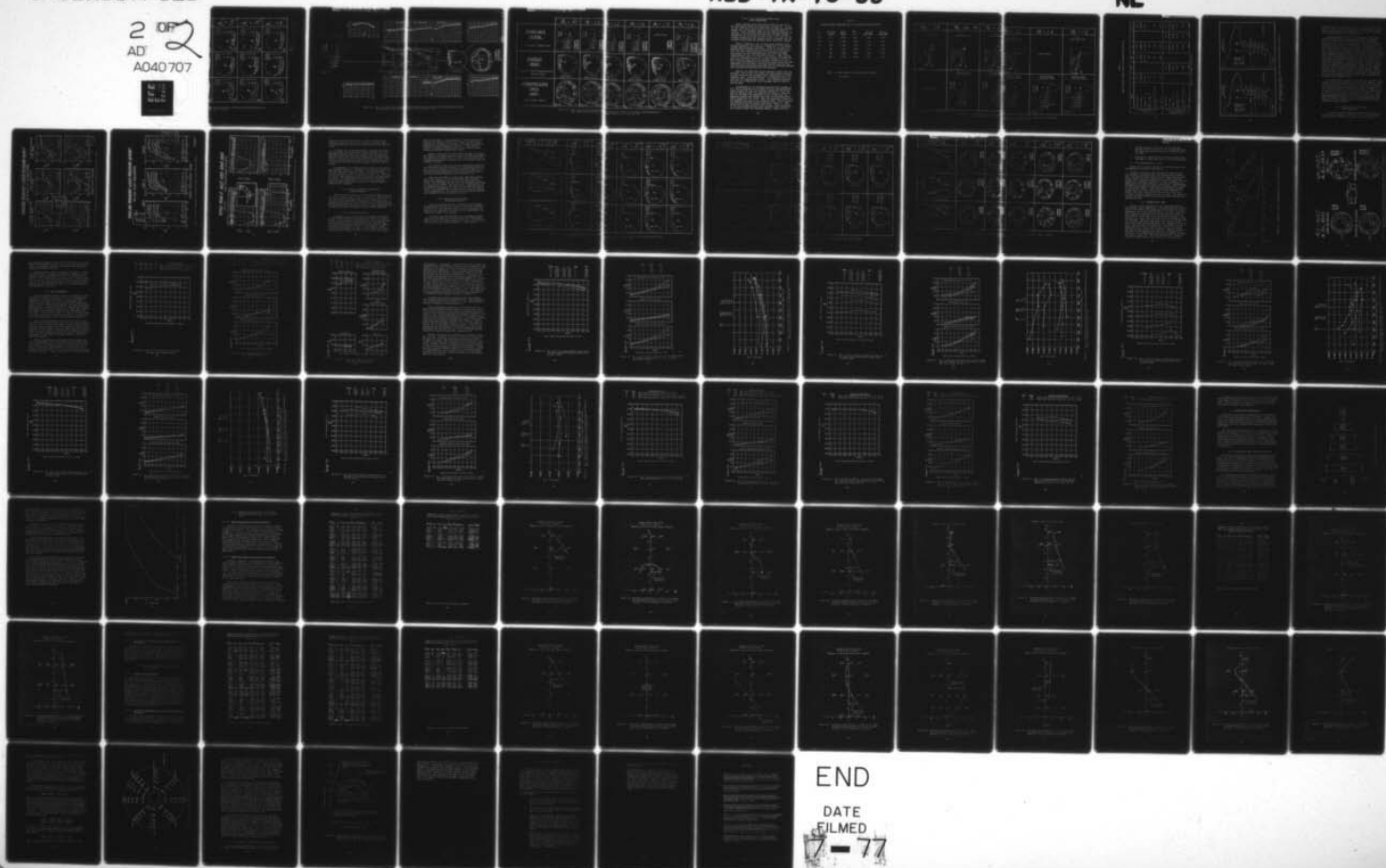
F33615-75-C-5289

UNCLASSIFIED

ASD-TR-76-35

NL

2 OF 2
AD
A040 707

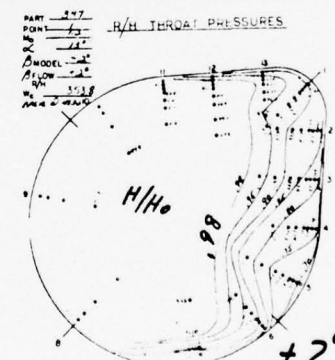
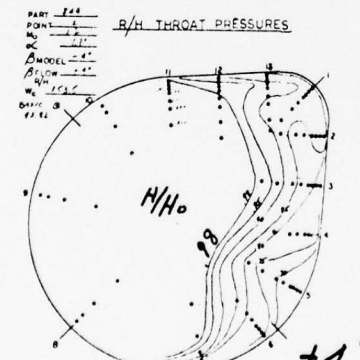
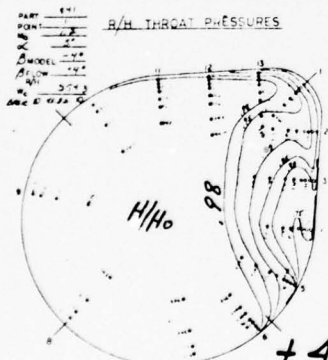
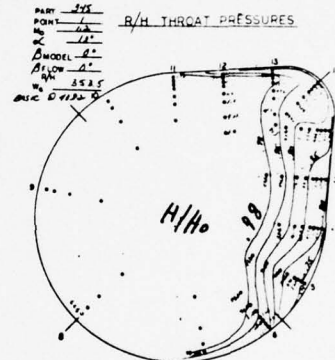
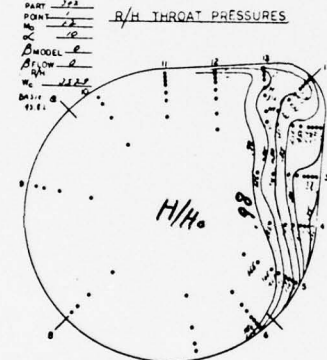
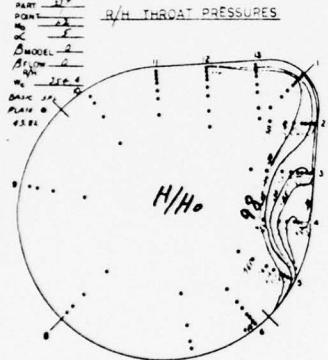
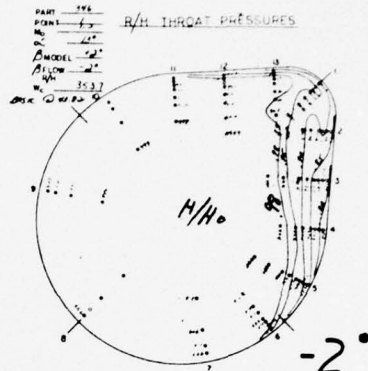
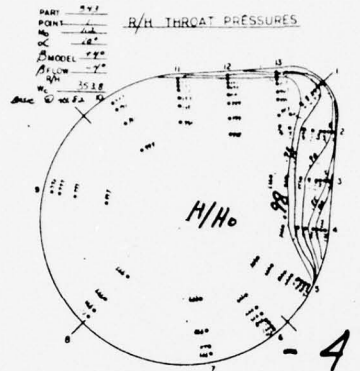
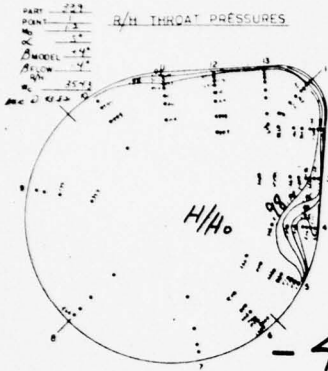


BEST AVAILABLE COPY

$\alpha = 5^\circ$

$\alpha = 10^\circ$

$\alpha = 13^\circ$



2°

ake contour maps for the Basic Long-Plow/Splitter-Plate
82 at $W_c = 354$ pps.

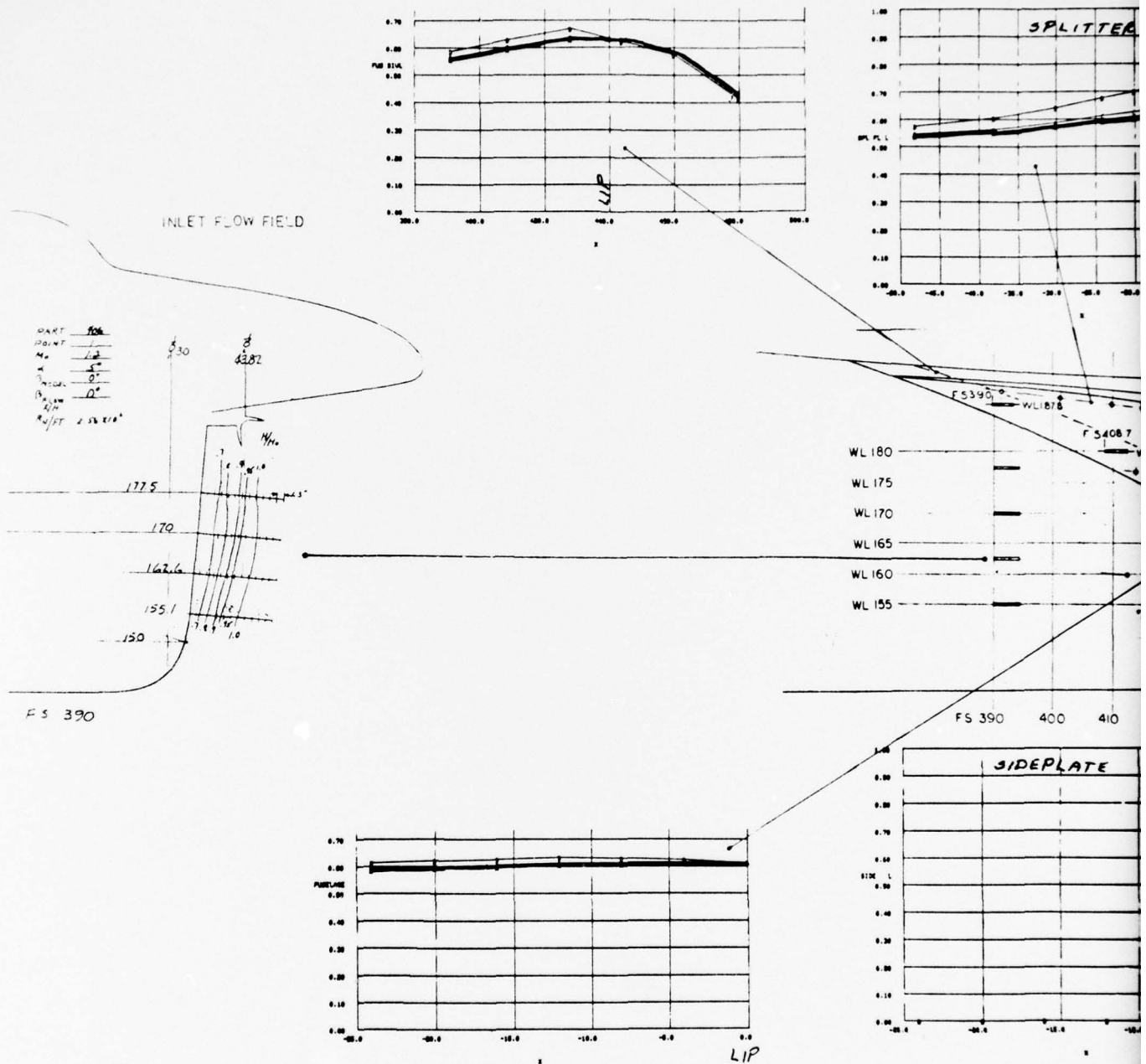
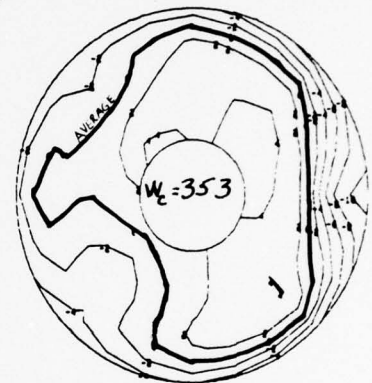
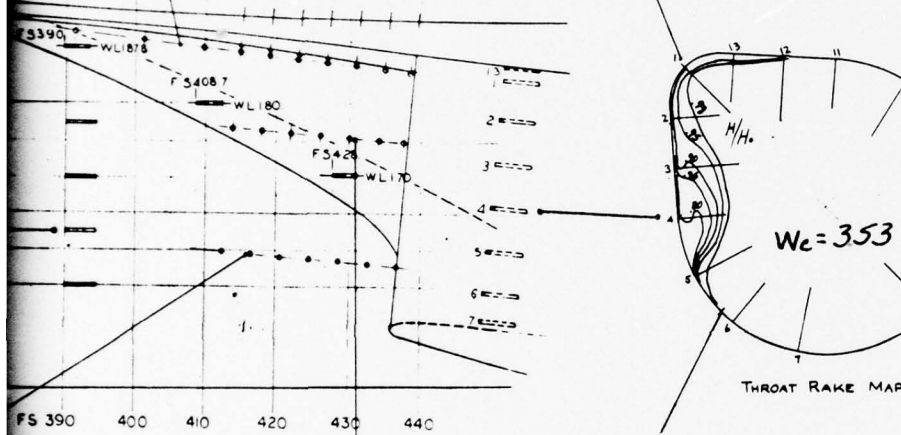
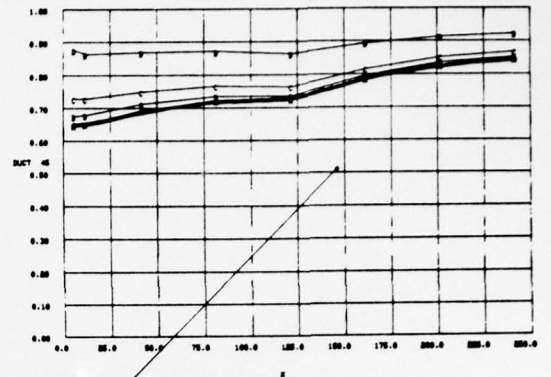
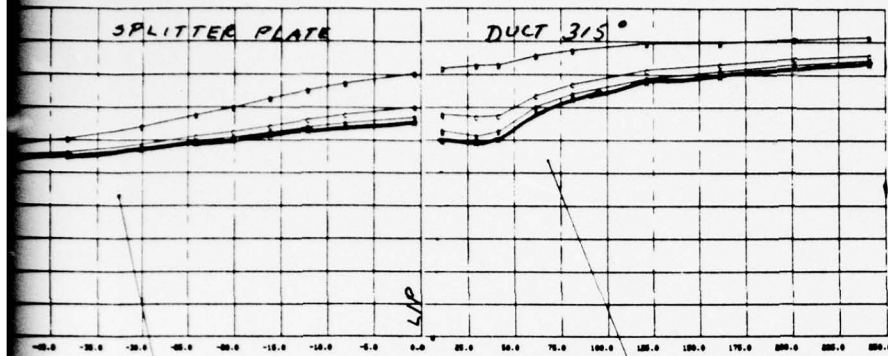


Figure 37. $M_0 = 1.2$ inlet-flow-field
Inlet at B.L. 43.82 at $\alpha = 0^\circ$

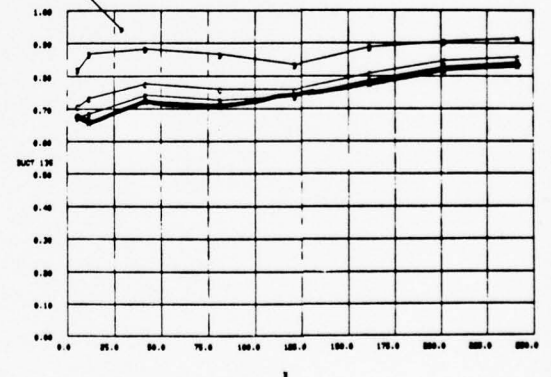
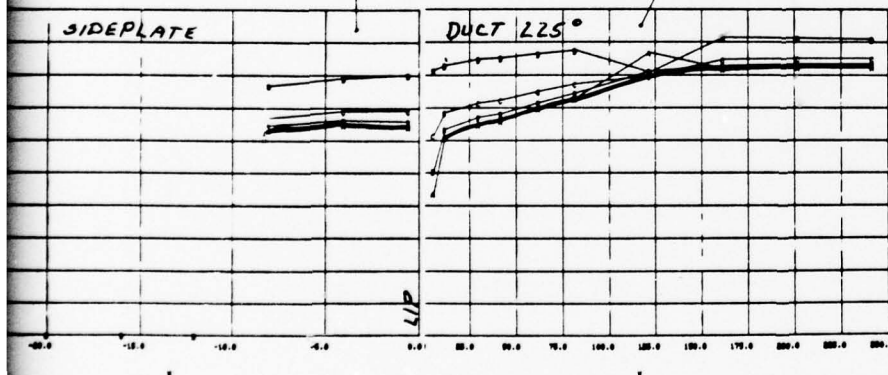


```

S.S.PART337.000
POINT 1.000
RACH 1.200
ALPHA 5.0:0
BETA -0.004
RECL 0.950
PMS-AUG3.0:1
IDCLMAX 0.070
IDCLMAX 0.030
JWFS 353.0:0
AUG 1.000
LEV INC 0.020

```

→ OUTED



t-flow-field data for the Basic Long-Flow/Splitter-Plate
43.82 at $\alpha = 5^\circ$ and $\beta = 0^\circ$.

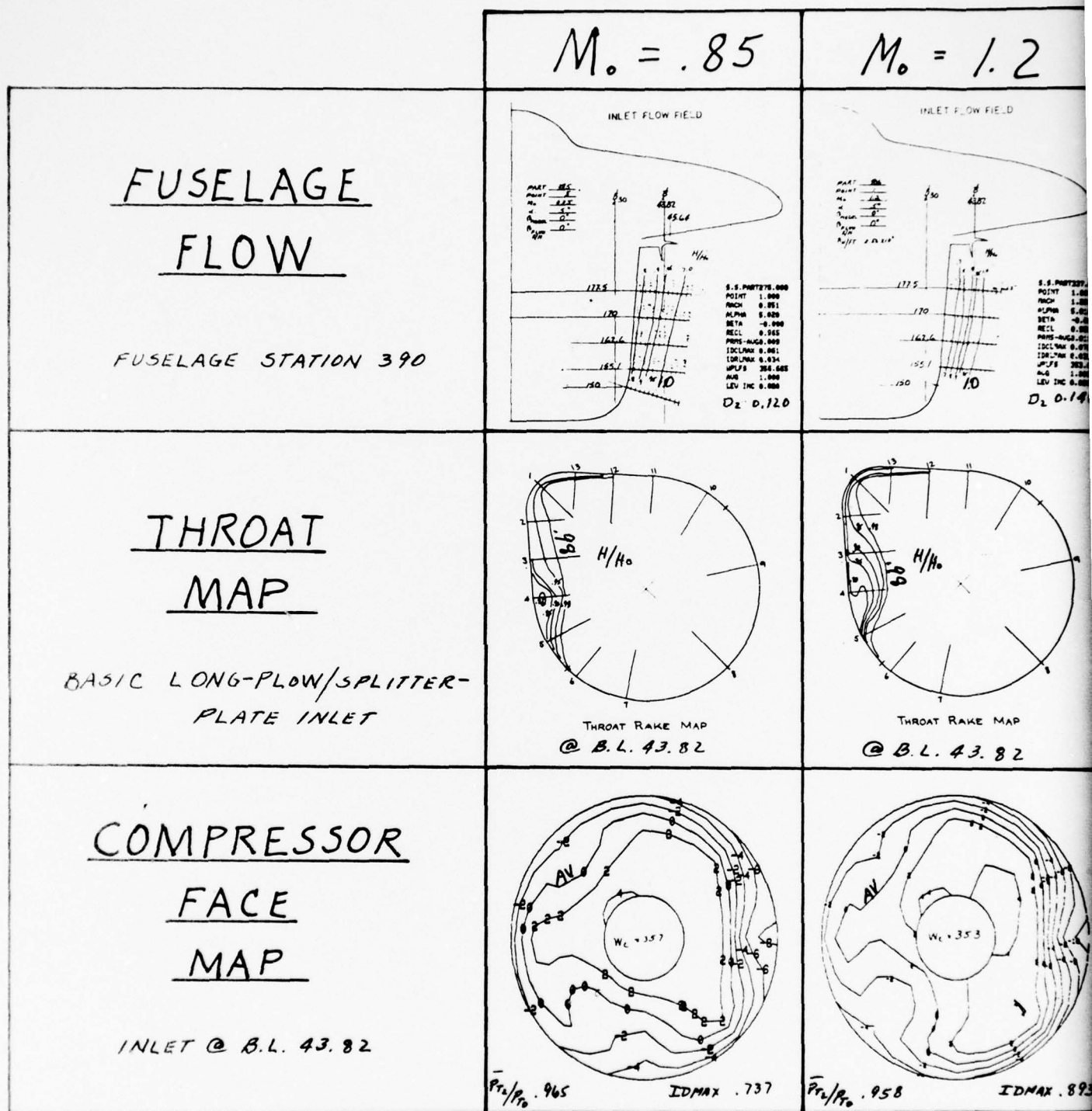
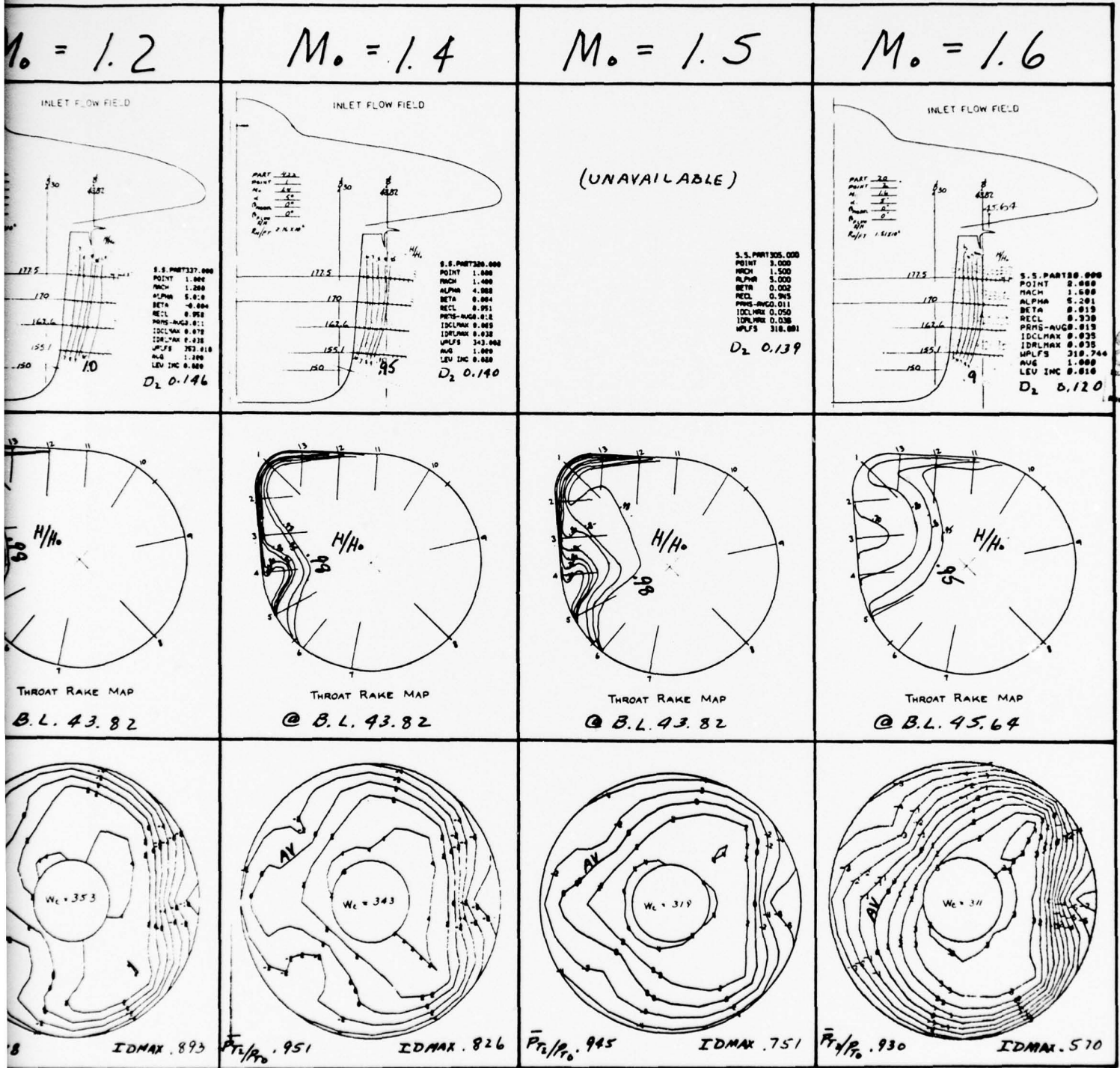


Figure 38. Inlet flow field versus Mach number
Plate Inlet at B.L. 43.82 at $\alpha = 0^\circ$



d versus Mach number for the Basic Long-Flow/Splitter-
B.L. 43.82 at $\alpha = 5^\circ$ and $\beta = 0^\circ$.

4.1.6 F-111 and Research-Model Flow Field Comparisons

Model fuselage flow-field survey data for the F-111 and the research model are presented in Figure 39. It can be seen from these contour plots that the flows are similar except that the boundary layer on the research model is thicker. Some increased thickness was expected because the fuselage on the research model extends 73 inches further forward of the inlet than it does on the F-111, but the increased thickness on the research model is greater than anticipated from turbulent boundary-layer flat-plate theory.

Table 3 contains a list of flat-plate boundary-layer heights predicted, with the aid of Reference 4, for several assumed Mach-altitude conditions. Shown in the table are boundary-layer thicknesses calculated at F.S. 390 and F.S. 440. For the conditions shown, the predicted increased thicknesses for the research model over the F-111 would range between 1 and 1.2 inches (full scale). Thus, moving the inlet outboard to B.L. 45.64 (the location at which the splitter-plate-rake data were recorded at Mach 1.6) from B.L. 43.82 (a movement of 1.82 inches) should have more than compensated for the added thickness expected and the flow into the inlet should have been good if the fuselage boundary-layer system was accepting its flow properly.

However, an additional factor possibly enters into the analysis. All of the F-111 model test data shown in Figure 39 were obtained with boundary-layer transition grit on the fuselage nose. As stated earlier, no transition strip was used for the research model tests. This omission possibly resulted in an abnormally thick boundary layer on the research model.

A comparison of the fuselage-boundary-layer heights at F.S. 390 as measured on the models and the calculated flat-plate heights for the test Reynolds numbers for the F-111 and the research model are presented in Table 4. When the data in the table are examined, it can be seen that the measured heights were always less than the calculated flat-plate heights for the F-111. With the exception of Mach 1.6, the opposite was true on the research model. And the greatest difference (0.418 inches) occurred at Mach 1.2. The difference at Mach 0.85 was 0.384 inches. Shown in Figure 40 are the calculated flat-plate boundary-layer heights for the research model test Reynolds number, relative to the

Table 3

RESEARCH MODEL PREDICTED FLAT-PLATE BOUNDARY-LAYER HEIGHTS

<u>M_O</u>	<u>Altitude- Feet</u>	<u>R_N/Ft X10⁻⁶</u>	<u>δ/l</u>	<u>δ - in. (Sta.390)</u>	<u>δ - in. (Sta.440)</u>
.55	S.L.	3.905	.016	7.46	8.26
.85	S.L.	6.035	.0154	7.18	7.95
.85	30K	2.420	.0167	7.78	8.62
1.4	30K	3.987	.0159	7.41	8.20
1.6	50K	1.888	.0169	7.88	8.72
2.0	50K	2.359	.0165	7.69	8.51

NOTE: l = 466 inches at Sta.390 and 516 inches
at Sta.440

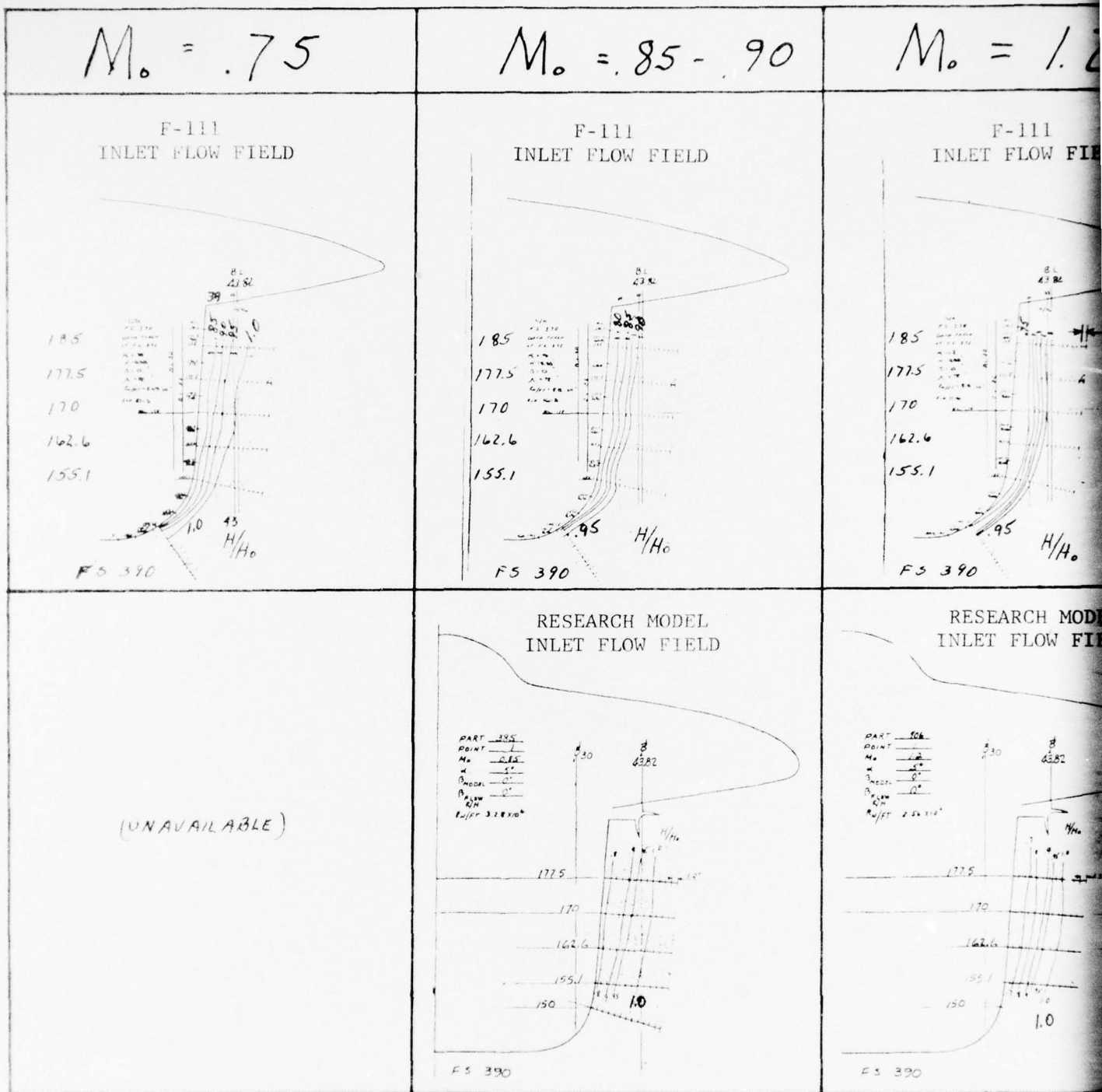
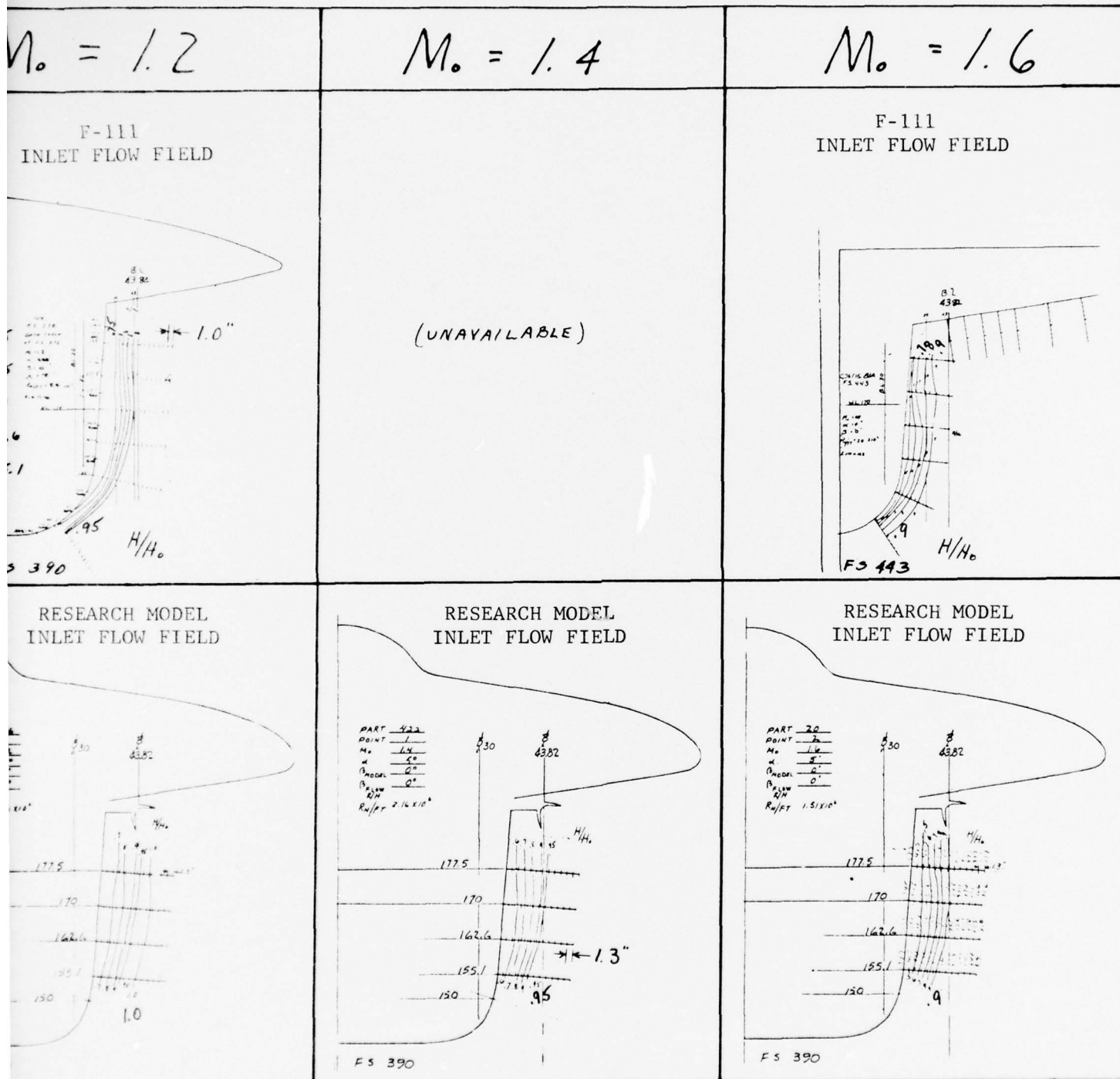


Figure 39. A comparison of the fuselage bo research models for Mach 0.75 t



the fuselage boundary layers measured on the F-111 and for Mach 0.75 to Mach 1.6.

Table 4

MODEL BOUNDARY LAYER HEIGHT AT FUSELAGE STATION 390

	MACH	.75	.85	.90	1.2	1.4	1.6
F-111 WITH TRANSITION GRIT	Model Scale	1/15	-	1/15	1/15	-	1/10
	Test R_N /Ft	2.49×10^6	-	2.5×10^6	2.5×10^6	-	7.4×10^6
	Length, l - in.	25.767	-	25.767	25.767	-	42.75^*
	Meas. δ' - in. on W.L. 170	.533	-	.533	.533	-	.7
	Flat-Plate δ @ Test R_N - in.	.577	-	.577	.582	-	.81
	$\delta' - \delta$, in.	-.044	-	-.044	-.049	-	-.11
RESEARCH MODEL NO TRANSITION STRIP	Model Scale	-	1/5.2	-	1/5.2	1/5.2	1/5.2
	Test R_N /Ft	-	3.28×10^6	-	2.56×10^6	2.16×10^6	1.51×10^6
	Length, l - in.	-	88.56	-	88.56	88.56	88.56
	Meas. δ' - in. on W.L. 170	-	2.067	-	2.154	1.961	1.79
	Flat-Plate δ @ Test R_N - in.	-	1.683	-	1.736	1.771	1.842
	$\delta' - \delta$, in.	-	.384	-	.418	.190	-.052

*Survey at Fuselage Station 443

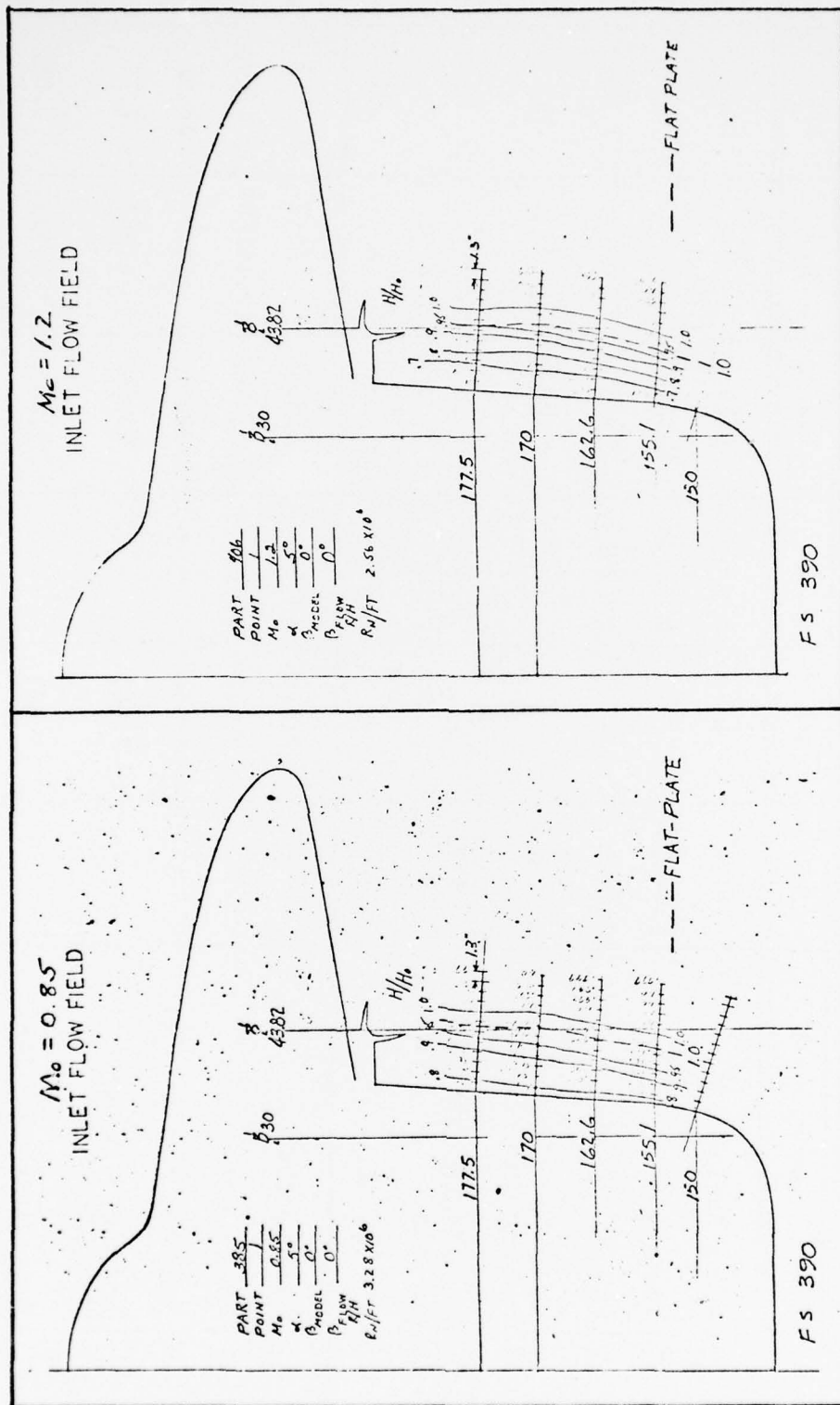


Figure 40. Theoretical flat-plate versus measured boundary-layer heights at $M_0 = 0.85$ and $M_0 = 1.2$.

measured data, for Mach 0.85 and 1.2. Making an adjustment of this type to the research model's boundary-layer data to account for the lack of a transition strip seems reasonable after examining the F-111 test results.

An additional search of F-111 model and flight test data was conducted to ensure that the above adjustments to the research model's boundary layer were reasonable. Shown in Figure 41 are some comparison data of the fuselage boundary-layer profiles as measured on a flight-test airplane and on the 1/6-scale inlet model. It can be seen from the figure that the full-scale airplane has the better profile at the TP II inlet spacing. Therefore, since the airplane boundary-layer profile is better than the model boundary-layer profile obtained (as well as it can be established at this time) with transition grit for the F-111 and since the boundary-layer profiles measured on the F-111 models when tested with transition grit show a thinner boundary layer than that calculated by flat-plate theory, it seems conservative to adjust the boundary-layer height on the research model to the theoretical flat-plate height to compensate for the lack of transition grit during the tests. With a boundary layer of this thickness or less, spillage into the inlet may have been minimized or eliminated. Undoubtedly, the inlet's performance and operation would have been enhanced if this had been true.

The data shown in Figure 41 for Mach 2.2 represent the similar results prevailing at the lower Mach numbers. Additional inlet flow-field data drawn from the F-111 program are shown in Figures 42 and 43. In Figure 42, flight-test fuselage boundary-layer profiles are shown for Mach 1.6 to 2.2. Shown in Figure 43 are model inlet-face pressure data at Mach 2.2 for the TP II inlet, located at B.L. 43, that can be used with the model data shown in Figure 41. These data indicate good flow to the TP II inlet up through 16° angle of attack - spillage of the boundary-layer air into the inlet is not a problem when the boundary-layer system handles the flow properly.

4.1.7 Alternate Splitter-Plate Configurations

The data analysis performed immediately following the test in 16S allowed the conclusion that a classical shock-boundary layer interaction problem existed at Mach 1.6

FUSELAGE BOUNDARY LAYER PRESSURE SURVEY

• M=2.2 • A/P VS 1/6 SCALE MODEL

○ 55° A/P 15 FLT. 107
 △ 55° A/P MODEL

○ 105° A/P 15 FLT. 107
 △ 10° MODEL

○ 148° A/P 15 FLT. 107
 △ 16° MODEL

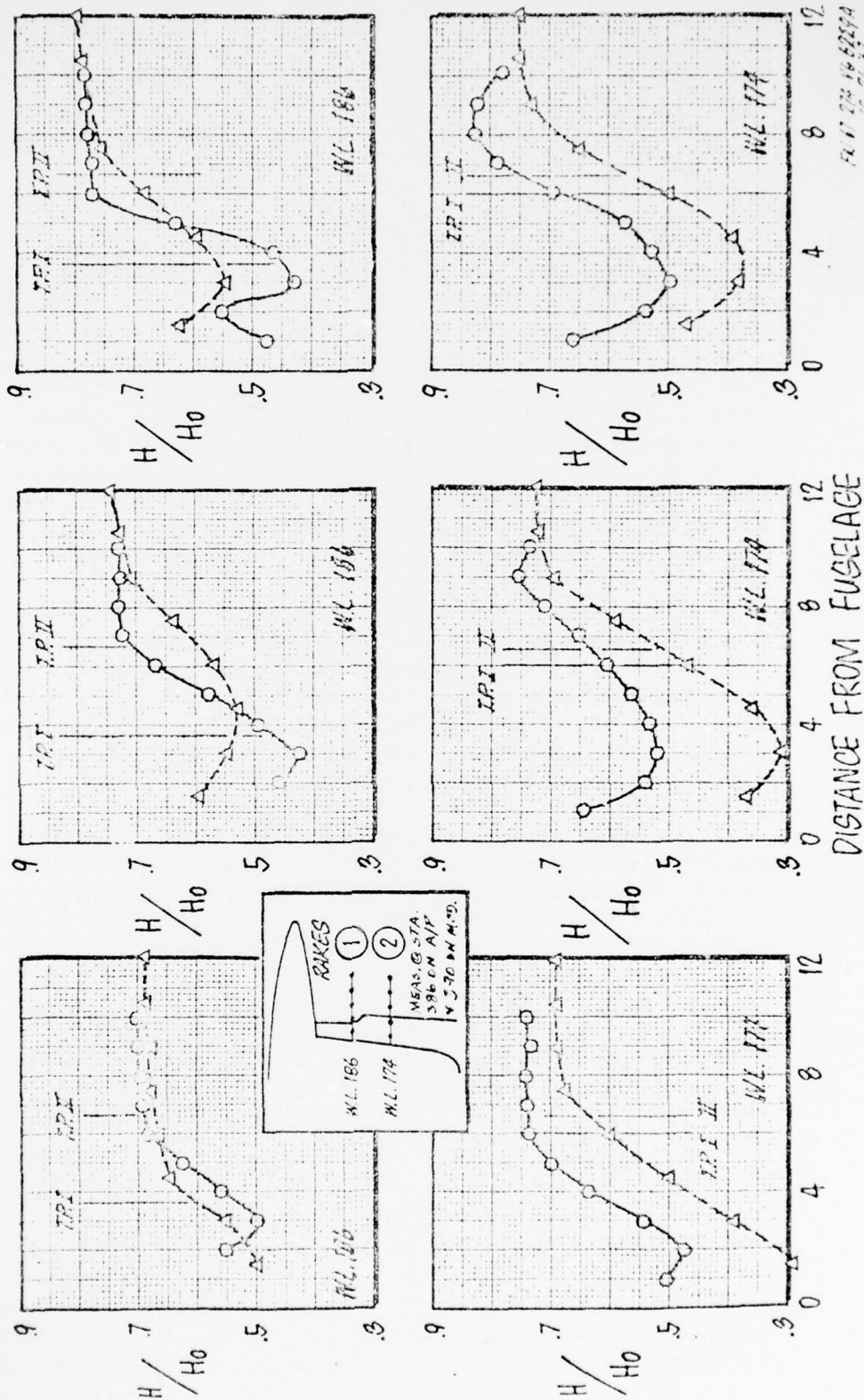


Figure 41. F-111 airplane and model-fuselage-boundary-layer pressure survey.

FUSELAGE BOUNDARY LAYER PRESSURE SURVEY

FOR LEVEL FLIGHT ACCELERATION

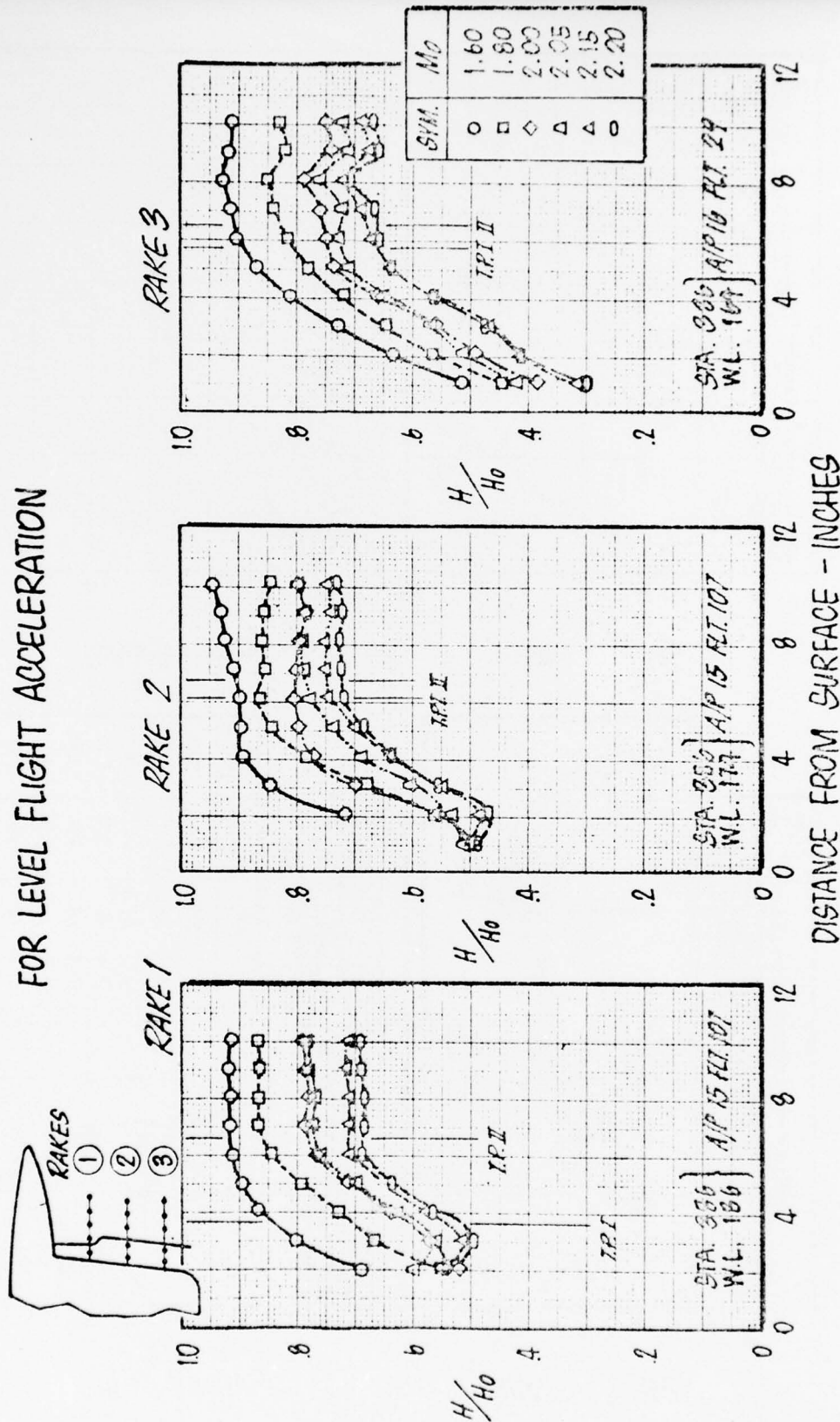


Figure 42. F-111 flight-test fuselage-boundary-layer pressure survey.

FM 672415 6218
10 24 67

TRIPLE FLOW II INLET FACE RAKE DATA

• $M = 2.2$ • FULL OPEN BOUNDARY LAYER BLEED

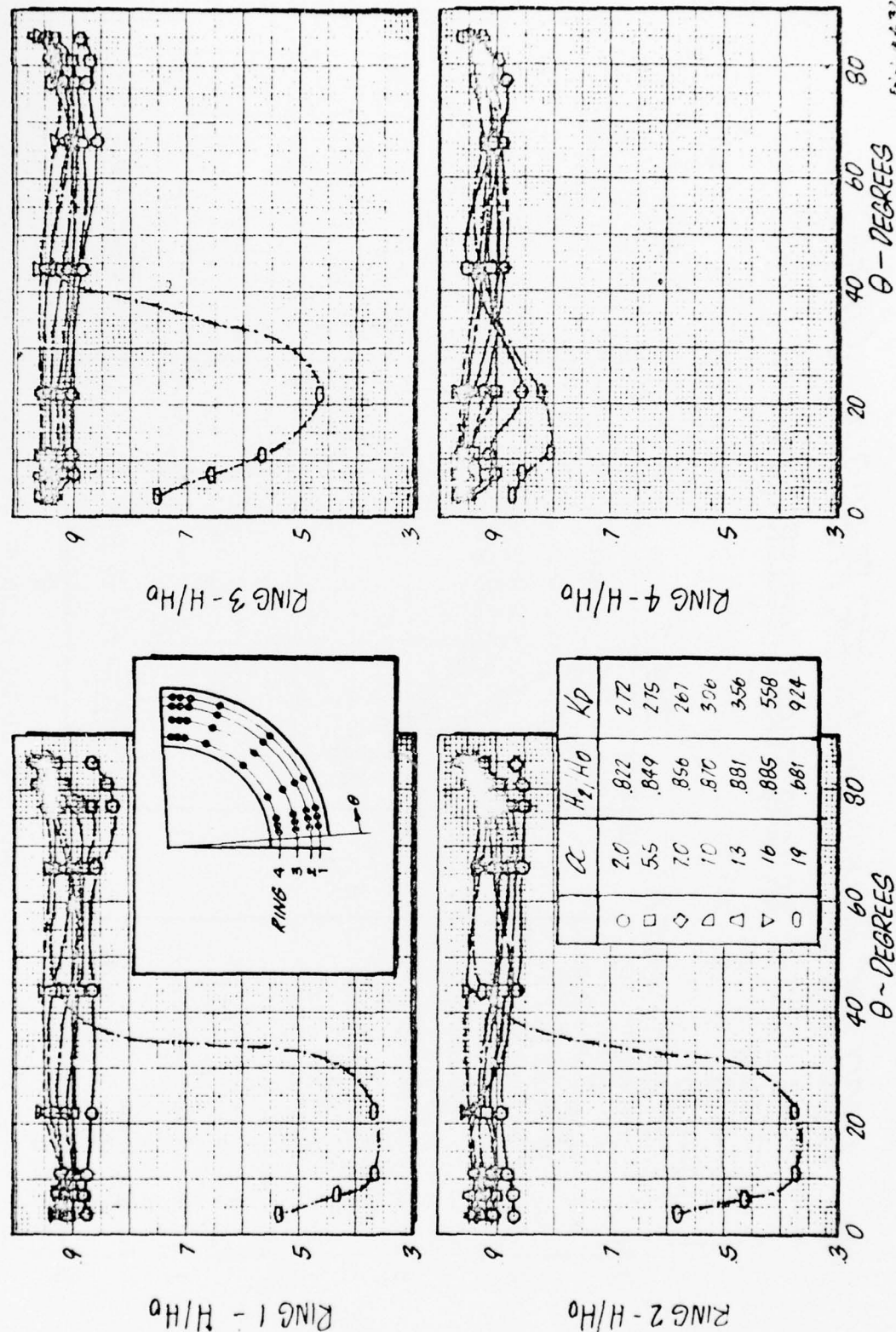


Figure 43. F-111 Triple Flow II inlet-model face-rake data.

between the normal shock and the fuselage boundary layer. Because of that conclusion, two alternate splitter-plate configurations were designed and fabricated for the PWT 16T tests.

In Figure 44, throat-map data for the Basic Long-Plow/ Splitter-Plate Inlet, Alternate Splitter-Plate No. 1, and Alternate Splitter-Plate No. 2 at Mach 0.85 are presented. Indications are that each modification made an improvement. However, as angle of attack was increased on all the configurations and the fuselage boundary layer thickened as seen in Figures 30 and 33, increased spillage into the inlet occurred.

A comparison of the Basic Splitter Plate and the Alternate Splitter-Plate No. 2 at Mach 1.5 is shown in Figure 45. The gain that was observed at Mach 0.85 with Alternate Splitter-Plate No. 2 was not realized at Mach 1.5. Instead, the throat maps indicate degraded flow with the larger splitter plate. This degradation is attributed to the spillage resulting from insufficient divergence of the fuselage boundary-layer-flow channel between the enlarged splitter plate and the fuselage.

4.1.8 Effect of Splitter-Plate Size/ Standoff-Distance

Since throat-map data are not available at Mach 0.85 for the inlet located at B.L. 45.64, the effect of splitter-plate size and standoff distance must be analyzed by use of the compressor-face maps shown in Figure 46. From the figure, it appears that moving the inlet outboard makes a bigger improvement than enlarging the splitter plates. This conclusion was reinforced by lower distortion in the outboard position.

4.1.9 Flow Field Summary

A summary of all of the flow-field analyses discussed in the previous subsections is presented here. As stated earlier, the conclusion reached after the 16S tests was that a shock-boundary layer interaction problem was occurring. This conclusion was based primarily on the works of Seddon contained in References 5 and 6. In his papers, Seddon shows that separation will occur on flat plates from shock boundary-layer interaction when the strength of the normal

shock exceeds Mach 1.3 (approximately) unless special precautions are taken to prevent it. Since the data being analyzed was for Mach 1.6 and above and since the pressure data depicted flow conditions similar to those shown by Seddon, a logical conclusion that a shock boundary-layer interaction problem existed was reached.

However, after the 16T tests, when the Mach 0.85 data was analyzed and showed similar throat-flow patterns without the presence of normal shocks, it had to be concluded that fuselage-boundary-layer spillage past the splitter plate was entering the inlet.

The spillage theory was further substantiated from the 16T tests when the inlet-throat flow conditions at Mach 1.2 and 1.4 did not improve over those recorded at Mach 1.6 in 16S although the strength of the normal shock was reduced below the predicted separation Mach number of 1.3.

Thus, with the Mach 1.6 flow-field rake data and subsonic test results, it is now concluded that spillage, rather than separation due to shock boundary-layer interaction, is the primary problem with the research model inlet as designed and tested. As noted before, modifications to the fuselage boundary-layer system can be made that should result in an improvement to inlet operation and to engine/inlet compatibility. The details of the proposed revisions are discussed in the following subsection.

4.1.10 Fuselage Boundary-Layer System Modifications

In the preceding sections, spillage of the fuselage-boundary-layer air into the inlet was discussed in detail. Correction of this spillage problem would be desirable to improve inlet operation and engine/inlet compatibility for operation to Mach 1.6 or higher.

An exact cause for spillage of the fuselage boundary layer into the inlet has not been definitely established. However, with the testing that has been done, the following potential solutions are recommended. These include:

SPLITTER

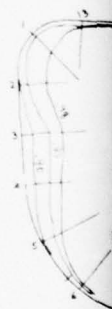
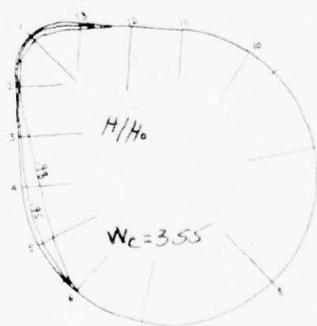
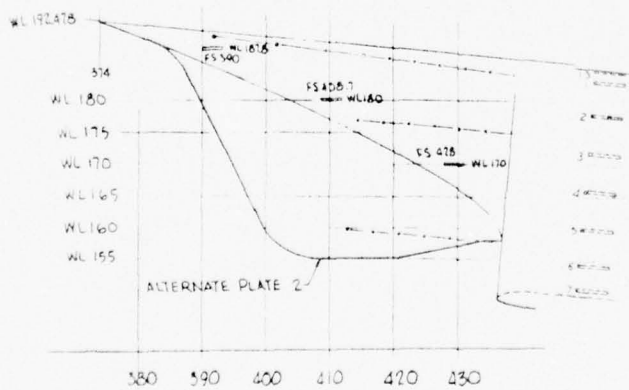
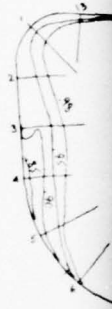
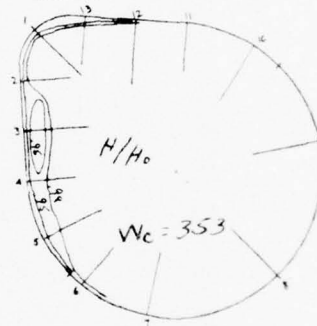
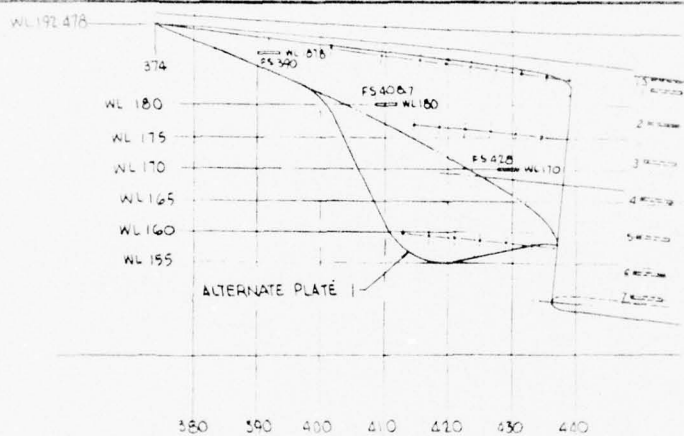
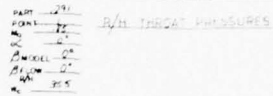
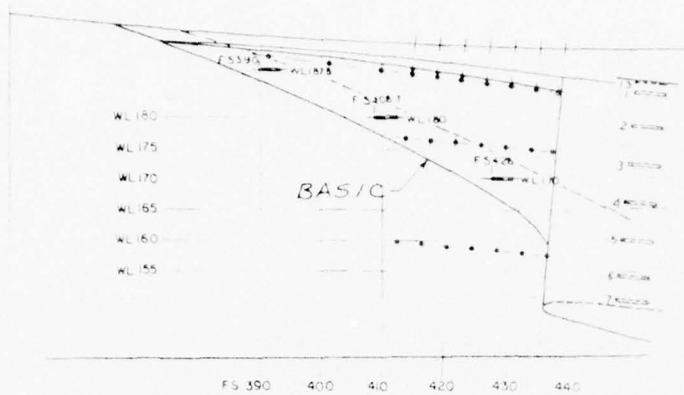
$$\mathcal{L} = 0^0$$
 α 

Figure 44. Effect of splitter-plate size and shape for the inlet at B.L. 43.82.

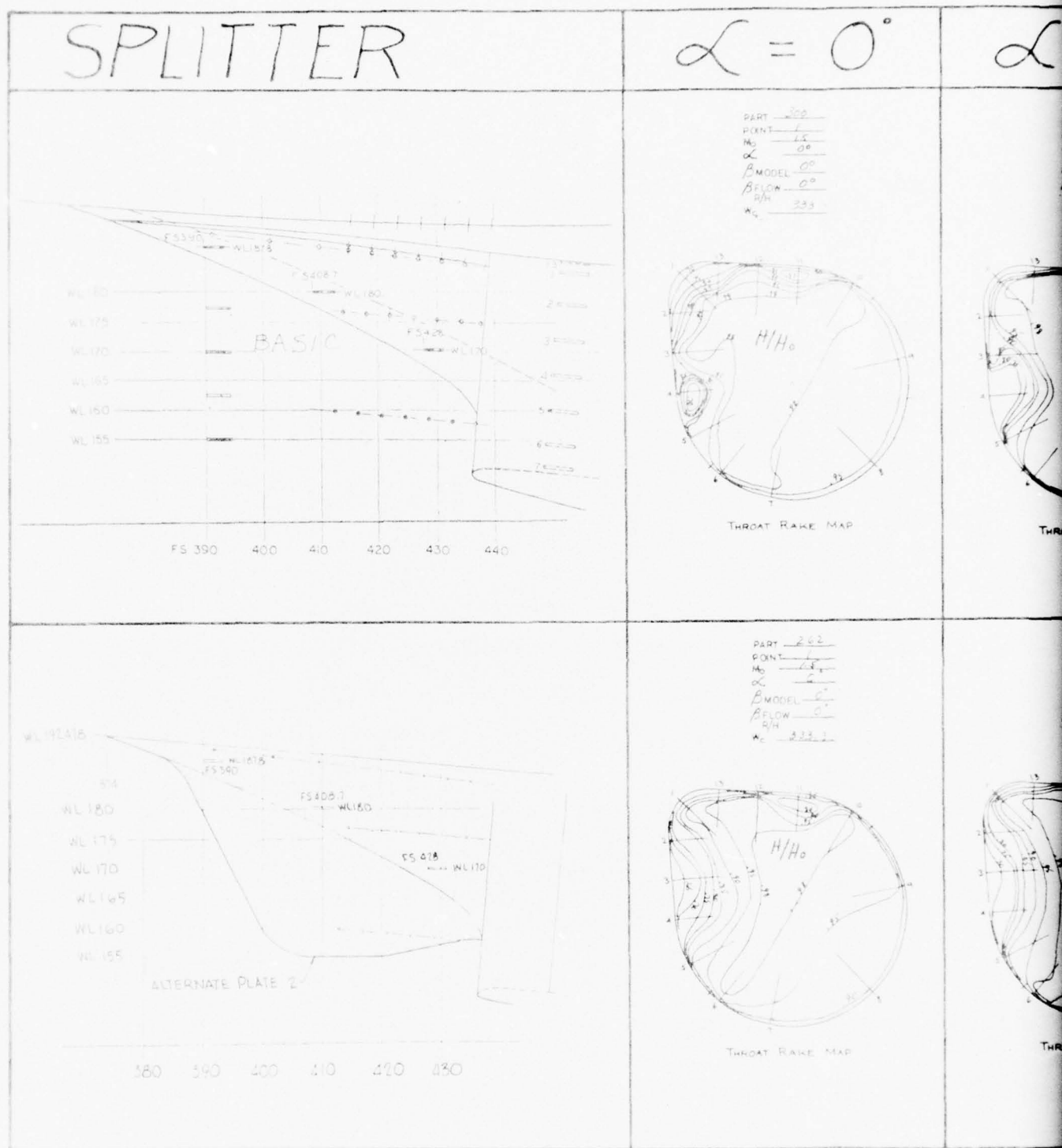
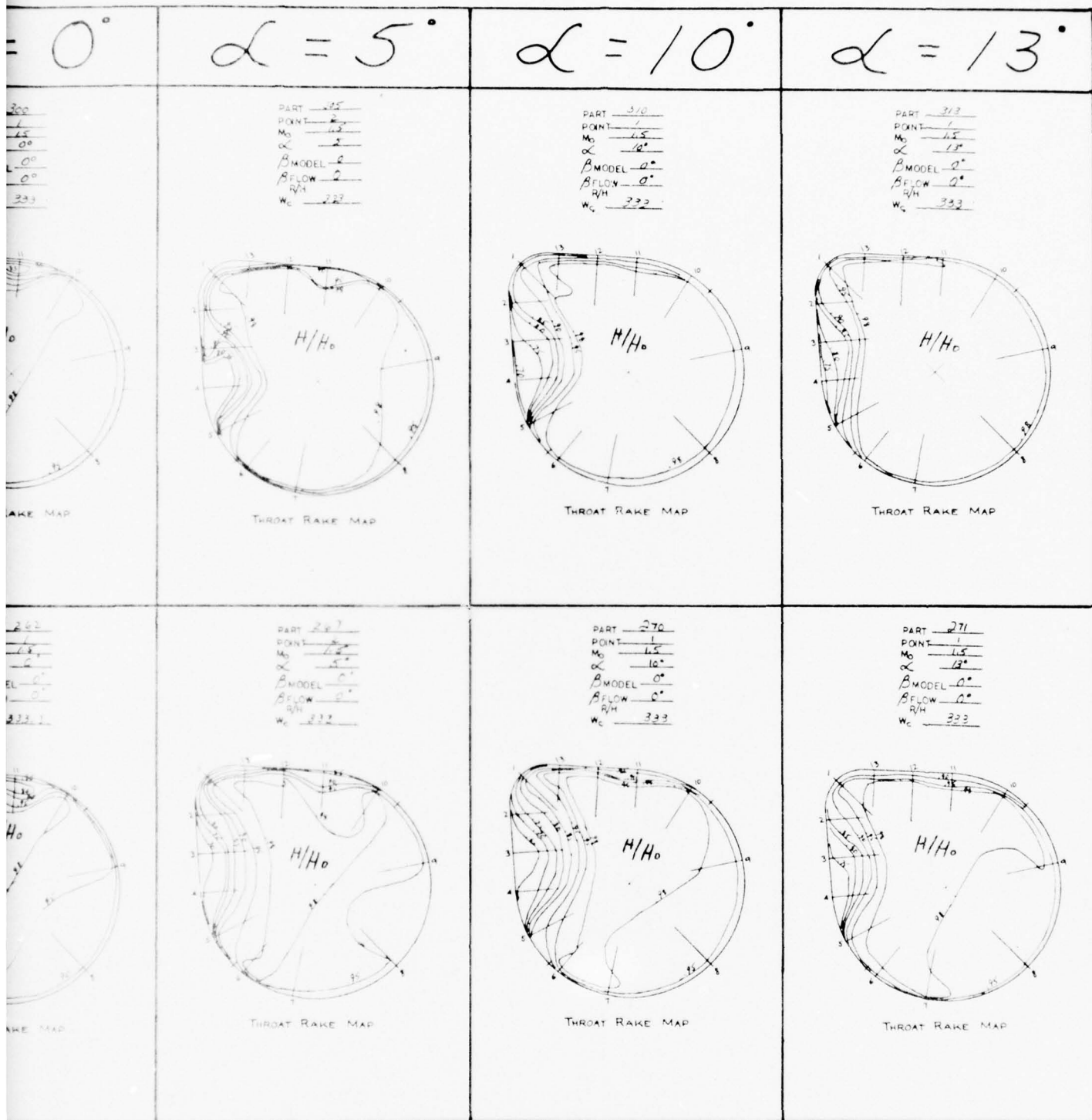


Figure 45. Effect of splitter-plates at $M_0 = 1.5$ at B.L. 43.82.



r-plates at $M_0 = 1.5$ on inlet-throat flow for the inlet

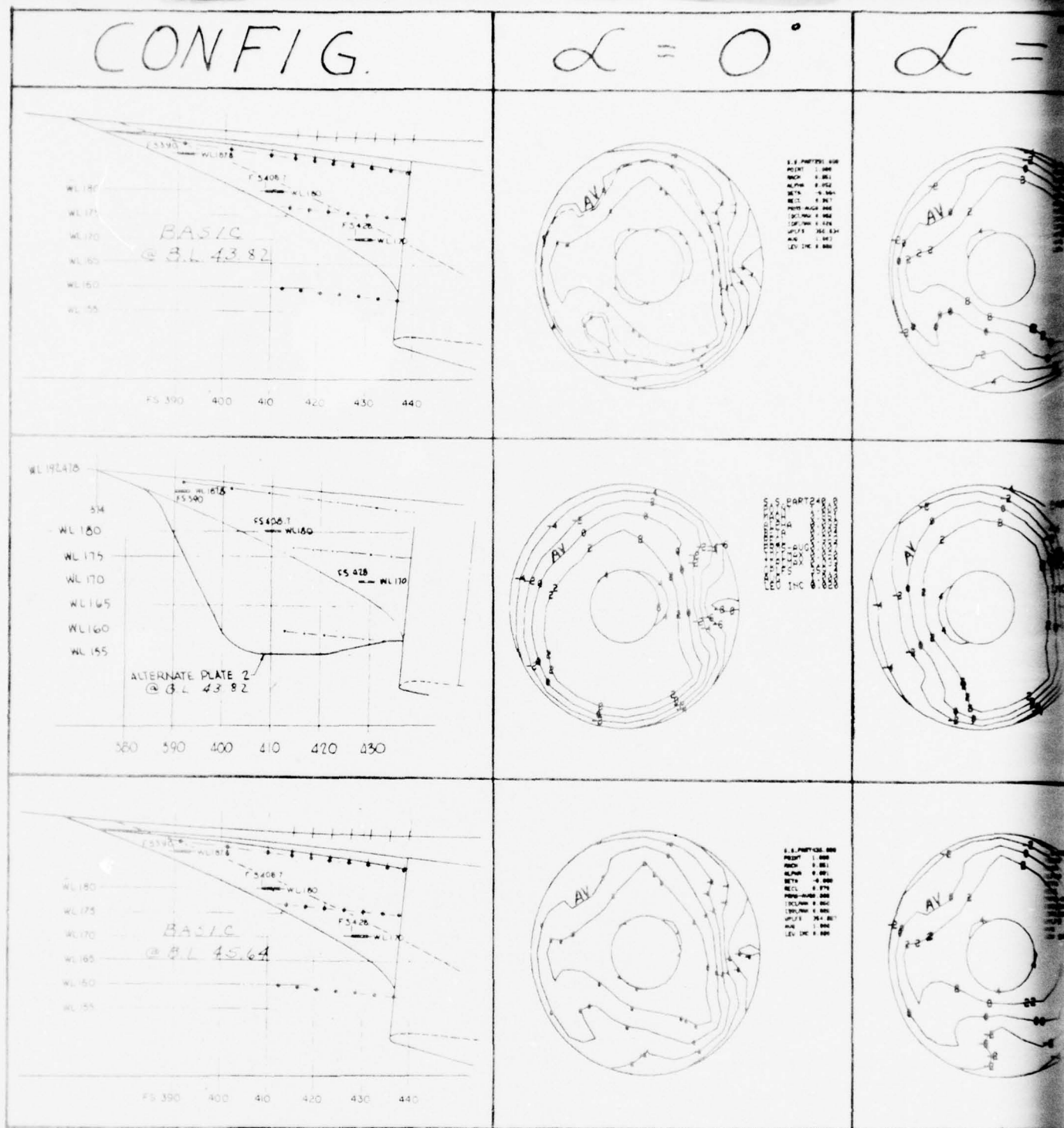


Figure 46. Effect of splitter-plate shape and step on compressor-face-pressure contour maps.

1. Providing greater flow area for the fuselage boundary layer by indenting the fuselage and using the short plow with the long or a modified splitter plate.
2. Blunting or cambering-in the splitter-plate leading edge to reduce any effect of flow misalignment.
3. Some combination of 1 and 2.

Figure 47 is a sketch showing the modified system that incorporates the changes listed above.

As shown, the short plow replaces the long plow and the fuselage is indented along the splitter-plate leading edge. The barred region shows the increased flow area that is obtainable with such a modification. Other potential changes are to combine modifying the splitter-plate size and shape with a fuselage indentation to match and blunting or cambering-in the splitter-plate leading edge. Modifications of these types could be tested and evaluated with a minimum of additional testing. Such modifications would provide greater splitter plate leading edge to plow distance, increased flow area, improved flow divergence, and a more favorable pressure gradient behind the plate. The right combination of these configuration changes will alleviate the spillage problem.

4.2 INTERNAL DUCT FLOW

Earlier in the discussion it was mentioned that the low-pressure region appearing in the compressor-face contour maps at the three o'clock position was the result of flow separation due to the outboard bend in the duct. This bend can be seen by referring to the sketch shown in Figure 5. But inasmuch as this was not a development program, a revision to the inlet duct lines was beyond the scope of this test program. But since the flow defect was recognized from the 16S data, alternate approaches, such as duct vortex generators (VGs) and duct blowing, were evaluated in the 16T test. Both the VGs and blowing were installed on the inboard duct wall in an effort to energize the low-energy spillage air but neither are effective. However, both the VGs and the duct blowing were effective in improving the flow along the outboard-wall bend where separation occurred as shown in Figure 48. Both are effective at 5° angle of attack and below but are not effective at 10° and above.

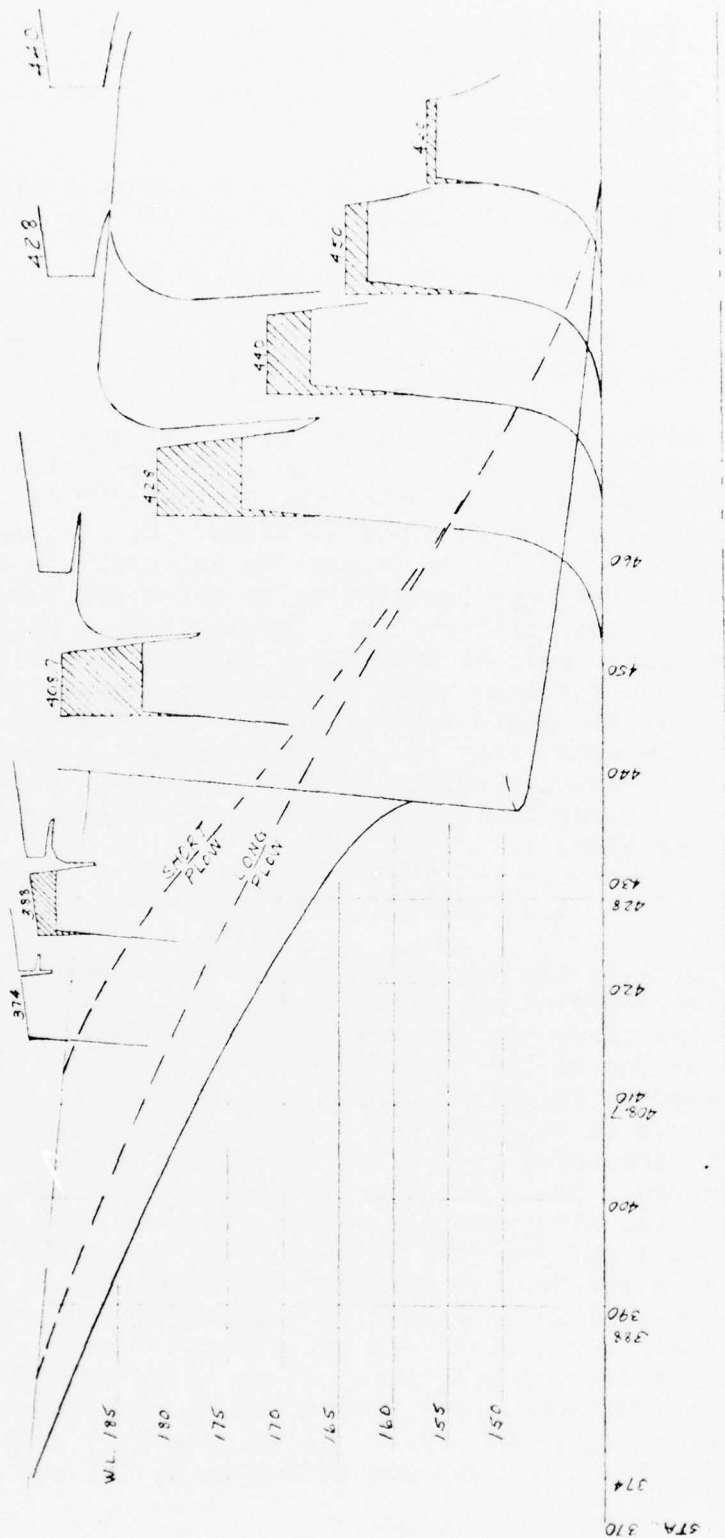


Figure 47. A potential fuselage-boundary-layer system modification.

The reason is because the high-energy air entering the inlet tends to flow along the upper part of the duct as angle of attack is increased, pushing the separated low-energy air toward the bottom of the duct.

Inlet pressure recovery decreased from 0.967 to 0.964 with VG Pattern 3, as shown in Figure 48. However, inlet pressure recovery increased from 0.972 to 0.975 with duct blowing. This improvement was obtained with a blowing flow rate of less than 1% of the inlet (engine) airflow. Consequently, it was demonstrated that the duct-bend separation problem can be corrected with VGs or duct blowing without redesigning the inlet duct.

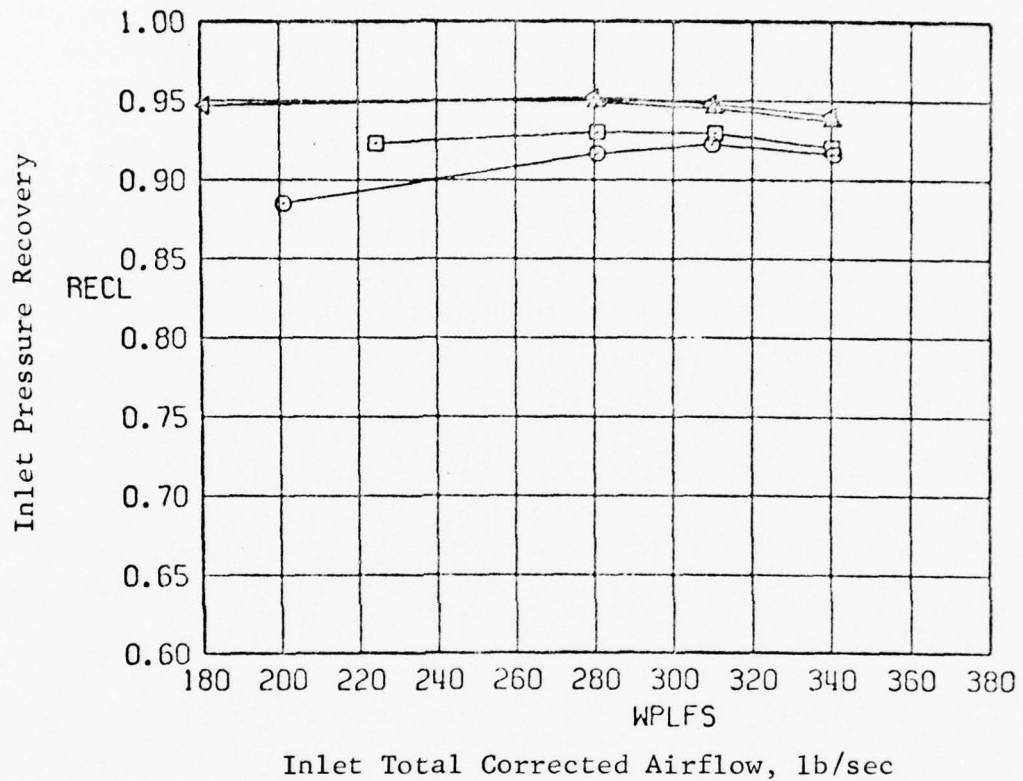
4.3 INLET PERFORMANCE

Inlet performance (pressure recovery, distortion, and turbulence) at Mach 1.6 for the four inlet configurations evaluated on the left-hand side of the model is shown in Figures 49, 50, and 51. All four configurations were tested with the same inlet duct designed for a throat Mach number of 0.8. A fifth configuration, the Basic Long-Plow/Splitter-Plate located at B.L. 45.64, designed for a throat Mach number of 0.7, was evaluated on the right-hand side of the model. No performance data for the right-hand inlet are shown in this report because the smaller inlet had good performance and was the primary configuration. Right-hand inlet performance data may be obtained from Reference 3.

From the data presented in Figure 49, it can be seen that the Short Splitter-Plate Inlet had the higher pressure recovery. Also, a very small gain in pressure recovery was realized when this inlet was moved outboard to B.L. 45.64 from B.L. 43.82. However, when the Basic Long-Plow/Splitter-Plate Inlet was moved to the most outboard position of B.L. 47.45, a loss in pressure recovery occurred. This loss is attributed to the higher local Mach numbers to which the inlet was exposed.

Purely on the basis of the performance of these four inlet configurations, the Short-Plow and Splitter-Plate Inlet at B.L. 43.82 would have been selected. However, this was a research inlet test program to determine how well a simple, open-nose, normal-shock inlet would operate in a wing-body flow field with the intent to extend the data base for inlet designs. It was not intended to select an optimum

Sym	Part	M_0	α	β	Inlet Configuration
□	20	1.62	5.2	0	Basic Long Plow/Splitter Plate @ B.L. 43.82
○	41	1.62	5.0	0	Basic Long Plow/Splitter Plate @ B.L. 47.45
△	63	1.60	5.1	0	Short Plow/Splitter Plate @ B.L. 43.82
◊	90	1.60	5.0	0	Short Plow/Splitter Plate @ B.L. 45.64



DATE 12-19-75
PROJ-P11-129
AFG INC

Figure 49. $M_0 = 1.6$ inlet pressure recovery of four inlet configurations.

Sym	Part	M_0	α	β	Inlet Configuration
□	20	1.62	5.2	0	Basic Long Plow/Splitter Plate @ B.L. 43.82
○	41	1.62	5.0	0	Basic Long Plow/Splitter Plate @ B.L. 47.45
△	63	1.60	5.1	0	Short Plow/Splitter Plate @ B.L. 43.82
4	90	1.60	5.0	0	Short Plow/Splitter Plate @ B.L. 45.64

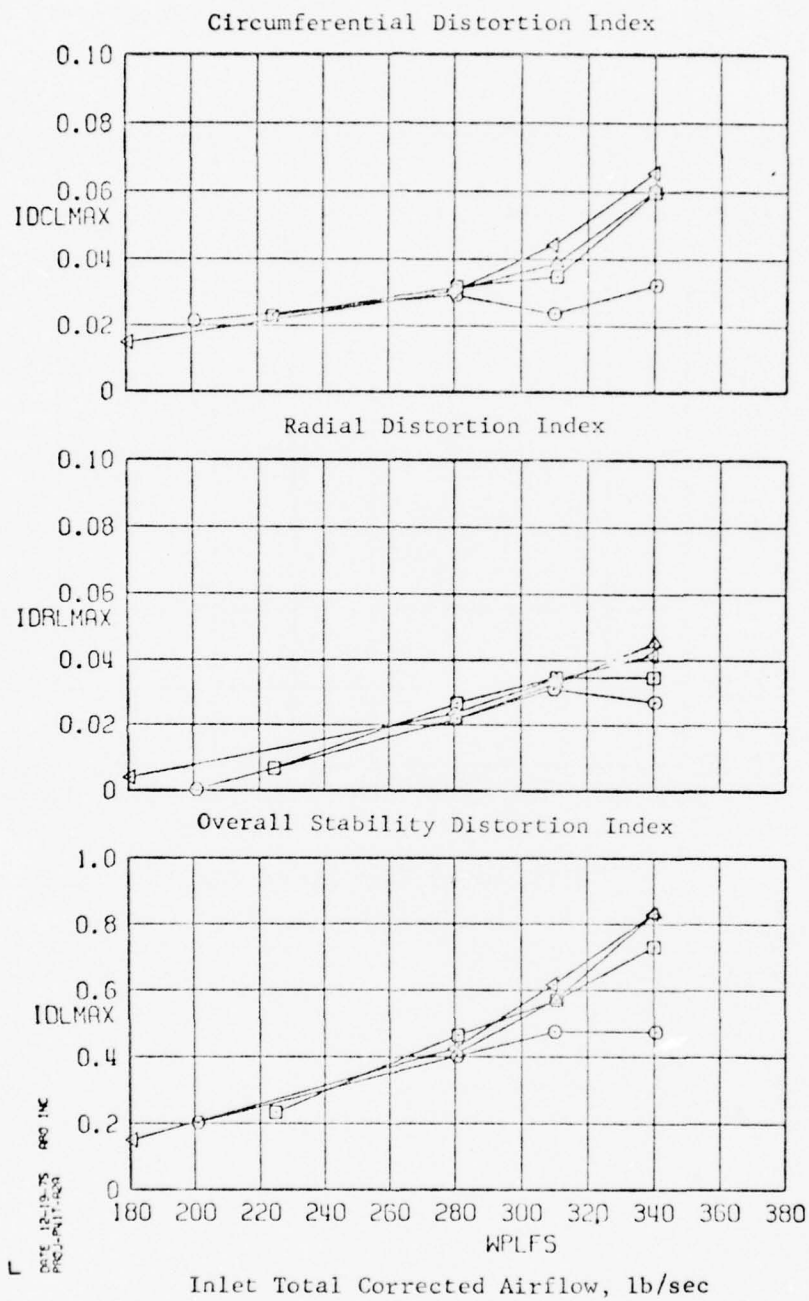


Figure 50. $M_0 = 1.6$ inlet distortion of four inlet configurations.

Sym	Part	M ₀	α	β	Inlet Configuration
U	20	1.62	5.2	0	Basic Long Flow/Splitter Plate @ B.L. 43.82
O	41	1.62	5.0	0	Basic Long Flow/Splitter Plate @ B.L. 47.45
A	63	1.60	5.1	0	Short Flow/Splitter Plate @ B.L. 43.82
Δ	90	1.60	5.0	0	Short Flow/Splitter Plate @ B.L. 45.64

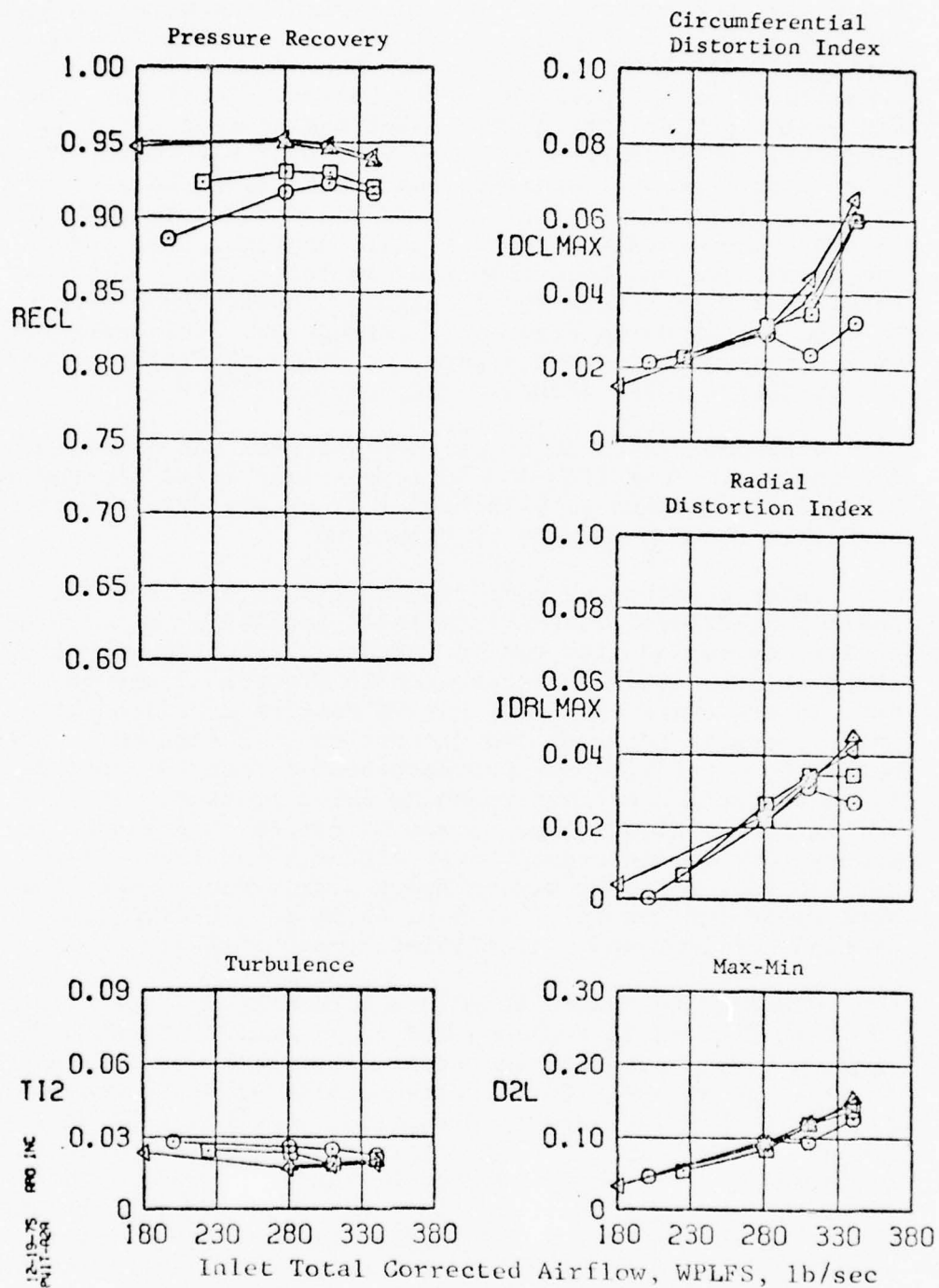


Figure 51. $M_0 = 1.6$ inlet performance of four inlet configurations.

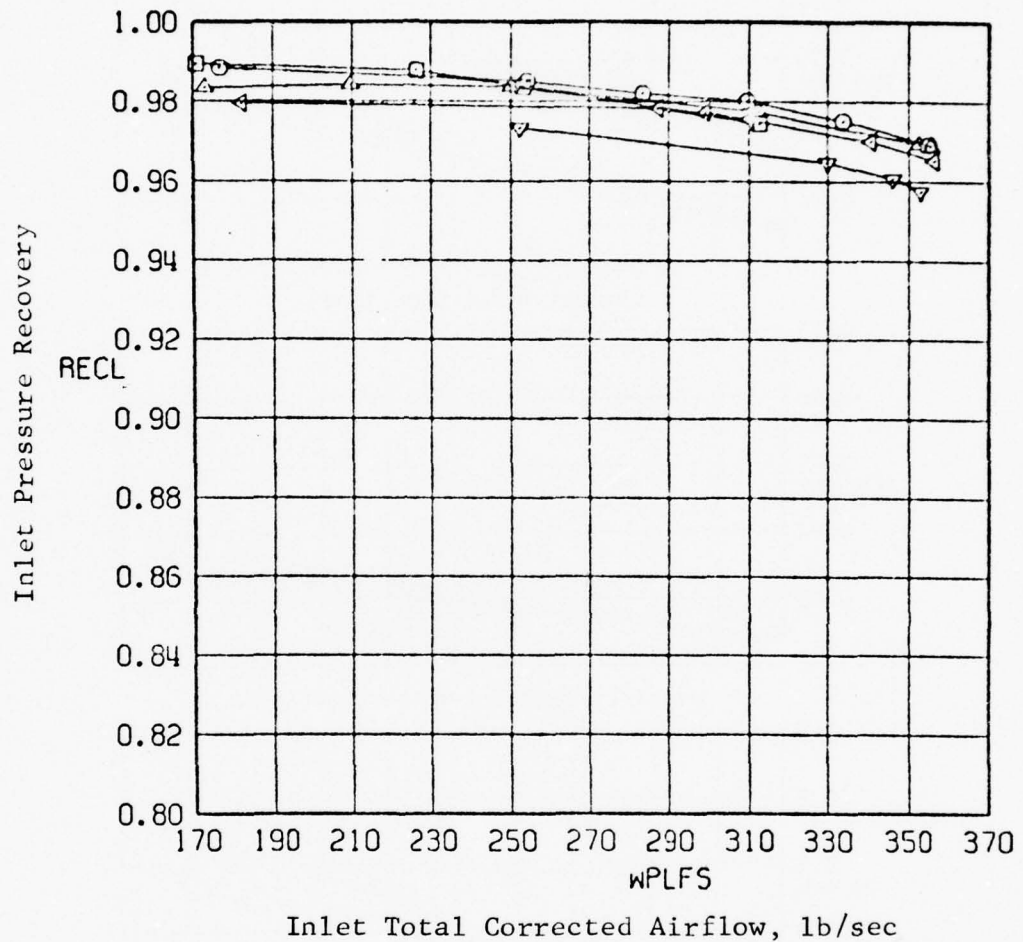
configuration. In addition, this research inlet program was dollar-limited, which did not permit great flexibility. Consequently, the number of inlet configurations were limited and had to be preselected. Thus, the Basic Long-Plow and Splitter-Plate Inlet with a throat Mach number of 0.8 was preselected as the primary configuration. Similarly, the Short-Plow and Splitter-Plate Inlet was preselected as a secondary configuration to be evaluated at Mach 1.6. Therefore, a performance documentation of the Basic Long-Plow/Splitter-Plate Inlet at B.L. 43.82 was made up to Mach 2.0 in 16S. Documentation of this basic configuration across the Mach range was then completed in 16T. The full set of inlet performance data for 5° alpha, 0° beta, from Mach 0.55 to 2.0, are shown in Figures 52 through 60. This same set of inlet pressure recovery data was presented relative to the predicted inlet pressure recovery in Figure 2.

A second set of inlet performance data was obtained for the Basic Long-Plow and Splitter-Plate Inlet located at B.L. 45.64 for Mach 0.55 to Mach 1.5. These data are presented in Figures 61 through Figure 66.

Inlet performance comparisons at Mach 0.85 for the Basic Long-Plow/Splitter-Plate Inlet located at B.L. 43.82, at B.L. 45.64, and for two VG patterns installed with the inlet at B.L. 45.64 are presented in Figures 67 and 68. The data in these figures show that VG Pattern 2 reduced both inlet pressure recovery and distortion. VG Pattern 3, which worked on correcting the outboard-bend defect, decreased inlet distortion without reducing inlet pressure recovery. Moving the inlet outboard showed no effect on pressure recovery, but it did reduce inlet distortion. Thus, it was decided to test and document inlet performance across the Mach range for the inlet at B.L. 45.64 as a backup configuration for improved engine/inlet compatibility.

Finally, the Basic Inlet and Alternate Splitter Plate No. 2 at B.L. 43.82 are compared in Figures 69 through 72. At Mach 0.85, no change in pressure recovery was seen at 5° angle of attack. But Alternate Splitter Plate No. 2 resulted in some increase in distortion at those test conditions. At Mach 1.5, the alternate splitter plate resulted in losses in both pressure recovery and distortion. Consequently, Alternate Splitter Plate No. 2 by itself, without any modification to the fuselage to improve the fuselage boundary-layer flow path, did not achieve the improvements that were anticipated.

SYMBOL	M_o	α	β	CONF	PART
□	0.55	5.0	0.0	1	368
○	0.65	5.0	0.0	1	363
△	0.75	5.0	0.0	1	352
◁	0.85	5.0	0.0	1	276
▽	1.20	5.0	0.0	1	337



DATE 04-22-75
PROJ-PAT-02R
880 INC

Figure 52. $M_o = 0.55-1.2$ inlet pressure recovery for the Basic Long-Flow/Splitter-Plate Inlet at B.L. 43.82.

Sym	Part	M_0
□	368	0.55
○	363	0.65
△	352	0.75
◁	276	0.85
▽	337	1.20

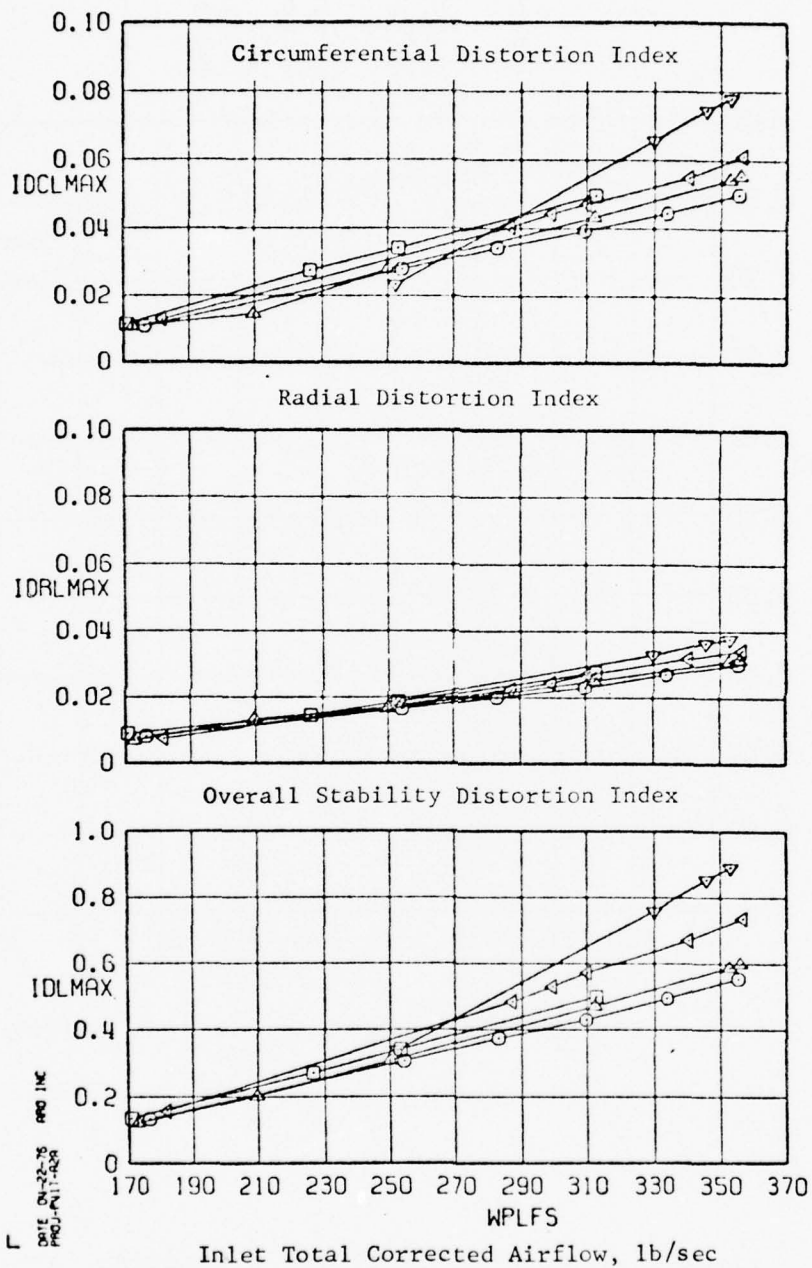


Figure 53. $M_0 = 0.55-1.2$ inlet distortion of the Basic Long-Plow/Splitter-Plate Inlet at B.L. 43.82 for $\alpha = 50^\circ$ and $\beta = 00^\circ$.

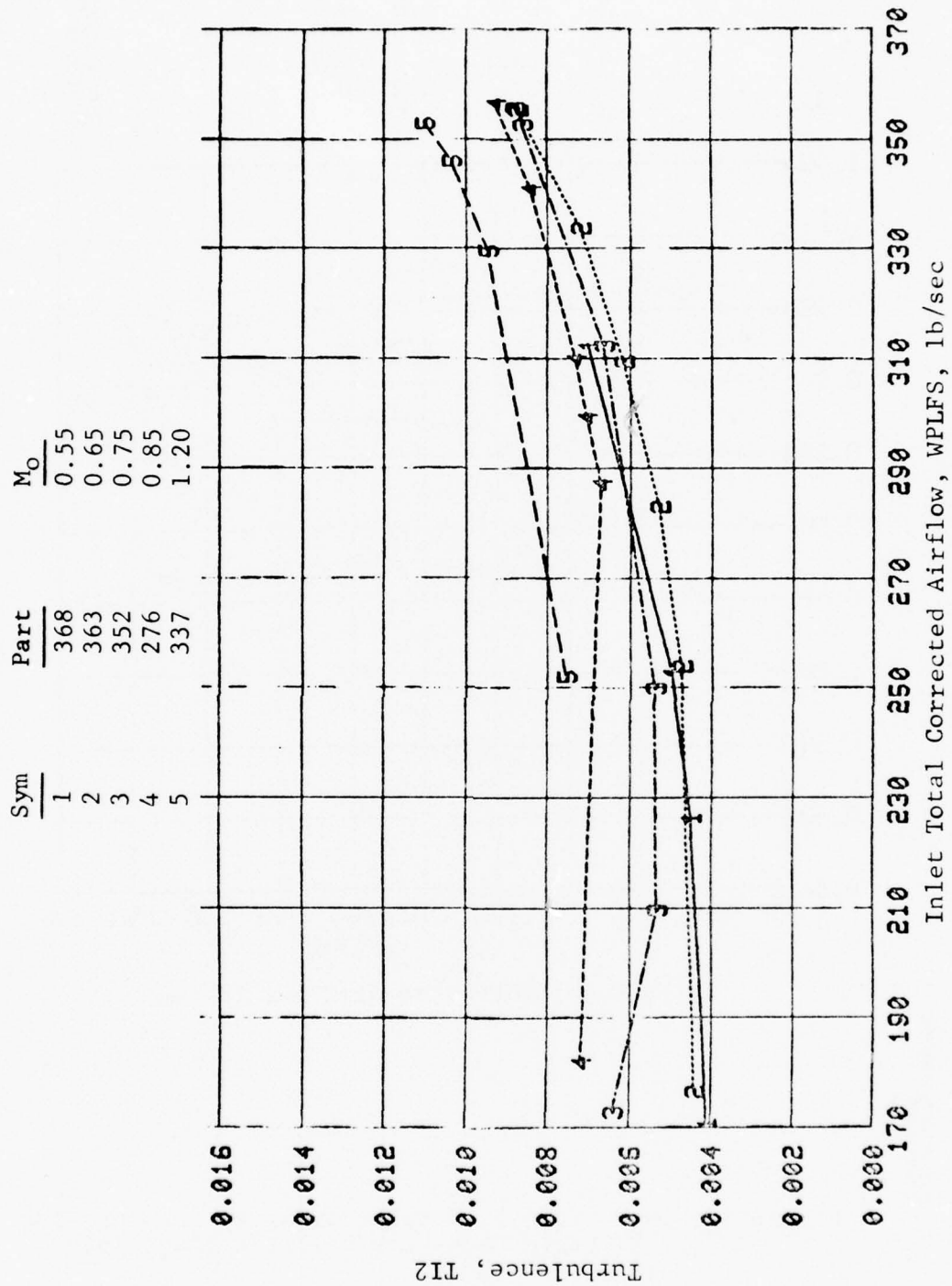


Figure 54. $M_o = 0.55$ -1.2 inlet turbulence of the Basic Long-Flow/Splitter-Plate Inlet at B.L. 43.82 for $\alpha = 5^\circ$ and $\beta = 0^\circ$.

SYMBOL	M_o	α	β	CONF	PART
□	1.20	5.0	0.0	1	337
○	1.40	5.0	0.0	1	320
△	1.50	5.0	0.0	1	305
◁	1.62	5.0	0.0	1	20
▽	1.70	5.0	0.0	1	155

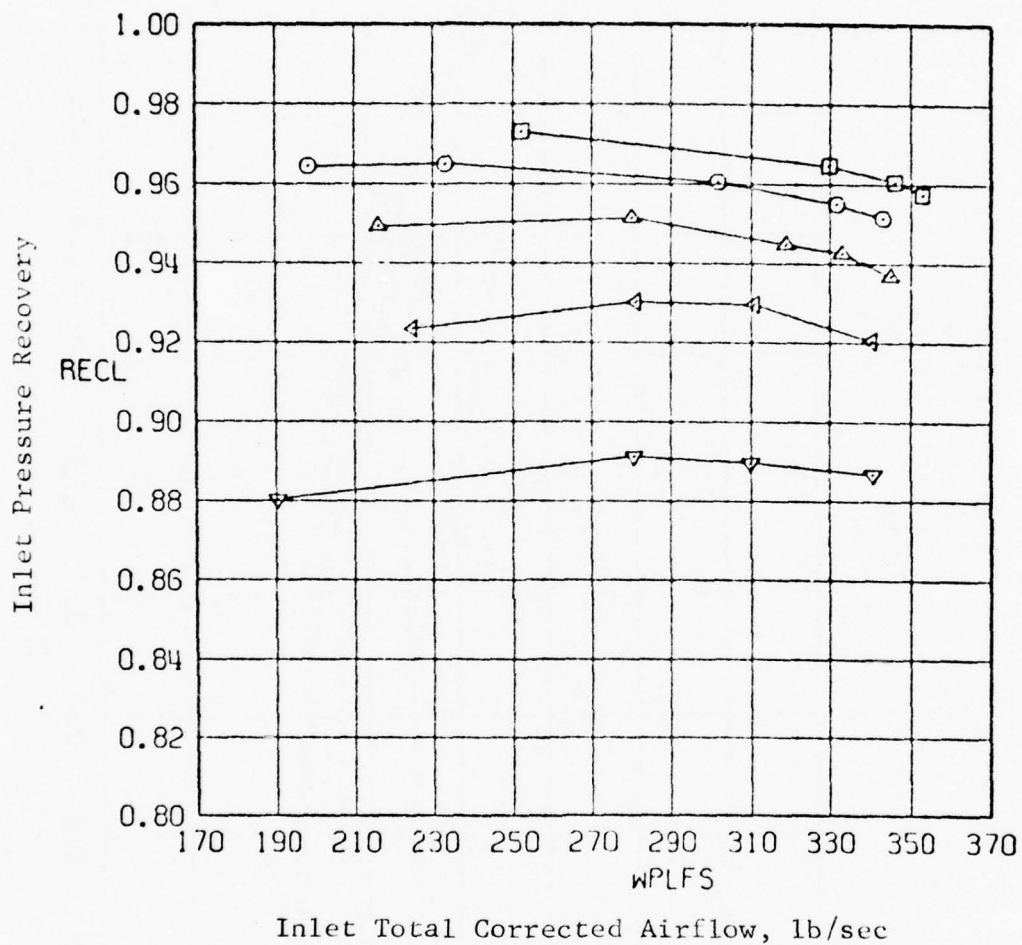


Figure 55. $M_o = 1.20-1.70$ inlet pressure recovery for the Basic Long-Plow/Splitter-Plate Inlet at B.L. 43.82.

Sym	Part	M_o
□	337	1.2
○	320	1.4
△	305	1.5
◁	20	1.62
▽	155	1.70

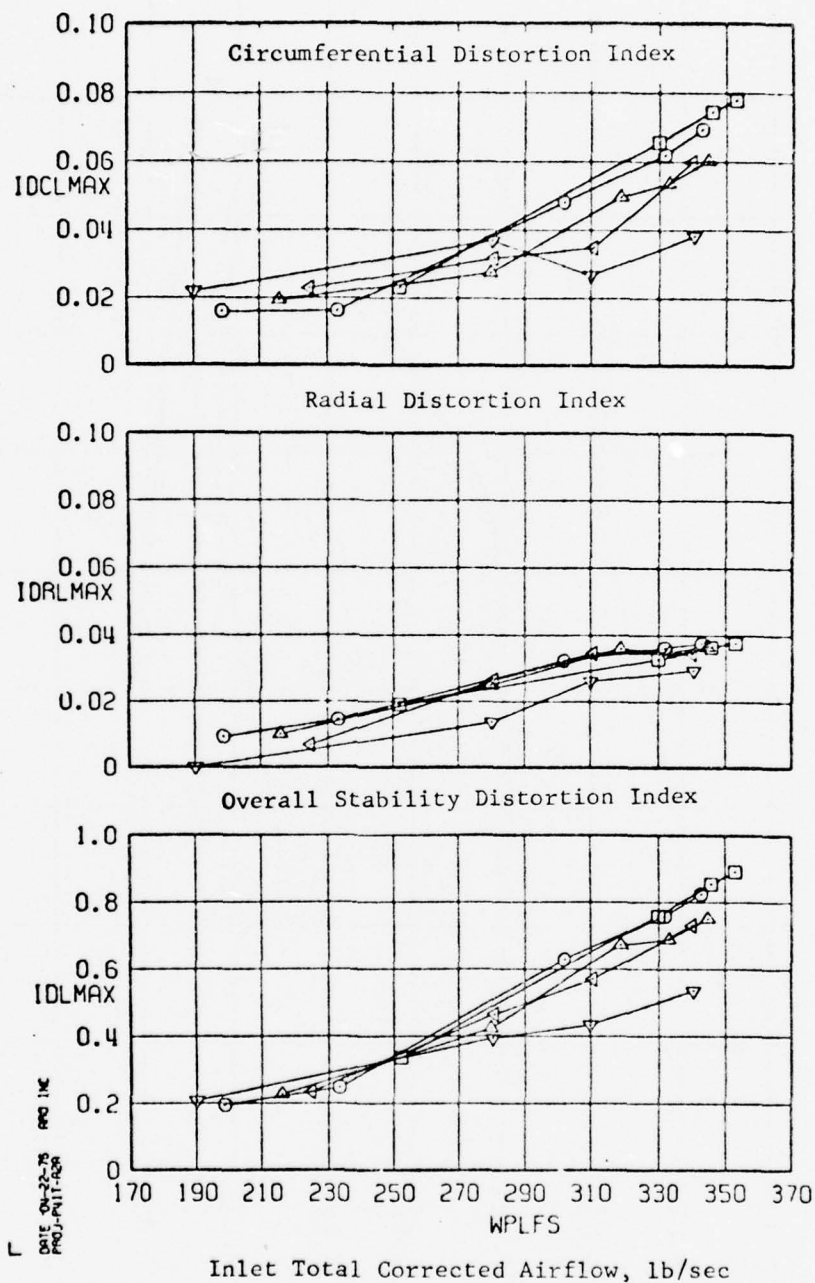


Figure 56. $M_o = 1.20-1.70$ inlet distortion for the Basic Long-Plow/Splitter-Plate Inlet at B.L. 43.82 for $\alpha = 5^\circ$ and $\beta = 0^\circ$.

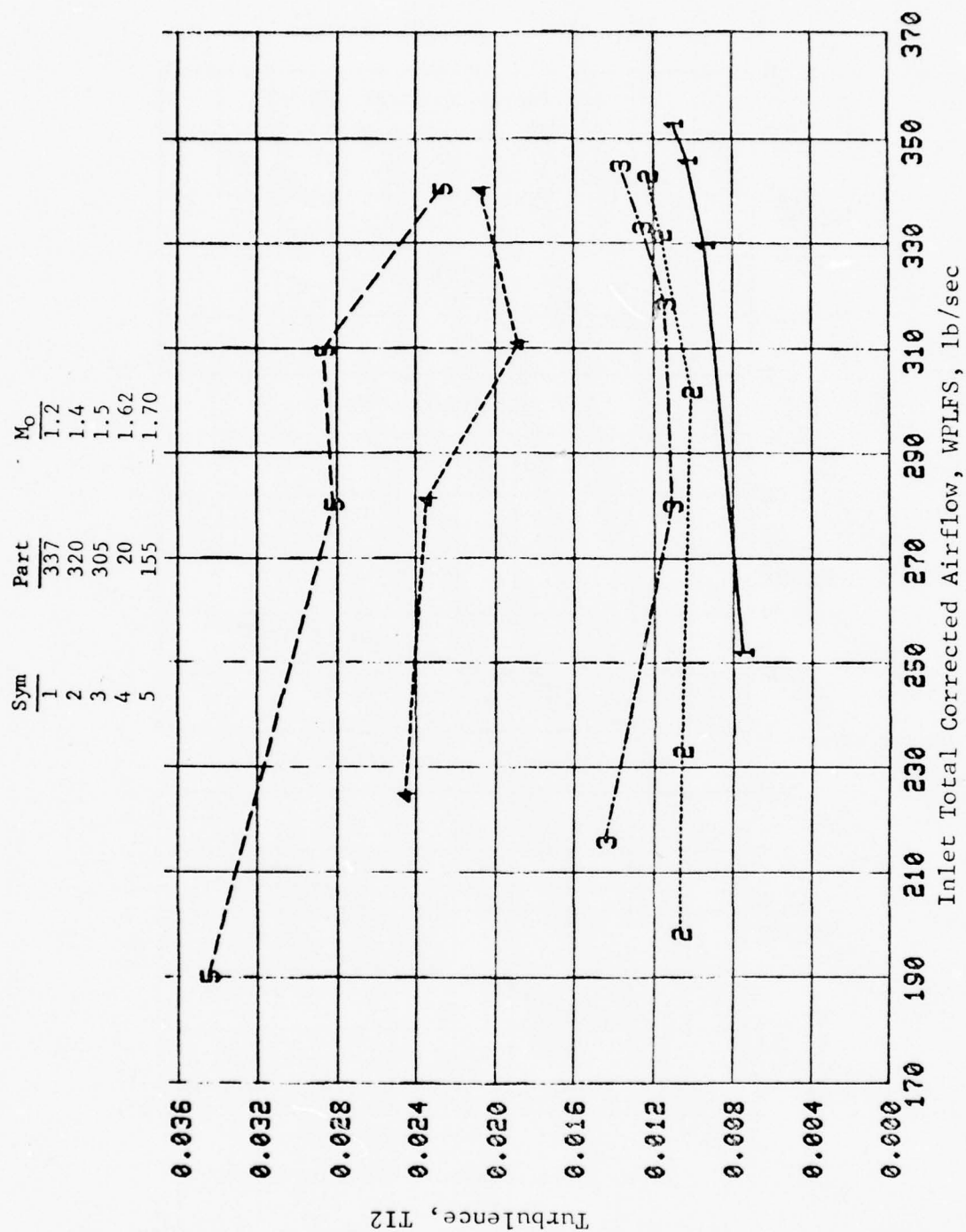


Figure 57. $M_0 = 1.20-1.70$ inlet turbulence for the Basic Long-Flow/Splitter-Plate Inlet at B.L. 43.82 for $\alpha = 5^\circ$ and $\beta = 0^\circ$.

SYMBOL	M_o	α	β	CONF	PART
□	1.62	5.0	0.0	1	20
○	1.70	5.0	0.0	1	155
△	1.80	5.0	0.0	1	123
◁	1.90	5.0	0.0	1	144
▽	2.00	5.0	0.0	1	141

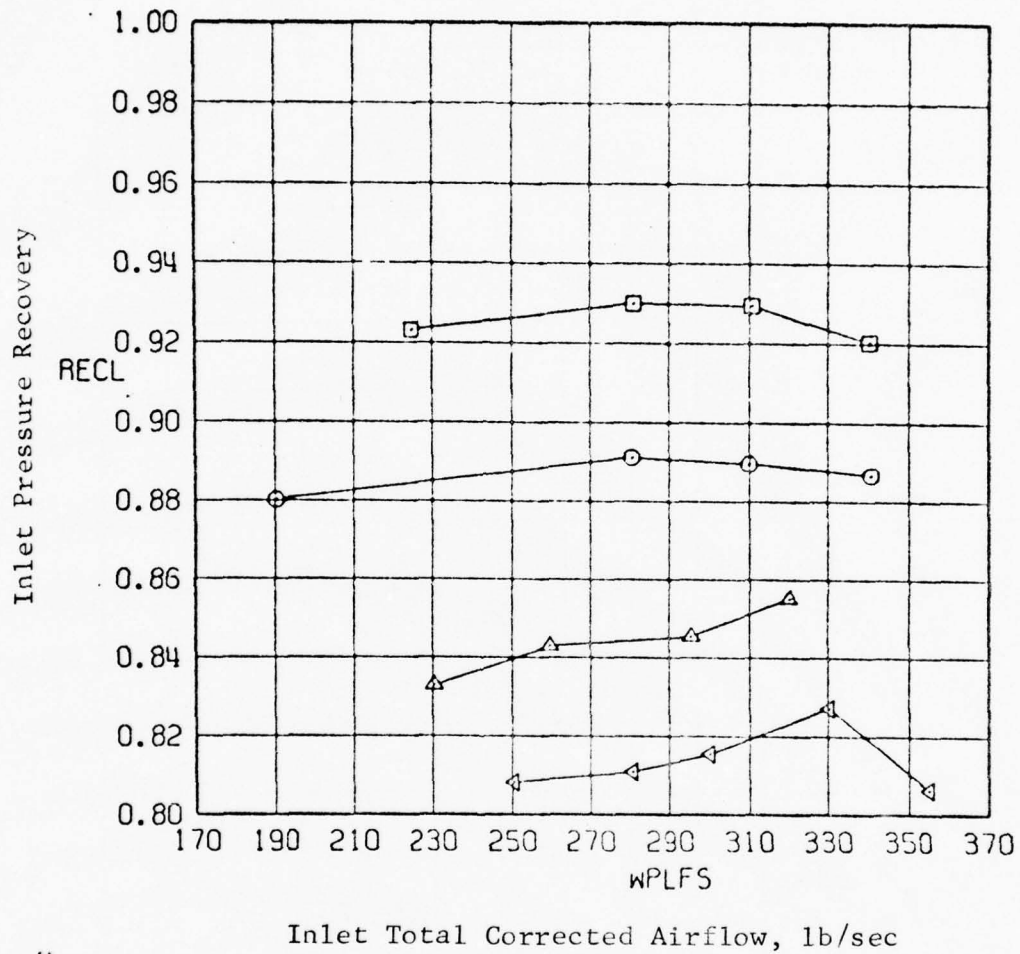


Figure 58. $M_o = 1.62-2.00$ inlet pressure recovery for the Basic Long-Plow/Splitter-Plate Inlet at B.L. 43.82.

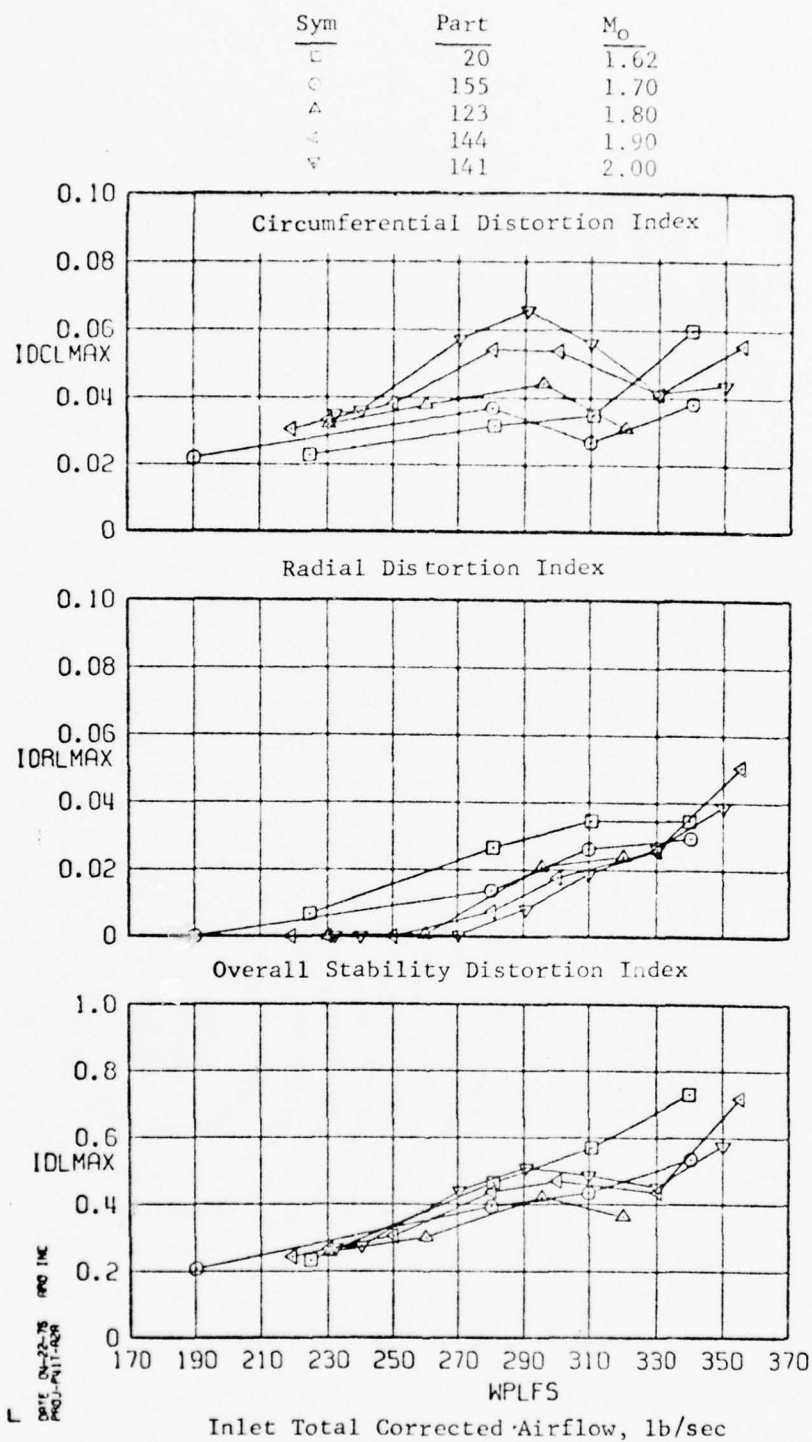


Figure 59. $M_o = 1.62-2.00$ inlet distortion for the Basic Long-Plow/Splitter-Plate Inlet at B.L. 43.82 for $\alpha = 5^\circ$ and $\beta = 0^\circ$.

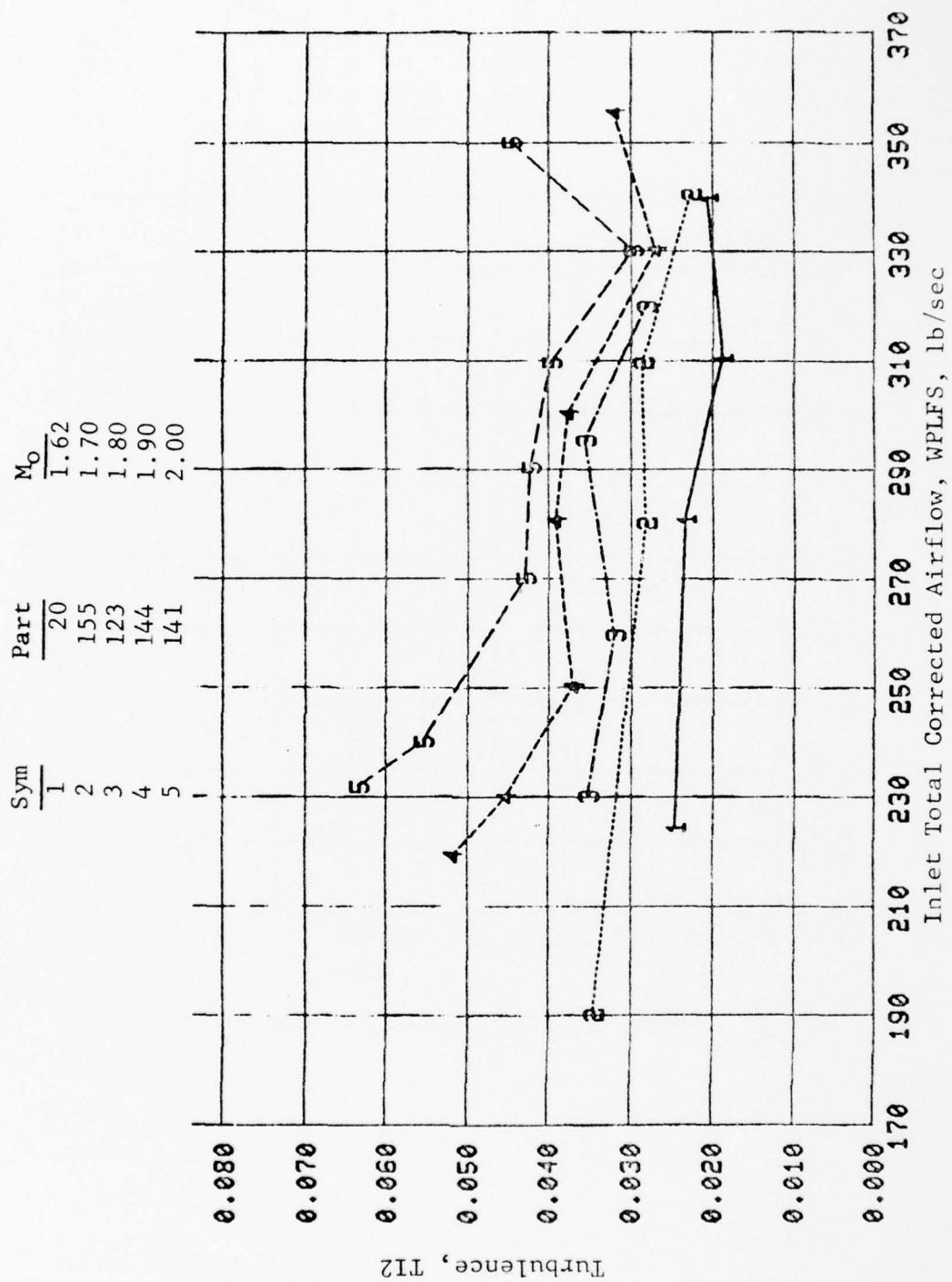


Figure 60. M_o = Mach 1.62-2.00 inlet turbulence for the Basic Long-Plow/Splitter-Plate Inlet at B.L. 43.82 for $\alpha = 5^\circ$ and $\beta = 0^\circ$.

SYMBOL	M_∞	α	β	CONF	PART
□	0.55	5.0	0.0	5	528
○	0.65	5.0	0.0	5	530
△	0.75	5.0	0.0	5	532
◁	0.85	5.0	0.0	5	440

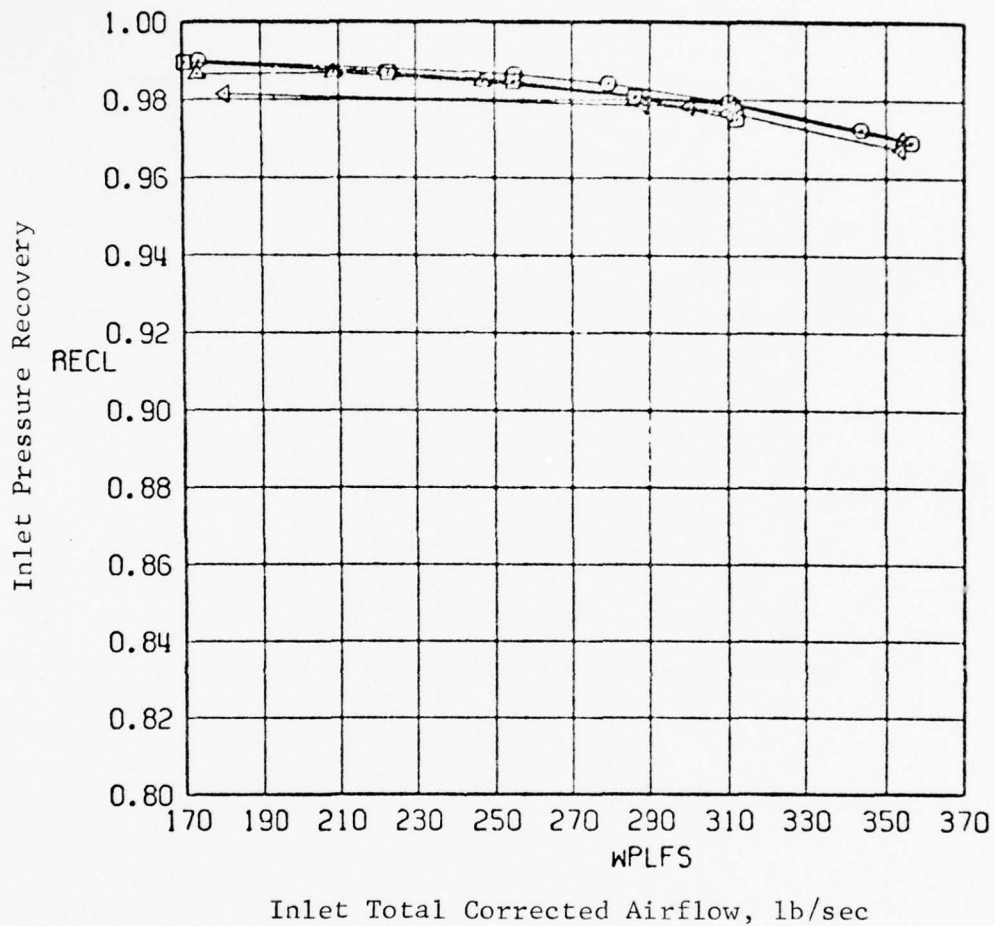


Figure 61. $M_\infty = 0.55-0.85$ inlet pressure recovery for the Basic Long-Plow/Splitter-Plate Inlet at B.L. 45.64.

Sym	Part	M ₀
□	528	0.55
○	530	0.65
△	532	0.75
<	440	0.85

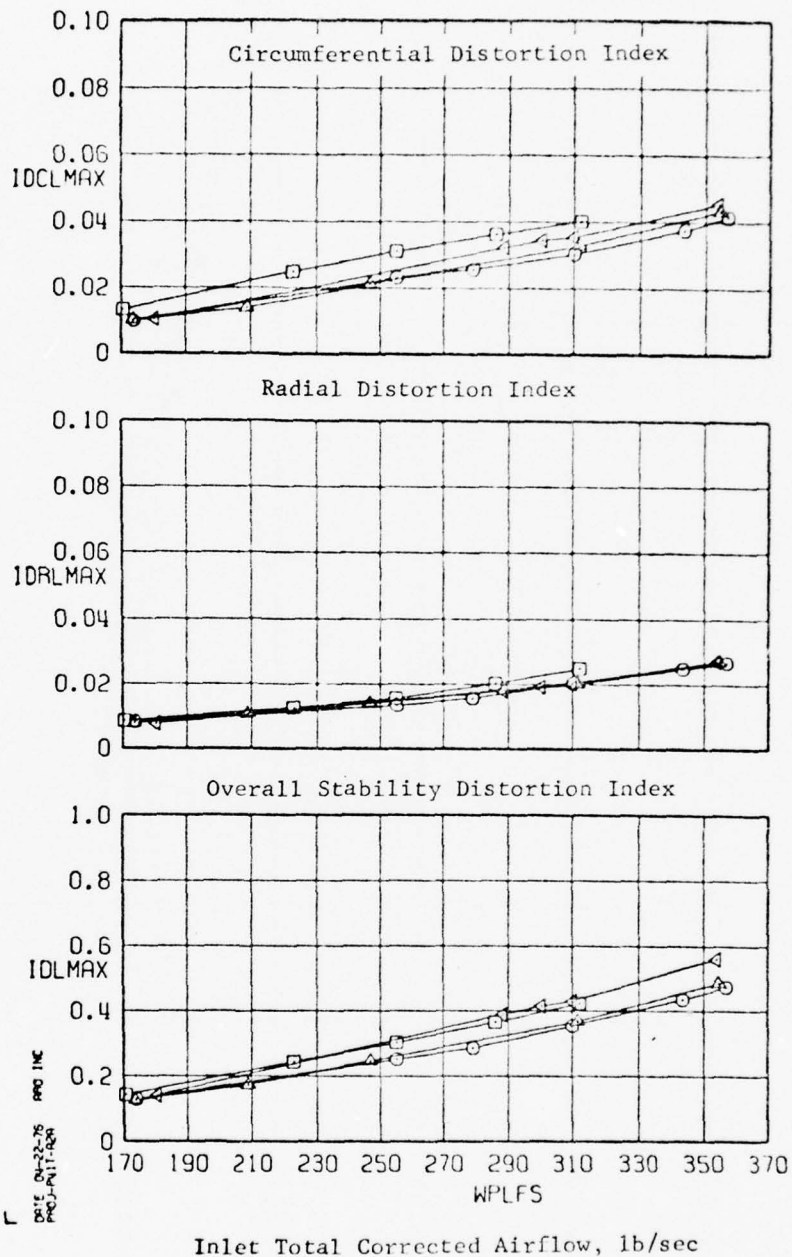


Figure 62. $M_0 = 0.55-0.85$ inlet distortion for the Basic Long-Plow/Splitter-Plate Inlet at B.L. 45.64 for $\alpha = 5^\circ$ and $\beta = 0^\circ$.

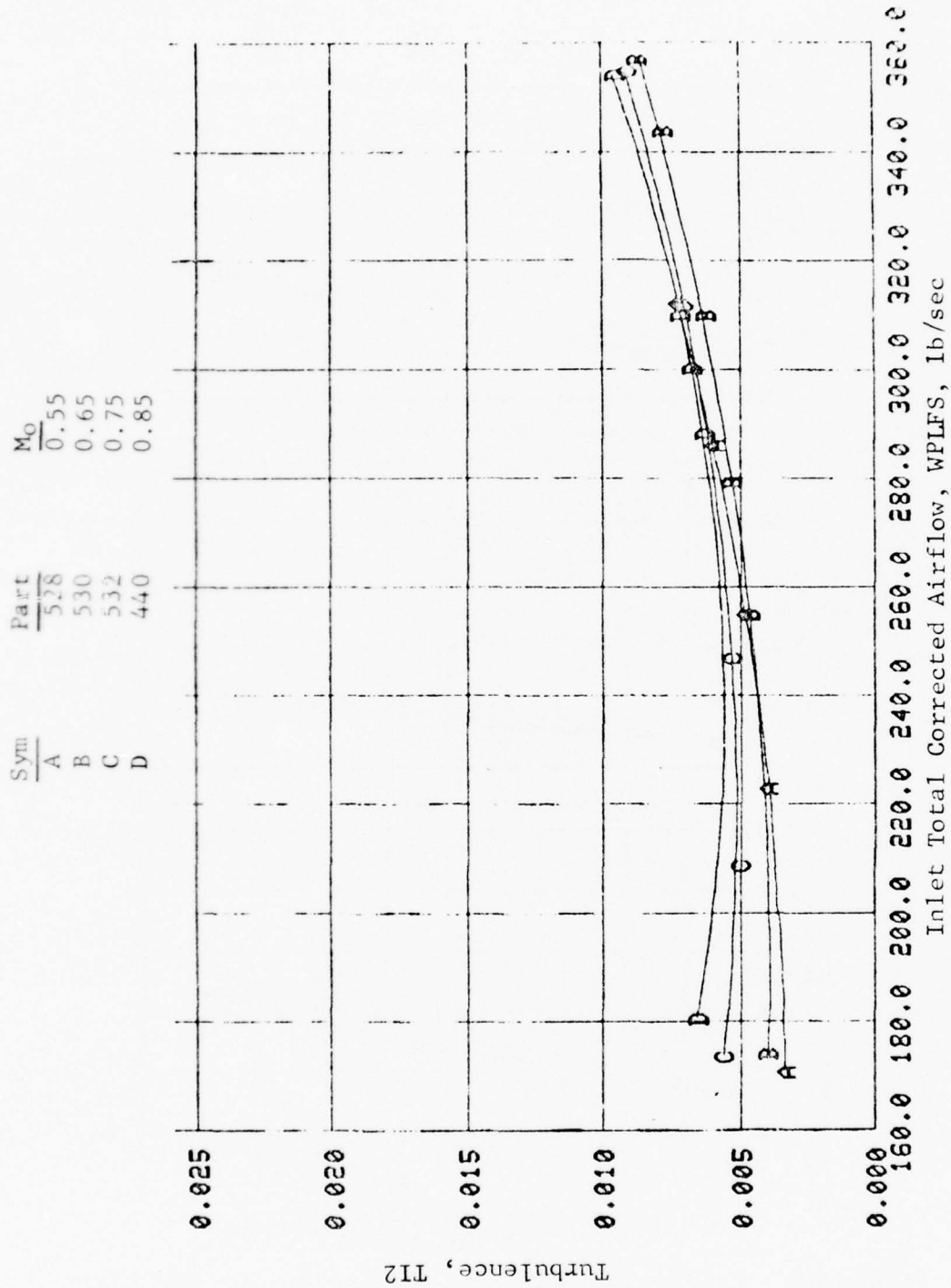


Figure 63. $M_0 = 0.55$ - 0.85 inlet turbulence for the Basic Long-Flow/Splitter-Plate Inlet at B.L. 45.64 for $\alpha = 5^\circ$ and $\beta = 0^\circ$.

SYMBOL	M	α	β	CONF	PART
□	1.20	5.0	0.0	5	456
○	1.40	5.0	0.0	5	471
△	1.50	5.0	0.0	5	545

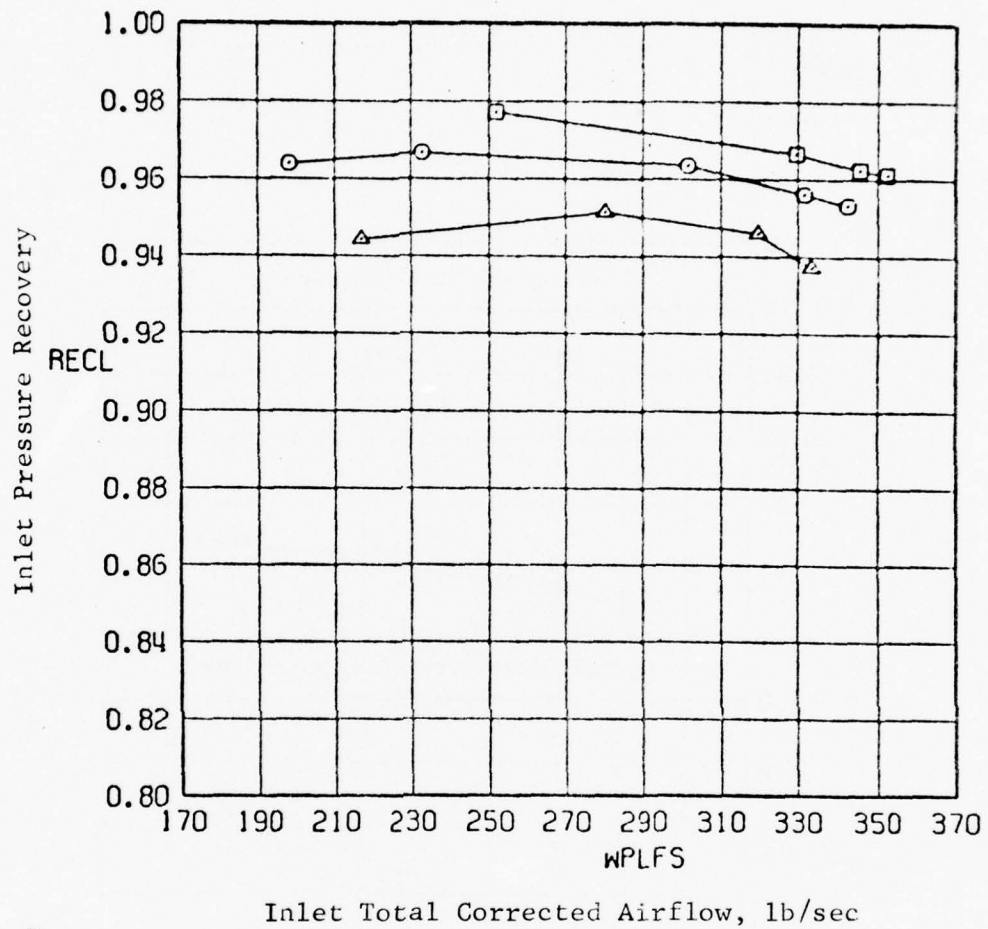


Figure 64. $M_0 = 1.20-1.50$ inlet pressure recovery of the Basic Long-Flow/Splitter-Plate Inlet at B.L. 45.64.

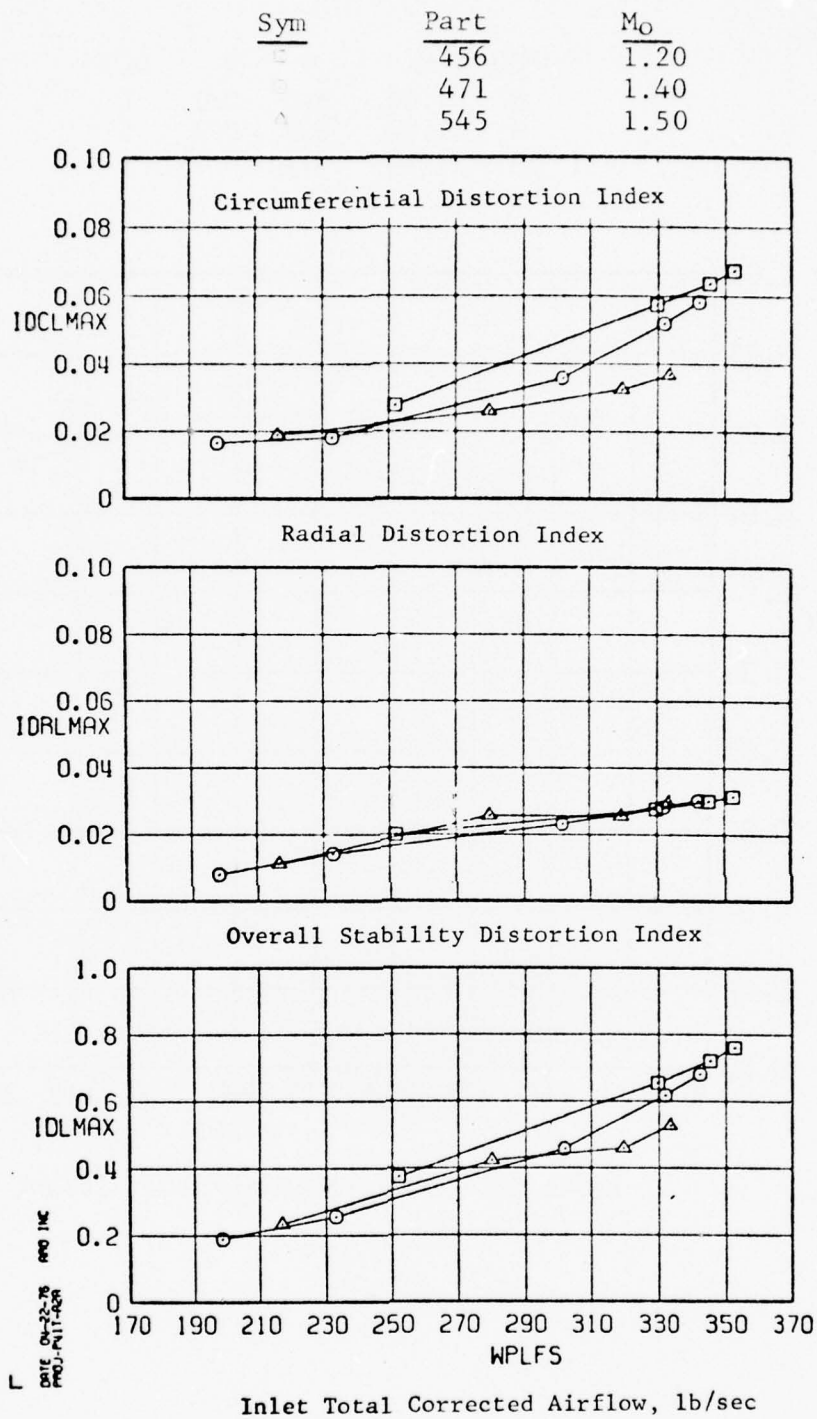


Figure 65. $M_0 = 1.20-1.50$ inlet distortion for the Basic Long-Plow/Splitter-Plate Inlet at B.L. 45.64 for $\alpha = 5^\circ$ and $\beta = 0^\circ$.

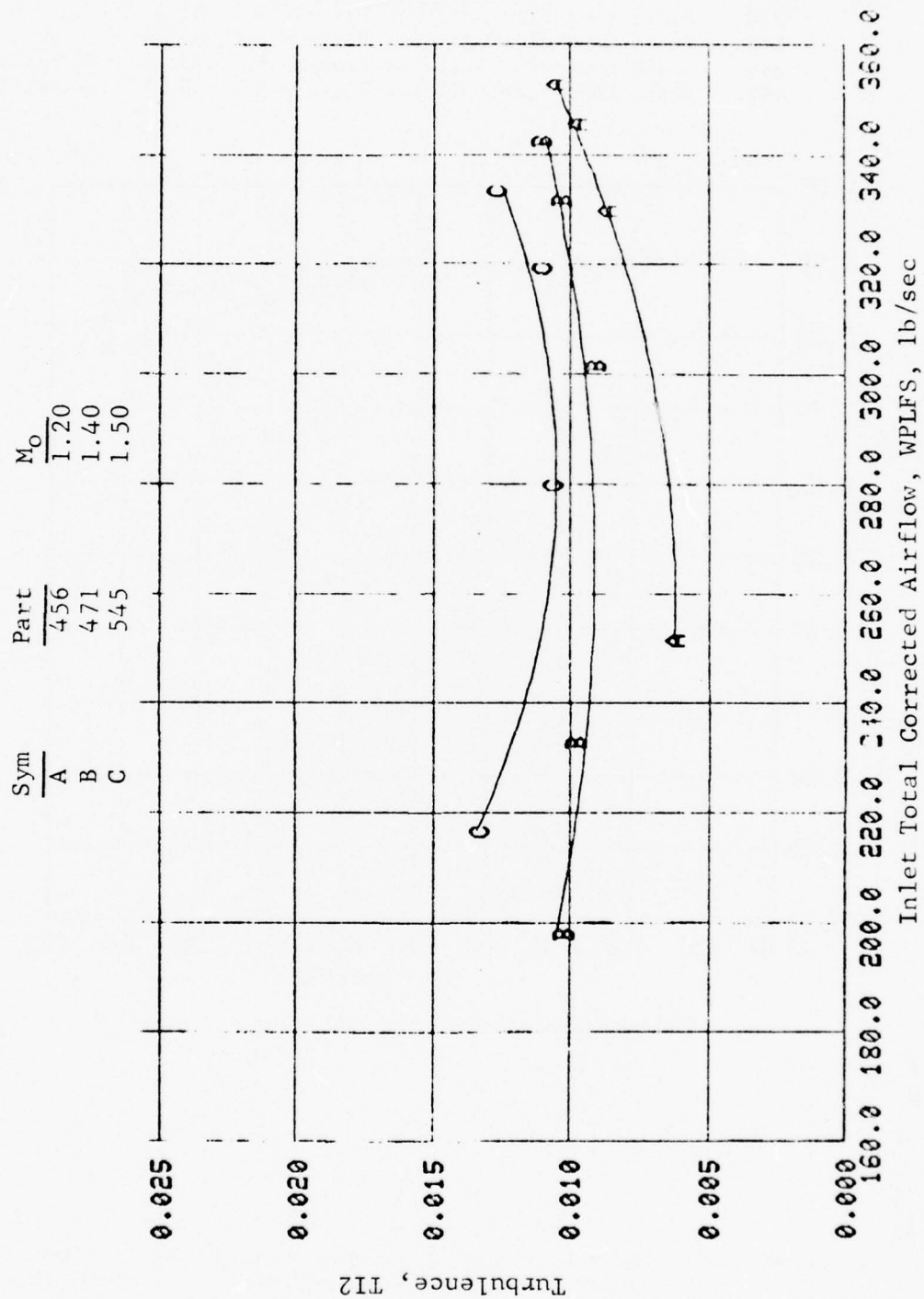


Figure 66. $M_o = 1.20$ - 1.50 inlet turbulence for the Basic Long-Flow/Splitter-Plate Inlet at B.L. 45.64 for $\alpha = 5^\circ$ and $\beta = 0^\circ$.

Sym	Part	Inlet Configuration
□	276	Basic Long Plow/Splitter Plate @ B.L. 43.82
○	440	Basic Long Plow/Splitter Plate @ B.L. 45.64
△	385	Basic Long Plow/Splitter Plate @ B.L. 45.64 + VG Pat 2
◊	492	Basic Long Plow/Splitter Plate @ B.L. 45.64 + VG Pat 3

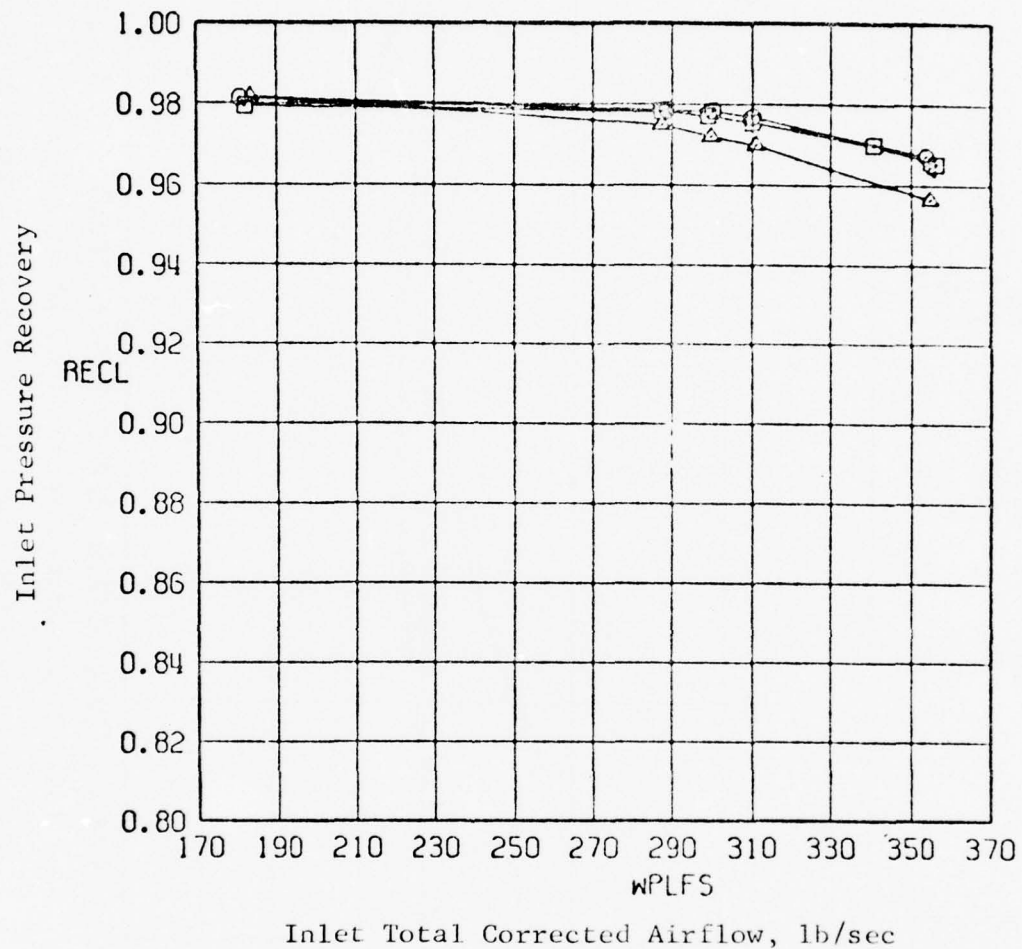


Figure 67. $M_0 = 0.85$ inlet pressure recovery of four inlet configurations at $\alpha = 5^\circ$ and $\beta = 0^\circ$.

Sym	Part	Inlet Configuration
□	276	Basic Long Plow/Splitter Plate @ B.L. 43.82
○	440	Basic Long Plow/Splitter Plate @ B.L. 45.64
△	385	Basic Long Plow/Splitter Plate @ B.L. 45.64 + VG Pat 2
◄	492	Basic Long Plow/Splitter Plate @ B.L. 45.64 + VG Pat 3

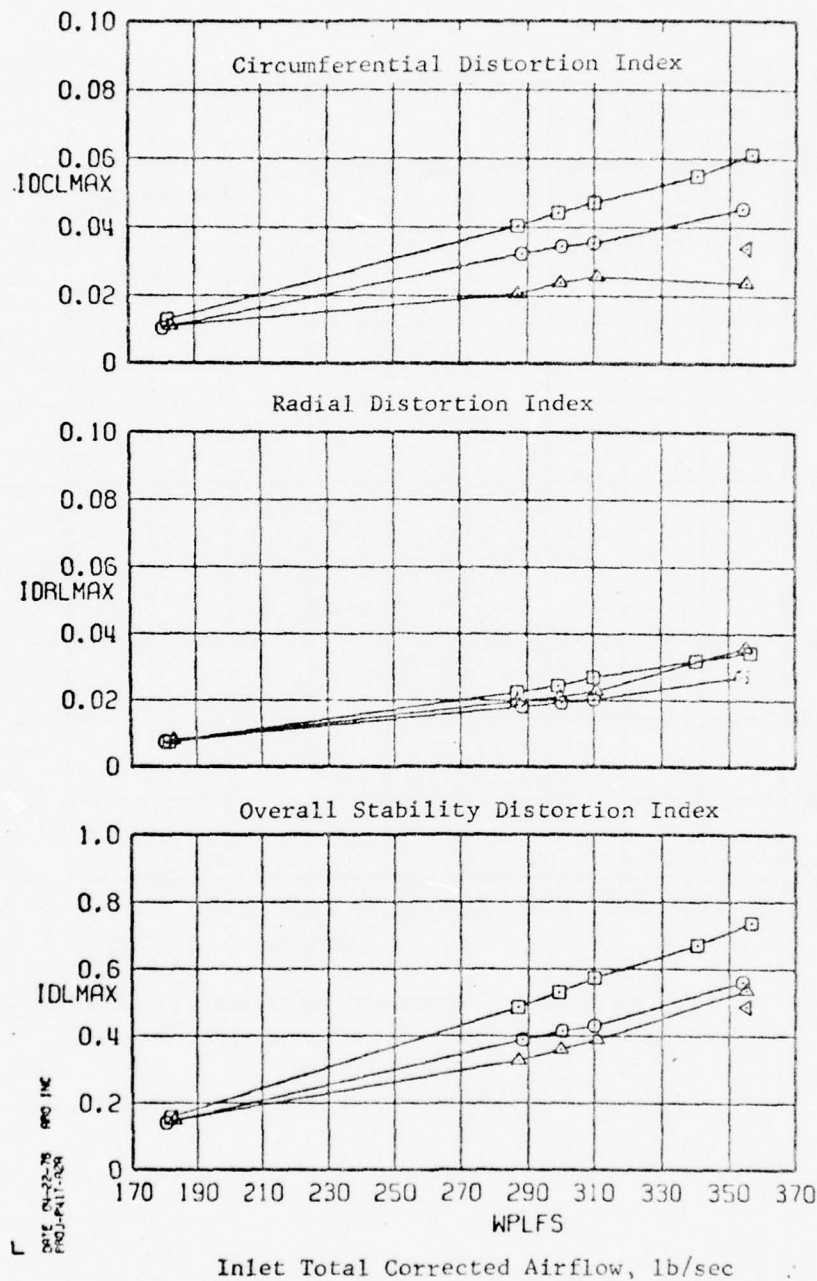


Figure 68. $M_0 = 0.85$ inlet distortion of four inlet configurations at $\alpha = 5^\circ$ and $\beta = 0^\circ$.

Sym	Part	Inlet Configuration
□	276	Basic Long-Flow/Splitter-Plate @ B.L. 43.82
○	245	Alternate Splitter-Plate No. 2 @ B.L. 43.82

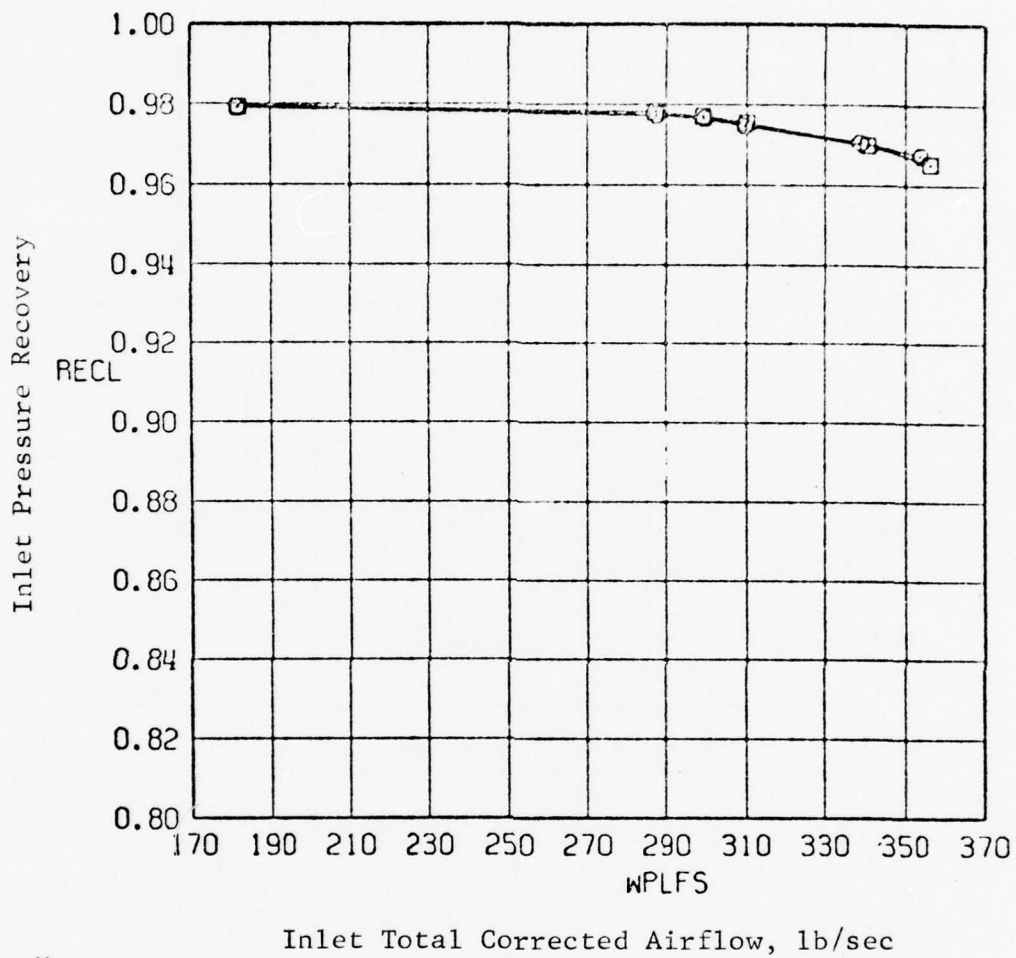


Figure 69. $M_0 = 0.85$ inlet pressure recovery of the Basic Long Splitter Plate and Alternate Splitter Plate No. 2 at $\alpha = 5^\circ$ and $\beta = 0^\circ$.

Sym	Part	Inlet Configuration
□	276	Basic Long Plow/Splitter Plate @ B.L. 43.82
○	245	Alternate Splitter Plate No. 2 @ B.L. 43.82

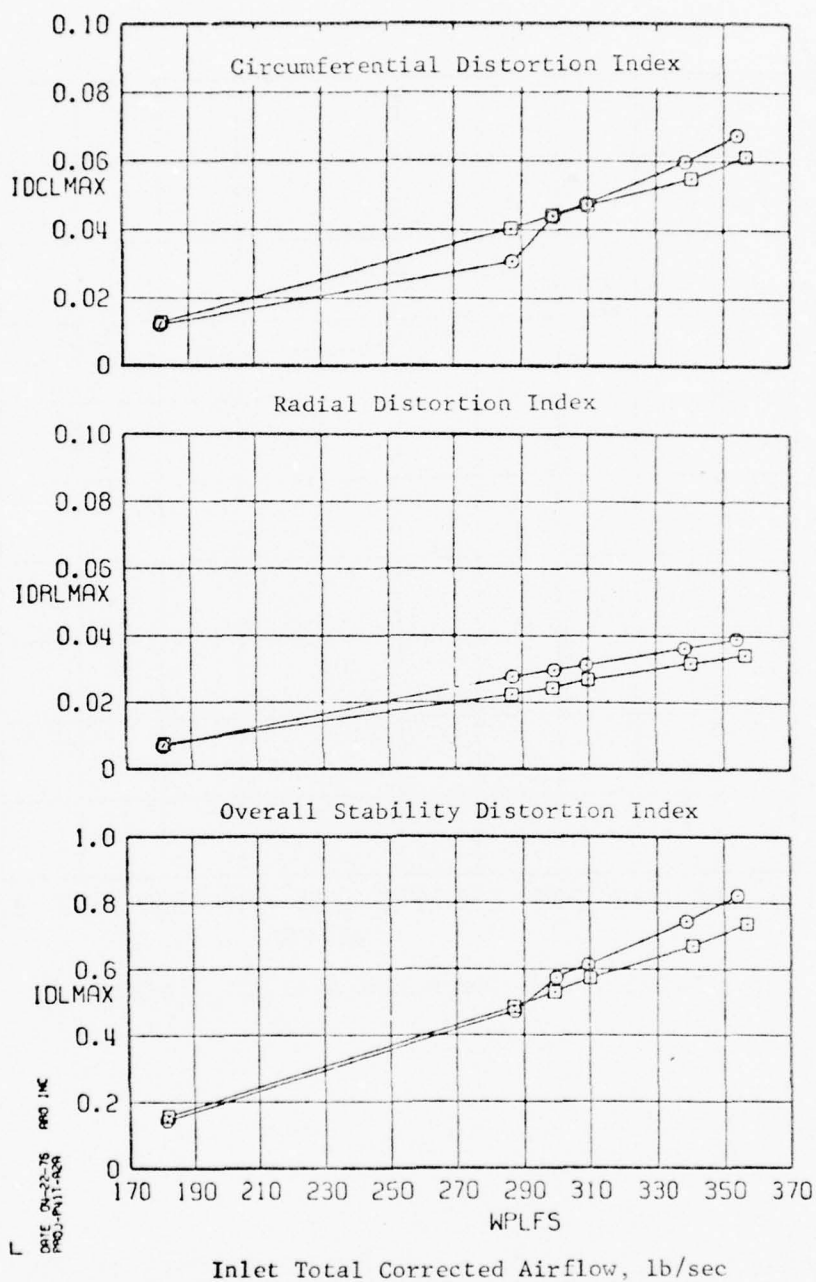
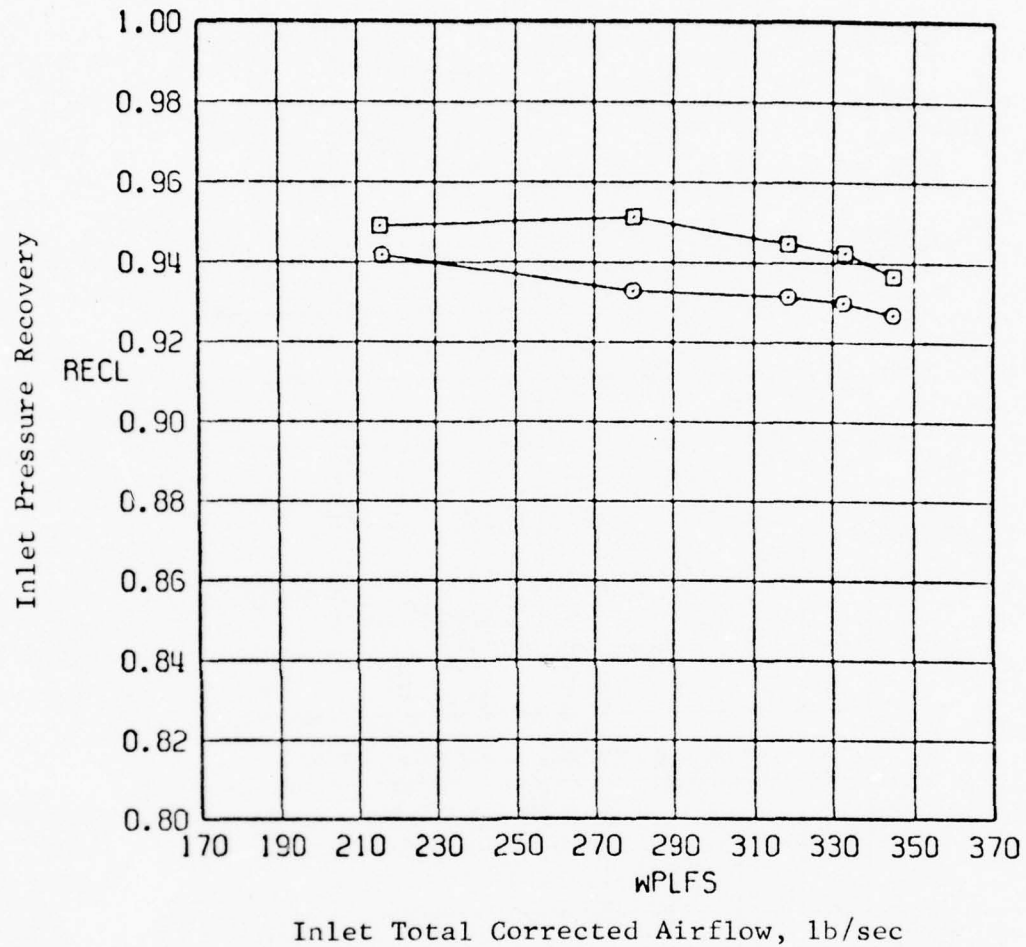


Figure 70. $M_0 = 0.85$ inlet distortion of the Basic Long Splitter Plate and Alternate Splitter No. 2 at $\alpha = 5^\circ$ and $\beta = 0^\circ$.

Sym	Part	Inlet Configuration
E	305	Basic Long Flow/Splitter Plate @ B.L. 43.82
C	267	Alternate Splitter Plate No. 2 @ B.L. 43.82



Date: 04-22-76
 PROJ: P-11-408
 RPO INC

Figure 71. $M_0 = 1.5$ inlet pressure recovery of the Basic Long Splitter Plate and Alternate Splitter No. 2 at $\alpha = 5^\circ$ and $\beta = 0^\circ$.

Sym	Part	Inlet Configuration
□	305	Basic Long Plow/Splitter Plate @ B.L. 43.82
○	267	Alternate Splitter Plate No. 2 @ B.L. 43.82

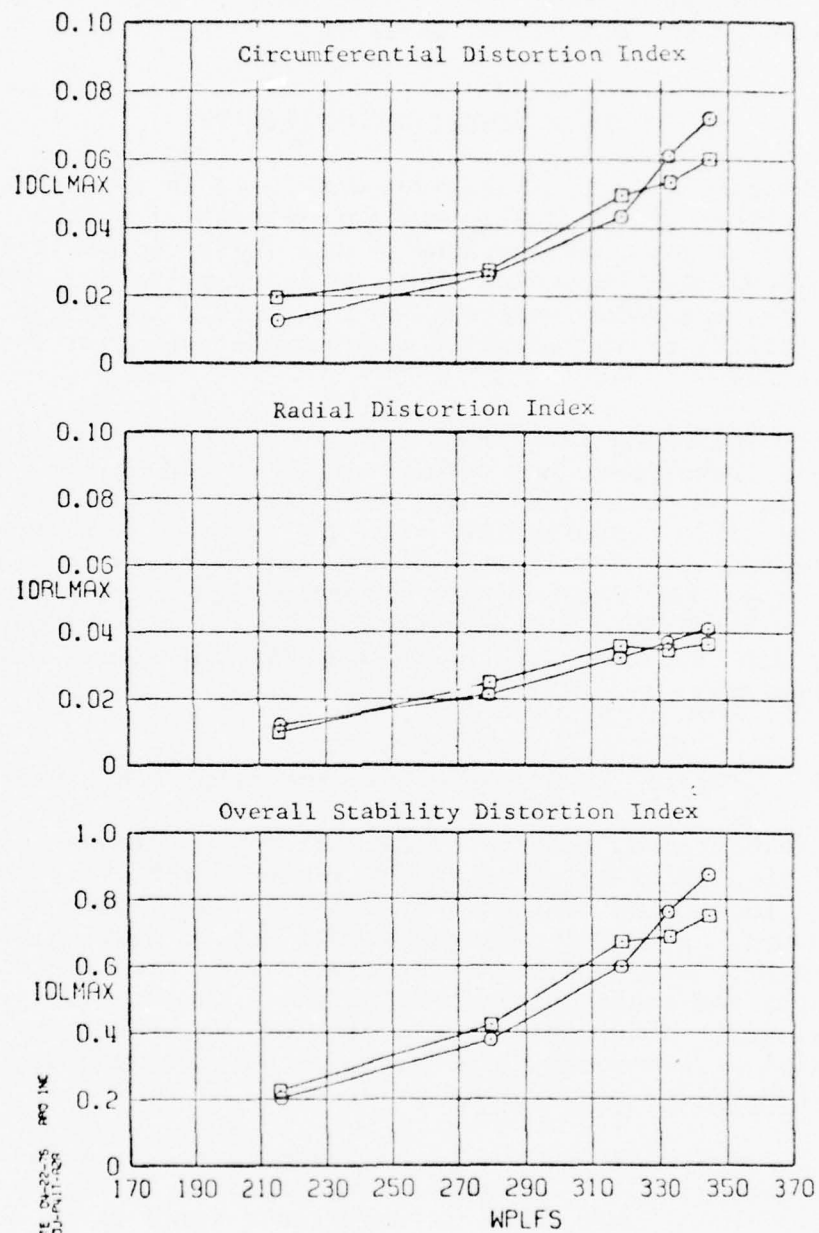


Figure 72. $M_0 = 1.5$ inlet distortion of the Basic Long Splitter Plate and Alternate Splitter No. 2 at $\alpha = 5^\circ$ and $\beta = 0^\circ$.

In summary, inlet pressure recovery for the Basic Long-Plow/Splitter-Plate Inlet is acceptable over the full-Mach range tested in either the B.L. 43.82 or B.L. 45.64 position. Inlet distortion is somewhat lower, however, with the inlet in the B.L. 45.64 position.

4.4 ENGINE/INLET COMPATIBILITY

Acceptable engine/inlet compatibility is an important consideration in the design and development of modern inlets. In certain applications of the inlet, compatibility can be even more important than the inlet pressure recovery. Therefore, extensive analyses were performed to assess the compatibility of the research-model open-nose inlet and the F101 engine.

The following paragraphs contain a description of the analysis techniques, the results of the compatibility assessments, and an extension of the test results to predict the improvement in compatibility when the low-energy defect (Subsection 4.2) is eliminated from the compressor face. It is shown that engine/inlet compatibility is very good with the Basic Long-Plow/Splitter-Plate Inlet positioned at either B.L. 43.82 or B.L. 45.64 when the low-energy defect is corrected.

4.4.1 Hi-Response Data Analysis Techniques

The left-hand compressor face of the model was instrumented with 40 hi-response and 40 steady-state pressure probes, located on centroids of equal areas (Figure 20). The purpose of the hi-response probes was to provide time-variant data with which instantaneous distortion could be evaluated and subsequently, engine/inlet compatibility could be assessed. A complete description of the hi-response data acquisition, recording, processing techniques, and distortion methodology is given in Reference 7.

The various steps of the hi-response analysis leading to the compatibility assessment are depicted in Figure 73. From the total number of test conditions for a given configuration, various conditions are selected for screening on the Analog Distortion Analyzer (ADA). The ADA continuously calculates distortion for the entire 30 seconds of recorded data and denotes the peak value of distortion and

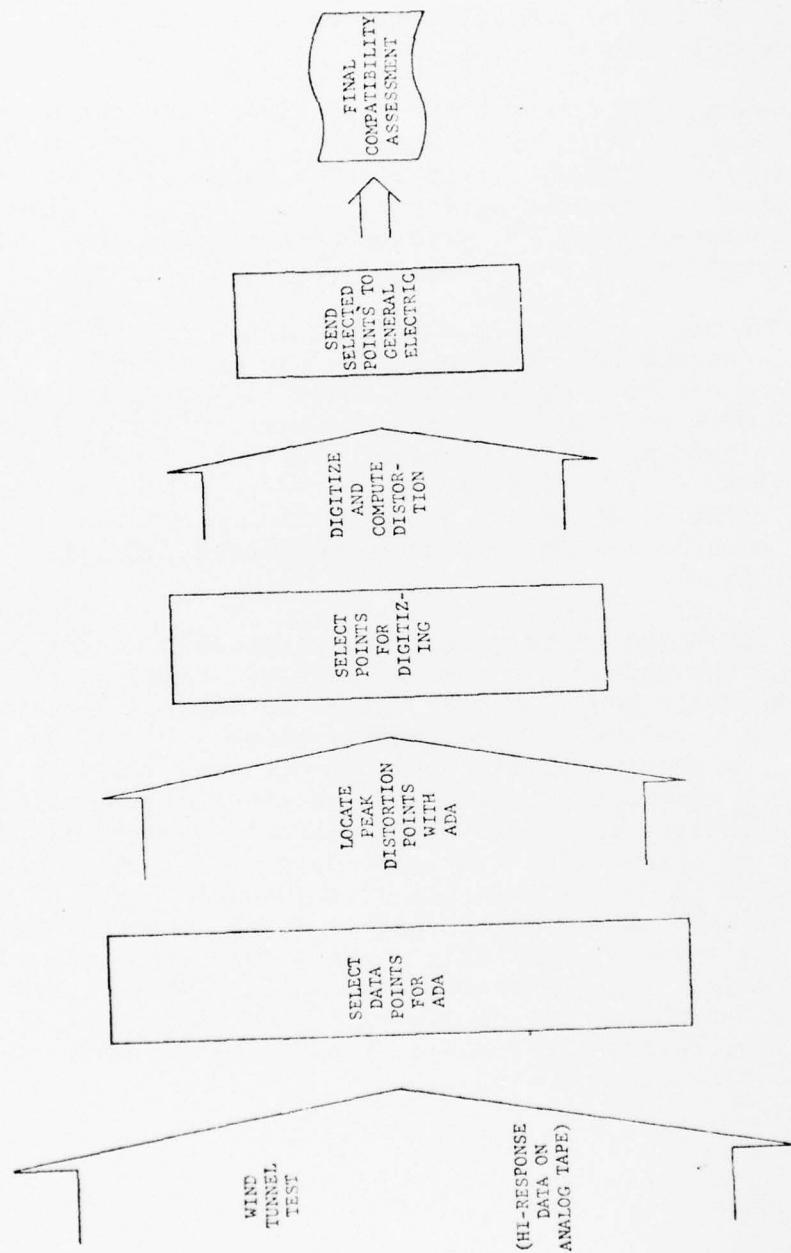


Figure 73. Hi-response analysis procedure.

where it occurs in time. Then, for most of the screened test conditions, a 0.2-second sample of data containing the peak value of distortion is digitized and processed through GE's digital distortion deck (on production at General Dynamics). The digital values of distortion are then used to plot an estimated compatibility envelope at various Mach-altitude combinations.

Throughout this report the term ID denotes the GE stability index. A value of ID less than 1 indicates acceptable engine/inlet compatibility, and a value equal to or greater than 1 indicates potential engine surge. Values of ID superscripted by an "*" were computed on the ADA; non-superscripted values were computed digitally.

The GE distortion deck also calculates values of the distortion parameters, KD2, used for the TF30 engines. It was pointed out earlier that the inlet flow field of this research inlet and the F-111 are similar. Since TF30 engines were used in all versions of the F-111, the value of KD2 generated by the compressor-face pattern that produced the peak value of ID is given herein as a convenient reference for those who wish to compare this research inlet to the F-111 inlets.

The engine/inlet compatibility assessment of the F101 engine and the advanced research inlet was based on the flight (Mach-altitude) envelope given in Figure 74. Although this flight envelope was arbitrarily chosen, it is thought to be representative of the requirements that would be imposed on an aircraft utilizing this engine/inlet combination. The compatibility envelopes that follow are presented from the point of view of the L/H inlet only; i.e., at positive β the inlet is on the lee side of the fuselage and at negative β it is on the windward side. Hence, the negative β side of the envelope typically shows a larger area of surge-free operation than the positive β side. However, for a twin-engine airplane the compatibility envelope must be a mirror-image (symmetrical about $\beta = 0^\circ$) of the most restrictive direction of sideslip.

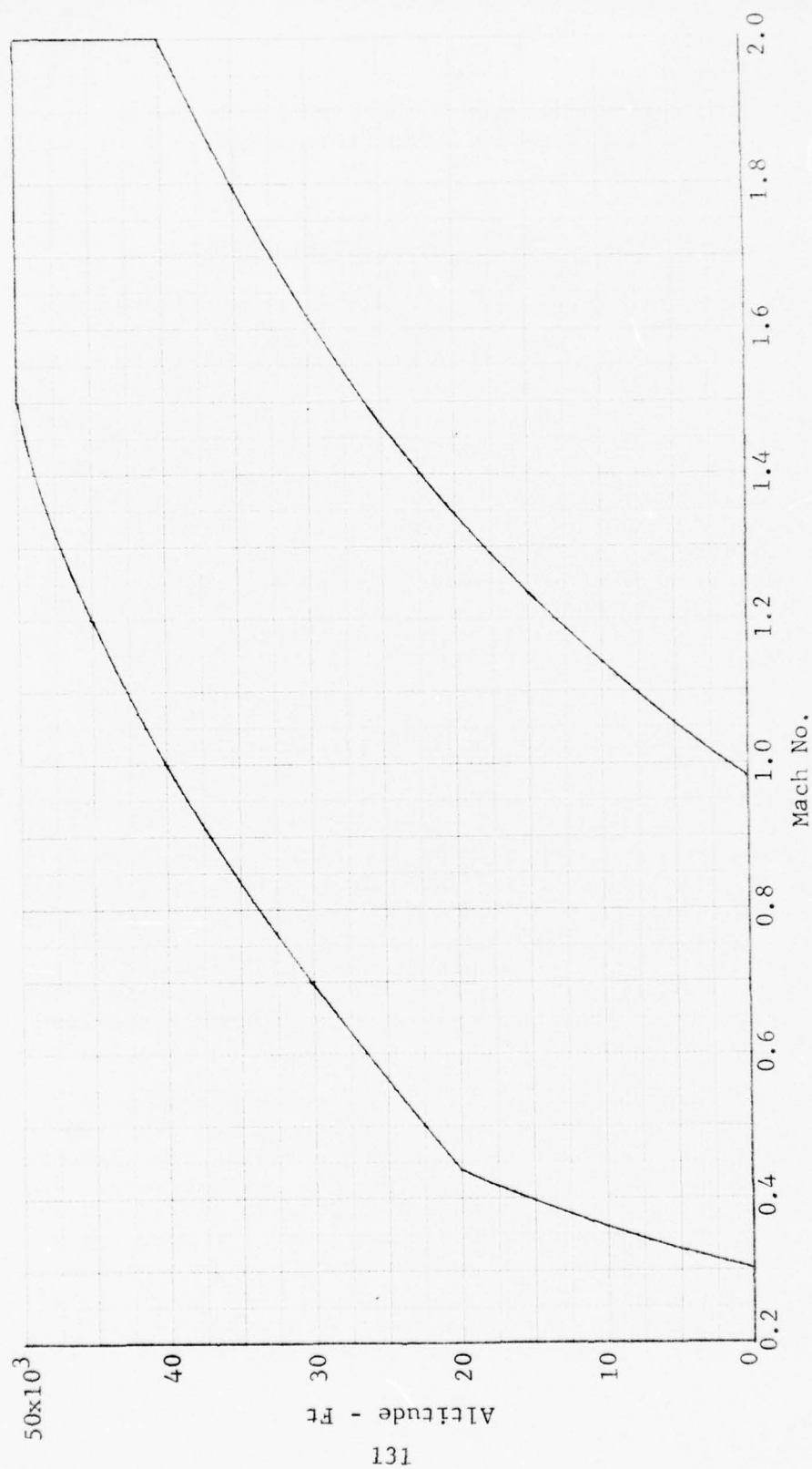


Figure 74. Mach-altitude envelope selected for engine/inlet compatibility analysis.

4.4.2 Compatibility Assessment of the Basic Long-Plow/Splitter-Plate Inlet at B.L. 45.64

4.4.2.1 Basic Inlet Without Vortex Generators

The test conditions selected for hi-response analysis of the Basic Inlet configuration at B.L. 45.64 are listed in Table 5 (2 pages). The estimated compatibility envelopes at Mach 0.85, 1.2, 1.4, and 1.5 are given in Figures 75 through 78. A region of surge-free operation is available at all Mach numbers; the largest region is available at Mach 0.85 and the smallest at Mach 1.2. These envelopes were generated for altitudes along the upper boundary of the assumed flight envelope which are the most adverse flight conditions for engine/inlet compatibility. Figures 79 through 81 present estimated compatibility envelopes for lower altitudes at Mach 1.2, 1.4, and 1.5. The regions of surge-free operation are enlarged significantly at each Mach number.

4.4.2.2 Basic Inlet With Vortex Generator Pattern 3

Earlier in Section 4 it was pointed out that a low-energy region existed at the compressor-face as a result of flow separation over the bend in the duct. VG Pattern 3, Figure 13, was tested on the Basic Long-Plow/Splitter-Plate Inlet at B.L. 45.64 to evaluate its effect on the low-energy region. This configuration was tested at Mach 0.85 and 1.4. The data show a great improvement in the steady-state compressor-face patterns, Figure 48, demonstrating that the low-energy region can be corrected without major redesign of the inlet and duct.

Those test conditions selected for the hi-response analysis of this configuration are given in Table 6. The compatibility envelopes for this configuration are given in Figures 82 and 83 for Mach 0.85 and 1.4, respectively. At Mach 0.85, surge-free operation is available at all tested angle-of-attack and sideslip combinations. At Mach 1.4 surge-free operation is available out to a sideslip of 2° for angle of attack between 0° and 10.6° , and at 0° sideslip surge-free operation is indicated up to a angle of attack of 15° or more. These envelopes were generated for altitudes

Table 5

SUMMARY OF POINTS SELECTED FOR HI-RESPONSE ANALYSIS
 BASIC LONG-PLOW/SPLITTER-PLATE INLET AT B.L. 45.64
 (Page 1 of 2)

Part- Pt.	M ₀	α/β	W _{C2}	\bar{F}_2/\bar{P}_0	\bar{F}_{2my}/\bar{P}_2	ID _{s-s}	ID _{inst}	KD2) _{ro}
436-1	.85	0/0	355	.970	0.75%	.714	*.895	—
438-1		5/-4	353	.971	0.79	.691	*.886	—
440-1		5/0	354	.967	0.96	.561	.839	648
442-1		5/4	356	.956	1.29	.545	.806	585
443-1		10/4	355	.945	1.71	.679	1.024	1154
444-1		10/2	357	.950	1.54	.630	.946	863
445-1		10/0	358	.954	1.37	.573	*.891	—
447-1		10/-4	358	.963	1.08	.512	*.728	—
448-1		13/-2	358	.953	1.36	.582	*.870	—
449-1		13/0	357	.948	1.56	.596	.957	890
450-1	.85	13/2	355	.943	1.85	.641	1.033	1029
452-1	1.2	0/0	353	.962	0.88	.841	*.966	—
453-2		0/2		.962	0.93	.801	*.987	—
454-1		0/-2		.962	0.89	.853	.972	579
455-1		5/-4		.963	0.91	.845	*.013	—
455-2		5/-2		.963	0.95	.815	.996	585
456-1		5/0		.961	1.06	.762	.969	588
457-1		5/2		.949	1.33	.717	.999	786
458-1		5/4		.938	1.64	.777	1.171	981
459-1		10/4		.916	2.44	.836	*1.271	—
460-1		10/0		.944	1.50	.768	1.075	759
461-1		10/-4		.957	1.08	.822	*1.035	—
462-1		13/-2		.949	1.41	.765	*1.040	—
463-1	1.2	13/0	353	.942	1.78	.704	1.046	863
464-1	1.2	13/2	353	.923	2.36%	.810	*1.264	—
466-1	1.4	0/0	343	.946	1.11	.631	.882	—
471-1		5/0		.953	1.11	.681	.965	552
472-1		5/2		.944	1.44	.615	.943	806
473-1		5/4		.929	1.92	.724	*1.164	—
474-1		10/4		.921	2.23	.692	*1.323	—
475-1		10/0		.948	1.36	.758	1.003	728
476-1		10/-4		.958	1.02	.832	*.995	—
477-1		13/-2		.957	1.09	.814	*.992	—
478-1		13/0		.951	1.26	.792	.985	771
479-1		13/2		.936	1.70	.807	1.178	1210
480-1		10/2		.941	1.69	.705	1.087	959
481-1	1.4	10/-2	343	.953	1.15	.792	.969	707
542-2	1.5	0/0	333	.929	1.40	.508	*.776	—
543-1	1.5	0/-2	333	.930	1.29	.678	*.893	—
544-1	1.5	0/2	333	.925	1.54	.475	*.765	—

*Denotes value of ID from analog computer

Table 5 (Cont'd)

SUMMARY OF POINTS SELECTED FOR HI-RESPONSE ANALYSIS
 BASIC LONG-PLOW/SPLITTER-PLATE INLET AT B.L. 45.64
 (Page 2 of 2)

Part Pt.	M ₀	α/β	W _{c2}	\bar{R}_1/\bar{R}_{c0}	\bar{R}_{1rms}/\bar{R}_2	ID _{S-S}	ID _{inst}	KD2 _{1D}
545-1	1.5	5/0	333	.937	1.27	.527	*.809	—
546-1		5/4		.914	2.19	.693	1.068	1173
547-1		5/2		.932	1.62	.559	*.902	851
548-1		5/-2		.945	1.11	.582	*.832	—
549-1		5/-4		.944	1.05	.643	*.886	—
550-1		10/0		.942	1.40	.625	*.939	738
551-1		10/-4		.953	1.05	.715	*.922	—
552-1		10/-2		.949	1.19	.677	*.910	—
553-1	1.5	10/2	333	.935	1.69%	.724	1.094	992
555-1		13/2		.938	1.51	.787	1.092	1254
556-1		13/0		.950	1.13	.769	.962	669
557-1	1.5	13/-2	333	.953	1.00	.778	*.959	—

*Denotes value of ID from analog computer

Numbers shown are values
of ID given in Table 5

*Denotes value of ID from analog computer.

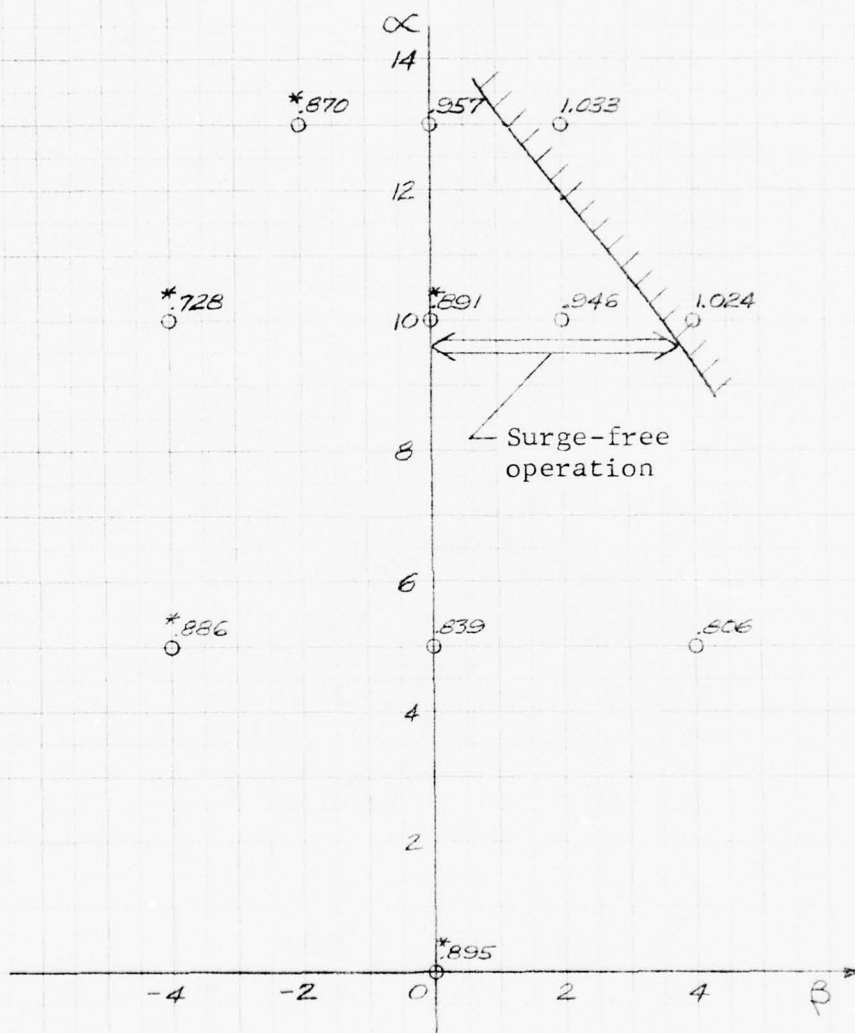


Figure 75. Estimated compatibility envelope of the Basic Long-Plow/Splitter-Plate Inlet at B.L. 45.64 with $M_0 = 0.85$ and altitude = 35,500 ft.

Numbers shown are values
of ID given in Table 5
*Denotes value of ID from analog computer.

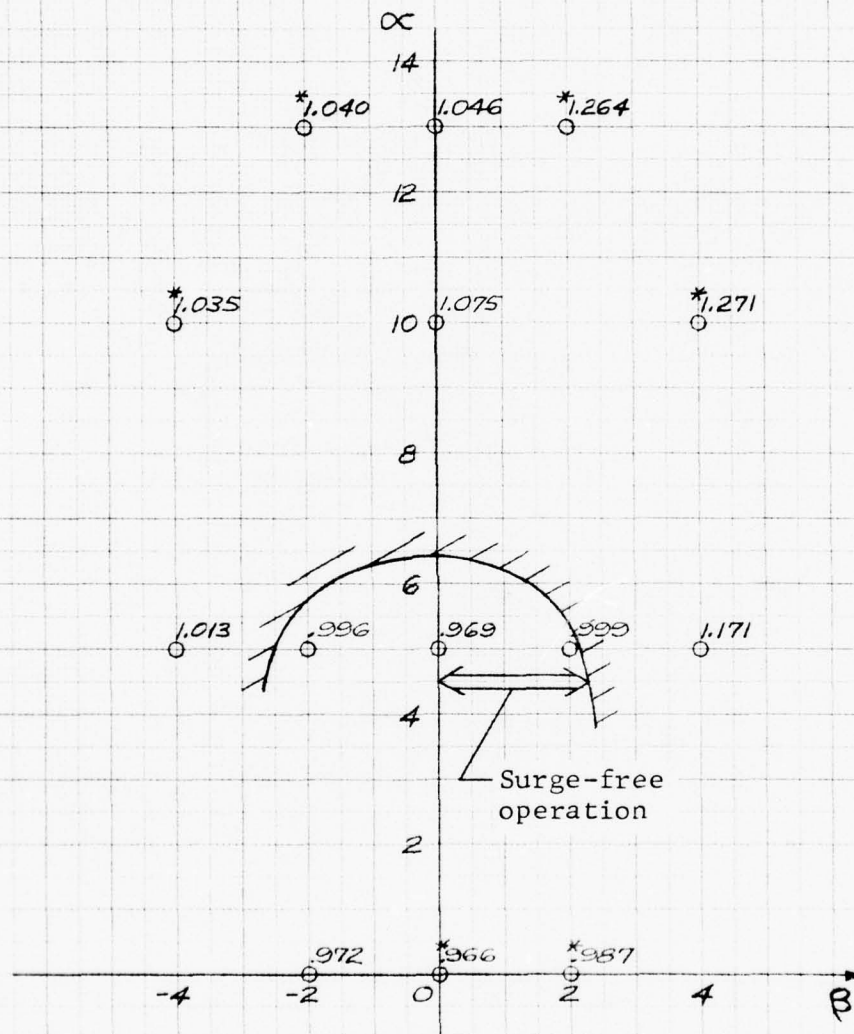


Figure 76. Estimated compatibility envelope of the Basic Long-Plow/Splitter-Plate Inlet at B.L. 45.64 with $M_0 = 1.2$ and altitude = 45,000 ft.

Numbers shown are values
of ID given in Table 5
*Denotes value of ID from analog computer.

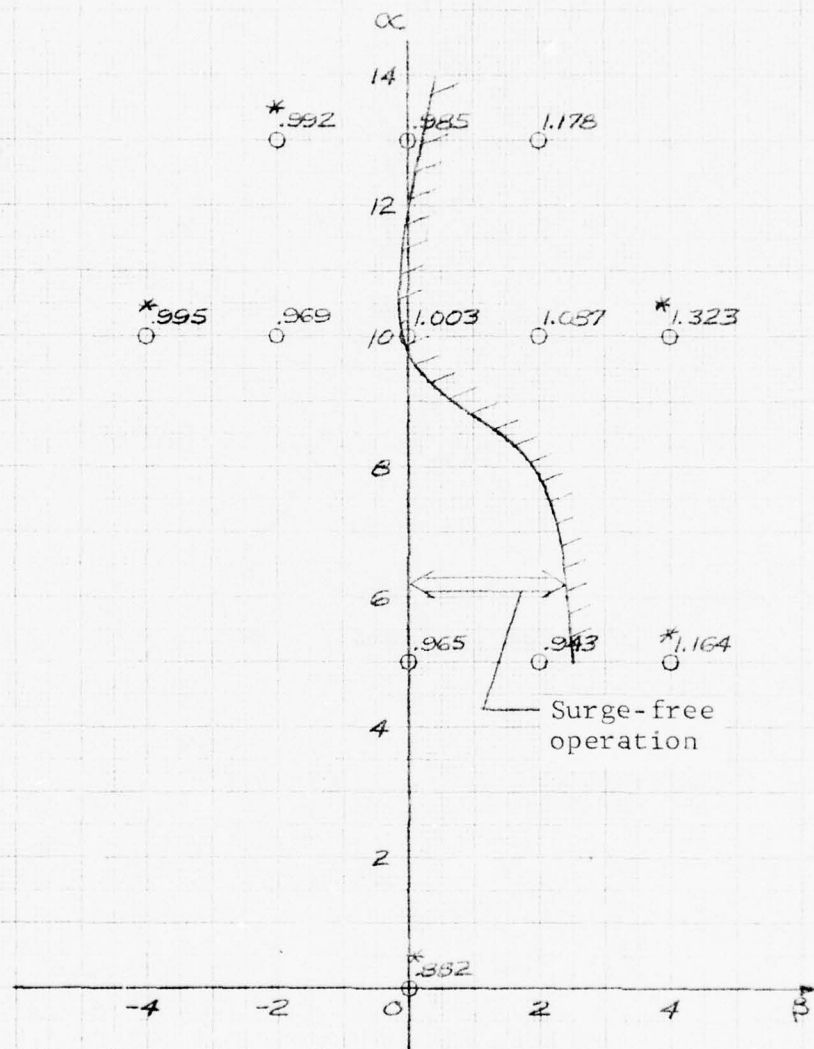


Figure 77. Estimated compatibility envelope of the Basic Long-Plow/Splitter-Plate Inlet at B.L. 45.64 with $M_0 = 1.4$ and altitude = 48,000 ft.

Numbers shown are values
of ID given in Table 5

*Denotes value of ID from analog computer.

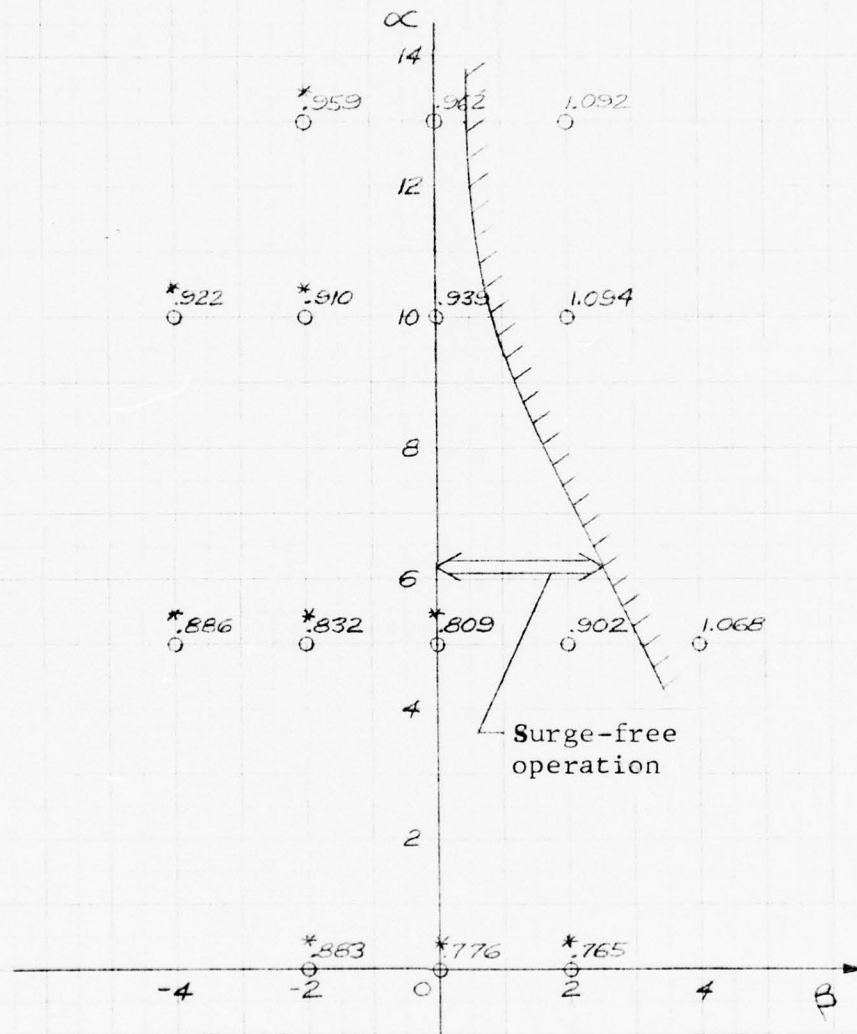


Figure 78. Estimated compatibility envelope of the Basic Long-Plow/Splitter-Plate Inlet at B.L. 45.64 with $M_0 = 1.5$ and altitude = 49,500 ft.

Numbers shown are values of ID

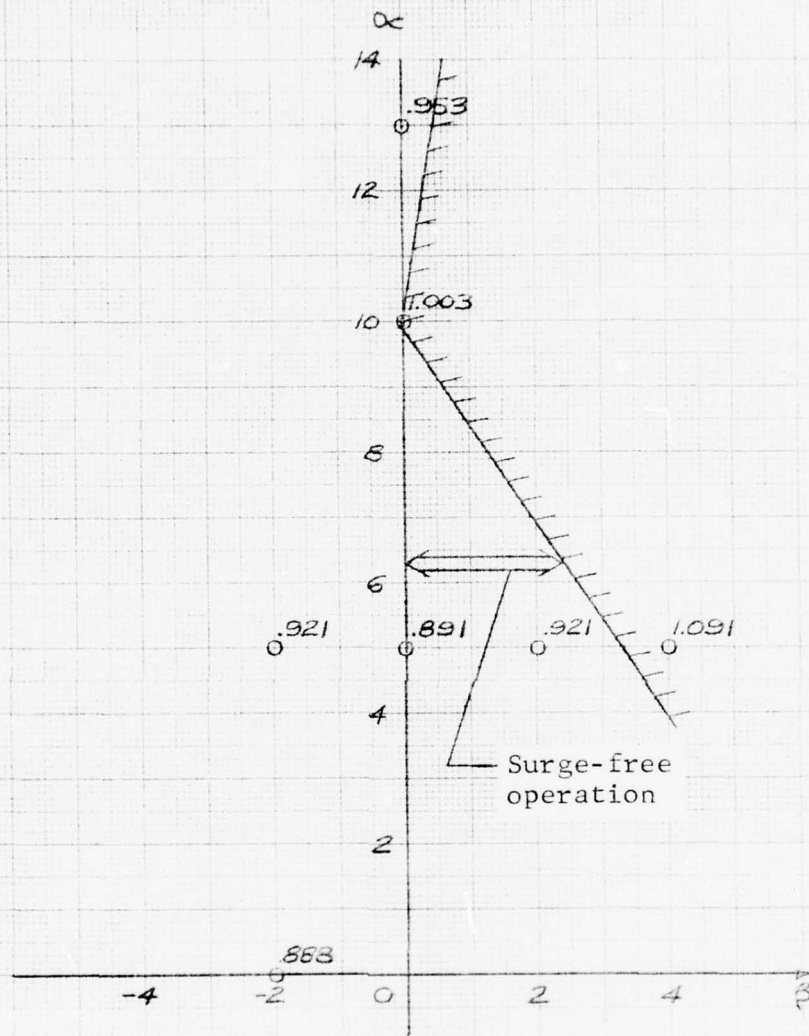


Figure 79. Estimated compatibility envelope of the Basic Long-Plow/Splitter-Plate Inlet at B.L. 45.64 with $M_0 = 1.2$ and altitude = 36,000 ft.

Numbers shown are values of ID

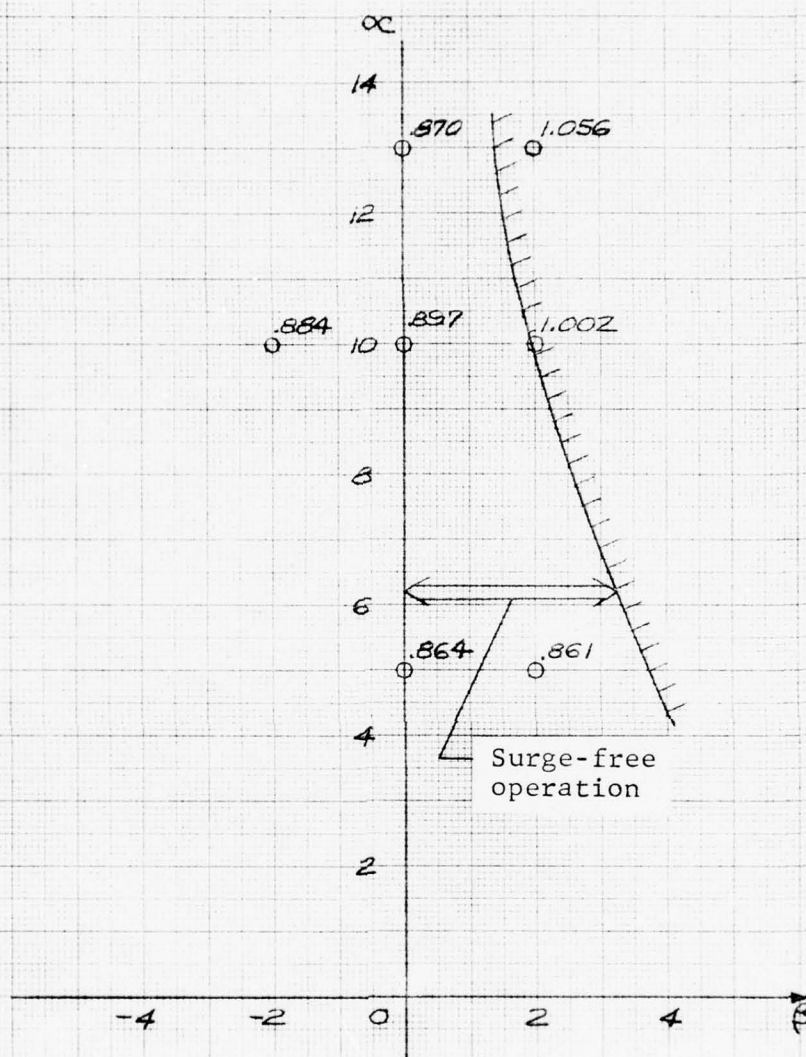


Figure 80. Estimated compatibility envelope of the Basic Long-Plow/Splitter-Plate Inlet at B.L. 45.64 with $M_0 = 1.4$ and altitude = 40,000 ft.

Numbers shown are values of ID

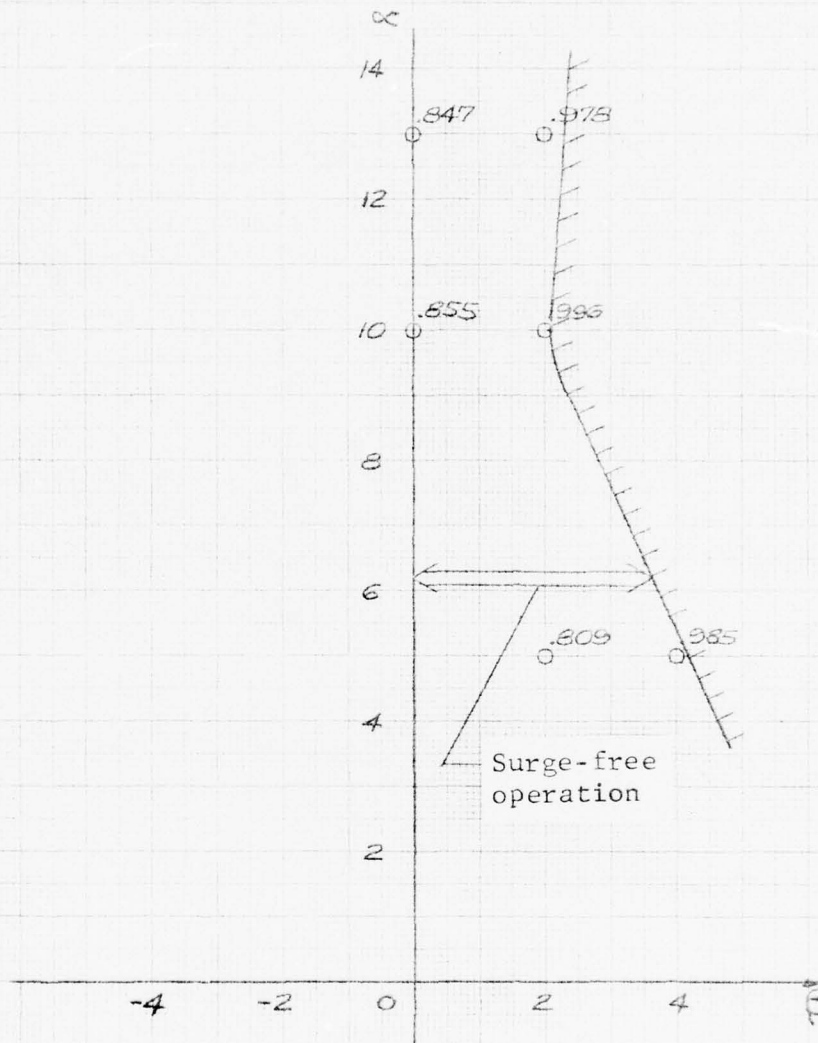


Figure 81. Estimated compatibility envelope of the Basic Long-Plow/Splitter-Plate Inlet at B.L. 45.64 with $M_0 = 1.5$ and altitude = 44,000 ft.

Table 6

SUMMARY OF POINTS SELECTED FOR HI-RESPONSE ANALYSIS
 BASIC LONG-PLOW/SPLITTER-PLATE INLET AT B.L. 45.64
 VORTEX GENERATOR PATTERN 3

Part- Pt.	M ₀	∞/β	W _{C2}	\overline{P}_{t2}/P_{t0}	$\overline{P}_{t2max}/\overline{P}_{t2}$	ID _{SS}	ID _{INST}	KD2 _{TD}
433-2	0.85	0/2	355	.968	0.76%	.466	*.596	—
431-1		5/-2		.967	0.81	.480	*.610	—
432-2		5/0		.964	0.87	.486	.642	618
499-1		5/2		.958	1.02	.515	*.739	—
500-1		5/4		.953	1.14	.542	*.785	—
501-1		10/4		.941	1.65	.651	.922	893
502-1		10/2		.947	1.33	.632	.938	904
503-1		10/0		.950	1.20	.571	*.846	—
506-2		10/-2		.955	1.09	.515	*.789	—
509-1		13/-2		.949	1.19	.588	*.900	—
510-1		13/0		.946	1.35	.616	.929	1106
512-1	0.85	13/2	355	.940	1.70	.609	.895	1012
514-2	.40	5/-4	343	.958	0.94%	.512	*.642	—
515-1		5/-2		.951	0.96	.435	*.671	—
516-1		5/0		.950	1.04	.476	.684	557
515-1		5/2		.940	1.32	.572	.653	536
519-1		5/4		.926	1.67	.707	1.145	1092
520-1		10/4		.916	2.12	.662	*.842	—
520-2		10/2		.937	1.85	.663	.891	797
521-1		10/0		.943	1.32	.643	.878	794
522-1		10/-2		.948	1.13	.563	*.822	—
523-1	.40	10/-4	343	.955	1.01	.494	*.741	—

*Denotes value of ID from analog computer

Numbers shown are values
of ID given in Table 6
*Denotes value of ID from analog computer.

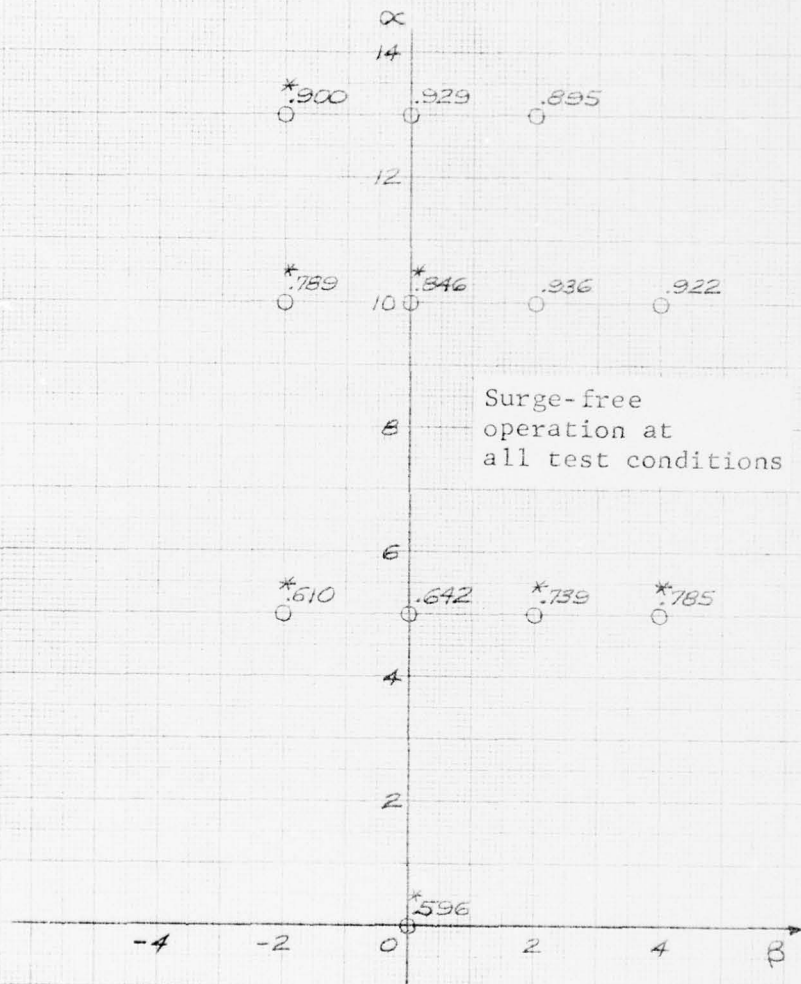


Figure 82. Estimated compatibility of the Basic Long-Plow/
Splitter-Plate Inlet, with Vortex Generator
Pattern 3, at B.L. 45.64 with $M_0 = 0.85$ and
altitude = 35,500 ft.

Numbers shown are values
of ID given in Table 6
*Denotes value of ID from analog computer.

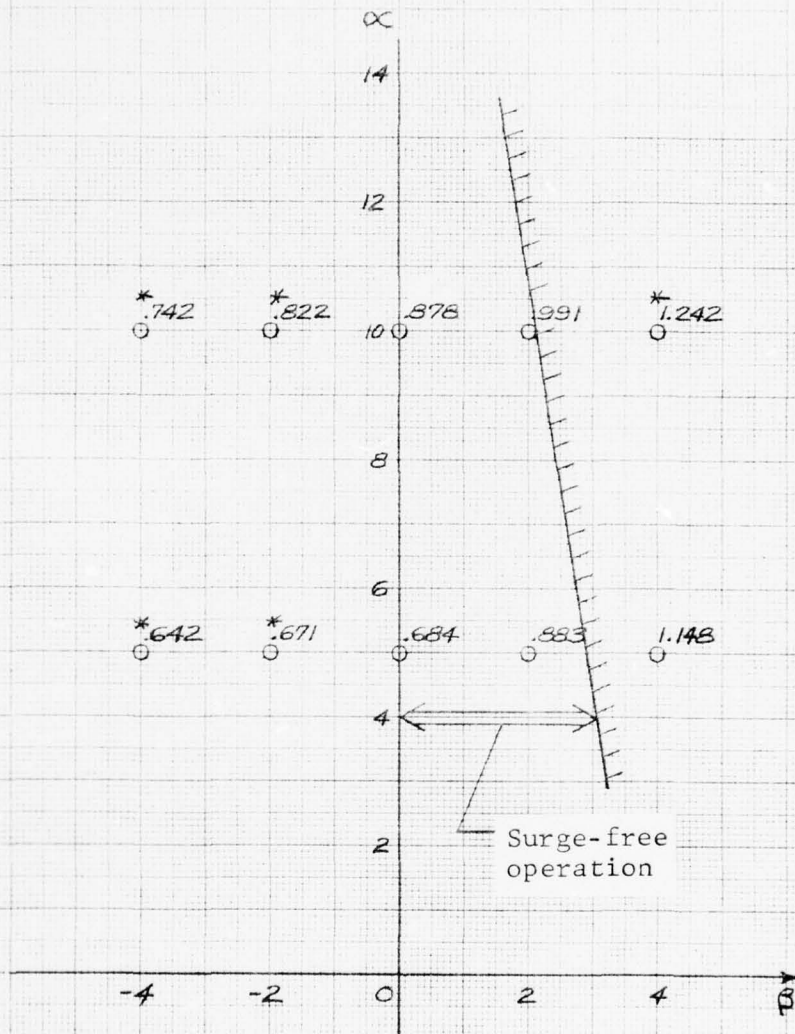


Figure 83. Estimated compatibility of the Basic Long-Plow/Splitter-Plate Inlet, with Vortex Generator Pattern 3, at B.L. 45.64 with $M_0 = 1.4$ and altitude = 48,000 ft.

along the upper boundary of the assumed flight envelope; compatibility is even better at lower altitudes.

4.4.2.3 Evaluation of VG Pattern 3 on Engine/Inlet Compatibility

Comparison of Figures 75 and 82, and Figures 77 and 83 reveals the effect of the vortex generators on compatibility. With the VGs installed, compatibility is enhanced at both Mach 0.85 and 1.4. This supports the conclusion of Subsection 4.2 that this VG pattern does correct the defect. Also, these results illustrate that some modification to the duct bend should be considered prior to further tests of the research inlet.

4.4.3 Basic Long-Plow/Splitter-Plate Inlet at B.L. 43.82

4.4.3.1 Compatibility Assessment

The points selected for the hi-response analysis of the Basic Inlet configuration at B.L. 43.82 are listed in Table 7. The estimated compatibility envelopes for Mach 0.85, 1.2, 1.4, 1.5, 1.6, and 1.7 are given in Figures 84 through 89, respectively. Regions of surge-free operation are available at all Mach numbers except 1.2; however, the regions at Mach 1.4 and 1.5 are smaller than desired. Again, these envelopes are for altitudes along the upper boundary of the assumed flight envelope. Figures 90 through 92 present the estimated compatibility envelopes at lower altitudes for Mach 1.2, 1.4, and 1.5. At each Mach number the region of surge-free operation is enlarged. However, the most significant difference occurs at Mach 1.2; at the lower altitude a region of surge-free operation is available whereas at the higher altitude there was none.

4.4.3.2 Predicted Compatibility With the Low-Energy Defect Corrected

The Basic Long-Plow/Splitter-Plate Inlet at B.L. 43.82 was not tested with VG Pattern 3. However, the improvement in compatibility, which can be achieved by correcting the low-energy defect, can be predicted by use of the available

Table 7

SUMMARY OF POINTS SELECTED FOR HI-RESPONSE ANALYSIS
 BASIC LONG-PLOW/SPLITTER-PLATE INLET AT B.L. 43.82
 (Page 1 of 3)

Part- Pt.	M ₀	α/β	W _{c2}	\bar{R}_2/\bar{R}_0	\bar{R}_{max}/\bar{R}_0	ID _{s-s}	ID _{inst}	KD2 ₁₀
169-1	.50	2/2	312	.978	1.11%	.472	.569	355
170-1	.50	2/-2	312	.980	1.06	.452	.553	484
171-1	.50	5/0	310	.978	1.15	.465	.556	352
276-1	.85	5/0	357	.965	0.93	.737	*.917	—
280-1		5/4	355	.956	1.25	.683	.930	533
281-1		10/0	357	.955	1.32	.663	.991	687
282-1		13/0	356	.951	1.45	.647	.978	990
283-1		10/2	354	.951	1.35	.696	.992	911
284-1		10/-2	355	.961	1.15	.617	*.865	—
292-1		0/2	356	.967	0.81	.844	*.924	—
293-1		0/-2	355	.971	0.74	.740	*.681	—
294-1		10/4	354	.945	1.73	.664	1.059	1008
297-2	.85	13/2	356	.945	1.82	.614	1.039	638
334-1	1.2	0/2	353	.961	1.02	.860	*1.032	—
335-1		0/-2		.963	0.63	.854	1.001	678
336-1		0/0		.963	0.87	.873	1.010	618
337-1		5/0		.958	1.10	.893	1.046	677
338-1		5/2		.945	1.49	.832	*1.141	1057
339-1		5/4		.933	1.80	.901	*1.239	—
340-1		5/-2		.963	0.95	.892	1.042	693
341-1		5/-4		.964	0.89	.885	*1.014	—
342-1		10/0		.939	1.69	.886	1.285	1030
343-1		10/4		.905	2.57	.977	*1.403	—
344-2	1.2	10/-4	353	.958	1.13	.922	1.079	705
345-1	1.2	13/0	353	.935	1.86%	.813	1.153	1198
346-1	1.2	13/2	353	.916	2.47	.807	*1.265	—
347-1	1.2	13/-2	353	.947	1.42	.826	*1.119	—
317-1	1.4	0/0	343	.949	1.01	.747	*.938	—
318-1		0/2		.947	1.17	.677	.934	482
319-1		0/-2		.948	0.96	.765	*.924	—
320-1		5/0		.951	1.23	.826	1.017	550
321-1		5/4		.923	2.24	.885	*1.351	—
322-1		5/2		.937	1.75	.779	1.090	1124
323-1		5/-2		.955	1.06	.841	.973	583
324-1		5/-4		.957	0.98	.831	*.966	—
325-1		10/0		.940	1.71	.834	1.191	907
326-1		10/4		.908	2.66	.923	*1.338	—
327-1		10/-4		.956	1.12	.896	1.016	630
328-1		13/-2		.952	1.35	.829	*1.027	—
329-1	1.4	13/0	343	.947	1.56	.724	1.057	905

*Denotes value of ID from analog computer

Table 7 (Cont'd)

SUMMARY OF POINTS SELECTED FOR HI-RESPONSE ANALYSIS
 BASIC LONG-PLOW/SPLITTER-PLATE INLET AT B.L. 43.82
 (Page 2 of 3)

Part-Pt.	M ₀	α/β	W _{CZ}	\bar{F}_2/R_0	\bar{F}_{2rms}/\bar{F}_2	ID _{S-S}	ID _{inst}	KD2) _{ID}
330-1	1.4	13/2	343	.926	2.11	.855	*.1259	—
300-1	1.5	0/0	333	.934	1.28	.664	*.886	—
302-1		0/2		.930	1.43	.591	*.864	—
303-1		0/-2		.932	1.21	.729	*.912	—
305-2		5/0		.943	1.26	.669	.928	479
306-1		5/2		.929	1.63	.669	.1073	720
307-1		5/4		.912	2.47	.793	.1249	1205
308-1	1.5	5/-2	333	.946	1.04	.758	*.922	—
309-1	1.5	5/-4	333	.948	0.96%	.767	*.905	—
310-1		10/0		.937	1.70	.799	.1161	1108
311-1		10/4		.909	2.58	.844	*.1324	—
312-1		10/-4		.952	1.14	.828	*.961	—
313-1		13/0		.948	1.40	.769	.1009	806
314-1		13/2		.933	1.86	.802	.1124	1279
315-1	1.5	13/-2	333	.952	1.22	.802	*.973	—
12-2	1.6	-2.3/0	310	.891	2.96	.516	.1303	2101
13-1		2/0	365	.889	2.48	.923	.1110	554
13-2			340	.913	2.16	.690	.935	645
13-3			324	.916	2.31	.617	*.931	—
13-5			310	.919	2.05	.579	.779	474
13-6			281	.909	2.82	.426	.909	1515
13-8			250	.900	2.93	.331	*.829	—
13-9		2/0	195	.888	4.77	.165	*.931	—
14-3		2/2	310	.914	2.79	.489	.811	646
15-2		2/4		.885	3.73	.619	.1534	1912
17-3		2/-2		.916	2.09	.553	.932	588
18-2		2/-4	310	.911	2.73	.493	.958	1057
20-1		5/0	340	.920	2.08	.731	.956	502
20-2			310	.930	1.88	.570	.815	705
20-3			281	.930	2.35	.465	*.844	—
20-4		5/0	224	.923	2.46	.233	*.669	—
21-2	1.6	5/2	310	.920	2.59	.542	.888	756
22-2	1.6	5/4	310	.901	3.19%	.529	.1012	1302
23-2		5/-2		.930	1.78	.666	*.865	—
24-2		5/-4		.930	1.75	.669	*.847	—
25-2		10/0		.936	2.23	.563	.910	725
26-2		10/2		.929	2.50	.593	.843	647
27-2		10/4		.913	3.22	.591	.1040	1314
28-2		10/-2		.940	1.97	.613	*.935	—
29-2	1.6	16/-4	310	.945	1.72	.653	.820	433

*Denotes value of ID from analog computer

Table 7 (Cont'd)

SUMMARY OF POINTS SELECTED FOR HI-RESPONSE ANALYSIS
 BASIC LONG-PLOW/SPLITTER-PLATE INLET AT B.L. 43.82
 (Page 3 of 3)

Part- Pt	M ₀	α/β	W _{cz}	\bar{P}_z/\bar{P}_0	\bar{P}_{rms}/\bar{P}_z	ID _{S-S}	ID _{inst}	KD2) _{ID}
30-3	1.6	13/0	310	.955	1.64	.720	.804	296
147-2	1.7	2.4/0		.837	3.72	.647	*1.344	—
148-2		2/2		.870	3.33	.460	1.306	1677
149-2		2/4		.845	4.15	.601	1.640	2229
150-3		2/0		.872	3.27	.468	1.066	1419
151-2		2/-2		.874	3.10	.541	1.265	1230
154-2		5/2		.895	2.81	.429	.872	1175
155-2		5/0		.890	2.87	.433	.979	1735
156-4		5/2		.882	3.13	.477	1.016	1380
158-2		10/4		.889	3.77	.519	1.387	1575
159-2		10/2		.902	3.15	.544	1.065	863
160-2		10/0		.914	2.62	.495	.910	816
161-2		10/-2		.922	2.34	.528	.765	764
164-2	1.7	13/0	310	.935	1.70	.576	*.880	—
120-2	1.8	2/-4	295	.828	3.78	.402	1.321	1878
123-2	1.8	5/0	295	.845	3.58	.421	1.042	1822
127-2	1.8	10/4	295	.850	4.41	.351	1.389	2057
129-2	1.8	10/2	295	.888	2.84	.397	.871	1132
144-4	1.9	5/0	280	.811	3.92	.347	1.436	1320
141-3	2.0	5/0	271	.767	4.22	.440	1.381	1561

*Denotes value of ID from analog computer

Numbers shown are values
of ID given in Table 7

*Denotes value of ID from analog computer

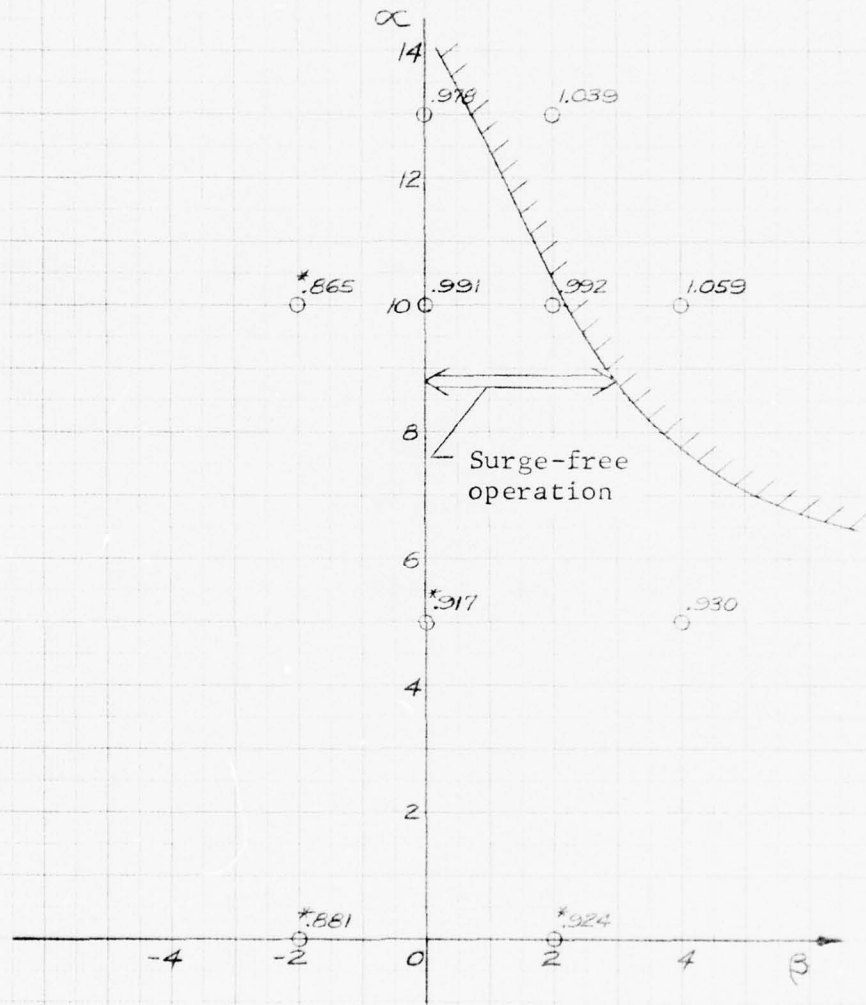


Figure 84. Estimated compatibility envelope of the Basic Long-Flow/Splitter-Plate Inlet at B.L. 43.82 with $M_0 = 0.85$ and altitude = 35,500 ft.

Numbers shown are values
of ID given in Table 7

*Denotes value of ID from analog computer

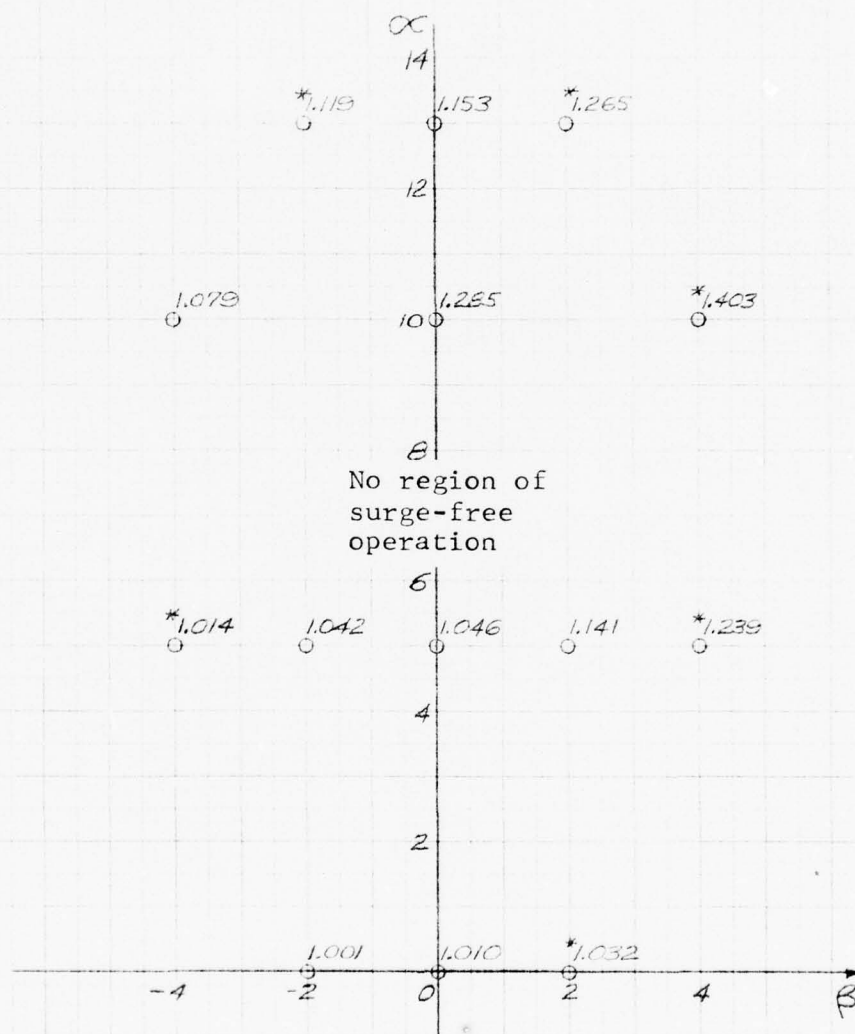


Figure 85. Estimated compatibility envelope of the Basic Long-Plow/Splitter-Plate Inlet at B.L. 43.82 with $M_0 = 1.2$ and altitude = 45,000 ft.

Numbers shown are values
of ID given in Table 7

*Denotes value of ID from analog computer

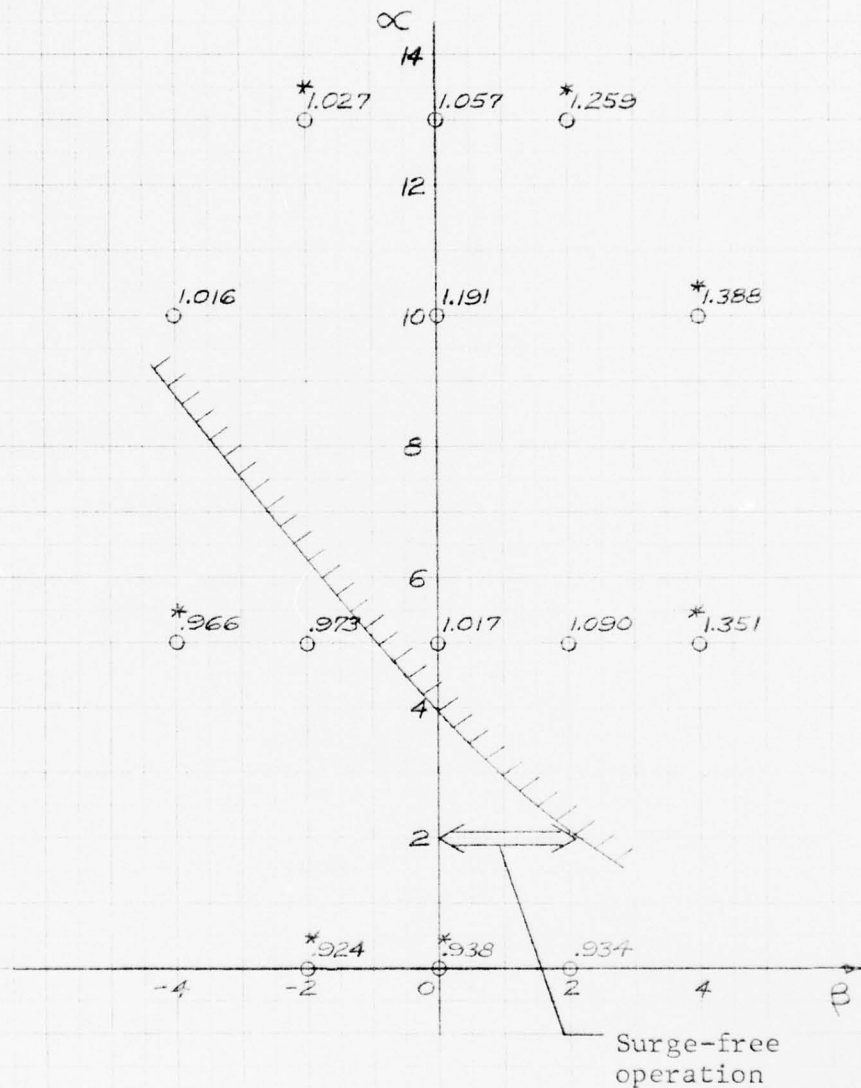


Figure 86. Estimated compatibility envelope of the Basic Long-Plow/Splitter-Plate Inlet at B.L. 43.82 with $M_0 = 1.4$ and altitude = 48,000 ft.

Numbers shown are values
of ID given in Table 7
*Denotes value of ID from analog computer

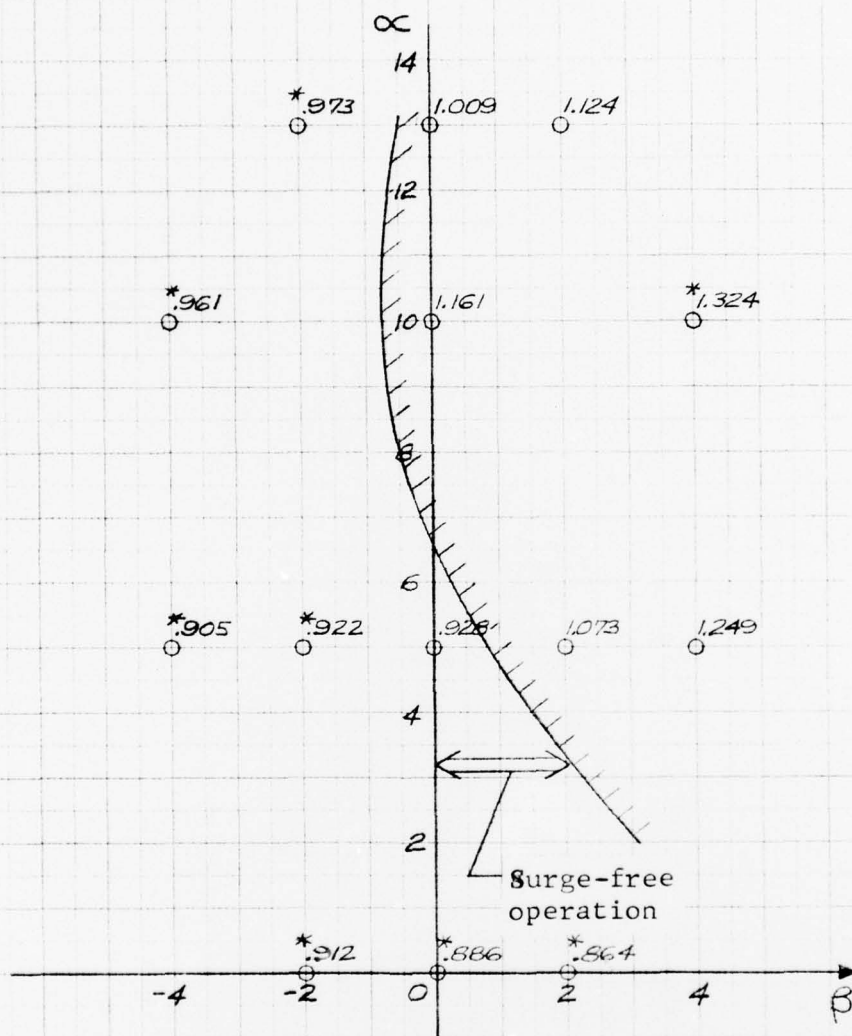


Figure 87. Estimated compatibility envelope of the Basic Long-Plow/Splitter-Plate Inlet at B.L. 43.82 with $M_0 = 1.5$ and altitude = 49,500 ft.

Numbers shown are values
of ID given in Table 7

*Denotes value of ID from analog computer

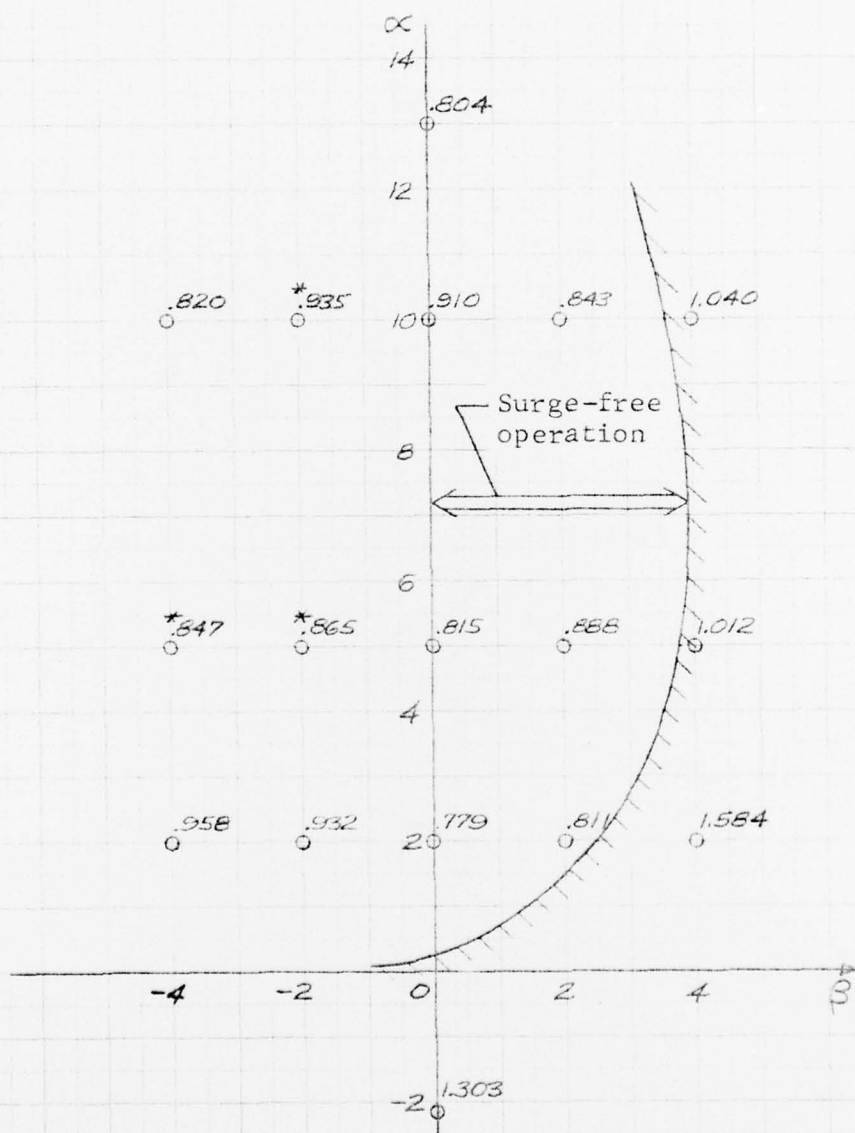


Figure 88. Estimated compatibility envelope of the Basic Long-Flow/Splitter-Plate Inlet at B.L. 43.82 with $M_0 = 1.6$ and altitude = 50,000 ft.

Numbers shown are values
of ID given in Table 7

*Denotes value of ID from analog computer

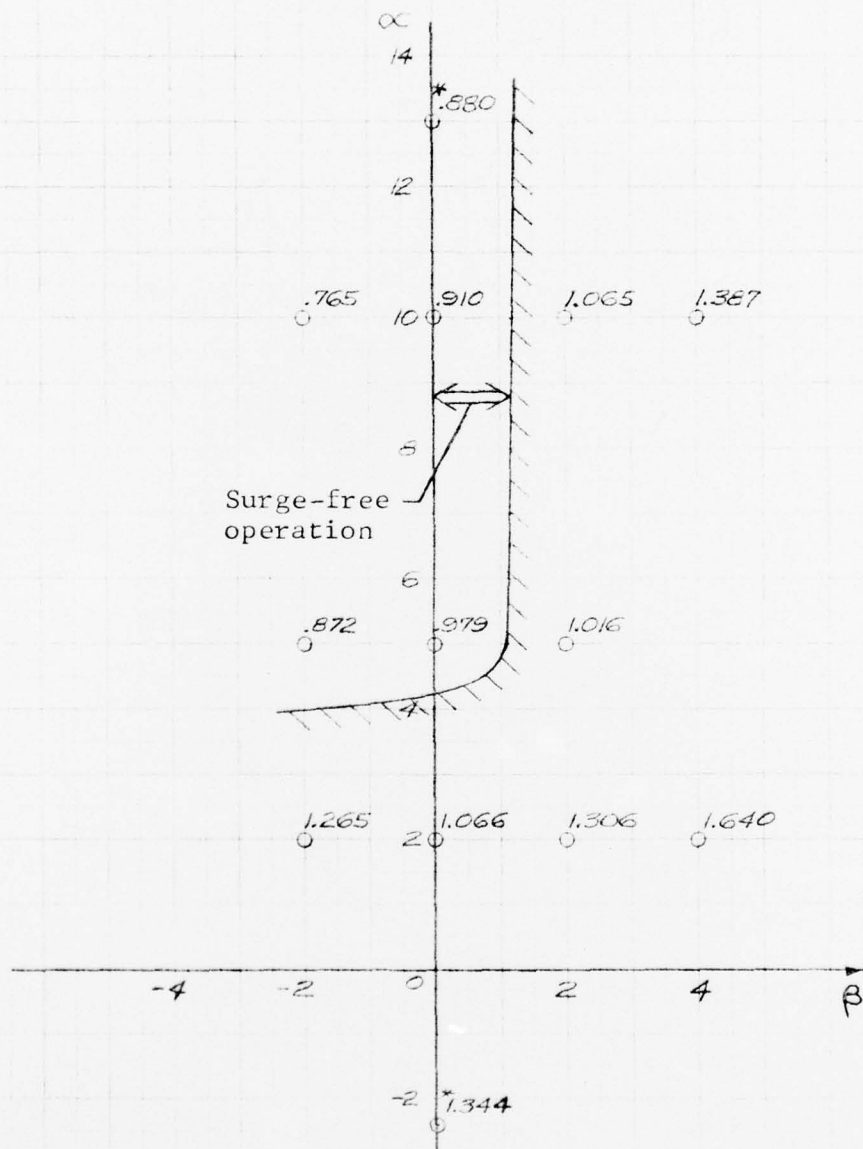


Figure 89. Estimated compatibility envelope of the Basic Long-Plow/Splitter-Plate Inlet at B.L. 43.82 with $M_0 = 1.7$ and altitude = 50,500 ft.

Numbers shown are values of ID

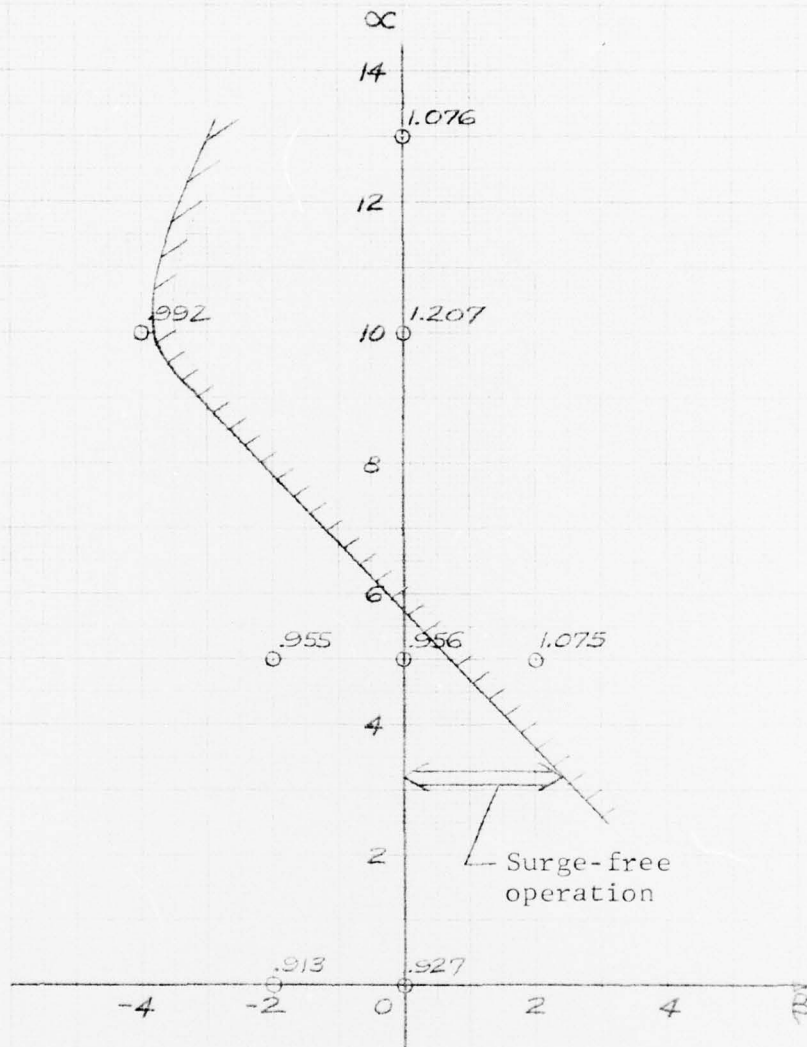


Figure 90. Estimated compatibility envelope of the Basic Long-Plow/Splitter-Plate Inlet at B.L. 43.82 with $M_0 = 1.2$ and altitude = 36,000 ft.

Numbers shown are values of ID

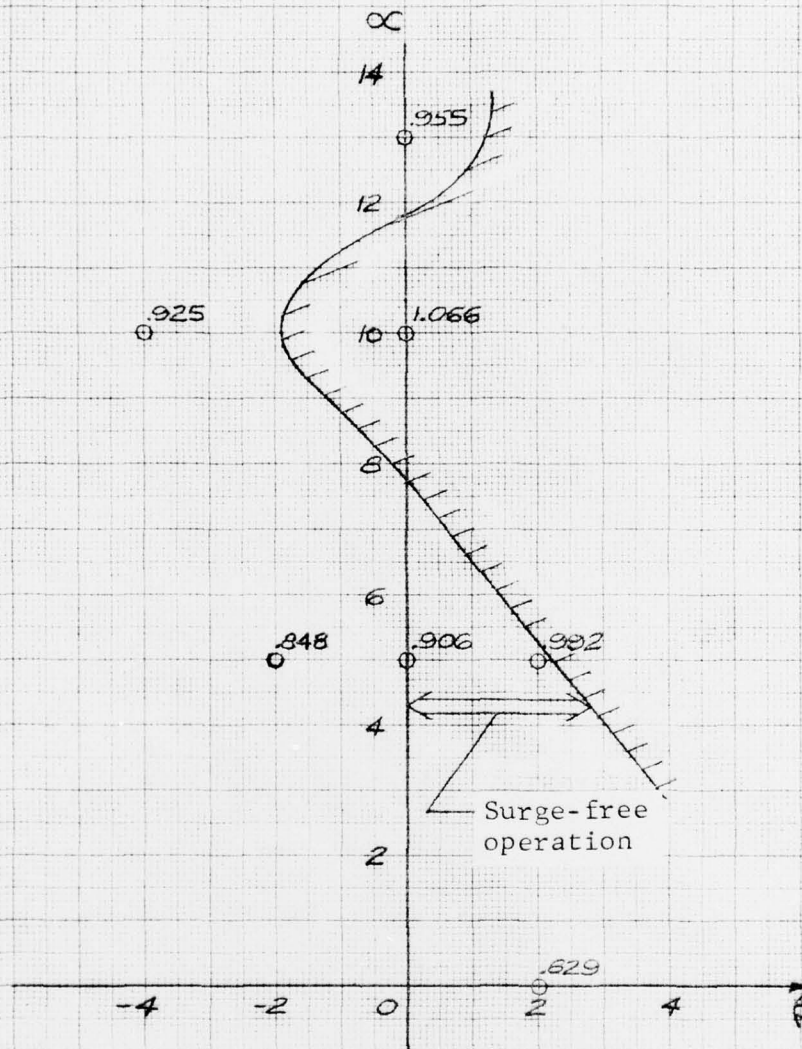


Figure 91. Estimated compatibility envelope of the Basic Long-Plow/Splitter-Plate Inlet at B.L. 43.82 with $M_0 = 1.4$ and altitude = 40,000 ft.

Numbers shown are values of ID

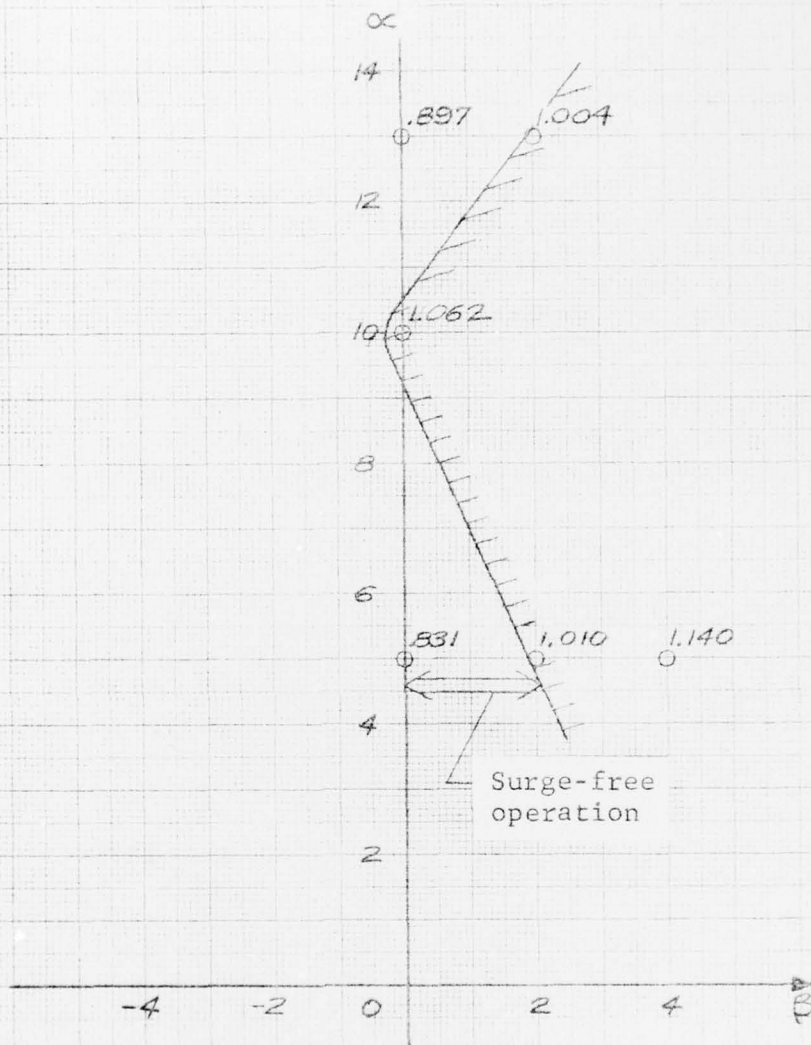


Figure 92. Estimated compatibility envelope of the Basic Long-Plow/Splitter-Plate Inlet at B.L. 43.82 with $M_0 = 1.5$ and altitude = 44,000 ft.

data. The prediction technique and the predicted compatibility improvement are given below.

In Subsection 4.2, it was shown that the airflow separates off the back side of the duct bend and creates a region of low-energy air on the outboard side of the compressor face. This region is typically located about probes 33, 43, and 53, shown in Figure 93. This pocket of low-energy air causes a very high level of steady-state distortion because the GE distortion methodology is supersensitive to a low reading on any probe in Rings 1, 2, 4, or 5 of the compressor-face instrumentation. An excessive level of steady-state distortion can dominate the instantaneous, or dynamic, level of distortion if the inlet turbulence level is low.

Functionally the dynamic distortion may be expressed as the sum of the steady-state distortion and some function of the turbulence level at the compressor face; i.e.,

$$ID_{DYN} = ID_{SS} + f(\bar{P}_{trms}/\bar{P}_{t2})$$

Thus, if a duct configuration change produces a reduction in the steady-state distortion level without increasing the turbulence level, then the dynamic-distortion level will be reduced accordingly. To illustrate this in a quantitative manner, realistic compressor-face patterns for an "improved" duct can be generated by substituting new values for the pressures in the low-energy region with the following averaging scheme. Consider Figure 93; substitution values, denoted by primes, for probes CF33, CF43, and CF53 can be generated as follows:

$$\begin{aligned} CF33' &= (CF23 + CF32 + CF34)/3 \\ CF43' &= (CF33' + CF42 + CF44)/3 \\ CF53' &= (CF43' + CF52 + CF54)/3 \end{aligned}$$

By use of the substitution values for these three probes, a new value of steady-state distortion, ID_{SS}' , is computed. Then the new value of dynamic distortion, ID_{DYN}' , can be calculated by

$$ID_{DYN}' = ID_{SS}' + [ID_{DYN} - ID_{SS}]$$

where the term in brackets is determined from the values given in Table 7.

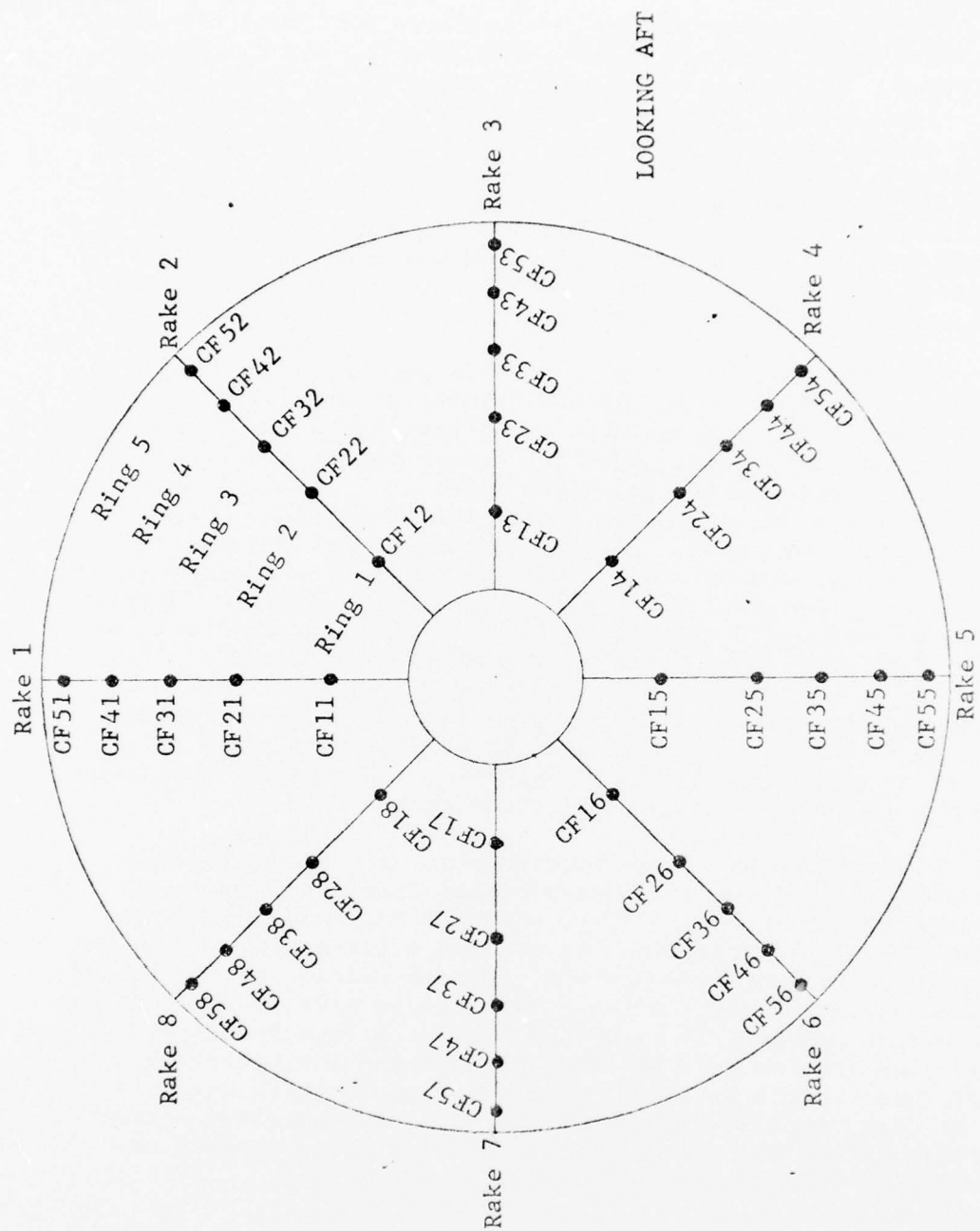


Figure 93. Left-Hand Compressor-Face Probe Designation

This technique was applied to those test conditions in Table 7 at 5° angle-of-attack, 0° sideslip, and the design airflow. The resulting values of ID_{SS} , ID_{DYN} , ID'_{SS} and ID'_{DYN} are plotted in Figure 94. These values of ID were computed for altitudes along the upper boundary of the assumed flight envelope. Note that the dynamic distortion level, ID'_{DYN} , for an "improved" duct configuration is less than the steady-state distortion level for the present duct. Also, from Mach 0.85 to 1.6 the dynamic distortion level does not exceed 0.8, which means the compatibility barrier at 1.2 Mach (Figure 85) has been eliminated.

Recall that the purpose of this prediction technique was to illustrate that the Basic Inlet at B.L. 43.82 would have acceptable engine/inlet compatibility if the low-energy defect was corrected. Further, recall that a prediction was not necessary for the Basic Inlet at B.L. 45.64 because data was available to show that, with VG Pattern 3, compatibility was very good. Because the low-energy defect is a duct problem and not related to the inlet flow field or inlet location, the predicted improvement for the inboard location should agree with the test data from the outboard location. The data in Figures 75, 77, 82, and 83 at 5° angle-of-attack and 0° sideslip, show a decrease in ID of .25 at Mach 0.85 and .28 at Mach 1.4. From Figure 94 the predicted decrease in ID is .22 at Mach 0.85 and .32 at Mach 1.4. This is excellent agreement; thus the validity of the prediction technique is strongly supported by the test data.

In Figure 94, it appears that at Mach 1.6 and above elimination of the low-energy region does not improve the distortion level. Actually, what has happened is that the boundary-layer ingestion has created a low-energy region on the upper inboard side of the compressor-face that dominates the distortion calculation. This can be seen in the compressor-face patterns in Figure 23. If the boundary-layer ingestion problem were eliminated, then the low-energy region produced by the duct-bend separation would again dominate the distortion level. Above Mach 1.6 the increment between steady-state and dynamic distortion increases sharply because of a rapid increase in turbulence level.

4.4.4 Summary of Engine/Inlet Compatibility

In the preceding subsections, it has been shown that the Basic Long-Plow/Splitter-Plate Inlet, positioned at

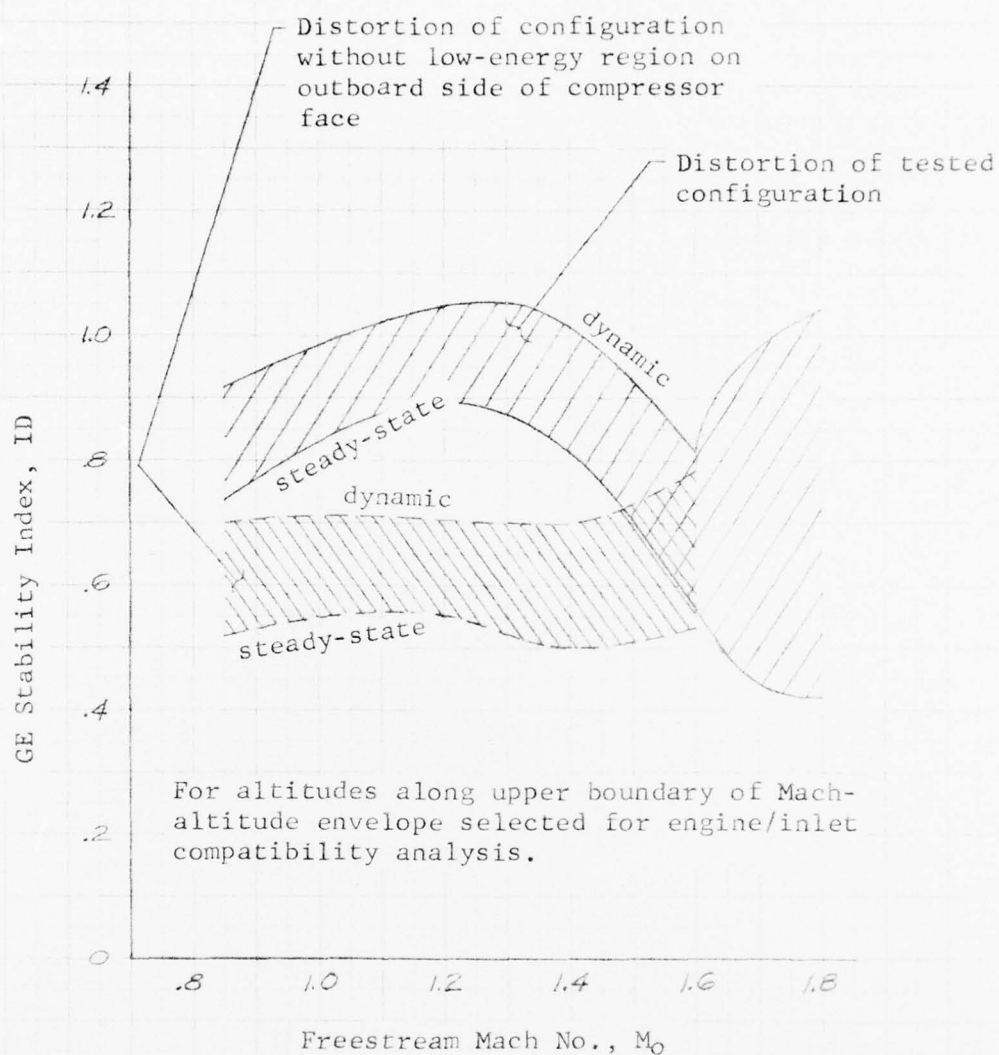


Figure 94. Compatibility prediction of the Basic Long-Flow/ Splitter-Plate Inlet with the low-energy defect corrected: $\alpha = 5^\circ$, $\beta = 0^\circ$, and design airflows.

either B.L. 43.82 or B.L. 45.64, has very good compatibility with the F101 engine when the low-energy defect at the compressor face is corrected. Further, it has been shown that VG Pattern 3 corrects the low-energy defect. These comments apply to altitudes along the upper boundary of the assumed flight envelope, which are the most adverse altitudes for compatibility. Even without correction of the low-energy defect, it has been shown that the Basic Inlet at either B.L. 43.82 or B.L. 45.64 has acceptable compatibility at lower altitudes.

5. CONCLUSIONS

It is concluded from this program that a simple, open-nose, normal-shock inlet can operate while in the influence of a wing-body flow field. The Basic Long-Plow/Splitter-Plate Inlet at either B.L. 43.82 or B.L. 45.64 has acceptable inlet pressure recovery. Likewise, engine/inlet compatibility of the Basic Long-Plow/Splitter-Plate Inlet with VG Pattern 3 is very good in either position throughout the selected Mach-altitude envelope. Without VG Pattern 3, the Basic Inlet has acceptable engine/inlet compatibility in either position at conditions slightly below the upper left-hand boundary of the selected Mach-altitude envelope.

Other specific conclusions drawn from the analysis of the test data are:

1. The fuselage boundary-layer on the research model as tested was thicker than the thickness calculated by flat-plate theory, whereas the opposite was true for the F-111.
2. The flow-field surveys show the fuselage boundary layer to be vortex-free throughout the Mach-alpha-beta envelopes tested.
3. Spillage of the fuselage boundary layer past the splitter plates into the inlet degraded inlet performance, distortion, and engine/inlet compatibility at all test conditions regardless of inlet standoff position. It was concluded, however, that an improved inlet configuration can be produced by modifying the fuselage-boundary-layer system.
4. The outboard duct bend resulted in some flow separation that increased inlet distortion. However, the separation phenomena is correctible with duct vortex generators or duct blowing without redesigning the duct. This was demonstrated during the tests and results in a significant decrease in distortion and subsequent marked improvement in engine/inlet compatibility.

5. The inlet was free from lip separation at all conditions tested.
6. The separation off the back of the duct bend created a region of low-energy air at the compressor face, which significantly increased the steady-state distortion. Although the fluctuating component of distortion was at a realistic level, the high steady-state component biased the compatibility analysis. It has been shown that when the problem at the duct bend is corrected, the dynamic distortion level (steady-state + fluctuating component) is acceptable across the Mach range.

REFERENCES

1. Cawthon, J. A., Truax, P. P., Steenken, W. G., Supersonic Inlet Design and Airframe - Inlet Integration Program (Project Tailor-Mate), Air Force Flight Dynamics Laboratory Report AFFDL-TR-71-124, Col. III, Composite Inlet Investigation, May 1973.
2. Model and Test Information Report, 1/5.2-Scale Composite Inlet Model Test in AEDC PWT 16T, 16S - October 1975, General Dynamics Fort Worth Division Report FZT-267, 15 August 1975.
3. Wind Tunnel Data Report, 1/5.2-Scale Fuselage-Inlet Model, AEDC, PWT Tests SF-178 and TF-399, November 1975 and March 1976, General Dynamics Fort Worth Division Report FZT-284, 27 April 1976.
4. Working Curves for the Characteristics of the Smooth Flat Plate Turbulent Boundary Layer, Convair, A Division of General Dynamics Corporation (Fort Worth) Report MR-A-1121, 21 May 1957.
5. Seddon, J., Boundary Layer Interaction Effects In Intakes With Particular Reference to Those Designed for Dual Subsonic and Supersonic Performance, Royal Aircraft Establishment TR66099, March 1966.
6. Seddon, J., The Flow Produced by Interaction of a Turbulent Boundary Layer With a Normal Shock Wave of Strength Sufficient to Cause Separation, Royal Aircraft Establishment, Aeronautical Research Council R&M 3502 (Tech. Memo No. Aero. 667), 11 March 1960.
7. Hi-Response Data Plan for the 1/5.2-Scale Advanced Research Inlet Test in the AEDC PWT 16T/16S Tunnels, General Dynamics Fort Worth Division Report MR-P-376, 14 October 1975.